INFORMATION TO USERS

This manuscript has been reproduced from the microfilm master. UMI films the text directly from the original or copy submitted. Thus, some thesis and dissertation copies are in typewriter face, while others may be from any type of computer printer.

The quality of this reproduction is dependent upon the quality of the copy submitted. Broken or indistinct print, colored or poor quality illustrations and photographs, print bleedthrough, substandard margins, and improper alignment can adversely affect reproduction.

In the unlikely event that the author did not send UMI a complete manuscript and there are missing pages, these will be noted. Also, if unauthorized copyright material had to be removed, a note will indicate the deletion.

Oversize materials (e.g., maps, drawings, charts) are reproduced by sectioning the original, beginning at the upper left-hand corner and continuing from left to right in equal sections with small overlaps. Each original is also photographed in one exposure and is included in reduced form at the back of the book.

Photographs included in the original manuscript have been reproduced xerographically in this copy. Higher quality 6" x 9" black and white photographic prints are available for any photographs or illustrations appearing in this copy for an additional charge. Contact UMI directly to order.

UMI

A Bell & Howell Information Company
300 North Zeeb Road, Ann Arbor MI 48106-1346 USA
313/761-4700 800/521-0600

Downloaded from SHAREOK. Persistent Handle URL: https://hdl.handle.net/11244/5574

THE UNIVERSITY OF OKLAHOMA

GRADUATE COLLEGE

A NEW CONCEPTUAL APPROACH TO SHALE STABILITY

A DISSERTATION

SUBMITTED TO THE GRADUATE FACULTY

in partial fulfillment of the requirements for the

degree of

DOCTOR OF PHILOSOPHY

by

HELIO M. R. SANTOS

Norman, Oklahoma

1997

UMI Number: 9812263

UMI Microform 9812263
Copyright 1998, by UMI Company. All rights reserved.

This microform edition is protected against unauthorized copying under Title 17, United States Code.

UMI
300 North Zeeb Road
Ann Arbor, MI 48103

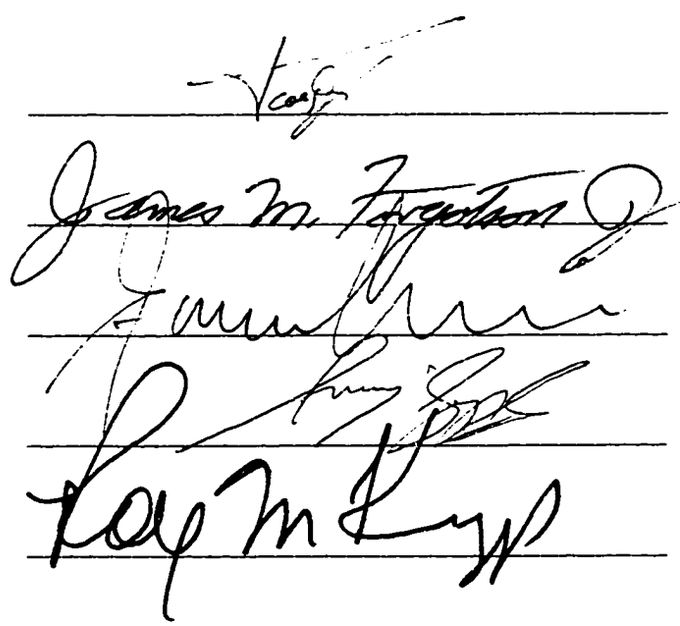
© Copyright by Helio M. R. Santos 1997
All Rights Reserved

A NEW CONCEPTUAL APPROACH TO SHALE STABILITY

A DISSERTATION APPROVED

FOR THE SCHOOL OF PETROLEUM AND GEOLOGICAL ENGINEERING

By



This dissertation is dedicated to the memory of my father Helio, to my mother Gilda, to my wife Denise, and to our three sons, Felipe, Eduardo, and Mauricio. Without their guidance, support, love, encouragement, undestanding, sacrifices, and patience, the completion of this work would not be possible.

Acknowledgments

I would like to acknowledge Petrobras for the opportunity given to me to pursue this Ph.D. degree, with all the financial and technical support throughout this venture.

I would like to express my sincere gratitude to Dr. Jean-Claude Roegiers for his support in all matters related to the difficult challenge imposed by the shale stability project, without it the results presented here would not be obtained. His technical guidance in Rock Mechanics was outstanding, allowing me to improve my knowledge and views of this subject. Thanks are also due to Dr. Anuj Gupta, who introduced me to new technology in thermal analysis, an important component of this work, Dr. Roy Knapp, Dr. Faruk Civan, and Dr. James Forgotson, for accepting to serve as members of the doctoral advisory committee and for revising this document. Important technical concepts were acquired during courses taken with them, as well as with informal conversations that, in one way or another, contributed somehow to the successful completion of this dissertation.

Special thanks go to Dr. Adel Diek for his invaluable contribution to this work. He was always available when I needed some help. His expertise in

several areas and scientific-oriented mind were decisive for my growth as an engineer and scientist.

Great appreciation also goes to several individuals and institutions:

Sergio A. B. da Fontoura, who introduced me to both the fascinating Rock Mechanics subject and to Dr. Roegiers, for his constant interest in exchanging ideas and discussing all the polemic points;

Dr. Thurmman Scott, Mike Shaw, Tammie Nelson, Alfonso Varela, and Timothy Freije for their help and support in all laboratory-related aspects, from trivial points to design of sophisticated and innovative laboratory experiments.

Fersheed Mody, Marty Stokke, Eric van Oort, Michelle Thomas, Gangerico Ramos, and Jack Estes helped in several ways with technical discussions, giving advice and suggestions on how to conduct and improve the various experiments. The companies affiliated in the Rock Mechanics Consortium, especially ARCO, Conoco, EXXON, PEMEX, Petrobras, Shell, and Sperry-Sun, as well as EDTI, provided invaluable contributions such as: laboratory tests, preserved and non-preserved shale cores, and allowing their employees to participate in events at the University of Oklahoma, such as workshops and technical meetings.

Mauricio Almeida, Luis Felipe Rego, Rafael Amorim, Joao Carlos Placido, Wellington Campos, and Maria das Gracas Silva, all friends from Petrobras, decisively helped me even before the arrival at the University of Oklahoma.

Their continuing support, advice, and encouragement paved the road for this successful work.

Abstract

Shale instability is today, probably, the largest single problem during drilling accounting for heavy losses for the oil industry. Research has been focused mainly in the chemical aspect, since shale is considered a very reactive rock when in contact with water. Solutions have quite often pointed to new additives with the aim of turning the drilling fluid more inhibitive. The observation that strong reaction with water occurs only in partially-dried shales led to the conclusion that a deep understanding of the actual downhole shale-fluid interaction was still missing.

This study concentrates on this last point, with emphasis on laboratory experiments. With the availability of well-preserved shale cores from offshore wells, an extensive laboratory research was conducted in order to investigate concepts and ideas used by the industry to optimize the drilling fluid. The results showed that inappropriate sample handling procedure generate the false notion that shales strongly swell in contact with water. Even though shale swelling has been questioned before, the results presented in this study provide a strong and irrefutable evidence that instabilities in shales are mainly originated from mechanical rather than chemical causes.

A new methodology to characterize shales based on thermal analysis is proposed. The need to better define the water distribution in a shale was the main driving force for the search of a methodology capable of substituting the X-Ray diffraction method. All the important features of a shaly rock can be described, including the clay minerals and the different water types associated with them.

In order to closely mimic the downhole conditions, especially pressure, a new triaxial laboratory test was developed to evaluate shale-fluid interaction. Tests conducted with three different shale types confirmed the results obtained with immersion tests under atmospheric conditions: the preserved samples did not swell when in contact with water. On the other hand, a strong reaction was observed with all partially-dried specimens.

Based on this broad investigation, the most probable instability mechanism is the creation of cracks with subsequent penetration of the drilling fluid into the fractures. An innovative conceptual model to analyze wellbore stability is presented, based on energy concepts. When the internal energy level of the rock reaches a critical limit, fracture surfaces are created to reduce the internal energy level to an acceptable level. The most important energetic events during drilling a wellbore are described; an energy balance should be performed in order to ascertain if the critical limit for the rock is achieved. New laboratory experiments are proposed so that the internal energy limit for the rock be measured. In addition, these experiments will allow the validation of the proposed mechanism. Field cases are described showing that the

adoption of non-penetrating fluid strongly reduced, and sometimes completely eliminated, severe problems in areas prone of instability.

Contents

Acknowledgments v

Abstract viii

Contents xi

List of Tables xv

List of Figures xvi

1. Introduction 1

1.1 General Overview 1

1.2 Objectives of the Study 4

1.3 Dissertation Overview 5

2. Critical Literature Review 9

2.1 Introduction 9

2.2 Mud Selection Criteria 10

2.3 Shale-Fluid Interaction 12

2.3.1 Swelling Clay Minerals 13

2.3.2 Shale Swelling Mechanisms 14

2.3.3 Capillary Effects 16

2.3.4 Swelling Pressure 17

2.3.5 Shale Activity 18

2.3.6 Driving Forces and Flows 21

2.4 Wellbore Stability Analyses 25

3. Influence of Water Content and Distribution on Shale Reactivity 29

3.1 Introduction 29
3.2 Shale Samples 32
3.2.1 Characterization Tests 33
3.3 New methodology of water content determination 37
3.4 Laboratory tests and evidences 43
3.4.1 Water Content and Shale Reactivity - Immersion tests 44
3.4.2 Rock Strength Variation 47
3.4.3 Water content 49
3.4.4 Water redistribution 52
3.4.5 Dehydration methods 59
3.4.6 Shale reaction in air-free samples 65
3.4.7 Mechanical work 66
3.5 How water content and distribution control shale reactivity - preliminary reflections 68
3.6 Shale preservation and laboratory sample handling recommendations 73
3.7 Practical implications and consequences 76
3.8 Summary 78

4. Shale Characterization with Thermal Analysis **80**
4.1 Introduction 80
4.2 Limitations of the XRD Method 82
4.3 Thermal Analysis as a Characterization Tool 87
4.4 Characterization Results 98
4.5 Discussion 108
4.6 Summary 110

5. Shale-Reactivity Test: A Novel Approach to Evaluate Shale-Fluid Interaction **112**
5.1 Introduction 112
5.2 Previous works 114
5.3 Test description 116
5.3.1 Sample Preparation 117

5.3.2 Test Procedure 121
5.4 Results 122
5.5 Discussion 128
5.6 Conclusions 130
5.7 Summary 131

6. Misconceptions Related to Shale-Fluid Interaction **132**
6.1 Introduction 132
6.2 Concepts or Misconceptions? 133
6.2.1 Swelling Clay Minerals 134
6.2.2 Shale Swelling Mechanisms 135
6.2.3 Capillary Effects 138
6.2.4 Swelling Pressure 144
6.2.5 Chemical Potential as a Driving Force 147
6.2.6 Analysis of Shale Structure Alteration with TGA 157
6.2.7 Semi-Permeable Membrane and Osmotic Pressure. 200
6.2.8 Shale Structure 203
6.2.9 Pore Pressure in Shales 205
6.2.10 Pore-Pressure Induced by Chemical Potential 208
6.3 Suggested Interaction Mechanisms for WBM and OBM 209
6.4 Conclusions 211
6.5 Summary 212

7. An Energy Approach to Wellbore Stability Analysis **214**
7.1 Introduction 214
7.2 Distribution of the Excess Energy during Rock Fracture Failure 215
7.3 Most Relevant Energetic Processes in a Wellbore 221
7.3.1 Drill String Vibration (Mechanical Energy) 221
7.3.2 Rock Deformation (Strain Energy) 228
7.3.3 Heat (Thermal Energy) 240
7.3.4 Chemical Rock Alteration 249
7.4 Proposed Instability Mechanism 255

7.5 Need for Laboratory Tests to Determine the Required Parameters... 258
7.6 Effective Minimization of the Wellbore Stability Problems..... 259
7.7 Relevance of the Various Energy Terms in the Overall Energy Balance..... 263
7.8 Summary..... 265

8. Conclusions and Recommendations **267**
8.1 Conclusions..... 267
8.2 Recommendations..... 269

Nomenclature **271**

References **273**

Appendix A **287**

Appendix B **316**

Appendix C **357**

List of Tables

Table 2.1: Different mechanisms and molecular species flow for each associated driving force (Mody & Hale, 1993) 24
Table 3.1: Pore fluid composition for shales from the Campos Basin and the Gulf of Mexico (ND = not detected).**Error! Bookmark not defined.**
Table 3.2: Cation Exchange Capacity (CEC) for shales from the Campos Basin, the North Sea, and Pierre shale. 35
Table 3.3: Mineralogy (%) of shales from the Campos Basin, the North Sea, and Pierre shale. 36
Table 3.4: Detailed mineralogy and average water content (usual methodology) of some shales from the Campos Basin. 36
Table 3.5: Water content (usual methodology) for different boxes (depths) - Shale B. 37
Table 3.6: Water content on the surface at different times for water redistribution evaluation. 53
Table 3.7: Water content on different surfaces (mechanically prepared and natural). 67
Table 6.1: Free water (%) as a function of time for the samples immersed in different solutions. 151
Table 6.2: Free water as a function of time for the samples immersed in OBM with different water-phase activities. 154
Table 6.3: Solution composition after 5 hrs. immersed in de-ionized water (mg/l) (ND = not detected). 201
Table 7.1: Evaluation of the various energy contributions for a 2.5g sample in the microfracturing process of rocks. 264
Table A.1: Classification scheme for phyllosilicates with six-membered rings of SiO_4 tetrahedra (Mackenzie, 1965) 301

List of Figures

Figure 3.1: Thermogravimetric Analyzer (TGA 50).**Error! Bookmark not defined.**
Figure 3.2: TGA 50 with the acquisition data system and plotter. Nitrogen gas (cylinder in the back) is used to purge any evolved gas from the sample. 40
Figure 3.3: Complete water content determination of a preserved sample. 43
Figure 3.4: Sample 0 after immersion in water for 3 days. 45
Figure 3.5: Sample 22 after immersion in water for 24 and 35 minutes. 45
Figure 3.6: Rex durometer Type C Model 1600. On the left, shale samples in a beaker immersed in mineral oil before testing. The samples are tested without removing them from the solution to avoid air exposure. ... 48
Figure 3.7: Strength index as a function of time for different drying periods. 48
Figure 3.8: Strength index as a function of time for preserved samples in de-ionized water and various KCl solutions. No significant change was observed. 49
Figure 3.9: Water content - sample 0 (no drying) 50
Figure 3.10: Water content - sample 22. 51
Figure 3.11: First 40 minutes of water content determination - sample 0 (no drying) 51
Figure 3.12: Size of the sample used to measure water content compared to the whole shale sample (approximate real scale; shale sample dimensions: 2 in. x 3 in.) 52
Figure 3.13: Shale reaction in water after 2-hour air drying, without water redistribution. 55
Figure 3.14: Shale reaction in water after being immersed in oil for 2 weeks to allow water redistribution. 56
Figure 3.15: Water redistribution experiment: shale coated with paraffin to avoid further dehydration and contamination with oil. 57
Figure 3.16: Free water (weight loss between room temperature and 110°C) at the surface: original value, after 2 hours in air, and after 5, 19, and 55 days equilibrating. 58
Figure 3.17: Bound water (weight loss between 110°C and 250°C) at the surface: original value, after 2 hours in air, and after 5, 19, and 55 days equilibrating. 59
Figure 3.18: Crystalline water (weight loss between 250°C and 800°C) at the surface: original value, after 2 hours in air, and after 5, 19, and 55 days equilibrating. 59
Figure 3.19: Weight loss for different dehydration processes. 63

Figure 3.20: Shale reaction after dehydration in alcohol - no air allowed in the sample. 66
Figure 3.21: Comparison between mechanically cut and naturally opened surfaces — a thin powder is generated on the mechanically opened surfaces (light color) whereas nothing is observed on the other one. 67
Figure 3.22: Fiberglass container used to preserve shale cores since the time they arrived at the rig floor. Sealing must be periodically checked for any leakage. 74
Figure 3.23: Pieces cut from cores are immediately immersed in mineral oil, and kept immersed until the beginning of any test. 75
Figure 4.1: XRD mineralogy of shale Petr_B: Total clay = smectite + illite + kaolinite + chlorite. 84
Figure 4.2: XRD mineralogy of shale Petr_D: Total clay = smectite + illite + kaolinite + chlorite. 84
Figure 4.3: XRD mineralogy of shale Petr_C: Total clay = smectite + illite + kaolinite + chlorite. 85
Figure 4.4: XRD mineralogy of shale Petr_E: Total clay = smectite + illite + kaolinite + chlorite. 85
Figure 4.5: XRD mineralogy of shale Pem_1: Total clay = smectite + illite + kaolinite + chlorite. 86
Figure 4.6: XRD mineralogy of shale Pem_2: Total clay = smectite + illite + kaolinite + chlorite. 86
Figure 4.7: XRD mineralogy of shale Pem_7: Total clay = smectite + illite + kaolinite + chlorite. 86
Figure 4.8: XRD mineralogy of shale Pem_22: Total clay = smectite + illite + kaolinite + chlorite. 87
Figure 4.9: TGA curve of kaolinite KGa-1 showing mass loss due to dehydroxylation (10.61-mg sample, 10°C/min. heating rate, 50-cm^3/min. N_2 purge) (Bish & Duffy, 1990). 92
Figure 4.10: TGA curve of ripidolite chlorite, CCa-1, California (13.12-mg sample, 10°C/min. heating rate, 50-cm^3/min. N_2 purge) (Bish & Duffy, 1990). 92
Figure 4.11: TGA curve for smectite SWy-1 (Na-montmorillonite) showing two-stage low-temperature dehydration and dehydroxylation (13.64-mg sample, 10°C/min. heating rate, 50-cm^3/min. N_2 purge) (Bish & Duffy, 1990). 93
Figure 4.12: TGA curve for smectite SAz-1 (Ca-montmorillonite) showing two-stage low-temperature dehydration and dehydroxylation (15.52-mg sample, 10°C/min. heating rate, 50-cm^3/min. N_2 purge) (Bish & Duffy, 1990). 93
Figure 4.13: TGA curve of calcite showing decarbonation (11.48-mg sample, 10°C/min. heating rate, 50-cm^3/min. N_2 purge) (Bish & Duffy, 1990). 96
Figure 4.14: TGA curve of brick component from Acme Brick Company, showing mass losses due to dehydration of smectite, dehydroxylation of kaolinite and smectite, and decarbonation of calcite (20.83-mg

sample, 20°C/min. heating rate, 50-cm^3/min. N_2 purge) (Bish & Duffy, 1990)..... 97
Figure 4.15: TGA of Wyoming bentonite. No free water was found. Top curve: weight retained; bottom curve: derivative of the weight with respect to temperature..... 99
Figure 4.16: TGA of shale Petr_C. Observe free water and inflection due to interlayer water..... 100
Figure 4.17: TGA of shale Petr_E. Smectite is similar to the one present in the Wyoming bentonite..... 101
Figure 4.18: TGA (10°C/min.) of shale B - native state - high calcite content..... 101
Figure 4.19: TGA (10°C/min.) of shale D - native state - high calcite content..... 102
Figure 4.20: TGA of shale Pem_1. Isolated peak for illite, and no presence of calcite..... 103
Figure 4.21: TGA of shale Pem_2. No interlayer water signals absence of smectite..... 103
Figure 4.22: TGA of shale Pem_7. Similar to the previous one..... 104
Figure 4.23: TGA of shale Pem_22. Isolated peak of interlayer water signals high amount of smectite. Even dried, this shale presents a high amount of "free" and interlayer water. This water cannot be considered totally free, being attached to the smectite, and does not evaporate at room temperature..... 104
Figure 4.24: TGA of shale Speeton. High clay content, no calcite..... 105
Figure 4.25: TGA of chalk. Peak at 200°C might indicate presence of organic matter in the rock..... 106
Figure 4.26: TGA of shale Petr_D - Native state..... 107
Figure 4.27: TGA of the remaining sample of the previous chart left exposed to air for 3.5 hrs. No free water, just interlayer water..... 108
Figure 4.28: TGA of the sample from the surface of a big piece dried for 3.5 hrs. Free and interlayer water present in the sample..... 108
Figure 5.1: Schematic representation of the equipment for the shale-reactivity test..... 118
Figure 5.2: Sample after the test showing the metal screen around it..... 119
Figure 5.3: Detail of the sample with the metal screen and jacket, with bottom and top caps..... 119
Figure 5.4: Sample ready to start the shale reactivity test. Preservation is provided by the oil surrounding the sample..... 121
Figure 5.5: Circumferential length variation for the aluminum sample..... 123
Figure 5.6: Circumferential length variation for a dried shale..... 124
Figure 5.7: Enlarged time scale for the dried shale..... 125
Figure 5.8: Circumferential length variation for a preserved shale..... 126
Figure 5.9: Enlarged time scale for the preserved sample..... 127
Figure 5.10: Picture of the whole equipment during a test. A plastic beaker is used to collect the outlet fluid for future analysis..... 128

Figure 6.1: Immersion in de-ionized water of different sample conditions. All the samples are from the same shale, with pieces taken from the same core box. Top, from left to right: preserved sample after 3 days immersed in water; sample dried in air for 2 hrs., after 2 hrs. immersed in water; sample dried in air for 22 hrs., after 24 min. immersed in water. Bottom, from left to right: sample dehydrated in alcohol and immersed in water for 2 days; sample dried in air for 2 hrs., equilibrated in oil for 4 weeks, and immersed in water for 2 days; sample dried in air for 2 hrs., equilibrated in oil for 1 year, after immersion in water for 24 hours..... 137
Figure 6.2: Immersion of dry shale in mineral oil: penetration into the rock indicated by gain in submersed weight..... 139
Figure 6.3: Rock-fluid interaction loop: dried outcrop shale (100% smectite) with fresh water; reaction throughout the sample..... 140
Figure 6.4: Rock-fluid interaction loop: dried outcrop shale (100% smectite) with oil; hole in gauge and no reaction whatsoever, despite penetration of oil into the shale (see dark shade around the horizontal hole)..... 140
Figure 6.5: Oil spreading on a dried shale: initial stage..... 141
Figure 6.6: Same as Figure 6.5, minutes later: penetration is faster in the fracture than into the matrix..... 142
Figure 6.7: Same as Figure 6.6, minutes later: front advance is seen on the left, as well as penetration into the rock around the fracture. Oil does not evaporate at room temperature and penetrates deeper into the rock. No reaction occurs..... 142
Figure 6.8: Water drop on a dried shale: penetration in the fracture, but most of the water remains steady..... 143
Figure 6.9: Shale surface after water has evaporated: signs of reaction visible on the surface, despite little penetration into the rock..... 143
Figure 6.10: Shale reactivity test of an air-dried shale D sample: expansion in the vertical direction and contraction followed by expansion in the circumferential direction. Final volume smaller than the initial one.145
Figure 6.11: Shale reactivity test of a preserved shale D sample: no reaction was observed after pumping water..... 145
Figure 6.12: Shale reactivity test: shale Petr_E, dried for 24 hrs. with de-ionized water as the test fluid. Final sample volume greater than before water gets in contact..... 146
Figure 6.13: Submersed weight as a function of time in different solutions: all samples of shale D and well preserved..... 149
Figure 6.14: First 2.5 hrs. of the previous graph..... 150
Figure 6.15: Weight in air before and after immersion in different solutions: samples and solutions are the same as in Figure 6.13..... 150
Figure 6.16: Penetrometer index as a function of time. Preserved samples immersed in quasi-saturated salt solutions, alcohol, and de-ionized water..... 152

Figure 6.17: Submersed weight as a function of time in different oil solutions: all samples of shale D and well preserved. 153
Figure 6.18: Weight in air before and after immersion in different oil solutions: samples and solutions the same as in Figure 6.17. 153
Figure 6.19: First 4 hrs. of Figure 6.17. Contrary to the immersion in the water-based solutions, all the samples increased the weight in the beginning. This trend was reversed after a few hours. 154
Figure 6.20: Strength (penetrometer index) as a function of immersion time. After 5 days immersed in different OBM, the samples were immersed in de-ionized water. 155
Figure 6.21: TGA (10°C/min.) of shale D - Native state - Immersion in $CaCl_2$. 158
Figure 6.22: TGA (10°C/min.) of shale D after 24 hrs. immersed in $CaCl_2$ 35% w/w (A_w = 0.50) 159
Figure 6.23: TGA (10°C/min.) of shale D after 48 hrs. immersed in $CaCl_2$ 35% w/w (A_w = 0.50) 159
Figure 6.24: TGA (10°C/min.) of shale D after 72 hrs. immersed in $CaCl_2$ 35% w/w (A_w = 0.50) 160
Figure 6.25: TGA (10°C/min.) of shale D after 96 hrs. immersed in $CaCl_2$ 35% w/w (A_w = 0.50) 160
Figure 6.26: TGA (10°C/min.) of shale D after 120 hrs. immersed in $CaCl_2$ 35% w/w (A_w = 0.50). 161
Figure 6.27: TGA (10°C/min.) of shale D after 144 hrs. immersed in $CaCl_2$ 35% w/w (A_w = 0.50). 161
Figure 6.28: TGA (10°C/min.) of shale D after 144 hrs. immersed in $CaCl_2$ 35% w/w (A_w = 0.50), then immersed in de-ionized water for 24 hrs. 162
Figure 6.29: TGA (10°C/min.) of shale D after 144 hrs. immersed in $CaCl_2$ 35% w/w (A_w = 0.50), then immersed in de-ionized water for 48 hrs. 162
Figure 6.30: TGA (10°C/min.) of shale D after 144 hrs. immersed in $CaCl_2$ 35% w/w (A_w = 0.50), then immersed in de-ionized water for 72 hrs. 163
Figure 6.31: TGA (10°C/min.) of shale D - Native state - Immersion in NaCl. 164
Figure 6.32: TGA (10°C/min.) of shale D after 24 hrs. immersed in NaCl 24% w/w (A_w = 0.78) 164
Figure 6.33: TGA (10°C/min.) of shale D after 48 hrs. immersed in NaCl 24% w/w (A_w = 0.78) 165
Figure 6.34: TGA (10°C/min.) of shale D after 72 hrs. immersed in NaCl 24% w/w (A_w = 0.78) 165
Figure 6.35: TGA (10°C/min.) of shale D after 96 hrs. immersed in NaCl 24 % w/w (A_w = 0.78) 166
Figure 6.36: TGA (10°C/min.) of shale D after 96 hrs. immersed in NaCl 24% w/w (A_w = 0.78), then in de-ionized water for 24 hrs. 166

Figure 6.37: TGA (10°C/min.) of shale D after 96 hrs. immersed in NaCl 24% w/w (A_w = 0.78), then in de-ionized water for 48 hrs. 167
Figure 6.38: TGA (10°C/min.) of shale D - Native state - Immersion in KCl. 168
Figure 6.39: TGA (10°C/min.) of shale D after 24 hrs. immersed in KCl 26% w/w (A_w = 0.85)..... 168
Figure 6.40: TGA (10°C/min.) of shale D after 48 hrs. immersed in KCl 26% w/w (A_w = 0.85)..... 169
Figure 6.41: TGA (10°C/min.) of shale D after 72 hrs. immersed in KCl 26% w/w (A_w = 0.85)..... 169
Figure 6.42: TGA (10°C/min.) of shale D after 96 hrs. immersed in KCl 26% w/w (A_w = 0.85)..... 170
Figure 6.43: TGA (10°C/min.) of shale D after 96 hrs. immersed in KCl 26% w/w (A_w = 0.85), then in de-ionized water for 24 hrs. 170
Figure 6.44: TGA (10°C/min.) of shale D after 96 hrs. immersed in KCl 26% w/w (A_w = 0.85), then in de-ionized water for 48 hrs. 171
Figure 6.45: TGA (10°C/min.) of shale D - Native state - Immersion in de-ionized water..... 172
Figure 6.46: TGA (10°C/min.) of shale D after 24 hrs. immersed in de-ionized water. 172
Figure 6.47: TGA (10°C/min.) of shale D after 48 hrs. immersed in de-ionized water. 173
Figure 6.48: TGA (10°C/min.) of shale D after 72 hrs. immersed in de-ionized water. 173
Figure 6.49: TGA (10°C/min.) of shale D - Native state - Immersion in alcohol..... 175
Figure 6.50: TGA (10°C/min.) of shale D after 24 hrs. immersed in alcohol. 175
Figure 6.51: TGA (10°C/min.) of shale D after 48 hrs. immersed in alcohol. 176
Figure 6.52: TGA (10°C/min.) of shale D after 72 hrs. immersed in alcohol. 176
Figure 6.53: TGA (10°C/min.) of shale D after 96 hrs. immersed in alcohol. 177
Figure 6.54: TGA (10°C/min.) of shale D after 120 hrs. immersed in alcohol. 177
Figure 6.55: TGA (10°C/min.) of shale D after 120 hrs. immersed in alcohol, then in de-ionized water..... 178
Figure 6.56: TGA (10°C/min.) of shale D - Native state - Immersion in OBM with $CaCl_2$ (A_w = 0.39) as water phase. 181
Figure 6.57: TGA (10°C/min.) of shale D after 24 hrs. immersed in OBM with $CaCl_2$ (A_w = 0.39) as water phase. 181
Figure 6.58: TGA (10°C/min.) of shale D after 48 hrs. immersed in OBM with $CaCl_2$ (A_w = 0.39) as water phase. 182
Figure 6.59: TGA (10°C/min.) of shale D after 72 hrs. immersed in OBM with $CaCl_2$ (A_w = 0.39) as water phase. 182
Figure 6.60: TGA (10°C/min.) of shale D after 96 hrs. immersed in OBM with $CaCl_2$ (A_w = 0.39) as water phase. 183
Figure 6.61: TGA (10°C/min.) of shale D after 96 hrs. immersed in OBM with $CaCl_2$ (A_w = 0.39) as water phase, then in de-ionized water for 24 hrs..... 183

Figure 6.62: TGA (10°C/min.) of shale D after 96 hrs. immersed in OBM with $CaCl_2$ (A_w = 0.39) as water phase, then in de-ionized water for 48 hrs. 184
Figure 6.63: TGA (10°C/min.) of shale D after 96 hrs. immersed in OBM with $CaCl_2$ (A_w = 0.39) as water phase, then in de-ionized water for 72 hrs. 184
Figure 6.64: TGA (10°C/min.) of shale D - Native state - Immersion in OBM with KCl (A_w = 0.84) as water phase. 185
Figure 6.65: TGA (10°C/min.) of shale D after 24 hrs. immersed in OBM with KCl (A_w = 0.84) as water phase. 186
Figure 6.66: TGA (10°C/min.) of shale D after 48 hrs. immersed in OBM with KCl (A_w = 0.84) as water phase. 186
Figure 6.67: TGA (10°C/min.) of shale D after 72 hrs. immersed in OBM with KCl (A_w = 0.84) as water phase. 187
Figure 6.68: TGA (10°C/min.) of shale D after 96 hrs. immersed in OBM with KCl (A_w = 0.84) as water phase. 187
Figure 6.69: TGA (10°C/min.) of shale D after 120 hrs. immersed in OBM with KCl (A_w = 0.84) as water phase. 188
Figure 6.70: TGA (10°C/min.) of shale D after 120 hrs. immersed in OBM with KCl (A_w = 0.84) as water phase, then in de-ionized water for 24 hrs. 188
Figure 6.71: TGA (10°C/min.) of shale D after 120 hrs. immersed in OBM with KCl (A_w = 0.84) as water phase, then in de-ionized water for 48 hrs. 189
Figure 6.72: TGA (10°C/min.) of shale D - Native state - Immersion in OBM with NaCl (A_w = 0.75) as water phase. 190
Figure 6.73: TGA (10°C/min.) of shale D after 24 hrs. immersed in OBM with NaCl (A_w = 0.75) as water phase. 190
Figure 6.74: TGA (10°C/min.) of shale D after 48 hrs. immersed in OBM with NaCl (A_w = 0.75) as water phase. 191
Figure 6.75: TGA (10°C/min.) of shale D after 72 hrs. immersed in OBM with NaCl (A_w = 0.75) as water phase. 191
Figure 6.76: TGA (10°C/min.) of shale D after 96 hrs. immersed in OBM with NaCl (A_w = 0.75) as water phase. 192
Figure 6.77: TGA (10°C/min.) of shale D after 120 hrs. immersed in OBM with NaCl (A_w = 0.75) as water phase. 192
Figure 6.78: TGA (10°C/min.) of shale D after 120 hrs. immersed in OBM with NaCl (A_w = 0.75) as water phase, then in de-ionized water for 24 hrs. 193
Figure 6.79: TGA (10°C/min.) of shale D after 120 hrs. immersed in OBM with NaCl (A_w = 0.75) as water phase, then in de-ionized water for 48 hrs. 193
Figure 6.80: TGA (10°C/min.) of shale D - Native state - Immersion in OBM with fresh water (A_w = 0.99) as water phase 194
Figure 6.81: TGA (10°C/min.) of shale D after 24 hrs. immersed in OBM with fresh water (A_w = 0.99) as water phase 195

Figure 6.82: TGA (10°C/min.) of shale D after 48 hrs. immersed in OBM with fresh water (A_w = 0.99) as water phase. 195
Figure 6.83: TGA (10°C/min.) of shale D after 72 hrs. immersed in OBM with fresh water (A_w = 0.99) as water phase. 196
Figure 6.84: TGA (10°C/min.) of shale D after 96 hrs. immersed in OBM with fresh water (A_w = 0.99) as water phase. 196
Figure 6.85: TGA (10°C/min.) of shale D after 120 hrs. immersed in OBM with fresh water (A_w = 0.99) as water phase. 197
Figure 6.86: TGA (10°C/min.) of shale D after 120 hrs. immersed in OBM with fresh water (A_w = 0.99) as water phase, then in de-ionized water for 24 hrs. 197
Figure 6.87: TGA (10°C/min.) of shale D after 120 hrs. immersed in OBM with fresh water (A_w = 0.99) as water phase, then in de-ionized water for 48 hrs. 198
Figure 6.88: TGA (10°C/min.) of shale D after 120 hrs. immersed in OBM with fresh water (A_w = 0.99) as water phase, then in de-ionized water for 72 hrs. 198
Figure 6.89: Idealized structure for a granular material: pores and matrix. Shale structure cannot be represented by means of this simplified view. 204
Figure 6.90: More realistic structure representing a shale. When exposed to a water solution, interaction among all the components leads to a different structure when the final equilibrium is reached. 204
Figure 7.1: A composite representation of the complete stress-strain curve and the incremental radial stress-axial strain curve for a suite of triaxial compression tests done in a stiff-testing machine and in a stiff, sealed triaxial cell, using specimens of argillaceous quartzite prepared from a single piece of rock. The axial sections through specimens stopped at various stages of compression show the structural changes associated with the complete stress-strain curve and associated dilatancy (Jaeger & Cook, 1979). 217
Figure 7.2: The stress-strain characteristics and the envelope of micro-seismic activity for Tennessee marble loaded to fracture in compression (Cook, 1965). 219
Figure 7.3: The stress-strain characteristics and the envelope of micro-seismic activity for St. Cloud granite loaded to fracture in compression (Cook, 1965). 220
Figure 7.4: Peak stress vs. RPM. Resonances are indicated by high stresses, above the critical stress (Mitchell & Allen, 1987). 223
Figure 7.5: Displacement vs. rotary speed due to mass imbalance on the drill string. Both models predicted accurately the range of RPM in which resonance occurs. The magnitude of displacements is accurately predicted by the rig effect model (Dykstra *et al.*, 1995). 224
Figure 7.6: Hysteresis loop due to loading-unloading of an inelastic material. The area inside the loop gives the amount of internal energy stored in the material for this cycle (Langhaar, 1962). 230

Figure 7.7: Complete stress-strain curves for a specimen of norite loaded and unloaded through several cycles at a confining stress of 3,000 psi (Jaeger & Cook, 1979). 231
Figure 7.8: Effect of pipe rotation. Gullfaks B-32. 12 1/4" section. Water-based KCl/Polymer mud. PWD sensor 14 m behind the bit (Ward & Andreassen, 1997)..... 234
Figure 7.9: Swab/surge pressures. Statfjord C-22. 8 1/2" section. Synthetic Oil-based mud. PWD sensor 34.5 m behind the bit. (Ward & Andreassen, 1997)..... 234
Figure 7.10: Breaking gels. Gullfaks B-32. 9.4" section. Normal Oil-based mud. PWD sensor 27 m behind the bit (Ward & Andreassen, 1997)..... 235
Figure 7.11: Leak-off test/Formation integrity test (FIT). Gullfaks B-32. 12 1/4" section. KCl/Polymer mud. PWD sensor 14 m behind the bit. (Ward & Andreassen, 1997). 235
Figure 7.12: Cuttings load. Statfjord A15 A. 12 1/4" section. Synthetic Oil-based mud. PWD sensor 27 m behind the bit. (Ward & Andreassen, 1997)..... 236
Figure 7.13: Reaming down. Statfjord C-22. 8 1/2" section. Synthetic Oil-based mud. PWD sensor 34.5 m behind the bit. (Ward & Andreassen, 1997)..... 236
Figure 7.14: Lost circulation. Statfjord A-6 A. 8 1/2" section. Synthetic Oil-based mud. PWD sensor 8 m behind the bit. (Ward & Andreassen, 1997)..... 237
Figure 7.15: One driller still reaming fast. Statfjord A-35 A. 8 1/2" section. Synthetic Oil-based mud. PWD sensor 28.5 m behind the bit. (Ward & Andreassen, 1997). 237
Figure 7.16: Fatigue test on a medium-grained granite from the Socorro Granitic Complex, Sao Paulo, Brazil (Celestino *et al.*, 1995). 239
Figure 7.17: Typical profile for the circulating mud for different drilling phases (Maury & Guenot, 1995). 242
Figure 7.18: Mud and borehole wall temperature evolution when deepening (Maury & Guenot, 1995). 243
Figure 7.19: Effect of pipe rotation on downhole and outlet (measured on the surface) temperature (Guenot & Santarelli, 1989)..... 244
Figure 7.20: Stress-strain curves for granite at a confining pressure of 5 kilobars and various temperatures (Jaeger & Cook, 1979). 246
Figure 7.21: Complete axial stress-strain and radial strain-axial strain curves at different confining pressures for a suite of specimens prepared from a single piece of argillaceous quartzite. Uniaxial compression: curve 1. Triaxial compression: curves; (2) $\sigma_2 = \sigma_3 = 3.45$ MPa; (3) $\sigma_2 = \sigma_3 = 6.9$ MPa; (4) $\sigma_2 = \sigma_3 = 13.8$ MPa; (5) $\sigma_2 = \sigma_3 = 27.6$ MPa, cracked specimen; (6) $\sigma_2 = \sigma_3 = 27.6$ MPa (Jaeger & Cook, 1979)..... 249
Figure 7.22: DSC result of shale D, before and after 24 hrs. immersed in NaCl 24% w/w..... 255

Figure 7.23: Extensional fissures around a borehole due to insufficient mud pressure (Dusseault & Gray, 1992). 260
Figure 7.24: Pressure penetration into fractures blocked by gilsonite. Mud pressure greater than pore pressure guarantees wellbore stability (Dusseault & Gray, 1992). 261
Figure 7.25: Schematic of a wellbore with a drillstring and the REV at the wellbore wall (not in scale). 263
Figure 7.26: Schematic of multiple, randomly distributed cracks around the wellbore due to the excess energy stored in the rock (not in scale). 265
Figure A.1: Diagrammatic sketch showing (a) single silica tetrahedron and (b) the sheet structure of silica tetrahedrons arranged in an hexagonal network 289
Figure A.2: Tetrahedral and octahedral configurations in kaolin minerals. Broken lines represent the unit-cell boundary (Brindley, 1961)... 290
Figure A.3: Diagrammatic sketch showing (a) single octahedral unit and (b) the sheet structure of the octahedral unit 291
Figure A.4: Coordination in the octahedral sheet. (a) The six dimples in the plane of oxygen and hydroxyl ions make two sets of sites e.g., 1,3,5 (octahedral) and 2,4,6 (tetrahedral). (b) An octahedral site formed by cation in dimple 3 surrounded by six oxygens or hydroxyls, three above and three below 293
Figure A.5: Joining an octahedral sheet and a tetrahedral sheet into 1:1 layer silicate (general case) 294
Figure A.6: Thinning of trioctahedral sheet 295
Figure A.7: Dioctahedral sheet showing ion shifts that occur to minimize cation-cation repulsion. Dark circles are anions in the basal octahedral layer, while light circles are anions in the upper octahedral layer. The ones with bars are hydroxyls. Small circles are aluminum cations and v marks a vacant octahedral site. B) Shielding movement of anions causes rotation of upper and lower layers in opposite directions around triad axis. C) Anion shielding shortens shared edges (after Bailey, 1966) 296
Figure A.8: Diagrammatic projections of the structure of clay minerals. (a) Kaolinite; (b) montmorillonite; (c) mica; (d) chlorite; (e) sepiolite (Mackenzie and Mitchell, 1966) 299
Figure A.9: Kaolinite layer structure (after Gruner, 1932) 304
Figure A.10: Diagrammatic representation of the structure of kaolinite and halloysite $4H_2O$. (a) Arrangement of layers in kaolinite; (b) arrangement of layers in halloysite according to Hendricks (1938); (c) proposed arrangement of halloysite layers by Bates et al. (1950) 306
Figure A.11: Montmorillonite layer structure (after, Hendricks, 1942) 308
Figure A.12: Picture of an ultra-thin section of a smectite clay (Wyoming bentonite) showing stacks of smectite layers bifurcating, curling, and folding (Push and Guven, 1990) 310

Figure A.13: Sketch of Figure A.12 displaying interparticle and interaggregate pores in smectites (Push and Guven, 1990)..... 310
Figure A.14: Illite layer structure (after Jackson and West, 1930).....312
Figure A.15: Chlorite layer structure (after McMurchy, 1934).....314
Figure B.1: van der Waals forces, and oscillatory and monotonic structural forces decaying with distance of separation D of clay surfaces per liquid molecular diameter σ (Israelachvili, 1991)..... 320
Figure B.2: Hypothetical arrangement of oxygens and hydrogens in layer of water molecules between clay mineral sheets. One hydrogen atom in each of the molecules K, M, and O is not involved in bonding within the net, but serves to join the net to oxygens of the neighboring silicate layer (after Hendricks and Jefferson, 1938)..... 321
Figure B.3: Combination of water and vermiculite layers by binding through hydrogen. The oxygen atoms represented by large dotted circles are 2.73 Å below the plane of the water molecules (Hendricks and Jefferson, 1938)..... 322
Figure B.4: Probable structure of multiple water layers on the surfaces of clays. Small black or shaded circles represent silicon atoms Hendricks and Jefferson, 1938)..... 324
Figure B.5: Combined water layers in partially dehydrated vermiculite (Hendricks and Jefferson, 1938)..... 324
Figure B.6: Configuration of structured water bound to silicate sheets by hydrogen bondings (after Hendricks and Jefferson, 1938)..... 325
Figure B.7: Probable type of binding between hydroxyl groups in the kaolinite layers. Double circles represent aluminum atoms located about 1.1 Å above the plane of hydroxyl groups (Hendricks and Jefferson, 1938)..... 326
Figure B.8: Arrangement of a single layer of water molecules in hydrated halloysite (Hendricks and Jefferson, 1938)..... 327
Figure B.9: Arrangement of the water molecules in the interlayer space of montmorillonite and vermiculite (after Barshad, 1949)..... 329
Figure B.10: Forces per unit area between platelets of Ca^{2+}-montmorillonite in pure water in the absence of hydration forces (Kjellander et al., 1988). Net forces of van der Waals and electrostatic interactions including (solid line) or excluding (dotted line) ion-ion correlation effects..... 341
Figure B.11: Logarithm of the total pressure between clay platelets of Wyoming bentonite in 10^{-4} mole/liter salt solutions of various cations as a function of interlayer distance h: □-□ Li^+, Δ-Δ Na^+, •-• K^+, °-° Cs^+ (Lubetkin et al., 1984)..... 343
Figure B.12: Schematic drawing showing position of organic cation between montmorillonite layers (Hendricks, 1941)..... 348
Figure B.13: Effect of amine chain length on montmorillonite basal spacing. The total internal surface area per cation-exchange position calculated as 165 $Å^2$ (Jordan, 1949a)..... 349

Figure B.14: Increasing basal plane spacing on intercalation of n-alkylammonium ions with increasingly long alkyl chains; charge per half unit cell, x=0.67, (Weisss, 1963)..... 350
Figure B.15: Arrangements of alkylammonium mica-type layer silicates with different layer (Weiss, 1963). (a) Very low charge; (b) medium charge; (c) preferred arrangement with the formation of three hydrogen bonds per RNH_3^+ ion and with trans, trans-configuration; (d) as (c) but with cis, trans-configuration; (e) high charge. Hatched areas: silicate layers..... 351
Figure B.16: Relationship between the length of the alkyl chain, the layer charge x, and the swelling power of n-alkylammonium montmorillonites in water (Weiss, 1963): curve I: x=0.55; curve II: x=0.66; curve III: x=0.42; curve IV: x=0.33..... 353
Figure C.1: Diagram of the shale coring box..... 359
Figure C.2: Assembly diagram of shale coring set up..... 360
Figure C.3: Coring box, pumping system and coring machine..... 361
Figure C.4: Coring machine..... 363

Chapter 1

1. Introduction

1.1 General Overview

In any drilling project mud selection plays important technical and economical roles. Problems caused by improper selection of either the weight or composition of the drilling fluid can include: wall instability, stuck pipe, increased torque and drag, difficulties in casing and logging, and formation damage. In the worst situation, part of the well or even the entire well can be lost.

Several additives, such as viscosifiers, lubricants, fluid loss controllers, shale inhibitors, pH regulators, and others have been specifically developed to solve each problem. The drilling fluid cost is directly proportional to the amounts and types of additives added to the mud. Of the two mud types, oil-based muds (OBM) are more expensive than water-based muds (WBM). Regular OBM can reach up to US$ 150.00/bbl, while a cheap WBM can cost

as little as US$ 20.00/bbl. Synthetic oil muds are the most expensive muds. They can cost as much as US$ 300.00/bbl. The total well cost is also directly proportional to the time "lost" trying to solve the various problems previously described.

Even though significant research has been conducted to improve drilling fluid performance, persistent field problems have led to the obvious conclusion that more research must be done. Despite the fact that shale represents most of the drilled "length" and causes the majority of the problems, it has not received the research attention it deserves.

This dissertation focuses on wellbore stability problems during the drilling phase. Wellbore stability problems also occur during the production phase, when operators experience sand production; however, this issue is not addressed in this work. Wellbore stability-related problems cost the oil industry between 500 million to 1 billion dollars each year. Reducing instability problems is crucial to profitably recover hydrocarbon reserves in several parts of the world.

Wellbore instability occurs in all kinds of rocks, but shale is the rock type that causes the most problems. Shales are known to be very reactive rocks and interaction with the drilling fluid has been assumed to be the main factor in wellbore instability. However, as will be shown in this dissertation, this assumption may not be true for "downhole" conditions.

Traditionally, wellbore stability problems have been studied from a mechanical standpoint by comparing the stresses acting on the rock with the

rock strength. Two types of failure are recognized: tensile and shear. In the first case, when the tangential stress exceeds the tensile strength of the rock, fractures open and fluid is lost to the formation. In the second situation, a damaged zone is created around the wellbore, for both low and high values of mud weight.

When drilling shales the interaction between the rock and the drilling fluid is another effect that plays an important role. Shales are complex rocks. Electrical charges and surface forces affect their behavior when in contact with water solutions. In the past, OBM was successfully used to reduce instability problems in shale sections. However, due to environmental concerns, the use of OBM today is restricted. Increased use of WBMs while drilling in more hostile and geologically challenging environments has led to a surge in stability problems. Research toward better understanding of the shale-fluid interaction mechanisms was initiated in the beginning of the 90s.

Most of the shale-fluid interaction concepts and ideas were derived from laboratory tests conducted in the past 40 years. Only recently did the oil industry realize the importance of moisture content on shale reactivity when the rock is exposed to a water solution. As cores are rare, outcrop formations are sometimes used as reference shales. Even when available, shale cores have not been appropriately preserved and are usually partially-dried by the time reactivity tests are conducted. Most conclusions derived from dried sample conditions are not applicable to well conditions at depth and all test results obtained from outcrop samples and partially-dried downhole cores should be

questioned. Attempts to resaturate the sample are likely to cause changes in the rock behavior and display different structure and character from the actual downhole shale.

The traditional idea that the reaction of shale with the drilling fluid reduced the strength of the shale fits well with field observations. Failure usually starts after the open hole has been exposed to the drilling fluid for some time, known as time-delayed failure. Nevertheless, downhole shale swelling has been recently questioned. Swelling might be caused by laboratory procedures that allow sample exposure to air.

1.2 Objectives of the Study

This study was designed to eliminate the controversies of shale-fluid interaction mechanisms. With correct understanding of the interaction mechanisms, appropriate drilling operations and fluid solutions can be adopted to decrease wellbore stability problems. Two main objectives were then defined. First, develop a comprehensive understanding of actual "downhole" shale-fluid interaction mechanisms. Second, develop a new approach to analyze wellbore stability with most relevant drilling phenomena taken into account.

To accomplish the first objective a broad laboratory investigation considering both micro- and macro-scales was carried out. An essential condition for this phase was the availability of well-preserved "downhole"

shale samples. Petrobras provided cores from four wells from three different fields located in the Campos Basin, offshore Brazil. The cores were taken during a four-year shale stability project (Santos *et al.*, 1997). As soon as they arrived at the rig floor, the cores were cleaned to remove the mud and they were immediately immersed in mineral oil to preserve their moisture content.

Since well-preserved shale samples were available, a detailed laboratory investigation was conducted to check controversial concepts about shale-fluid interaction such as: shale swelling, effectiveness of osmotic pressure in shale-mud systems, presence of a semi-permeable membrane, and water flow in shales. From the results obtained in the laboratory, new ideas of how shales interact with both OBM and WBM were developed and are presented here.

With a deeper understanding of subsurface shale-fluid interactions, the second objective of analyzing wellbore stability could be accomplished by taking an energy balance approach. All major well drilling events and effects could be included in a simple way. This new approach can explain almost all field problems and help identify actual problem causes. As a result, procedures to solve shale stability problems can be more effectively implemented.

1.3 Dissertation Overview

A critical literature survey is presented in Chapter 2 to describe the current approaches to analyze wellbore stability. The most important concepts

developed and currently used to define the best drilling fluid composition are also reviewed. Some contradictions in the literature are emphasized.

Chapter 3 describes the laboratory study to check the influence of water content, amount, distribution, and water types, on shale reactivity. Even though it was known that any change in water content affects shale behavior, quantification had not previously been attempted. A new method using thermogravimetry (TGA) was developed to determine the water content and provided the opportunity to quantify water loss severity due to dehydration.

For a complete understanding of shale-fluid interaction, a more detailed characterization methodology was necessary. The most popular method used by the industry, X-Ray diffraction (XRD), has limitations with shale samples. The proposed methodology uses TGA and is presented in Chapter 4. It has several advantages when compared to XRD. The composition of the rock can easily be identified and structural changes of the rock can be observed.

Incorporating confining pressure in the immersion test was necessary to more closely reproduce downhole conditions. To overcome limitations of the current swelling pressure test, a new test, the *shale-reactivity test*, was designed and is described in Chapter 5. The test procedures, sample preparation, and interpretation of the results are completely new. It is shown that the shale-reactivity test gives more detailed information about the interaction of the shale with a fluid and avoids misinterpretations found in swelling pressure test results.

Chapter 6 presents the results of specially designed tests conducted to check some of the controversial concepts previously mentioned. Test results show that these concepts are not applicable to downhole conditions, and led to a new understanding of shale-fluid interactions.

These new concepts allowed a broader understanding of those interactions and led to development of a new analysis technique, based on energy, to evaluate wellbore stability. This is described in Chapter 7. This energy balance concept was used to develop a new comprehensive conceptual model to analyze wellbore stability. In this model, dominant important energy phenomena in the wellbore of temperature differences between the drilling fluid and rock formation, vibration of the drill string, chemical interactions, and wellbore wall deformation, were considered. Other phenomena can also be incorporated, if they can be described as energy.

Chapter 8 summarizes the results obtained, the new interaction mechanisms observed, and presents the conclusions of this study. Recommendations for future tests to expand and generalize the knowledge obtained are also proposed.

Three Appendices have been included to help the reader understand some crucial issues in shale stability. The first Appendix describes the structure of clay minerals present in significant amounts in shaly formations. The second Appendix presents some relevant features of clay interaction, including intermolecular forces. The third Appendix describes the equipment developed to prepare plugs for shale-reactivity tests without allowing sample

dehydration. The equipment and the procedure to prepare the specimens are both described in detail.

Chapter 2

2. Critical Literature Review

2.1 Introduction

This chapter presents a review of the most important concepts used by the oil industry in the wellbore stability area. The review is divided in two areas: one focused on shale-fluid interaction mechanisms, thought to be responsible for most problems encountered in the field, and the other focused on the methodology to analyze wellbore stability. Initially, how the industry selects a particular drilling fluid is reviewed, and the limitations of the procedures are discussed. Then, several concepts regarding shale-fluid interaction are presented. The latter involves the methodology and models used today to analyze and evaluate wellbore stability, and also emphasizes the limitations of the current approach.

Shale sections often present a caliper much larger than the bit size, creating problems in running and interpreting logs, running the casing, and,

finally, in cementing and providing a good zonal isolation. The interaction with the drilling mud, especially WBM, is assumed to be the most important cause of the problems when drilling through shales. Other factors are also relevant, such as abnormal pore-pressure, for example.

2.2 Mud Selection Criteria

Problems when drilling through shales are usually attributed to inadequate weight and/or composition of the drilling fluid. These are most often selected based on experience (trial-and-error) and on screen tests with available samples.

If the well is located in the same field where a successful mud has been used before, the same fluid is repeated. Sometimes, its composition is adjusted to minimize problems faced during drilling the previous wells. If severe problems are experienced, a radical change may occur, switching to OBM, for example. Even though OBM preserves hole integrity more efficiently than WBM, its use in exploratory wells is not recommended due to limitation in logging and in evaluating the reservoir. Such an approach very seldom leads to the optimum solution.

When shale samples are available, either from outcrop or downhole cores, screening tests (Darley & Gray, 1991) are conducted to evaluate different mud

compositions. Among these tests, the *hot rolling test*[1] is one of the most common. In some cases, only visual inspection of the shale samples after being immersed in the fluids provides the final evaluation and decision of the best composition. Since downhole samples are usually not available, tests are often conducted with a reference shale (outcrop formation, Gazaniol *et al.*, 1995), preferably a highly reactive one. Even though it is a cheap alternative, the use of outcrop shales to simulate downhole interaction can lead to wrong interpretation and understanding. Pore water content and composition, as well as the stresses on the surface are totally different from what is encountered downhole. In addition, the field to be drilled might have completely different shaly formations than the outcrop used for the laboratory tests. Cuttings also have been suggested to be used (Osisanya & Chenevert, 1987; Zausa *et al.*, 1997), with the advantage that immediate response, at the rig site, can be obtained. However, due to their small size it is very difficult to remove all drilling fluid contamination. Use of cuttings to evaluate reactivity of downhole shales is, therefore, highly subjected to disturbances.

Dried cores, not necessarily from the same field where the well will be drilled, are also often used. The results in these cases can lead to a complete misunderstanding of the actual downhole interaction mechanisms (Schmitt *et al.*, 1994). The worst situation occurs when reconstituted shale samples are

[1] The test consists of immersing a shale sample in a drilling fluid and rolling it inside an oven at a given temperature for a certain period of time (usually more than 8 hrs.) and at the end compare the initial and final sample weight. The smaller the reduction in weight the more compatible the fluid.

used (Darley & Gray, 1991). In these cases, shale samples are powdered, dried, and then reconstituted under pressure. Water is added to restore the original moisture content. Even aware of the importance of original moisture content preservation (Hale *et al.*, 1993; Forsans & Schmitt, 1994; Schmitt *et al.*, 1994), and the consequences that any change will cause to the rock, mud companies are still using these tests to evaluate some of their products. Recommendations based on the interactions observed between the mud and the reconstituted rock often lead to a more expensive fluid than actually needed. In some situations, OBM is suggested because it is the only drilling fluid capable of controlling the shale swelling. However, the swelling in these cases is artificially caused by dehydration and alteration of the rock and does not, necessarily, represent downhole behavior.

2.3 Shale-Fluid Interaction

The most accepted fact regarding shales is that these rocks present a potentially strong reaction (swelling) when in contact with a water solution. Most of the stability problems faced by the industry are attributed to the reaction of shale and WBM. Laboratory studies have been conducted for decades and several ideas and theories have been developed, in an attempt to reduce the swelling.

Even though shale swelling has been known for a long time, only relatively recently did the oil industry realize the difference in shale reactivity due to

water content variation, and started to preserve shale samples from dehydration (Santarelli *et al.*, 1992; Chenevert & Osisanya, 1990 & 1992; Bol *et al.*, 1994; Hale & Mody, 1992). Observing that moisture content variation alters shale reactivity, swelling of downhole shales has been questioned (Santarelli & Carminati, 1995). Studies have suggested that sample dehydration in the laboratory introduces artifacts (capillary effects) that cause the swelling (Forsans & Schmitt, 1994; Schmitt *et al.*, 1994; Onaisi *et al.*, 1994). Time consuming resaturation procedures have been suggested (Forsans & Schmitt, 1994) to eliminate the presence of air inside the samples, avoiding the bias introduced by the capillary effects in laboratory results.

2.3.1 Swelling Clay Minerals

Shales have very low permeability, with a significant amount of clay minerals and other accessory minerals, such as quartz, feldspars, and calcite. One clay mineral, smectite, when dried, shows a strong swelling when subsequently in contact with water (Darley & Gray, 1991; see Appendix A for more detailed clay mineralogy). It is believed that the higher the amount of smectite in a shale, the higher the potential of that shale to swell if a water-based solution gets in contact with the rock. In some situations, operators rely only on the amount of smectite in a shale to define the drilling fluid to be used. Wellbore stability problems are often associated with shales with high smectite content.

In order to quantify the amount of minerals present in a rock, the X-Ray diffraction (XRD) method is normally used. After conflicting results were

found from two laboratories, a blind test was decided to be conducted among three different companies. The results of these tests, shown in Chapter 4, reveal completely different values not only of the total clay content, but also the smectite content. It is clear that direct correlation between smectite content and instability problems in the field lacks support from these inconsistent results. The need of accurate rock characterization and the problems with the XRD method led to the development of a new methodology to characterize such rocks. This methodology, using thermal analysis, is presented in Chapter 4.

2.3.2 Shale Swelling Mechanisms

Even though all clay minerals absorb water, smectites concentrate almost all the attention due to the larger volumes of water they take up, compared to the other minerals. In order to explain clay swelling, theories have been developed based upon the behavior of a system of individual clay particles immersed in a given water solution, and the response of such a system has been extrapolated to actual, downhole shales. There are two basic clay particle swelling mechanisms: crystalline (or surface hydration) and osmotic (Darley & Gray, 1991). Adsorption of mono-molecular layers of water on the basal crystal surfaces (external or inter-layer) is called *crystalline swelling*. The bonds of this absorbed water, also called interlayer, bound or structural water, decrease with the distance from the clay particle surface. Due to its structured nature,

this water has quasi-crystalline properties, and its specific volume is less than that of free water (Darley & Gray, 1991).

Osmotic swelling derives from the high concentration of ions held by electrostatic forces in the vicinity of clay surfaces (Darley & Gray, 1991). Only certain clays of the smectite group, mainly sodium montmorillonite, develop interlayer osmotic swelling. Osmotic swelling causes a large increase in bulk volume, but swelling pressures are low. On the other hand, crystalline swelling, exhibited by all clays, develops high swelling pressures, but the increase in volume is relatively small. It should be emphasized that the intensity of clay swelling is proportional to the dryness state of the mineral. This is also applied to shales, which contains varying amounts and types of clay minerals. In Appendix B, some of the most important interaction forces, developed by clay in contact with some fluids are described.

The most problematic practice here is the extrapolation of the clay swelling mechanisms to downhole conditions. Since clay swelling is proportional to its dryness state, in shales this behavior should be similar. In addition, downhole shales are saturated and in equilibrium, and, therefore, its swelling should be carefully investigated. Chapter 3 presents several laboratory tests conducted in well-preserved and partially dried downhole shales with the aim of investigating their swelling characteristics. The experiments demonstrate the influence of water content and distribution on shale reactivity. Shale swelling was only observed when some of the original rock water was lost.

2.3.3 Capillary Effects

Allowing shales to dehydrate in air results in a non-saturated rock, with air and water in the pores. The relief of stress when the rock is cored and brought to surface most probably also introduces a second phase in the pores (vapor). When this now partially-saturated rock gets in contact with water, capillary pressure develops and water is sucked inside, eliminating the suction that increases the rock strength. Also, trapped air inside the pores generates tension, which might fissure the rock, expanding its total volume (Onaisi *et al.*, 1994). Swelling and breakage of shales have been explained through these capillary effects (Forsans & Schmitt, 1994; Schmitt *et al.*, 1994; Santarelli & Carminati, 1995; Onaisi *et al.*, 1994), and not through osmotic and swelling pressures. Capillary effects would explain, then, why a partially-dried shale swells in water, whereas a saturated sample remains intact. Rock breakage would then be the consequence of a mechanical effect, rather than a chemical one.

In order to eliminate the presence of air inside the samples, a careful resaturation procedure has been suggested (Schmitt *et al.*, 1994) avoiding disintegration of the rock, due to the reaction of the partially dried clay minerals in contact with water. Special laboratory tests were designed to check the assumption that the capillary effects were actually causing shale disintegration. With the basic understanding developed with simple tests (described in Chapter 3) it was possible to design more sophisticated tests

(described in Chapter 6) to reach a final conclusion, showing that the capillary effects are not solely responsible for the swelling and breakage of partially-dried shale samples.

2.3.4 Swelling Pressure

Water adsorption by clay minerals, mainly smectites, generates swelling pressures. However, these swelling pressures are generated when dry clay minerals are exposed to water. Since shales have clay minerals in their composition, an extrapolation of this concept to shales has been made. Equations to estimate the potential swelling pressure of shales have been suggested (Chenevert, 1969) as a function of the activity of the water in the shale:

$$p_s = -\frac{RT}{V}\ln\frac{p}{p_0} \qquad (2.1)$$

where p_s is the swelling pressure in atmospheres; T is the absolute temperature (°K); V is the partial molar volume of water (liters/mole); R is the universal gas constant (liter atmospheres/mole °K); and p/p_0 is the relative water vapor pressure at equilibrium with the shale which is approximately equal to the activity of the water in the shale.

In order to effectively measure the swelling pressure, laboratory tests were developed specifically for this purpose (Steiger, 1993; Mese, 1995). These tests were conducted under constant volume and reaction after the sample was

contacted by the test fluid changes the confining pressure. If the final pressure is greater than the original one, a swelling pressure is defined. Test preparation requires some time (usually more than 1 hour), from sample preparation to the final installation of all measuring devices, closure of the cell, and final test of instruments. Since shales are extremely sensitive to dehydration in air (tests described in chapter 3), by the time the sample is contacted by the test fluid, significant dehydration has already occurred. Knowing that swelling pressures develop in dry clay, it is expected that the dryness state of the shales are the cause for such swelling pressures. The results presented in the literature, showing that shales develop swelling pressure when in contact with a water solution, are thus highly questionable.

Two main limitations were found in the swelling pressure test: lack of sample preservation and not enough detailed data to interpret the results. A new approach, referred to as *shale-reactivity test*, provides a much more detailed interpretation of the results and a correct understanding of the interaction between the fluid and the rock. The necessity of a careful sample preparation to avoid any bias in the test results is also emphasized.

2.3.5 Shale Activity

The concept of activity has been used for a long time to define the salinity of drilling fluid (Chenevert, 1970a; O'Brien & Chenevert, 1973). The initial idea that a drilling fluid with the same salinity as the water in the shale would avoid swelling (Mondshine & Kercheville, 1966) was further evolved to equal

activity, rather than salinity (Chenevert, 1970b). In order to implement this concept, the activity of the shale needs to be somehow estimated and the drilling fluid is then prepared to match the rock's activity.

The two most common procedures to measure the activity of a solution are a hygrometer, or the isopiestic method (Carminati *et al.*, 1997). The first method consists of measuring, with a probe, the relative humidity (R.H.) of a closed vessel with the test solution inside it. The activity of the solution is given by the following relation:

$$a_w = \text{R.H.}/100 \qquad (2.2)$$

The latter method is more laborious. It requires a few high pressure closed desiccators, partially filled with solutions of known activity. In each of them, above the level of the solution, an open container with a known weight of the tested solution is left to equilibrate. The activity of the test solution is the one of the solution of known activity contained in the desiccator in which a zero weight change of the test solution was measured.

Measurement of shale activity has been extrapolated directly from these methods. It is thought that the activity of the water inside the shale can be measured using the same approach. This dissertation shows, in the next chapters, that shales have a highly complex water distribution. It is highly improbable, then, that the water inside the shale has just one activity. Ions are not equally distributed due to the high concentration of charges on the clay

mineral surfaces (see Appendices A and B for more details). Another major concern is the fact that both methods introduce air in the rock, dehydrating it. Therefore, since water has been lost to the atmosphere, it is not reasonable to assume anymore that the measurement is accurate and representative of the downhole state.

Even though shale's activity has been reported to reach values well below 1.0, the activity of de-ionized water (Chenevert & Osisanya, 1990), Carminati *et al.* (1997) present a detailed investigation of this issue showing that low rock activity values are a consequence of the partially dried state of the sample. Usually shale salinity (Chilingarian *et al.*, 1995) would produce a rock activity of 0.97[2] (assuming a saturated shale), considering the only salt is sodium chloride (Carminati *et al.*, 1997). Here, again, the influence of shale dehydration on concepts derived from laboratory measurements is clear.

The activity (of a certain solution) concept itself is very well established and proven. The major problem is to extend this concept to a rock with a highly complex structure. The assumption that the activity of the water inside the shale is what is being measured is not reasonable, since the ions distribution within the clay minerals is not uniform. In addition, if the shale dehydrates, the salinity of the water in the rock will increase, leading to a low activity value. Low shale activities has been reported to be caused by

[2] Solution activity is a function of concentration of different salts dissolved. This number was estimated from the concentration found in shale pore fluid, assuming just one salt type, for the sake of simplicity.

laboratory artifacts (Carminati *et al.*, 1997), and does not reproduce the downhole state of the same rock.

Chapter 6 describes a series of tests conducted with varying activity solutions showing the different effects in the shale produced by different salt types. Activity value alone is not enough to estimate the behavior of the rock. It is absolutely necessary to know the rock changes due to the interaction with any solution, now possible using the characterization methodology described in Chapter 4.

2.3.6 Driving Forces and Flows

Difference in activity between the drilling fluid and the shale has been argued to produce a flow of water to or from the rock, due to the generation of an osmotic pressure (Bourgoyne Jr. *et al.*, 1991; van Oort *et al.*, 1996; Sherwood, 1993; Tan *et al.*, 1996; Chenevert & Osisanya, 1992):

$$\pi = \frac{RT}{V} \ln\left(\frac{A_{df}}{A_{sh}}\right) \tag{2.3}$$

where R is the universal gas constant, T is the absolute temperature, V is the partial molar volume of water, and A_{sh} and A_{df} the activities of the shale and the drilling fluid, respectively. According to this equation, if the activity of the mud is greater than the shale activity, an osmotic pressure will be generated driving the water inside the shale, and vice-versa.

Shales are believed to behave as a semi-permeable membrane, and when OBM is used, this semi-permeable membrane is assumed to be perfect; that is, only solvent can enter or leave the shale (Hale *et al.*, 1993). The above equation would be, then, totally applied to this situation, since the osmotic pressure is only generated in the presence of a semi-permeable membrane system. On the other hand, when WBM is used, a perfect membrane is not present (solvent and solute can flow through the membrane). This concept has been used extensively in the oil industry to define the salinity of the water phase in OBM, and the salinity of the WBM. The basic idea is to have a low activity drilling fluid (in the case of OBM it is considered the activity of the water phase) so that water would flow from the rock into the well. Shale dehydration would increase its strength (Hale *et al.*, 1993), and also decrease the near wellbore pore pressure, improving the wellbore stability (Tan *et al.*, 1996).

Balanced activity muds are believed not to produce any alteration (swelling or contraction) of the shale. However, all samples of the same shale (most probably having all the same activity) unexpectedly expanded in linear swelling tests (Osisanya & Chenevert, 1987) conducted with solutions with higher and lower activities, compared to the shale activity (Amanullah & Chenevert, 1996; Fisk, 1996). These conflicting results raised questions concerning the effectiveness of the chemical potential (difference in activity) as a driving force. A complete understanding of this mechanism, often used to design drilling fluids, was then needed. Specific tests were designed and conducted

with both WBM and OBM to analyze the effects of chemical potential on shales. The surprising results, presented in Chapter 6, led to a totally new insight into the shale-fluid interaction mechanisms, contradicting what is established today. Furthermore, the idea that by dehydrating the shale the rock strength is increased might have serious side effects. Not only is the rock reactivity changed but also micro-fractures might be induced. In all cases the problems can overcome the benefits.

Today, not only the chemical potential, but also other potentials are being considered in order to drive water out of shale (Yuan *et al.*, 1995; van Oort *et al.*, 1994). The hydraulic and thermal potentials are always present when drilling a well, due to the difference in pressure and temperature between the drilling fluid and the formation. The electric potential has been recently studied, in order to induce a flow of water if an electric current can be established between the rock formation and the well. The basic equations used to define these potentials and the associated water flow, described with a non-equilibrium or irreversible thermodynamics framework, are given below (van Oort *et al.*, 1996):

$$J_v = - L_{11}\nabla P - L_{12}\nabla \mu_c - L_{13}\nabla E - L_{14}\nabla T \qquad (2.4)$$

$$J_D = - L_{21}\nabla P - L_{22}\nabla \mu_c - L_{23}\nabla E - L_{24}\nabla T \qquad (2.5)$$

$$I = - L_{31}\nabla P - L_{32}\nabla \mu_c - L_{33}\nabla E - L_{34}\nabla T \qquad (2.6)$$

$$Q = - L_{41}\nabla P - L_{42}\nabla \mu_c - L_{43}\nabla E - L_{44}\nabla T \qquad (2.7)$$

where J_v, J_D, I, and Q denote the flow of total solution (total volume), the diffusive flow of solute relative to the volume flow, the flow of current, and heat, respectively. ∇P, $\nabla \mu_c$,∇E, ∇T denote gradients in pressure, chemical potential, electrical potential, and temperatures existing between the drilling fluid and the shale, respectively. The values of the empirical constants L_{ij}, denoting the contribution of a certain gradient to a specific flow, can be obtained from experiments.

According to Mody & Hale (1993), the chemical and hydraulic potentials are the two most important driving forces. Considering just these two driving forces, these authors present a description of the mechanism for each driving force, and the associated species flow (Table 2.1).

Table 2.1: Different mechanisms and molecular species flow for each associated driving force (Mody & Hale, 1993)

Mechanism	Driving Force	Molecular Species
Osmotic Transport (Diffusion)	Chemical Potential of Water	Water in or out of shale
Reverse Osmosis	Hydraulic Pressure Difference[3]	Water into shale
Hydraulic Flow	Hydraulic Pressure Difference[3]	Bulk Water (cations, anions, and water) primarily into shale
Open Communication (Diffusion)	Chemical Potential of Ions and Water	Ions and water in or out of shale

In any sedimentary rock, including shales, flow induced by the hydraulic potential is always considered to follow Darcy's law. In Chapter 6 this

[3] It is assumed that the mud weight is greater than the pore pressure, the flow being primarily into the shale.

assumption is discussed, and due to the structure alteration observed when shale is in contact with a solution, this assumption might introduce serious mistakes. In this dissertation, focus is given to the study and evaluation of the chemical potential as a driving force, since chemical issues have been considered to play an important role in wellbore instability.

2.4 Wellbore Stability Analyses

Wellbore stability has been studied by the oil industry for a long time. The approach that has been applied is the same since the first models came out in the 40's: compare the stresses in the rock with its strength. Basically, two types of failure have been widely investigated; when the stresses overcome the tensile strength, on when the stresses are greater than the shear strength. In the first case a fracture is created, whereas in the second case it is assumed that a damaged zone is generated.

The whole idea is that the state of stress around the wellbore is changed by the pressure exerted by the drilling fluid. Just by drilling the well, the in-situ stresses are immediately replaced by the wellbore fluid pressure, which is equal in all directions. This fluid pressure oscillates sometimes intentionally, but in many other operations the pressure changes significantly due to some problems in the well or due to inadequate operational practices. Each fluid pressure change will induce a modification in the state of stress around the wellbore, and depending on the magnitude, it can induce failure of the walls.

Initially, the studies focused only on the fracturing side, due to the use of hydraulic fracturing to stimulate oil wells. In the beginning the models were simple and the rock was considered linear elastic, homogeneous, and isotropic, applied to vertical wells. Lately, models for inclined wells (Daneshy, 1973) and with more complex rock characteristics have been developed.

More recently, compressive failure have been introduced in the analysis (Bradley, 1979). It was observed that the state of stress around the well can produce a failure in shear also, not just in tension. These models could explain the collapse of the wells, very common during drilling. Since then, a mud weight window has been defined, with a lower limit for the drilling fluid weight given by the shear failure and an upper limit determined by the fracturing failure. For a safe drilling, the mud weight should be within these two boundaries.

Several models have been developed, increasing the complexity of the rock response (Hsiao, 1987; McLean and Addis, 1989). Santos (1989) identified the possibility of two other failure mechanisms: a lower fracturing failure, and an upper collapse failure. These two modes give new bounds to the mud weight window, restricting a little further the safe limit to be used in the field. This author, however, used a simple model, considering the rock isotropic, homogeneous, and linear elastic.

Further development in the models only added complexity to the type of rock to be analyzed. Anisotropic (Santos & da Fontoura, 1991; Ong, 1994) and fractured formations (Germanovich *et al.*, 1996) have been included lately.

Incorporation of complex constitutive relations also has been done. Introduction of poro-elastic concepts added new insights to the problem (Cui *et al.*, 1995; Abousleiman *et al.*, 1995; Frydman & da Fontoura, 1997).

In essence, models can be developed to take into account all the important phenomena into the wellbore. However, some phenomena are really difficult to be modeled, such as the effect of drill string vibrations and chemical alteration of the rock. The thermal effects have been considered in several works, with the development of various models, including thermoelastic, thermo-poroelastic, and even thermo-poroelastoplastic (Hojka & Dusseault, 1991; Wang & Dusseault, 1995). A solution coupling the conductive heat transfer and Darcy's fluid flow also has been recently presented (Wang *et al.*, 1996).

In some cases the strength of the rock is considered to be degrading, and a lower than original value has been used in the analyses. The major problem is the lack of available input parameters. The more complex the model, the more input parameters needed. Most of the time these parameters are not available, forcing the engineers to estimate some reasonable values. The results produced by the model, therefore, do not necessarily represent the actual situation one is trying to simulate, leading to failure in predicting the problems faced in the field. Experience has showed that the simpler the model, the better the predictions.

Even with all the model complexity available today, several problems cannot be explained or predicted. In shales, specifically, time-delayed failures are very common. Problems in the wellbore usually starts after the formations

have been exposed for some time (usually days). It is well accepted today that these problems are caused by the interaction between the drilling fluid, mainly WBM, and the shale. As has been mentioned before, however, these ideas have been questioned. Even with OBM some wells still have severe instability problems (Santarelli & Carminati, 1995). Poro-elastic effects also have been blamed to be causing time-delayed failures, due to the dissipation of the excess pore pressure, especially in low permeability formations.

Rocks fail if either the stresses are greater than the strength, or if the energy stored in the rock exceeds the acceptable limit for such material. Based on this last approach, and considering that the available models fail to explain several situations encountered in the field, an innovative conceptual model, based on energy, has been developed and it is presented in chapter 7.

Chapter 3

3. Influence of Water Content and Distribution on Shale Reactivity

3.1 Introduction

Proof that shale water content should be preserved as close as possible to in-situ conditions in order for the specimen to reproduce actual shale behavior is one of the most important recent conclusions. In the past, too little attention was paid to this fact; partially and sometimes completely dried shale samples were used in laboratory tests. Most of these tests were done to evaluate drilling fluid compatibility and optimize their composition. Shale instability problems are more severe when WBM are used. Using improperly preserved samples, several additives were suggested in order to prevent the shale from absorbing water and swelling (O'Brien & Chenevert, 1973; Steiger, 1981; Bol, 1986).

When it was observed that partially dried shales do not behave in the same manner as a preserved one when immersed in water solutions, the oil industry began to store shale cores in such a way as to avoid water losses. A number of preservation techniques were developed, suggested, and used by different companies; two of which are preferred: keep the shale in mineral oil, or wrap the rock with aluminum foil, plastic and finally coat it with paraffin. Both techniques were tested and checked for effectiveness; and it is proposed that a common procedure be adopted by the industry.

Although it is obvious that partially dried shales react differently than do preserved samples, it is not clear whether the presence of air is the main cause leading to this change in behavior. When shale dries, not only does air enter the sample, but water is also lost. Because water is part of the shale structure (see Appendix A for more details), the innate structure is altered and the rock is changed. Therefore, there still remain unanswered questions such as:

1. How does a change in structure affect shale behavior?
2. After losing water, how does the rock reach a new equilibrium?
3. Does shale water move, trying to compensate for that which was lost?
4. How does this movement (if it occurs) affect shale reactivity?

In order to get answers to these questions, research was conducted specifically on how water content and distribution affect shale reactivity. This chapter presents the first results, derived from a series of laboratory tests made on carefully preserved downhole samples. Initially, the idea was simply

to observe the shale reactivity when it was in contact with different solutions. Therefore, the majority of the early tests were done under laboratory conditions. Only after a better understanding of the rock behavior was achieved, triaxial tests were introduced to study the influence of confining pressure (see Chapter 5). By changing one parameter at a time, the influence of individual parameters affecting shale reactivity can be evaluated.

Standard characterization tests were done by Petrobras, and the most relevant results are presented here. A careful preservation procedure was used to keep the water content of the cores as close as possible to their in-situ conditions. As part of the study, the preservation procedure was also checked for effectiveness and for any change of the shale original surface properties.

Additionally, a new methodology to determine the different types of water present in a shale, free, bound, and crystalline water, is described. Standard procedures, now used by industry, do not give, indeed, sufficient details about those. Shale reactions under controlled conditions were recorded and show the important points to be stressed. From results of this study it is clear that changes in well-established procedures may be required to realistically view shale instability problems. The main goal of this chapter is to show how the water in the shale is affecting its reactivity. Comparison with preserved and partially dried shale samples are made. Even though it is well known that a dehydrated shale has a different behavior than the preserved one (Mody & Hale, 1993; Hale *et al.*, 1993; Schmitt *et al.*, 1994; Forsans & Schmitt, 1994), and that water redistribution within the shale has been mentioned before

(Mody & Hale, 1993), comparison between well-preserved downhole shale and partially dried samples of the same shale is made for the first time.

3.2 Shale Samples

Without having confidence about preservation of the shale sample, there is no sense in running laboratory experiments since results may be biased. In order to study the influence of water content on shale reactivity, test samples must remain as close as possible to their original in-situ state. All the samples used in this research were donated by Petrobras. Cores were taken from several wells located in the Campos Basin, offshore Brazil, in water depths varying from 450 m to more than 1000 m. These cores were retrieved to complete an internal shale stability project conducted by Petrobras, under the PROCAP 2000 program. A successful shale coring program must include procedures to be followed from the moment the rock reaches the rig floor until it arrives in the laboratory, including storage periods. The first core for the project was taken only after everybody involved (including rig personnel) was educated on the importance of preserving the in-situ nature of the core. Immediate immersion in mineral oil rather than wrapping with paraffin was chosen after investigating the pros and cons of each technique. Being a very simple operation, exposure time to air was minimized and water loss was not significant. As soon as the core arrived at the rig floor, it was cleaned with mineral oil (to remove the WBM used in the coring operation) and stored in

sealed fiberglass containers filled with mineral oil. From this point container leakage was monitored at all times. However, even these precautions do not prevent the sample from the unavoidable loss in saturation due to the expansion associated with stress relief and temperature changes.

3.2.1 Characterization Tests

Due to its highly complex structure, shale characterization requires a number of different tests, each one specifically dedicated to a certain property. The rock behavior is influenced not only by the amount, but also by how the components are distributed and arranged. Pore size distribution is directly related to the rock structure, influencing fluid flow through it. Internal forces developed in shales due to clay minerals (see Appendix B) are also dependent on the arrangement of the rock components. Both the individual constituents and the shale structure were characterized by Petrobras (Martins *et al.*, 1996), using most of the standard tests used by the oil industry:

. Specific surface

. Grain density

. Mineralogy

. Pore fluid composition

. Cation exchange capacity (CEC)

. Pore size distribution

. Rock density

. Water content (usual methodology, sample inside an oven at 105°C)

. Hot Rolling

. Capillary suction

. Granulometry

In addition to these tests, thin sections and images from the electronic microscope helped define the cementation and the microstructure of the shales. Presence of pyrite, for example, was clearly observed in one of the pictures (Martins *et al.*, 1996), although the results from the mineralogy did not indicate its presence in one of the shales.

Table 3.1 through Table 3.3 present the results of pore fluid composition, CEC, and mineralogy. These results were compared to others available in the literature (Schmidt, 1973). The total CEC value is similar, but the values for each specific cation is different. This difference explains the different behaviors of the shales when exposed to fluid solutions. Therefore, it is essential to report the CEC for each specific cation, in addition to its total value. The conclusion at this point is that only one or two parameters are not enough to characterize the shale to foresee how the rock will behave when in contact with fluid solutions.

Therefore, there was a need to develop a methodology that is able to quantify, in more detail, the water in a shale. The standard methodology used by the industry (heat the sample in an oven at 105°C and measure the difference in weight) does not permit differentiation among the water types present in the shale.

Table 3.1: Pore fluid composition for shales from the Campos Basin and the Gulf of Mexico (ND = not detected).

Ions	Concentration (mg/l)		
	Shale B	Gulf of Mexico (1)	Gulf of Mexico (2)
Li^+	ND	2.2	2.6
Na^+	14,439	23,800	20,700
K^+	370	133	141
Mg^{++}	137	5.2	5.3
Ca^{++}	927	47	66
Sr^{++}	ND	ND	ND
Cl^-	12,879	17,300	9,860
$SO_4^=$	9,470	26,800	27,500

Table 3.2: Cation Exchange Capacity (CEC) for shales from the Campos Basin, the North Sea, and Pierre shale[1].

Cation	CEC (meq/100g)			
	Shale B	Shale F	Pierre	North Sea
Na^+	7.07	3.82	18.8	25.2
K^+	4.23	1.07	0.2	1.0
Ca^{++}	14.62	15.20	11.7	3.2
Mg^{++}	1.83	3.27	3.5	6.3
Total	28.1	23.36	34.2	35.7

A detailed mineralogy of the clay minerals for some shales has also been determined by XRD. Not only clay content, but also smectite content are low, indicating a potentially low reactive shale (Table 3.4). The average water

[1] The CEC for Li^+ and Sr^{++} was zero.

content (usual methodology - heating in oven for 24 hrs. at 105°C) for each shale type is also reported, indicating similar values.

Table 3.3: Mineralogy (%) of shales from the Campos Basin, the North Sea, and Pierre shale.

Shale	Quartz	Calcite	Pyrite	Feldspars	Total Clay	Others
A	25	20	10	10	30	5
B	20	30	5	5	30	10
C	12	60	0	5	18	5
D	15	45	5	5	20	10
E	10	60	5	5	15	5
Pierre	20	6	0	4	70	0
North Sea	16	11	0	2	65	6

Table 3.4: Detailed mineralogy and average water content (usual methodology) of some shales from the Campos Basin.

	Shale B	Shale D	Shale E
Quartz	20	15	10
Calcite	30	45	60
Pyrite	5	5	5
Feldspars	5	5	5
Others	10	10	5
Total Clay	30	20	15
Kaolinite	3	1	1
Chlorite	0	0	1
Illite	15	10	7
Smectite	12	9	6
Water content (%) (Free water)	8.3	7.9	8.8

The importance of shale preservation can be observed by comparing the values of water content (usual methodology) for different coring boxes from the same well (Table 3.5). Some of the boxes leaked mineral oil, and this was clearly observed from the low water content values obtained. The cores with low water content values were not used for any interaction test.

Table 3.5: Water content (usual methodology) for different boxes (depths) - Shale B.

Box #	Water Content (%)
1	8.6
2	8.1
3	8.1
4	8.9
5	6.1
6	7.6
7	3.9
8	8.9

3.3 New methodology of water content determination

Even though it is well known that water content plays an important role in shale reactivity, there is no standard procedure followed by the oil industry to measure it. Usually, samples are placed in an oven and the difference in weight before and after drying is attributed to water loss. Typically, temperatures ranging from 65°C to 105°C and drying periods ranging from 1 hour to more

than 1 day (until weight stabilizes) are used (Hale *et al.*, 1993; Martins *et al.*, 1996; Fooks & Dusseault, 1996)[2]. In some instances, crushed samples were used to facilitate water loss (Fisk, 1996; da Fontoura & Rego, 1995). Rock fragments of different sizes and shapes are also used. Another method for water content determination consists of placing the sample in an airtight chamber containing 100 g of anhydrous calcium sulfate at 150°F until the weight of the sample or the calcium sulfate stabilizes (Hale *et al.*, 1993). Lack of uniformity in the techniques used to determine water content can, by itself, produce a wide range of results. All three factors, sample size, oven temperature, and drying time, affect water movement.

Shales are fine-grained detrital sedimentary rocks containing variable amounts of clay and accessory minerals such as quartz, carbonates, and feldspars that form a complex structure with a variable pore size distribution. Water distribution within such a system is another variable. In addition, it is important to separate shale water as free water, bound water, and crystalline water, since the rock pore structure retains the free water and clay minerals have water in the later two forms in their structure (see Appendix A). The free water is herein considered as filling macropores (> 10 μm) between clay aggregates and/or particles of accessory minerals as well as interparticle pores on the order of microns.

[2] The recommended ISRM procedure is to heat the sample in an oven at 105°C until the weight stabilizes (at least for 24 hrs.). Difference between the initial and final weight divided by the final (dried) sample weight is the water content, in %.

Because bound water occupies interlayer spacings within expandable clay particles (Appendix A), it requires a higher energy to be removed than does free water. Water molecules are confined to two-dimensional structures, or layers present in integral numbers as a function of relative humidity, i.e., water activity (Berend, 1991; see Appendix A). Clay particles composed of several unit layers can also contain internal lenticular pores up to 10 nm wide (Touret *et al.*, 1990). The most energetically bound water is associated with exchangeable cations (Berend, 1991), and temperatures above 100°C are necessary to remove it . In addition, crystalline water (structural hydroxyls), not usually considered as "water" in clays, when contained in the unit layer perhaps play the role of anion-exchange sites. The hydroxyl groups combine to form water at about 550°C (see Appendices A and B).

A big controversy about water classification in clays and shales still exists. The methodology described here was adopted in order to keep consistency with the most popular technique used in the oil industry (heat the sample in an oven at 105°C until weight stabilizes), and, thus, to allow comparisons. The terms free and bound water, and the temperature range defined in the methodology were chosen according to usual oil industry procedures (Fisk, 1995; Stokke, 1995; Sostebo & Horsrud; 1996, Low, 1961; Darley & Gray, 1991).

In order to determine in detail all the important water content by type; and study the effect of varying water type content on shale reactivity, a precise methodology is required. The Thermogravimetric Analyzer (TGA), TGA 50

(Figure 3.1 and Figure 3.2), provides an accurate measure of weight loss as a function of time and temperature (up to 800°C) and is suggested for use in all water content determinations. An advantage of this equipment is that it only requires very small samples (20 to 80 mg) which permits water content to be obtained from different locations in the same sample.

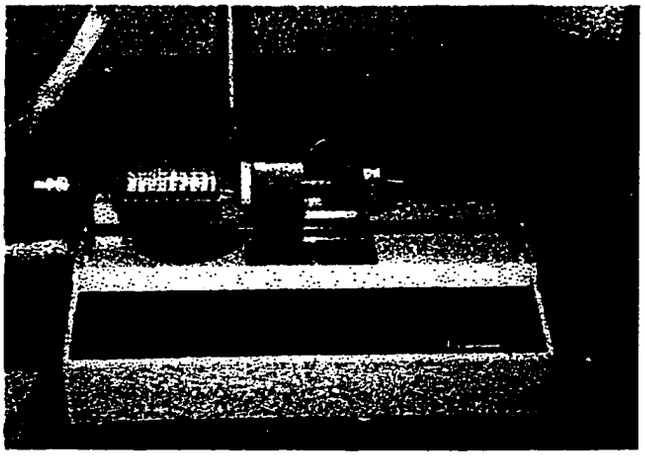


Figure 3.1: Thermogravimetric Analyzer (TGA 50).



Figure 3.2: TGA 50 with the acquisition data system and plotter. Nitrogen gas (cylinder in the back) is used to purge any evolved gas from the sample.

Time was spent in defining the optimum settings (temperature rate increase, periods of holding temperature, etc.) to be used. After 16 hours at room temperature (22°C), the sample does not lose any additional significant amount of water. After this period, temperature was increased at a rate of 2°C/min. up to 110°C. The sample was kept at this temperature for 3 hours, allowing all the so-called free water to escape. From this point up to 250°C, temperature was increased again at a rate of 2°C/min. to 250°C where it was held constant for another 3 hours. At this stage, all bound water should have been released. After this point the temperature increase rate was lowered to 0.1°C/min. to a test termination temperature of 800°C. Even though the term water is being used here, some other gases can evolve from the sample as it is heated. In the case of shales with calcite, for example, CO_2 is released between 700°C and 750°C. Since the term crystalline water involves all the evolved gases between 250°C and 800°C, the weight loss observed in the TGA test does not represent, necessarily, just the structural water from the clay minerals (see Chapter 4).

The complete curve of weight loss versus temperature for one shale tested indicates that, in this sample, the amount of free water is greater than the bound water (Figure 3.3). The free water content obtained from TGA, 8.3%, is very close to the value obtained with the usual methodology for the same shale (Table 3.4). It is important to note that for all TGA results the water content is the weight loss divided by the original total sample weight, whereas for the

ISRM recommended procedure the water content is the weight loss divided by the final dried sample weight. A simple conversion can be made in order to compare the two values. For shale E, the value of 8.8% in Table 3.4 is equivalent to 8.1%, if the initial total sample weight is considered. As can be seen, the value obtained from the TGA is quite similar to the one obtained with the oven method. The lower curve is the first derivative of the weight loss. When the derivative is close to zero, almost all the water possible to be removed at a certain temperature has escaped. Powdered samples rather than small solid pieces are preferable for use in the TGA (Wendlandt, 1986; Bish & Duffy, 1990; Daniels, 1973), reducing the time required to release all water at a certain temperature, and keeping consistency among the tests. If pieces are used, reproducibility of the results are more difficult since the shapes and sizes of the samples would vary widely. However, shale structure can be altered by crushing the rock. Scratching the surface of the specimen is, then, a preferred procedure to collect samples for TGA. Temperature variation rate can be different from the ones suggested above. However, the sample should be kept at a temperature long enough to guarantee that all water (free or bound) has already been released from the rock.

All water content results reported in this chapter were determined following the method previously described (except the results obtained by Petrobras, Martins *et al.*, 1996). By keeping the method constant, variation in water content can be compared from different samples and locations.

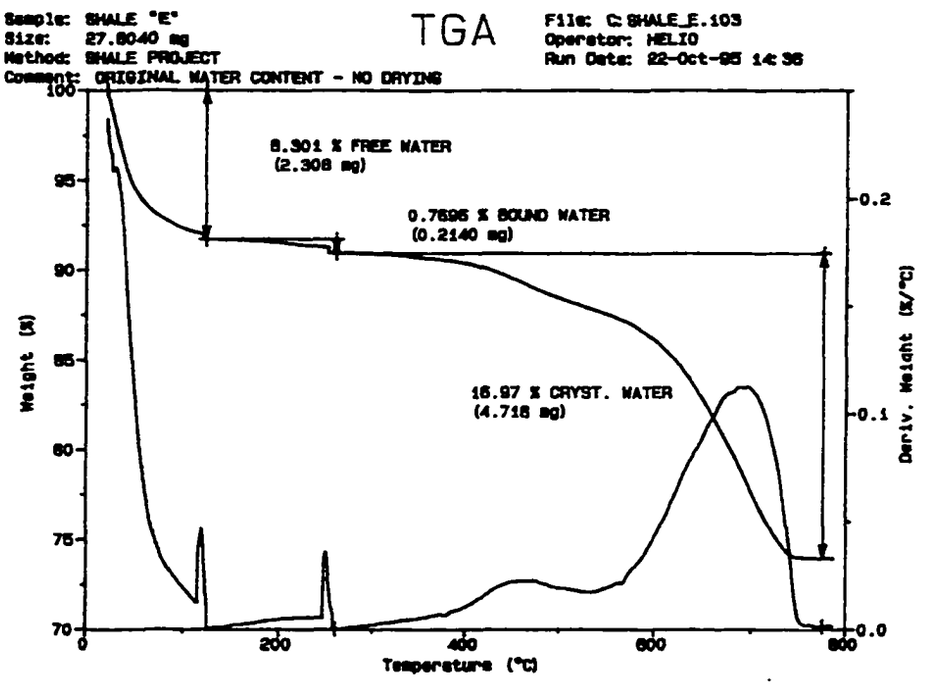


Figure 3.3: Complete water content determination of a preserved sample.

3.4 Laboratory tests and evidences

Even though shale dehydration has been known to affect shale reactivity when immersed in water, quantification of these effects has not yet been done. Hale *et al.* (1993) studied the effect of dehydration on the mechanical strength of shales. Under downhole conditions, the shale is in permanent exposure to a drilling fluid; therefore, reactivity and mechanical studies should be conducted together. A series of laboratory tests were conducted, in a preliminary stage, with carefully preserved and partially-dried shale samples. The aim was to demonstrate the influence of water content and distribution on shale reactivity

when immersed in water solutions, and to observe the most important aspects to provide the basis to understand the interaction mechanisms.

3.4.1 Water Content and Shale Reactivity - Immersion tests

The first tests were designed to be run under atmospheric conditions of pressure and temperature. Immersion tests were conducted by placing shale samples in different solutions, then monitoring and recording qualitative reactions with a video-camera.

Preliminary results of immersion tests clearly indicated that shale reactivity was proportional to the amount of water loss in the sample. One sample (shale E) was allowed to dry at ambient conditions (22°C) for 22 hours (sample 22). It was then immersed in mineral oil again until air bubbles no longer escaped from the sample; and, finally, it was immersed in de-ionized water. A second sample, adjacent to the previous one, was not pre-dried (sample 0). After 45 minutes, sample 22 was completely disintegrated while sample 0 remained almost intact for 5 days. The difference in reaction between these samples is readily visible to the unaided eye (Figure 3.4 and Figure 3.5). While the shape of sample 0 remained unchanged after 3 days of immersion, sample 22 strongly reacted on the surface, generating several spalled pieces after only a few minutes of immersion. As might be expected, the reaction intensity was, visually, clearly proportional to the drying period. Samples were also allowed to dry in air for 0.5 hr. and 3 hrs. Although not shown here, reaction was

much less intense in the 3-hr. dried sample than the one dried for 22 hrs. For the sample dried for just 0.5 hr. reaction was limited to a thin outside layer.

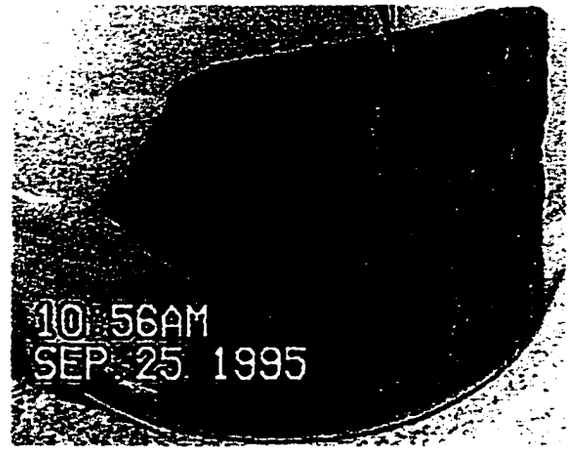


Figure 3.4: Sample 0 after immersion in water for 3 days.



Figure 3.5: Sample 22 after immersion in water for 24 and 35 minutes.

These results show that a shale can be in contact with a water solution (in this case de-ionized water) without reacting (swelling). The sample remained inside water for more than 1 year without almost any change. Even considering that all the exchange processes are very slow in shales due to its low permeability, this behavior was not expected. It is known that water

content influences shale behavior; a thorough and deep study to understand the real mechanisms, however, has not yet been conducted. With this unexpected result, the whole downhole shale swelling idea needed to be revisited.

Since the samples were preserved immersed in mineral oil, it was suspected that it was the mineral oil that impeded the reaction of the preserved samples, by changing somehow the shale surface characteristics. A specific investigation was carried out to clear this doubt. A piece of preserved core was taken out of the oil and fresh surfaces were opened using a wedge. By avoiding to cut the shale mechanically (with a saw) an original undisturbed surface was obtained. One of the fresh surface was immersed immediately in de-ionized water, without any prior contact with oil. This preserved surface did not present any reaction. The other surface, also without any prior oil contact, was left dehydrating in air for 2 hrs. After dehydration, the piece was immersed in oil prior to immersion in de-ionized water. Even with a film of mineral oil surrounding the surface, a strong reaction was seen. Even though this test was recorded, it was not possible to obtain good pictures of the surfaces. Consequently, the lack of reaction in samples preserved in oil was not due to a treatment artifact, but because the sample maintained its original (as close as possible, of course) water content.

3.4.2 Rock Strength Variation

The strength of the rock was measured as a function of time using a Rex durometer Type C model H-1600 (Figure 3.6) which provides an index value that can be used to compare the degree of weakening in different shale samples. The durometer is a pen-like device with a needle in one of the extremities that is pressured against the material to be tested. The penetration resistance offered by the material is measured with a gauge. Being a non-destructive test, it is very useful for studying rock strength as a function of immersion time. The durometer model should be selected so that the full range of strength expected for the material can be measured. If the durometer model is too strong, it will break the samples. A full scale reading would be the consequence of selecting a very weak durometer. The H-1600 model was selected based on previous experience with shaly rocks (Stokke, 1995; Mody, 1995; Chenevert, 1995), performing adequately with the available shales from the Campos Basin.

The durometer index varies as a function of drying time (Figure 3.7). Two samples were allowed to dry at ambient conditions (22°C): for 3 hours (sample 3) and 22 hours (sample 22). A third sample was not pre-dried (sample 0). As previously stated, before immersing in water, all samples were cleaned with a paper towel. By following this same procedure, the only difference among the samples is the water content and its distribution. The same shale E was used in these tests.

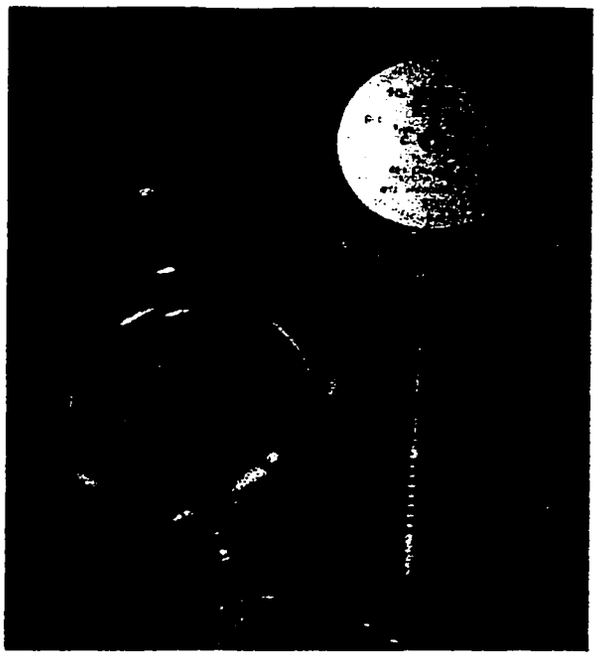


Figure 3.6: Rex durometer Type C Model 1600. On the left, shale samples in a beaker immersed in mineral oil before testing. The samples are tested without removing them from the solution to avoid air exposure.

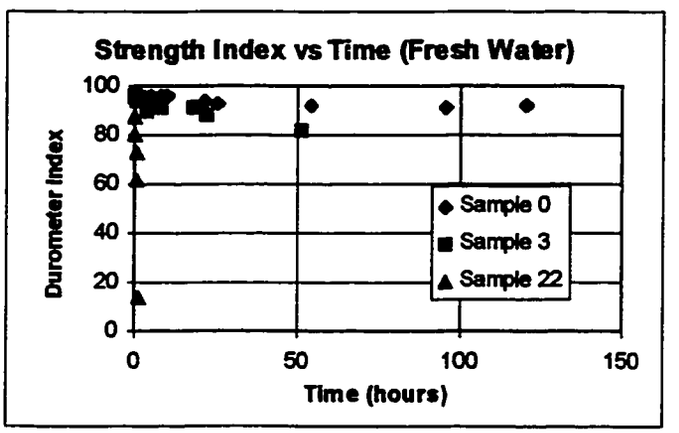


Figure 3.7: Strength index as a function of time for different drying periods.

In the next sequence, all the samples were preserved without any drying. These samples were immersed in solutions of different KCl concentrations (different activities), which eventually produced a constant durometer index as a function of time (Figure 3.8). Regardless of the solution activity no significant change in strength resulted. Even though Figure 3.8 shows the first 15 days of the test, after 1 year all the samples maintained unaltered their strength index.

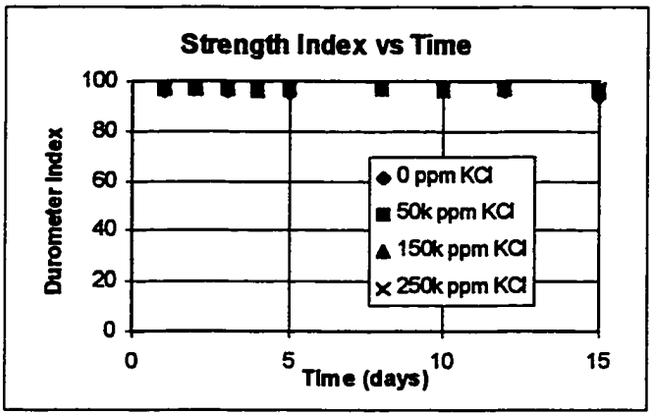


Figure 3.8: Strength index as a function of time for preserved samples in de-ionized water and various KCl solutions. No significant change was observed.

3.4.3 Water content

Water content was determined for samples 0 (no drying) and 22 before dropping them in water. At room temperature (22°C), sample 0 lost the majority (7.7%) of its free water (Figure 3.9). Total free water found with this test is in the same range obtained by the usual method (Table 3.5, Martins *et al.*, 1996). The amount of bound water released between 110°C and 250°C was 1.3%. A comparison with the results of sample 22 reveals that both the free

and bound water change from sample to sample (compare Figure 3.9 and Figure 3.10). Another interesting point is the shape of the curve at the beginning of the test (Figure 3.11). After 30 minutes the preserved sample lost 59% of the total water released in 24 hours at room temperature. These values will, of course, vary as a function of the ambient humidity in the testing environment. Results clearly indicate, however, that even 10 or 20 minutes of exposure to air is sufficient to completely alter the water content at the sample surface. The time from scratching the surface of the shale to collect the sample and the beginning of the TGA test is less than 1 min. Keeping this time small is absolutely essential to guarantee a minimum water loss.

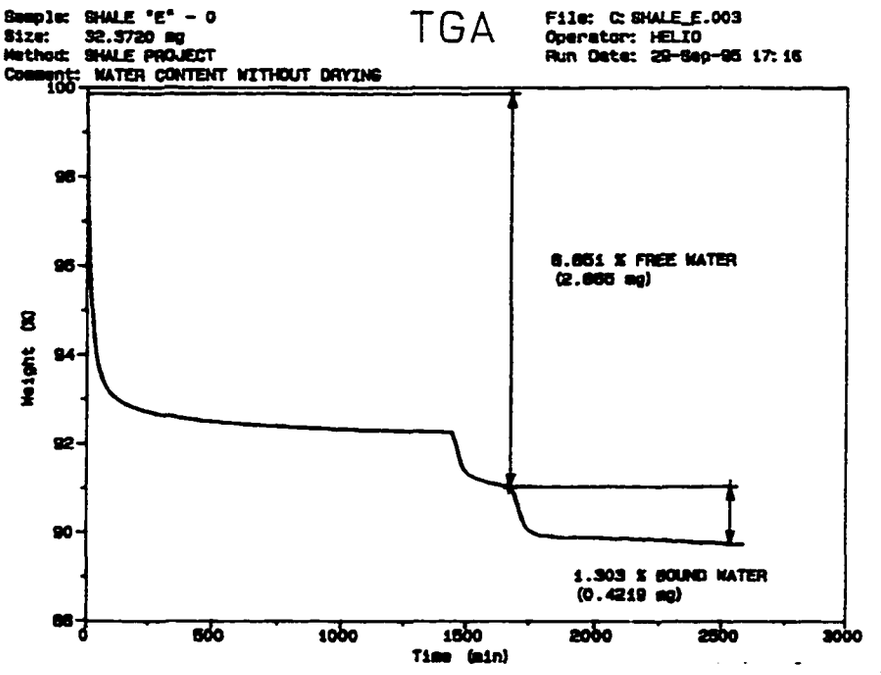


Figure 3.9: Water content - sample 0 (no drying).

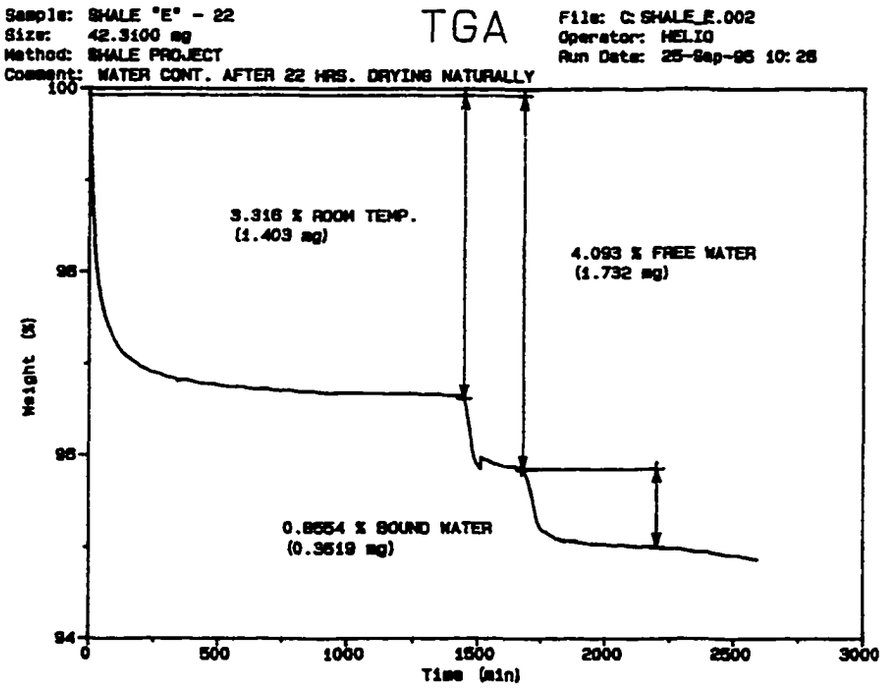


Figure 3.10: Water content - sample 22.

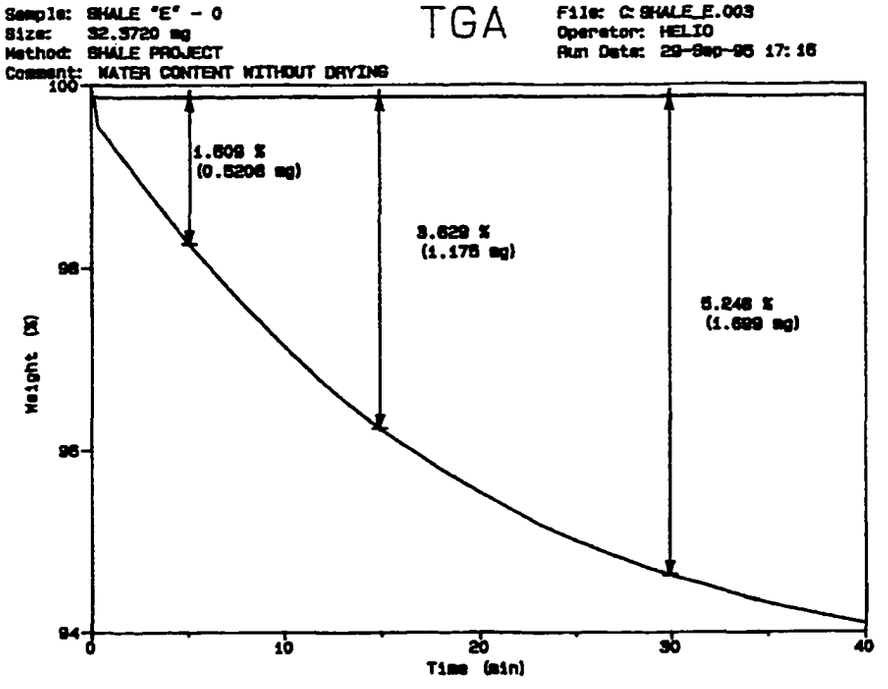


Figure 3.11: First 40 minutes of water content determination - sample 0 (no drying).

Because the methodology uses small amounts (20 to 60 mg) of rock, water content from different positions in the sample can be obtained (Figure 3.12). Ideally, more than one sample should be collected from the same specimen, to check for water content homogeneity.

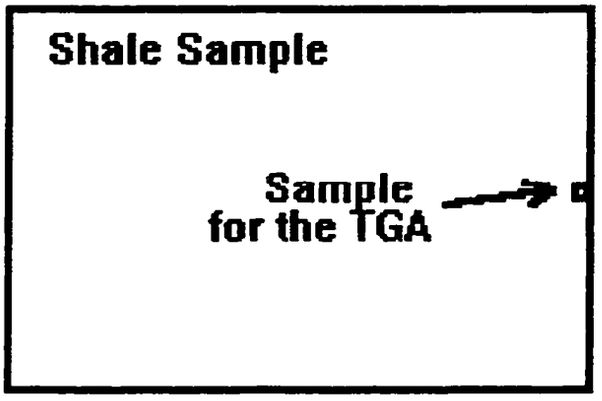


Figure 3.12: Size of the sample used to measure water content compared to the whole shale sample (approximate real scale; shale sample dimensions: 2 in. x 3 in.)

3.4.4 Water redistribution

By storing the sample in mineral oil after first being dried for some time, water in the sample is allowed to move from the inner to the outer parts of the sample. No extra water is lost, nor is more air allowed to penetrate. Mody & Hale (1993) mentioned the possibility of water being redistributed inside the shale sample after part of its water has been lost. However, quantification and proof of this concept have not yet been done due to lack of a water content

determination methodology capable to capture these localized features. With the TGA methodology described previously this is now possible.

In order to quantify this aspect, three samples were dried in air for 2 hours. The samples were adjacent pieces taken from a preserved core and all three were dried at the same time, one beside the other to permit later comparison of the results. After a 2-hour period, one sample was immersed in de-ionized water. The remaining two were immersed in mineral oil, in order to avoid any more drying and allow water redistribution, if, indeed, it occurred. After 2 weeks, one of the samples in oil was immersed in de-ionized water. The third sample was left for 4 weeks before exposing it to de-ionized water. On different occasions water content was measured in the sample that remained in oil for 4 weeks. Pieces for water content measurements were taken from adjacent locations on the surface, to ensure a good comparison. All three samples lost about 1% of their total weight after the 2-hour air exposure period.

Table 3.6: Water content on the surface at different times for water redistribution evaluation.

Description	Free water (%)	Bound water (%)	Crystalline water (%)
Original water content	7.08	0.81	17.88
After 2 hours drying in air	4.21	1.01	18.5
After 2 weeks immersed in oil	6.70	2.16	18.25
After 4 weeks immersed in oil	6.11	1.21	18.15

It is clear that not only free water but also bound water content changes with time (Table 3.6). Difference in free water after 2 and 4 weeks in oil might indicate that a complete equilibrium had not yet been achieved. Water redistribution does not appear to be an extremely slow process, but even after 4 weeks some water is still moving. Crystalline water is not much affected. However, differences in bound water are not small. Even though it is premature to assure that drying in air leads to bound water redistribution, these results might indicate that losing water at room temperature during shale drying is not a reversible process. It is obvious that original values will never again be reached, as confirmed from the results.

Direct observations indicated that the sample reaction is a function of how much original water is lost before testing; the larger the difference in water content from the original value, the stronger the reaction. Without any redistribution, surface reaction is intense. After the outer layers react, the inner part of the sample, still wet, remains intact (Figure 3.13). The sample that remained in oil for 2 weeks experienced quite a different reaction. Surface reaction was not intense, but, after 46 hours, the sample broke into three separate pieces. As water was redistributed, it moved from the inner part of the sample to equilibrate at the surface. Consequently, water content on the surface, though not exactly the same, approached its original value but the same redistribution caused the inside portion to dry. The net result was a more homogeneous water distribution so that reaction occurs throughout the sample, rather than just on the surface (Figure 3.14).

Likewise, sample C, being in oil for a longer period established a more homogeneous water distribution throughout the sample, and reacted in the manner described above. There is an indication that shale reaction is a function of both the amount and distribution of water in the shale and that these variables are not necessarily independent variables.

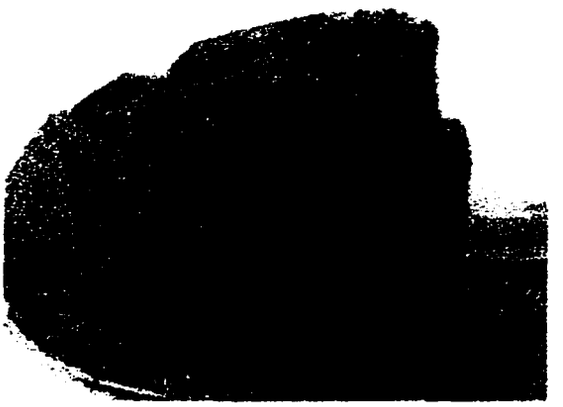


Figure 3.13: Shale reaction in water after 2-hour air drying, without water redistribution.

It is important to note here that all three samples lost the same amount of water when initially exposed to air and that the preserved sample did not react when immersed in de-ionized water, even though it was not completely saturated. According to da Fontoura & Rego (1995) this shale has around 80% saturation.

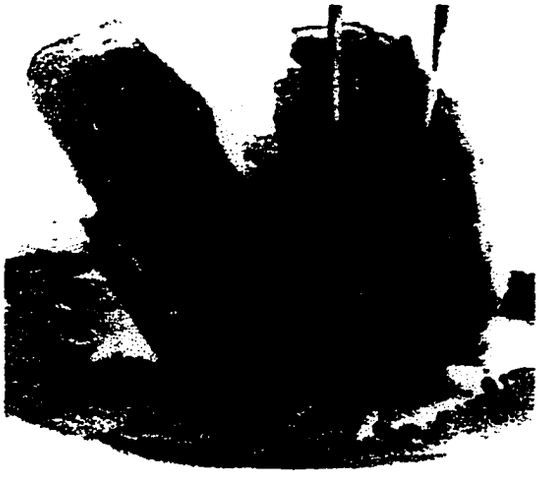


Figure 3.14: Shale reaction in water after being immersed in oil for 2 weeks to allow water redistribution.

Immersion in oil after being dehydrated in air might have introduced bias, since oil penetrates into the shale and might give a wrong result in the TGA water content determination. In order to eliminate any contamination, another test was designed, this time wrapping the sample with aluminum foil, plastic, and paraffin, after the 2-hour drying period (Figure 3.15). The idea was to block any further dehydration without contaminating the sample with another element. Effectiveness of the paraffin seal was checked by continuously weighing the sample. Weight change was not observed indicating that the paraffin was actually preserving the sample from dehydration.

The same procedure for water content determination was repeated. Measurements were taken before dehydration (native state), after a 2-hour drying period, and after 5, 19 and 55 days allowing water redistribution. Coating with paraffin is much more laborious; each TGA measurement requires the unwrapping and an immediate re-wrapping of the sample, in order

to minimize any further water loss. In this test, water redistribution also occurred within the sample. Not only free water, but also bound and crystalline rebounded after the huge change in the beginning (Figure 3.16 through Figure 3.18).

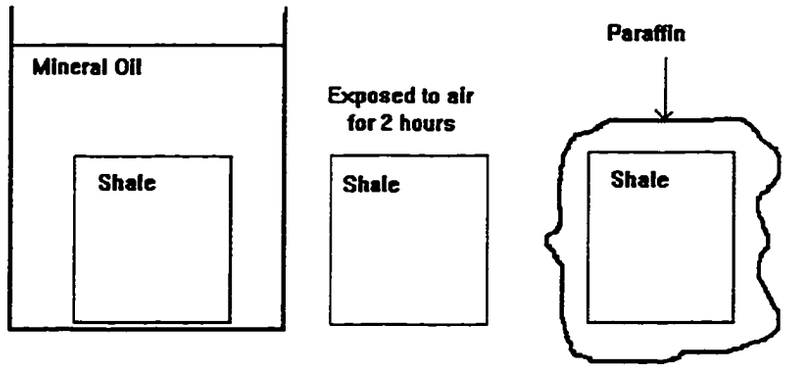


Figure 3.15: Water redistribution experiment: shale coated with paraffin to avoid further dehydration and contamination with oil.

During air dehydration, the sample lost 1% of its initial weight. It is assumed here that this weight loss corresponds to free water. This assumption is realistic since air exposure at room temperature can remove only the water that is not strongly held inside the sample. Since the sample initially had 7.5% of free water, its average free water content would be 6.5% after the drying period. The test was, then, interrupted after 55 days, when the free water content at the surface reached this amount. Even though water content was not determined inside the sample, it was assumed that the redistribution would be complete at this point.

The same behavior as the previous test is seen here. Free water is greatly reduced due to air exposure, and then slowly increased due to the movement of water from the inside portion of the sample to the outside. Bound and crystalline water have the opposite behavior: initially the values increased and then went down. Both the bound and crystalline water rebounded to values close to the original values. Free water, on the other hand, will not be restored to the original value, since some amount was irreversibly lost.

The same behavior was also observed for this sample when immersed in water. Very slight surface reaction was seen, but after a few days the sample broke and lost completely its strength, in a very similar way as for the tests previously described (Figure 3.14).

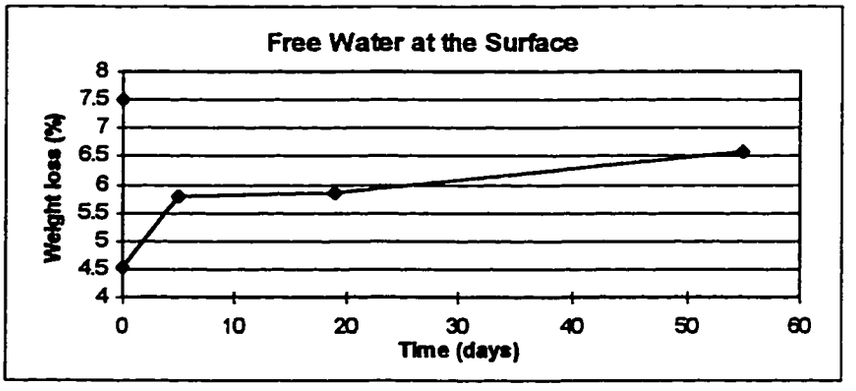


Figure 3.16: Free water (weight loss between room temperature and 110°C) at the surface: original value, after 2 hours in air, and after 5, 19, and 55 days equilibrating.

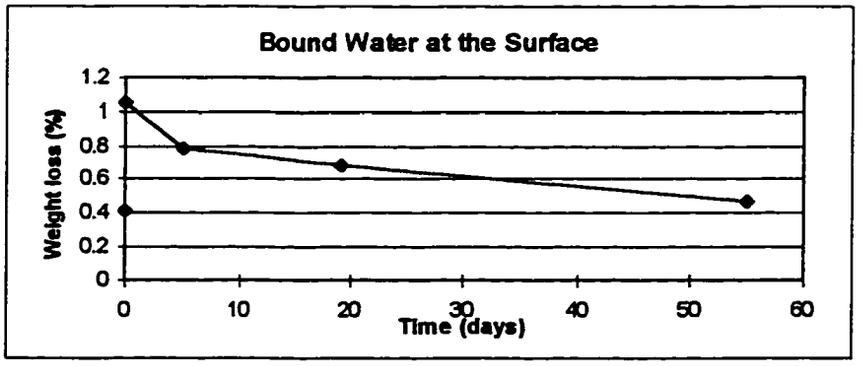


Figure 3.17: Bound water (weight loss between 110°C and 250°C) at the surface: original value, after 2 hours in air, and after 5, 19, and 55 days equilibrating.

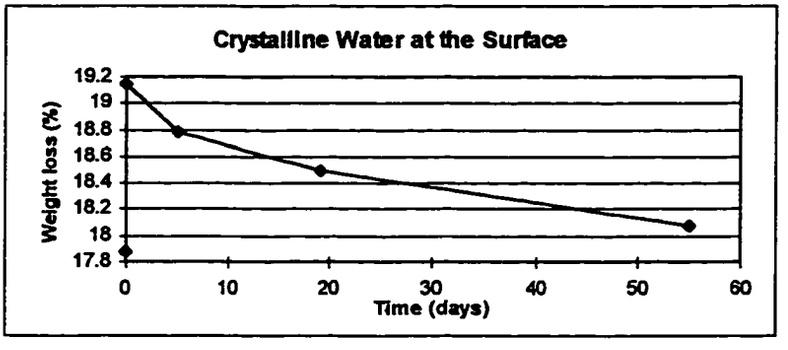


Figure 3.18: Crystalline water (weight loss between 250°C and 800°C) at the surface: original value, after 2 hours in air, and after 5, 19, and 55 days equilibrating.

3.4.5 Dehydration methods

So far, all samples were dehydrated by exposure to air, which permits air to enter the rock as water comes out. A new way to dry a shale sample without exposing it to air is, therefore, necessary to avoid air penetration into the rock and check the influence of capillary effects on shale reaction immersed in

water. The first attempt was to immerse a sample in OBM with a low activity water phase (Hale *et al.*, 1993). The fundamental driving force in this case is the chemical potential difference between the water phase in the OBM and the water in the shale, which creates an osmotic pressure, if an ideal semi-permeable membrane is assumed to exist between the rock and the fluid (Bourgoyne Jr. *et al.*, 1991). Based on the partial molar free energy differences of water among shales and the internal water phase of an OBM, the osmotic pressure generated is:

$$\pi = -\frac{RT}{V_w} \ln \frac{p_w}{p^o{}_w} \tag{3.1}$$

where V_w is the partial molar volume of water, R is the universal gas constant, T is absolute temperature, and p_w and $p^o{}_w$ are the partial pressure of the water vapor and vapor pressure of pure water at the same temperature T, respectively. This equation was derived for an ideal system, and in order to apply the same concepts to non-ideal systems, the partial pressure and vapor pressure terms are replaced by *fugacity*. The fugacity, f_i, of a component *i* in solution is the imaginary value of vapor pressure that would have to be used in Eq. 3.1 to make it apply accurately to a non-ideal system. The ratio of $f_i/f^o{}_i$ also is called the activity, a_i, of component *i*.

Activities of the drilling fluid and of the shale (it is assumed to be the activity of the water in the shale) are then used to estimate the osmotic

pressure generated when these activities are different. The differential pore-pressure resulting from the water activity differences between the shale and the drilling fluid is (Mody & Hale, 1993):

$$\frac{RT}{V_w}\ln\frac{A_{df}}{A_{sh}} = \pm\Delta p \qquad (3.2)$$

where A_{df} and A_{sh} are the activities of the drilling fluid and the shale, respectively, and Δp is the differential pressure generated in the rock. This pressure will be positive if the drilling fluid activity is greater than the rock's activity, and vice-versa.

Immersion in a low water phase activity OBM produced a decrease in the sample's weight; however, it was observed that the wettability of the sample surface was completely modified, in such a way that the sample was no longer water-wet. The surface was so strongly modified that after 48 hours in the OBM, the sample water loss ceased, even when exposed to air. Due to the presence of surfactants in OBM, used as emulsifiers, the mud created an impermeable layer on the surface (see Appendix B for more details in surfactants reaction with clay). The term surfactant is the standard contraction for surface active agent; these agents are adsorbed on surfaces and at interfaces, and lower the surface free energy. These surfactants can be cationic, anionic, or nonionic. Since clay minerals and most rock surfaces are negatively charged (see Appendix A), the electrostatic attraction causes the

cationic surfactants to be more strongly adsorbed. Anionic surfactants are adsorbed at the positive sites at the end of clay crystal lattices and at oil/water interfaces. On the other hand, nonionics compete with water for adsorption on the basal surfaces of clay crystals, thereby limiting the expansion of swelling clays such as bentonite. Then, depending on the type of shale, each surfactant will act in a different way, changing more or less the rock wettability. The OBM used in the test was received already prepared from a drilling fluid company; details about the type of emulsifier used were not disclosed. Due to this strong interaction between the shale and the drilling fluid, this dehydration procedure (dehydration was also not strong enough) could not be used for further evaluation of reactivity of the partially-dried shale with water. Since the surface became oil wet, water was totally repelled.

Assumption of an ideal semi-permeable membrane in this situation is also highly questionable. Further discussion on this topic, and the associated pore-pressure generation due to chemical potential difference is presented in Chapter 6.

Using ethanol anhydrous alcohol[3] was the next attempt. Water loss is more rapid by immersion in alcohol than in OBM and the surface maintains its original wettability. Therefore, sample reaction when immersed in water can be evaluated. Dehydration is conducted by removing the shale from mineral oil, cleaning the excess oil, and immediately immersing it in alcohol. By keeping

[3] The ethanol anhydrous type was chosen because it is safer than methanol, and the anyhydrous would give a stringer driving force to dehydrate the shale sample.

the sample submersed in alcohol, water is free to leave the rock but no air can enter the system. Sample weight is continuously monitored by suspending the immersed sample on a balance. In this way the shale can be kept at its original wettability without permitting air to invade the sample.

Different dehydration methods, including alcohol immersion, were used in order to compare how shale reacts when immersed in water solutions. Weight loss as a function of time was recorded for three situations: exposed to air at 22°C, immersed in alcohol, and immersed in OBM with 0.5 water phase activity (Figure 3.19). When exposed to air, the sample lost 1% of its weight in 2 hours, whereas it took 48 hrs. to lose the same amount of water when immersed in alcohol. Immersion in OBM creates the slowest water loss, and the sample did not lose water any further water after 48 hrs. of immersion, due to the wettability change.

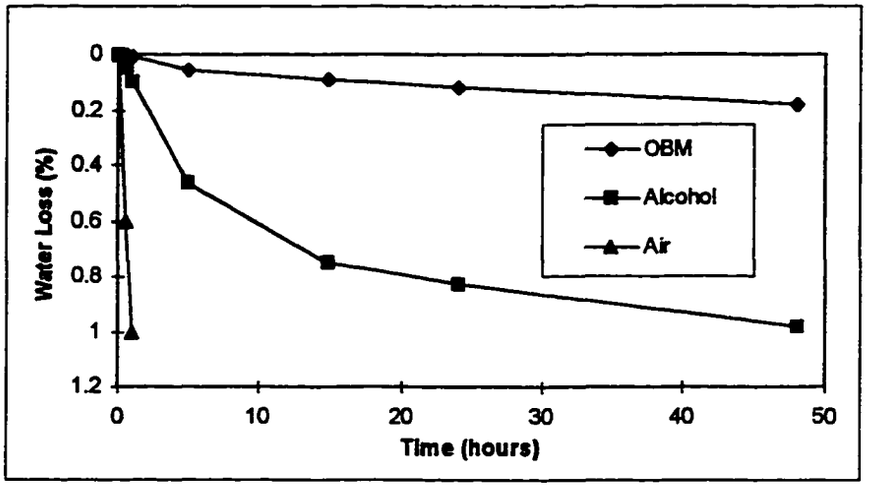


Figure 3.19: Weight loss for different dehydration processes.

It is clear from the results that water evaporation (due to air exposure) is much faster than removal of water induced by chemical potential (immersion in alcohol and in OBM).

For samples dehydrated in air, visible cracks were generated after less than 30 min. of exposure. If the drying process is too fast (as is the case of exposure to air), the shale structure cannot adjust to the new volume quickly enough to prevent cracking. According to Schmitt *et al.* (1994), when drying a specimen of shale or clay the release of water may first induce pore contraction, allowing the rock to remain saturated. These authors add that upon further drying, the compressibilities of pores can no longer accommodate the water loss, the air-entry point is reached and the sample saturation decreases. As cited in Schmitt *et al.* (1994), the experimental work of Biarez *et al.* (1987) and Ed Diny *et al.* (1992) shows clearly such phenomenon. The sample cracking starts when the compressibility of pores can no longer accommodate any further water loss.

If these samples are immersed in oil for 2 weeks (allowing water redistribution), the cracks are no longer visible to the naked eye. The water that had quickly evaporated was slowly replenished, and the clay minerals and the shale increase their volume, partially recovering the original one. The increase in volume closes the cracks, at least for the naked eye.

Dehydration in alcohol does not cause visible cracking. As the removal of water is not as fast as in air (as indicated by Figure 3.19), the rock structure does not suffer a violent contraction. Even though redistribution of water is a

slower process, the structure has time to rearrange without the sudden volume change that causes the cracks to form.

3.4.6 Shale reaction in air-free samples

In order to investigate which factor, presence of air (capillary effects) or lack of water, is actually controlling shale reaction, a sample was dried while immersed in alcohol until 1% weight loss was reached (1% weight loss permits comparison with the samples dried in air). In addition, the piece used in this test was also taken adjacent to the three earlier samples (see section 3.4.4). At 1% in weight loss, the sample was removed from alcohol and immediately immersed in de-ionized water.

The reaction pattern here was very similar to the one dried in air when water redistribution was permitted (Figure 3.14).No strong surface reaction was observed, but after 49 hours, the sample again broke into three pieces (Figure 3.20).

It is clear that such reaction is similar when samples lose equivalent amounts of total water and, most important, when water distribution is almost the same (compare Figure 3.20, Figure 3.14, and Figure 3.13). Even without permitting air to enter the sample, the rock still reacts. The reaction observed can only be attributed, therefore, to the fact that original water has changed in the sample. In other words, presence of air in sample (Figure 3.14) does not affect reaction in shale.



Figure 3.20: Shale reaction after dehydration in alcohol - no air allowed in the sample.

3.4.7 Mechanical work

Observations indicate that when mechanical work is done onto a sample, the surface reaction varies. For example, a thin powder is generated on a saw cut surface when a preserved sample is immersed in de-ionized water, whereas on a pre-existing surface where no mechanical work has been done, no reaction is observed (Figure 3.21). Water content was determined on different mechanically-induced and naturally-opened surfaces (Table 3.7). It can be seen that the amount of all three types of water is affected by doing mechanical work. While free and bound water are reduced, crystalline water increases. Reduction in bound water goes in an opposite direction compared to the results obtained after the sample had been dried in air. Change in crystalline water is an indication that damage on the surface was so severe that it affected

the structure of the rock. With the material on this surface being different from the natural one, a different reaction was expected. In addition, this mechanically-damaged surface was also dried. After the thin powder has been generated and removed from the damaged surface, no further reaction was observed, once the sample regains its original state.



Figure 3.21: Comparison between mechanically cut and naturally opened surfaces — a thin powder is generated on the mechanically opened surfaces (light color) whereas nothing is observed on the other one.

Table 3.7: Water content on different surfaces (mechanically prepared and natural).

Surface description	Free water (%)	Bound water (%)	Crystalline water (%)
Natural	6.964	0.738	18.57
Mechanically opened (sample 01)	6.193	0.413	21.86
Mechanically opened (sample 02)	5.808	0.582	21.07

Another observation was the generation of small pieces ($\cong$ 1 mm^3) on the surface of a preserved sample when a penetrometer is used to measure

strength. Application of stress with a penetrometer on a preserved sample surface apparently causes a mechanical disturbance to a small portion of the surface. When this sample was immersed in de-ionized water small pieces reacted and detached from the sample. The stress concentration applied by a penetrometer locally alters the structure of the shale. The altered shale then reacts with the water. Even though no water content results are available for these small pieces, an association with the previous observation, where mechanical work changes water content and affects reactivity, is justified.

Even though mechanical damage might have great influence during drilling a well (both the bit and the drill string produce damage) it was observed that the damage is very superficial. In addition, when a dilute (KCl) solution is used, no reactions were detected. Due to this minor impact in the reactivity relevance, these mechanical effects were not further investigated in this dissertation. However, these observations were crucial to correctly interpret the immersion tests conducted under pressure (see Chapter 5).

3.5 How water content and distribution control shale reactivity - preliminary reflections

It has been shown that the water present in a shale greatly influences how the rock reacts when exposed to a water solution. In shale, water plays a completely different role than in other sedimentary rocks, such as sandstone.

Not only crystalline water, but also bound water are part of the shale structure.

An imbalance of the intermolecular surface forces (attractive van der Waals, attractive ion-ion correlation, repulsive electric double-layer, and oscillatory or even monotonic repulsive hydration; see Appendix B for more details on these intermolecular forces) holding the shale structure in equilibrium is caused by any modification in the original water content, composition, and/or distribution in the shale (Diek & Santos, 1996).

In a well-preserved shale sample the charges on the internal and external surfaces of the clay particles are balanced. The interlayer hydrated cations form stable complexes with discrete two-dimensional water layers (see Appendix A). The balanced intermolecular surface forces are mainly attractive van der Waals, ion-ion correlation, repulsive electric double-layer, and oscillatory hydration forces. Any changes in the structure, or order of water adsorbed on the bare clay surface, or to interlayer cations, can cause additional repulsive forces called hydration forces that can generate crystalline swelling upon rehydration. In addition, salt dilution by taking up water by the partially-dried rock increases the magnitude of the electric double-layer forces and decreases the effects of attractive ion-ion correlation forces. As swelling progresses, surface separations increase and van der Waals attraction dies out. Therefore, upon rehydration of a partially-dried shale, the increase of repulsive hydration forces and electric double-layer forces outweighs the

attractive forces, leading to crystalline and osmotic swelling, respectively (Diek & Santos, 1996).

The following scenario may explain the redistribution of water and the modification of clay structure in a dried shale sample. As a shale sample dries in ambient conditions, the free or external water at the surface escapes first from the structure. This creates a temporary imbalance of relative humidity between the surface and the interior of the sample. The activity of free water at the surface is lower than in the interior. A chemical potential difference transports free water from the interior to the surface to equilibrate the relative humidity. If the sample is not allowed to dry further, i.e., by immersion in mineral oil, a new equilibrium of the relative humidity of free water in the whole sample is reached. Nevertheless, the new relative humidity (or activity) of the free water that remains in the external structure (macropores and interaggregate pores) is lower than that of the bound water in the internal structure (interlayers) of expandable clays, which is unchanged from the original sample. A chemical potential difference sets up a slow transport of bound water into the external structure until, if allowed enough time, a new equilibrium is attained when the relative humidity of the free and bound water are balanced with the intermolecular forces holding the water in the interlayers of clay minerals.

This process can irreversibly modify the clay microstructure of the shale sample. As the bound water desorbs and moves out of the interlayers, the two clay unit layers move closer together, come into adhesive contact, or even

reorient into a different configuration. All these manifestations depend on the amount of bound water withdrawn and the resultant modifications in the chemistry and physics in different portions of the interfaces (Diek *et al.*, 1996):

(a) increase of salt concentration leads to an increase in screening of the double-layer repulsion;

(b) dehydration of clay sheets and decrease in density of the bound water reduce the hydrophilicity of the surface and thereby the repulsive strength of hydration forces;

(c) presence of highly polarizable multivalent counterions within the diffuse double layers, and/or the discreteness of surface charges, increases the attractive ion-correlation forces;

(d) reduction of the separation between the clay layers enhances attraction and reorientation effects of van der Waals forces;

(e) surface potential, or charge of the clay unit layers, is lowered by increased ion binding.

The same forces operate on clay particles to stack them together into aggregates, to hold them together, to break aggregates apart, and to reorient particles within aggregates. The resultant shale fabric depends on the balance between forces operating to attract and hold particles together and those tending to disperse them (Diek *et al.* 1996). In turn, these forces are modified by the native water type and content (Diek & Santos, 1996). In addition, large surface tension forces occur at air/water interfaces in the clay matrix when

drying in air (Greene-Kelly, 1973), which, in turn, can lead to destructive retraction that damages the texture or fabric. Upon rehydrating a dry shale sample, the original internal micro-structure, including flaws or discontinuities, is not recovered. The readsortion of water into the internal structure can cause instabilities that lead to swelling and dispersion in the shale sample

Mineral composition of the shales tested indicates a low percentage of reactive clay minerals (< 8% illite/smectite). Although the results presented here cannot be extrapolated to cases with high smectite content, a speculation of what might happen can be made. For shales with a high content of reactive minerals, the critical amount of water loss, after which the structure is modified, should be much smaller than in a shale with a low content of those minerals.

It should be remembered that all results and observations presented here were made on the same type of shale, from pieces taken from the same core and from locations very close to each other. This permits comparisons for the different states tested to be valid.

For some time, swelling mechanisms observed in laboratory tests have been questioned (Santarelli & Carminati, 1995), and the idea that they may be a consequence of laboratory artifacts is fully supported by the results shown here. The artifact, however, is not only due to the presence of air in the shale but mainly due to loss of water, causing shale to become reactive, as shown in the experiment in which the sample was dehydrated immersed in alcohol.

3.6 Shale preservation and laboratory sample handling recommendations

Based on results described here, shale preservation and sample handling are two critical issues. Due to extreme sensitivity to air exposure, shales should be kept and manipulated in such a way so as to minimize such exposure. Wrapping with paraffin and immersion in mineral oil are the two most popular preservation techniques used today by the oil industry.

Preservation with paraffin involves a labor intensive procedure and, most important, exposure of the rock to air for some time. Exposure to air occurs every time the rock is unwrapped to prepare samples (cut the core, drill plugs, etc.). In order to save the remaining and unused pieces it is necessary to wrap them again. Therefore, the rock has already been exposed to air long enough to be somewhat dried. Another problem is that the paraffin does not always seal the rock completely. Paraffin is sometimes broken and humidity is lost. Also, storage of big pieces is not practical with paraffin. Consequently, wrapping with paraffin is not an appropriate way to store shale samples.

So far, the best preservation method is immersion in mineral oil. Contact with mineral oil does not alter the shale wettability, and oil does not prevent shale from reacting when a partially dried sample is in contact with water. Any use of chemicals (other than mineral oil) should be preceded by an analysis of how they affect shale properties. The biggest advantage of preserving shales

immersed in mineral oil is that, even when the rock is temporarily removed from the oil, a thin film of oil covers the sample, minimizing humidity loss. The procedure is very simple and does not require any equipment beyond containers and oil. The containers should, however, be checked periodically for leakage.

Immediately after the core arrives at the rig floor, mud should be removed with cloth and mineral oil, and the core should be put in a container filled with mineral oil (Figure 3.22). The container should be leakproof and well sealed. Transport to the laboratory or storage place should be done only after assuring that the containers are in good condition.



Figure 3.22: Fiberglass container used to preserve shale cores since the time they arrived at the rig floor. Sealing must be periodically checked for any leakage.

In order to guarantee good experimental results, handling procedure in the laboratory is another critical point. Several tests demand long sample preparation time. Even if the shale arrives at the laboratory in well-preserved condition, long exposure during preparation will dehydrate the shale, so the actual rock being tested does not represent the in-situ rock. As stated before, procedures to restore humidity should be avoided. Therefore, it is absolutely necessary that extreme care be exercised during sample preparation (preservation in oil helps here). The sample should remain surrounded by oil until the beginning of the test.

Cutting and drilling of cores should be done with the rock submersed in mineral oil. Both the plugs and the remaining pieces of the core should be immediately immersed in mineral oil again once the operation is completed (Figure 3.23). Every test should be reevaluated and procedures adapted to guarantee that the sample is not exposed to air for a long time.

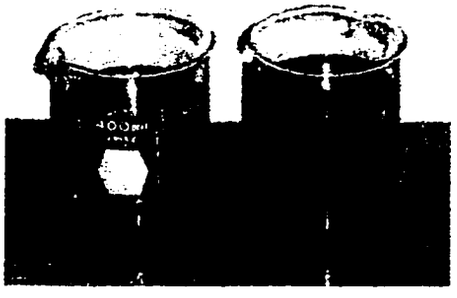


Figure 3.23: Pieces cut from cores are immediately immersed in mineral oil, and kept immersed until the beginning of any test.

This laboratory handling procedures and guidelines were used to design the more sophisticated tests described in Chapters 5 and 6, so that all the results be representative and not biased by introduction of handling artifacts.

3.7 Practical implications and consequences

Results shown here suggest that some procedures currently used in determining shale properties should be reevaluated. Only well-preserved samples should be used in testing conducted to better understand downhole behavior. Procedures that change water content of shales by trying to resaturate the rock should be avoided. Tests where dessicators are used to modify water content in shales to study rock-fluid interaction can give biased information. Mechanisms observed under these conditions do not represent downhole behavior.

If good preservation cannot be guaranteed, it is not worth running laboratory tests. All laboratory test procedures should be redesigned to guarantee sample preservation until the moment the test starts.

By knowing that a preserved shale does not react when immersed in de-ionized water it might be thought to be unnecessary to use complex muds to drill. It is obvious that this is not the case. Several additives are used for purposes other than preventing shale instability. What is essential, though, is a deeper understanding of how each additive performs together with other additives in a solution, and if their presence actually contributes to what the additive is designed for. When testing drilling mud suitability, most of the time

dried or partially dried shale samples are used, and drilling mud is selected by analyzing its reaction with these dried samples. This is obviously a poor approach; the mud selected using this method will not, necessarily, behave in the observed manner under downhole conditions. Cuttings might be used for this purpose only if a good preservation and removal of the contaminated layer can be assured.

If sample preparation requires keeping the sample in air for a few minutes, it is necessary to interrupt the procedure from time to time and reimmerse the sample in oil. This procedure is much simpler than using a special room with controlled humidity, and it is recommended for each laboratory test on shales.

Redistribution of shale water is another important issue when dealing with shale. The ideal situation is to completely avoid drying. In reality, however, some water will be lost during sample preparation. Water loss should be monitored to evaluate the sample state (amount and distribution of water) before running tests, especially reactivity tests. After preparing the sample and before running the test, enough time should be allowed for the water in the rock to equilibrate, otherwise differential reactivity may occur. There may be a critical amount of water loss beyond which the shale is strongly affected. Even though not quantified here (specific tests should be designed and conducted for this purpose), from the results obtained so far this amount of water might be small.

Alcohol is a good way to dehydrate shale without introducing air into the sample. Oil-base mud changes surface wettability and cannot be used as a

dehydration environment for further evaluation of shale reactivity, as suggested by Hale & Mody (1992).

3.8 Summary

Just a few years ago water content was identified as one of the main properties controlling shale reactivity in the laboratory. Partially dried shales behave differently than saturated shales when in contact with water solutions. Presence of air in the rock was thought to be the main cause of shale reaction, due to capillary pressure generated by the entrapped air. The experiments described in this chapter, conducted on well-preserved downhole shales, identifies the amount and distribution of water, rather than air in the sample, as the key property that actually controls shale reactivity. A new methodology for determining water content is proposed. Not only free water but also bound and crystalline water can be determined, using small samples. Movement of water in the sample as the shale dehydrates was observed with this new methodology. Several different tests were conducted and evidence is that shale reaction, when immersed in water, is controlled by both the amount and the distribution of water in the sample. A technique to preserve shale samples in their in-situ condition, as well as a laboratory handling procedure, are proposed. Furthermore, an industry wide, standard procedure should be adopted in order to be able to compare shale laboratory test results done in

different laboratories. Finally, practical implications to drilling mud selection, laboratory testing, and other applications are discussed.

Chapter 4

4. Shale Characterization with Thermal Analysis

4.1 Introduction

Shale-fluid interaction has been studied for a long time, using both simple (immersion with visual inspection, for example) and sophisticated tests (linear swelling and swelling pressure tests) (Darley & Gray, 1991), with the aim of selecting a drilling fluid composition capable of avoiding stability problems. However, results of shale composition after it has been contacted by a fluid are very few (Santarelli & Carminati, 1995), even though this information is crucial to monitor rock-fluid interaction. Lack of a simple and inexpensive methodology to characterize shales might be the most important reason for the absence of such results. The technique normally used by the industry, X-Ray diffraction (XRD), is relatively expensive (more than US$ 100.00/per sample),

requires special and sophisticated equipment, specialized personnel to operate and to interpret the results, and the results do not include characterization of the water associated with the different clay minerals. This last limitation is, for shale-fluid interaction studies, the most important one. It has been shown in Chapter 3 that water is an important component of clay minerals (being present in different ways: free, interlayer, bound, and crystalline), playing a decisive role in controlling the reactivity of a shale when in contact with a water solution. It has also been shown that the water in a shale, both its amount and distribution, actually controls the rock reactivity.

Search for a simple, quick, cost-effective, and detailed characterization technique pointed towards thermal analysis. Thermogravimetry (TGA) provides detailed information about the rock composition, so that it can be used in shale-fluid interaction studies. The technique can be used both in the laboratory and in the field, using cuttings or cores. Use of cuttings should, however, be done with extreme care, due to the possible contamination with drilling fluid. Contamination removal must be guaranteed in order to ensure characterization of the native rock. Shale alteration when in contact with different solutions can be monitored, providing a powerful method to screen drilling fluids. The methodology herein proposed has been available for quite some time (Wendlandt, 1986; Daniels, 1973; Todor, 1976; Bish & Duffy, 1990), but not for characterizing the water distribution in the clay minerals and the shale structure. In the oil industry, however, its use has been very

limited, just for determination of the free water content, but not reported in the literature.

This chapter initially presents the limitations of the XRD method, with controversial results obtained from 3 different laboratories. A brief description of TGA is given, followed by the proposed methodology. Results for different rock types and minerals are presented, showing the capability of the technique to identify detailed and important shale characteristics. Some applications are suggested and discussed.

4.2 Limitations of the XRD Method

XRD is the most widely method used to characterize the composition of rocks because, being a semi-quantitative method, it gives the relative amount of each mineral present. Based on the rock composition, decisions regarding the types of drilling and completion fluids are usually made. The method, however, has several limitations. Restrictions that the samples are usually not properly preserved, the different water types inside the shale cannot be characterized which led to searching for a new technique. In order to effectively understand the shale-fluid interaction mechanisms, a detailed characterization methodology is needed, so that not only the change in the different water types, but also in the minerals could be detected. Clearly, the XRD method is not the most appropriate technique for such detailed characterization.

Also, in order to check the reproducibility of the method, a blind test was carried out among laboratories of three big companies, including operating and service companies. Fooks & Dusseault (1996) presented mineralogy results for the Pierre I shale showing also discrepancies among the sources. However, since those results were not obtained from the same shale piece, it was not possible to conclude about the reproducibility of the XRD method. Adjacent pieces of core from 8 different wells were, then, sent to each laboratory, from 8 different wells. Four wells were from the Campos Basin, in Brazil, and the other four from the Gulf of Mexico (offshore south Mexico). Results from two laboratories show good agreement, but the third one is completely different (Figure 4.1 to Figure 4.8). Both the amount of clay minerals, and specifically the quantity of smectite and illite, indicated more than twice the values reported by the other two companies. One laboratory reported that shale B contained 69% of clay minerals, whereas the other two reported 30 and 32%. For the smectite content, the result was 30 in one case, and 12 and 13 for the other two laboratories. For shale D the results were similar. Total clay content of 60%, in contrast of 20 and 21 %. Disparity in the smectite value is even worse: 38% versus 9 and 8%. Shales C and D have the trend, even though the discrepancies are slightly smaller. All the shales from the Campos Basin have high calcite content (Figure 4.1 to Figure 4.4), especially shales C and E. Designation of each laboratory is the same for all the results presented herein. Laboratory A is the same laboratory in all the charts, as well as B and C.

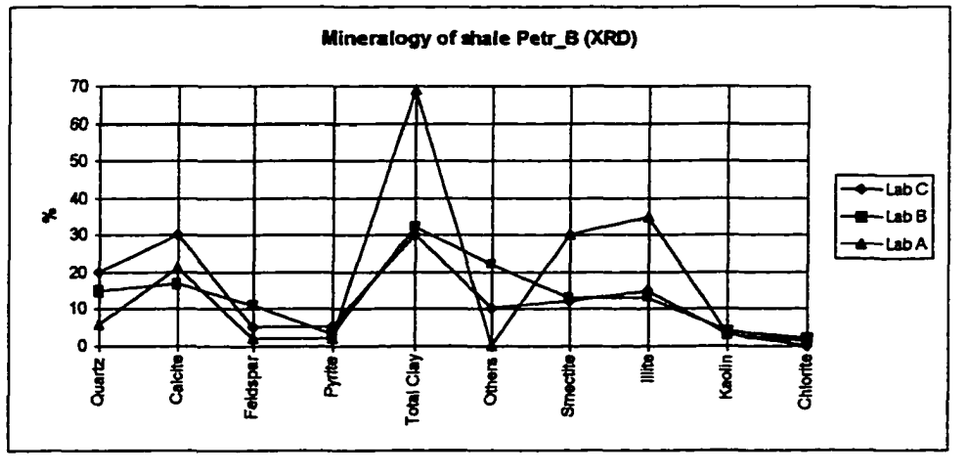


Figure 4.1: XRD mineralogy of shale Petr_B: Total clay = smectite + illite + kaolinite + chlorite.

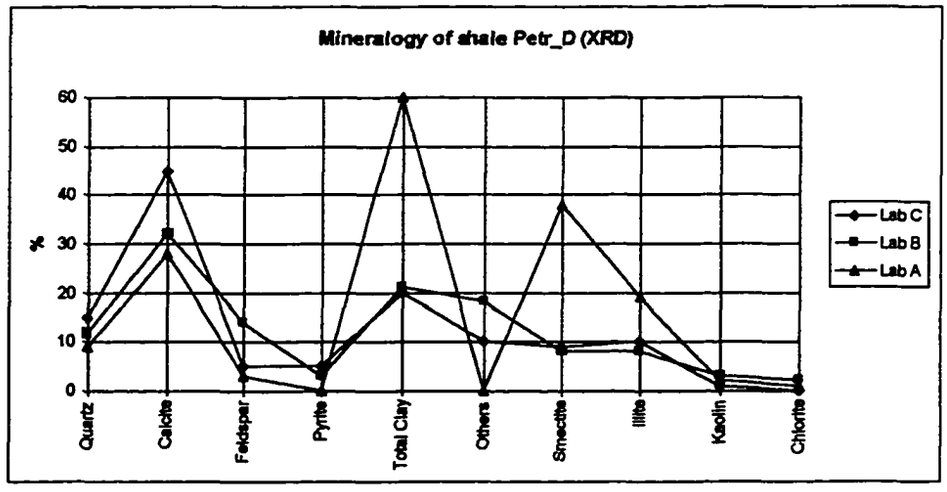


Figure 4.2: XRD mineralogy of shale Petr_D: Total clay = smectite + illite + kaolinite + chlorite.

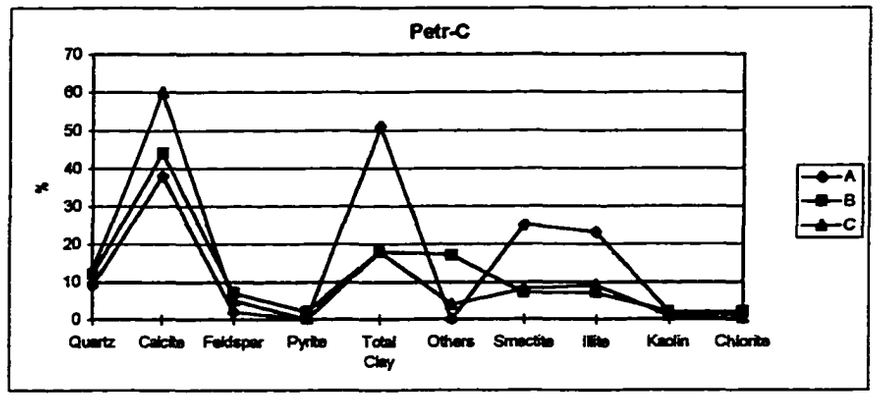


Figure 4.3: XRD mineralogy of shale Petr_C: Total clay = smectite + illite + kaolinite + chlorite.

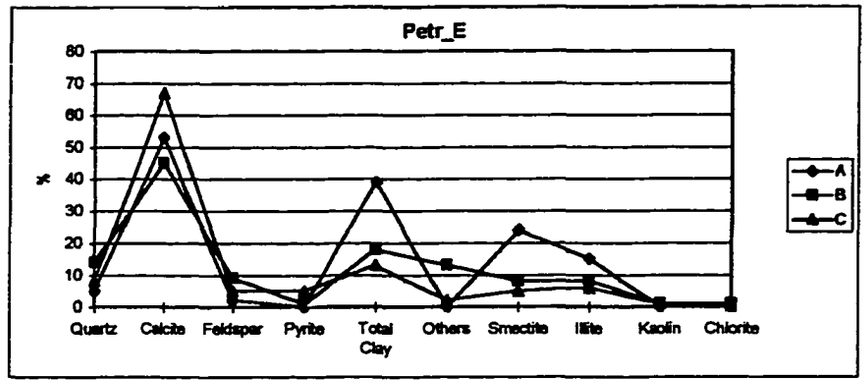


Figure 4.4: XRD mineralogy of shale Petr_E: Total clay = smectite + illite + kaolinite + chlorite.

Shales from the Gulf of Mexico have very different composition, with low calcite content, and very high clay content (Figure 4.5 to Figure 4.8). However, the same discrepancies persist. Laboratory A reported much higher values for total clay and smectite and illite content. In some cases, the difference exceeds 200%. Laboratories B and C reported closer results, as in the shales from the Campos Basin.

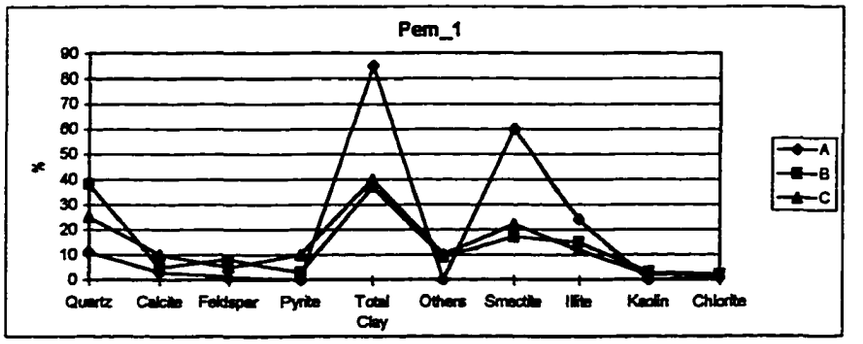


Figure 4.5: XRD mineralogy of shale Pem_1: Total clay = smectite + illite + kaolinite + chlorite.

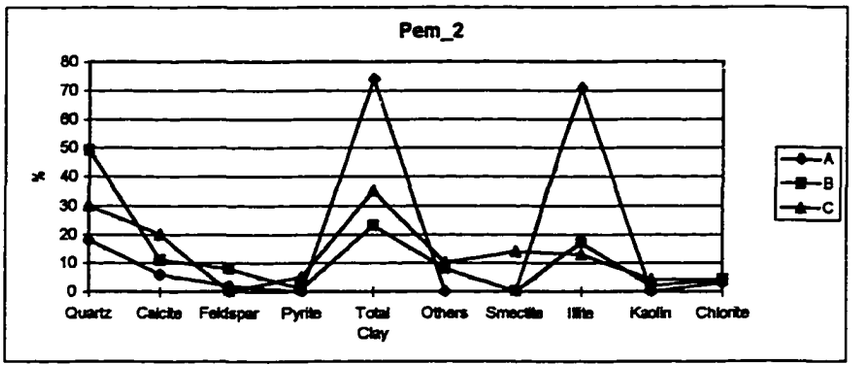


Figure 4.6: XRD mineralogy of shale Pem_2: Total clay = smectite + illite + kaolinite + chlorite.

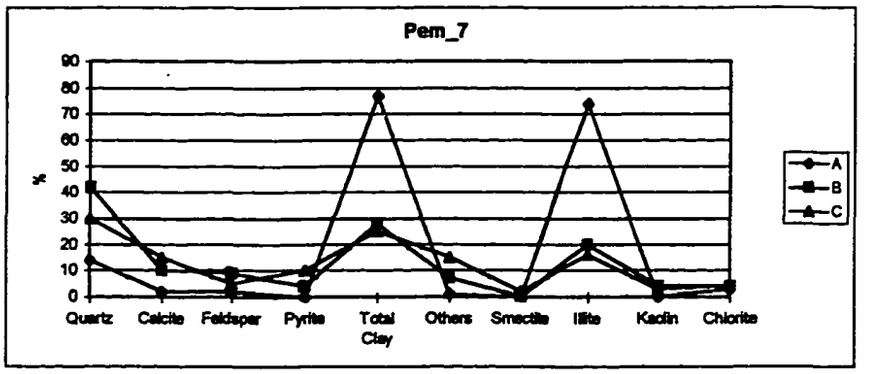


Figure 4.7: XRD mineralogy of shale Pem_7: Total clay = smectite + illite + kaolinite + chlorite.

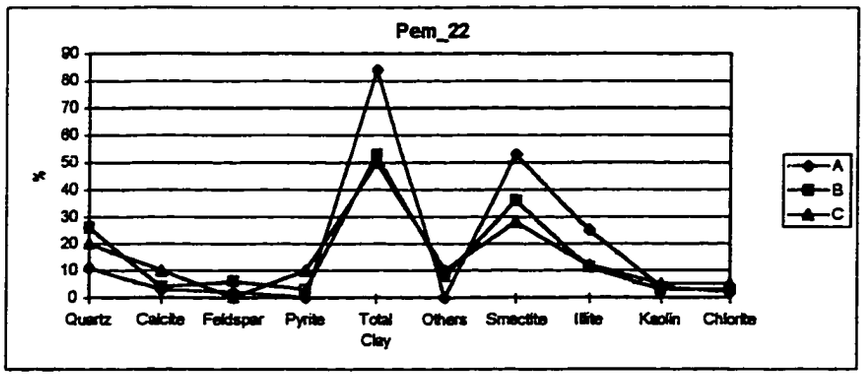


Figure 4.8: XRD mineralogy of shale Pem_22: Total clay = smectite + illite + kaolinite + chlorite.

It is reasonable to expect some discrepancy among the results, but the variation should be within a reasonable range. Since shale reactivity is usually associated with clay and smectite content, depending on the laboratory in charge of conducting the analysis, the conclusion would have been that shales B and D are highly reactive, or they have a very low potential to react with water. In the first case, the decision would be to use a lot of additives or even an OBM, increasing the mud cost, whereas in the second case a cheaper fluid could be used without major problems. These conflicting results show one should not just rely on this test to select a drilling fluid.

4.3 Thermal Analysis as a Characterization Tool

Thermal analysis offers an interesting alternative to characterize sedimentary rocks. Even though thermal analysis comprises a group of techniques, TGA alone was found to give enough information to qualitatively characterize a

rock. With further development and addition of other techniques, such as Differential Thermal Analysis, a quantitative methodology can be achieved. Despite the fact that some minerals can be quantified with TGA, the focus is on a qualitative method since an accurate quantification of all the minerals present in the rock with TGA is still difficult. Mass loss for each mineral transformation reaction must be defined so that a quantification of the mineral's amount be done. As it will be seen, since the rock is composed of several minerals mixed together, accurate isolation of all events is not always possible. A procedure to quantify the amount of mineral in the rock from the TGA results is presented here; even though it might be difficult to quantify all the species present in the rock, it might be possible to quantify some of the minerals. It only depends on the TGA results, as it will be seen later.

The advantages of TGA are various:

. it allows characterization of the different types of water in a shale: free, interlayer, bound, and crystalline;

. preserved samples can be tested;

. it requires very small samples (10 to 50 mg);

. the test is fast, taking less than a couple of hours;

. the equipment is simple (no requirement of specialized personnel or intensive training);

. the interpretation is straightforward;

. the test is inexpensive (less than US$ 1.00/per sample, excluding equipment depreciation and labor cost to run the test).

TGA determines the mass of a sample as a function of its temperature. As temperature increases, thermal reaction occurs and mass is lost as species become volatile and are removed from the sample. Sample weight is measured with a very accurate balance, placed inside a furnace, and an inert gas (typically nitrogen) is used to remove evolved gases. Different heating rates can be used, depending on the information needed, and even different temperature methods have been proposed (Chapter 3) to determine the water content in a shale. Even though it is a simple technique, TGA results are influenced by several factors (Wendlandt, 1986; Daniels, 1973; Todor, 1976):

. sample size: if pieces are used as samples, as the size increases, difficulty in liberation of the evolved gas from any reaction also increases. In some cases, reaction might not be totally completed if the piece is large and the temperature increase is too fast;

. heating rate: as pointed out before, if one uses a very high heating rate it might be possible that the reaction inside the sample would be incomplete. Also, the temperature for which each reaction is being processed cannot be precisely determined if a fast increase in temperature is used. A slow heating rate assures that the reaction will be completed. A compromise between experiment time length and accuracy must always be in place. Usually, a heating rate of 10°C/min. or 20°C/min. is used;

. furnace atmosphere (N_2, air, or other gas): the gas evolved from the sample should be removed immediately to avoid interference. The gas used to purge creates an environment around the sample that can react with the rock.

In order to avoid any reaction with the rock, an inert gas (nitrogen) is preferred. If air is used, for example, oxi-reduction reactions might be induced, changing artificially the test results;

. sample arrangement: powder distribution on the testing pan is another important consideration. If a large sample is used (more than 80 mg, for example), the powder will be arranged as a mountain, creating the same problem as described in the first item (sample size). Therefore, it is essential to guarantee an even distribution of the sample on the pan, so that any gas can be easily removed from the sample;

. sample particle size: by reducing the size of particles in a rock its structure might be permanently affected. As a consequence, any grinding or crushing procedure to prepare samples should be avoided. This is especially important when testing shales since water is part of the rock's structure.

Despite the fact that TGA is influenced by all these factors, by consistently following a common procedure, results can be easily reproduced. In order to minimize influence of sample size and shape, it is suggested that a powder sample be used. The sample can be obtained by scratching the surface of the rock, and this was the method employed to do all the tests presented herein. Absence of confining and pore pressures might influence the results. Unfortunately the TGA can only be conducted under atmospheric pressure. The excess oil (used for shale preservation) on the surface should be removed with paper towel to avoid contamination.

In addition to the mass curve, its derivative with respect to time or temperature is also recorded during the experiment. By keeping a constant heating rate (typically 10°C/min.), the derivative curve indicates different events with distinct peaks. Each peak characterizes a reaction with generation of a gas that is being removed. The importance of the derivative curve is that each mineral has a typical signature, with each peak occurring at a defined temperature. The derivative curve for a sample exhibits a signature that includes different events, since the rock is composed of several minerals, with varying proportions. By comparing the rock signature with the individual minerals curves, their presence can be identified. Quantification of each mineral would be possible by writing a chemical balance for the chemical transformation undergone by the mineral.

The characteristics of shales are most influenced by the constituent clay minerals - smectite, kaolinite, illite, and chlorite. Some shales have a high content of calcite and quartz, feldspar, pyrite, and other minerals are also present in smaller proportions. There is a temperature limit in some TGA equipment (900°C, for the one used here) which limits the identification of some minerals such as quartz, which undergoes reaction and gas liberation for temperatures above 900°C. Therefore, depending on the equipment capability, identification of minerals may be limited. For clay-rich rocks, such as shales, however, this limitation is not important. All the main features can be identified below 900°C. Use of these high temperatures in the experiment has

the solely purpose of characterizing the elements in the rock, and not to reproduce downhole temperatures, that seldomly exceeds 200°C.

TGA results (10°C/min. heating rate) for individual minerals are available in the literature. Kaolinite, chlorite, and Ca- and Na-montmorillonite are shown in Figure 4.9 to Figure 4.12.

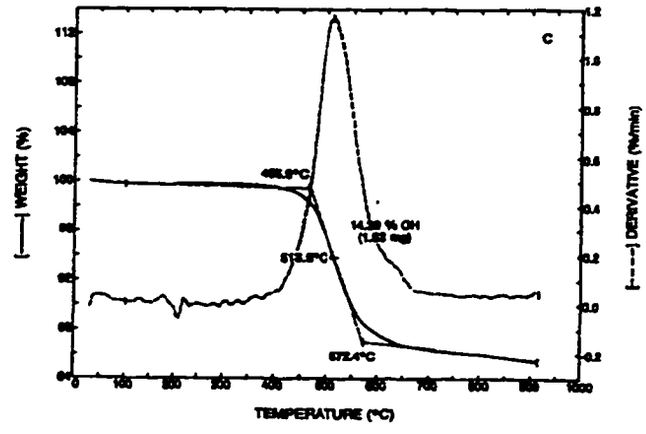


Figure 4.9: TGA curve of kaolinite KGa-1 showing mass loss due to dehydroxylation (10.61-mg sample, 10°C/min. heating rate, 50-cm^3/min. N_2 purge) (Bish & Duffy, 1990).

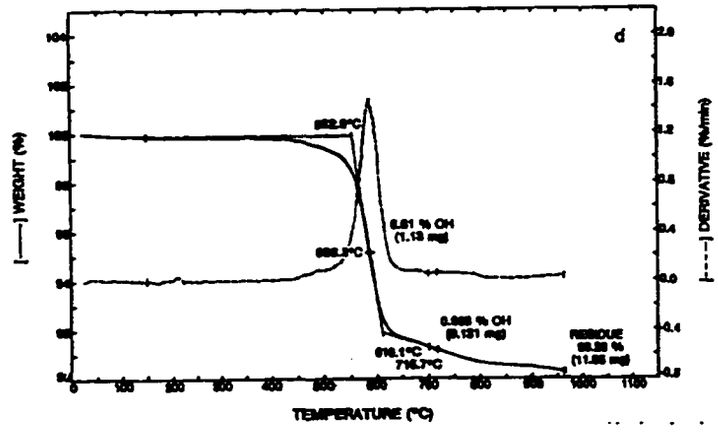


Figure 4.10: TGA curve of ripidolite chlorite, CCa-1, California (13.12-mg sample, 10°C/min. heating rate, 50-cm^3/min. N_2 purge) (Bish & Duffy, 1990).

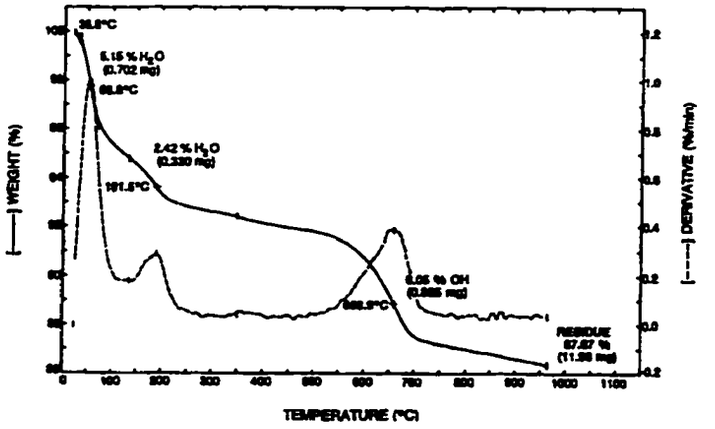


Figure 4.11: TGA curve for smectite SWy-1 (Na-montmorillonite) showing two-stage low-temperature dehydration and dehydroxylation (13.64-mg sample, 10°C/min. heating rate, 50-cm^3/min. N_2 purge) (Bish & Duffy, 1990).

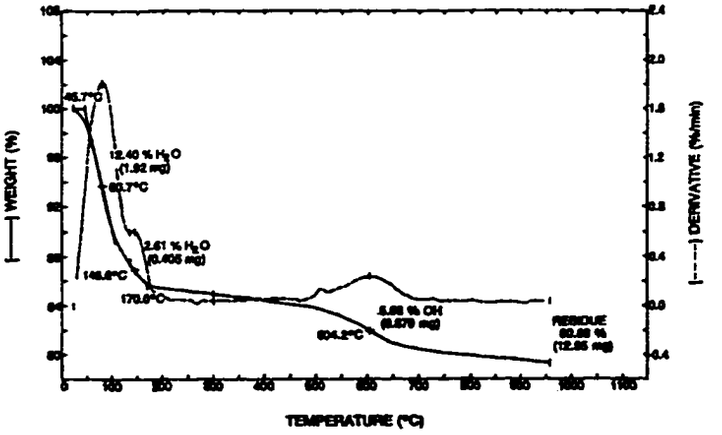


Figure 4.12: TGA curve for smectite SAz-1 (Ca-montmorillonite) showing two-stage low-temperature dehydration and dehydroxylation (15.52-mg sample, 10°C/min. heating rate, 50-cm^3/min. N_2 purge) (Bish & Duffy, 1990).

By heating kaolinite above 500°C, it breaks down to an essentially noncrystalline material, and the reaction can be represented by Eq. 4.1:

$$Al_2Si_2O_5(OH)_4\ (s) \rightarrow Al_2Si_2O_7\ (\text{noncrystalline})\ (s) + 2H_2O\ (g)\uparrow \qquad (4.1)$$

As can be seen from this equation, the mass loss observed when heating kaolinite is entirely due to the loss of water from structural hydroxyls (Bish & Duffy, 1990). All clay minerals show this dehydroxylation, which occurs in a temperature range of 450-900°C. The temperature at which the peak occurs varies depending on the mineral and its composition: for illite and kaolinite it is around 500°C (illites can have a broad spectrum of temperature peaks, depending on its composition); chlorite, 600°C; and montmorillonites, close to 700°C. For montmorillonites, however, the most visible event is dehydration (vaporization of the interlayer water). Smectite dehydration occurs in two steps, differently from the Na- and Ca-montmorillonite. Actually, the type of ion present in the smectite influences the TGA response (Bish & Duffy, 1990). Depending on the type of illite, dehydration also takes place, but to a lesser extent than in smectites. When the minerals are mixed together, smectite/illite, kaolinite/smectite/illite, for example, the events can change drastically. Both dehydroxylation and dehydration are affected. The temperature for the peaks can be completely altered (Todor, 1976), depending on the proportions of each mineral. Presence of organic matter, feldspar, pyrite, and other minerals also affects the accuracy and isolation of each event.

Calcite decomposition starts around 675°C, with the liberation of CO_2. The peak for this event can be seen around 750°C (Figure 4.13, 10°C/min. heating rate). Calcite decomposition follows Eq. 4.2, and the amount of calcite can be

estimated from the mass of CO_2 lost, if the peak can be isolated. According to Wendlandt (1986), the error of this estimation is of the same order as the estimation done by chemical determinations.

$$CaCO_3\ (s) \rightarrow CaO\ (s) + CO_2\ (g) \uparrow \qquad (4.2)$$

Calcite quantification can be done from the equation above, knowing the amount of CO_2 released. 1 mole of calcite will produce 1 mole of CO_2, which can be transformed in grams, adding the atomic mass of each element:

$$1 \text{ mole of } CaCO_3 = 40 + 12 + 3x16 = 100 \text{ g}$$

$$1 \text{ mole of } CO_2 = 12 + 2x16 = 44 \text{ g}$$

Therefore, 100 g of calcite produce 44 g of CO_2. From Figure 4.13, the total amount of CO_2 is 5.06 mg. The amount of calcite in that sample should be, then, equivalent to:

$$\text{Amount of calcite} = (100/44) \text{ x mass of } CO_2 = 2.27 \text{ x } 5.06 = 11.486 \text{ mg}$$

Since the sample has 11.48 mg, the percentage of calcite in that sample is 100%, as expected. A calcium carbonate laboratory sample was also tested in the TGA. The total weight of the sample was 12.27 mg, and the weight loss by CO_2 liberation was 5.138 mg. Repeating the same procedure described above,

the amount of $CaCO_3$ in the sample was found to be 11.66 mg. The calcium carbonate tested was, therefore, not 100% pure, but 95%.

When just one reaction (one peak) is present in the TGA chart, quantification of the mineral can be accurately done. Difficulty arises when several components are mixed together, and the peaks of different reaction overlap each other. The same procedure should be done in order to quantify any element. The chemical reaction should be known, and the peak in the TGA chart must be easily isolated.

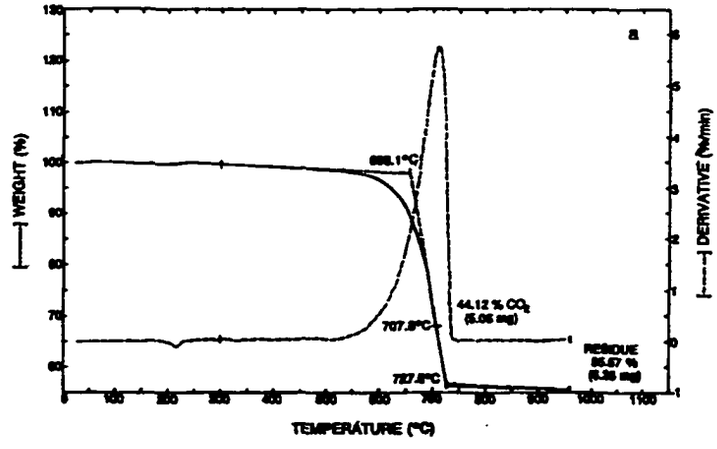


Figure 4.13: TGA curve of calcite showing decarbonation (11.48-mg sample, 10°C/min. heating rate, 50-cm^3/min. N_2 purge) (Bish & Duffy, 1990).

The methodology consists of comparing the TGA chart for the rock with the individual minerals. Figure 4.14 shows the results obtained from testing a brick material, containing smectite, kaolinite, and calcite. Some differences in the temperatures can be observed for which each peak is recorded, when

compared to the peaks of the minerals tested alone. An estimation of the relative amount of each element can be derived from the height of each peak. Quantification of what is being removed from the sample is straightforward (water or CO_2, for example), and is obtained directly from the weight curve. Correlation of these quantities with the corresponding mineral amount, however, can be done for some minerals, if the peak can be nicely isolated. Nevertheless, this is not possible for all the minerals.

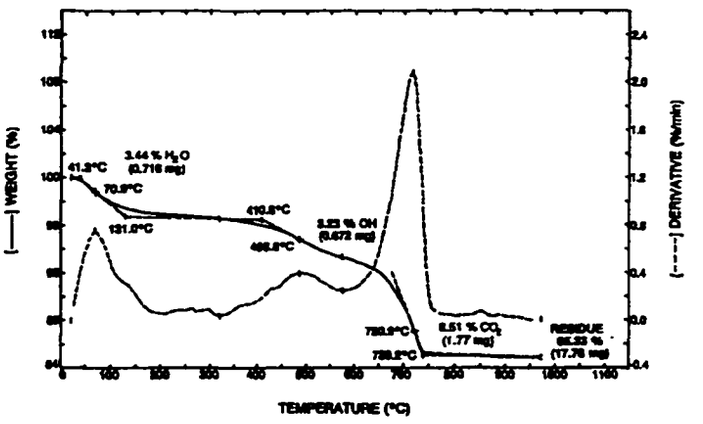


Figure 4.14: TGA curve of brick component from Acme Brick Company, showing mass losses due to dehydration of smectite, dehydroxylation of kaolinite and smectite, and decarbonation of calcite (20.83-mg sample, 20°C/min. heating rate, 50-cm^3/min. N_2 purge) (Bish & Duffy, 1990).

Some TGA equipment have the capability of direct the outflow of gas to a chromatography. In this case, an analysis of the evolved gas is also possible. Knowing which gas is coming out of the sample helps in better defining the reaction being processed inside the shale sample. Unfortunately, the equipment used for these tests did not have this capability ready to be used. A much more

accurate interpretation of the reactions is possible with this additional information.

4.4 Characterization Results

Wyoming bentonite has more than 85% of smectite in its composition and the results obtained from TGA confirms a high amount of interlayer water (Figure 4.15). The occurrence of a single peak in the derivative curve indicates only interlayer water and no free water (the sample tested was dried). Kaolinite is probably present, due to the temperature and shape of the dehydroxylation peak around 550°C. Due to its well-defined shape, the peak around 700°C might indicate the presence of some other clay mineral, illite, for example, or even, dehydroxylation of smectite. Since it occurs below 700°C, it is not probably due to calcite. For calcite, the peak should be around 750°C. It can be, however, due to feldspar. Since this peak can indicate several clay minerals, it is not possible to accurately characterize it. All the results presented herein show the derivative curve with respect to temperature, rather than with respect to time as showed from the pictures collected in the literature. The curve remains practically the same, regardless of with which variable the derivative is calculated.

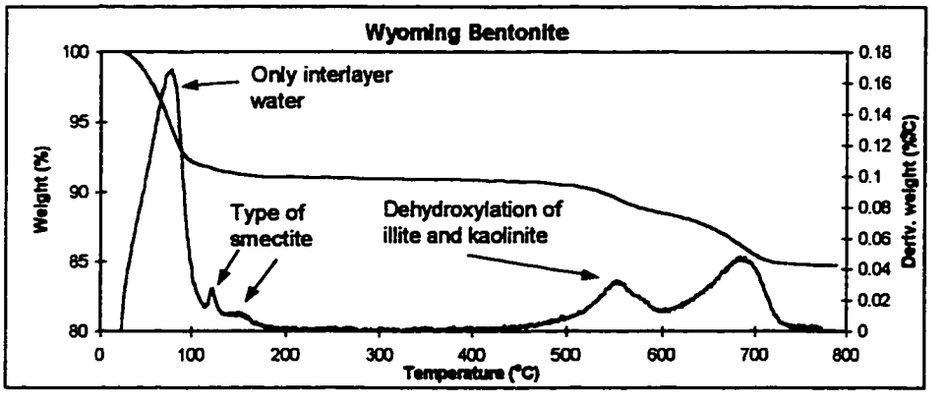


Figure 4.15: TGA of Wyoming bentonite. No free water was found. Top curve: weight retained; bottom curve: derivative of the weight with respect to temperature.

When the minerals are mixed together as in a shale sample, the temperatures for which the peaks are expected might change. Therefore, it is important also to "learn" how to read the results from TGA test on a shale, and XRD results might help to identify and clarify some peaks. TGA tests were conducted with the same shales shown in Figure 4.1 through Figure 4.8 for comparison purpose. It can be seen that Petr_C and Petr_E have a high calcite content, in agreement with XRD results (Figure 4.16 and Figure 4.17). However, clay content does not appear to be as high as reported by laboratory A (low peak due to dehydroxylation between 450°C and 700°C). Results from laboratories B and C tend, then, to be more reasonable.

Presence of smectite in a sample can be detected by observing the derivative curve up to 100°C. Since interlayer water requires more energy to be released than free water, there will be a different weight loss rate for each of these water types. As smectite is the only clay mineral that has interlayer

water, and the peak for the release of this water is around 65°C, an inflection (for low smectite content) or a separate peak (for high smectite content) on the derivative curve indicates the presence of this mineral. Inflection is very pronounced in Petr_C (Figure 4.16). Two distinct peaks of dehydroxylation can be seen, indicating probably illite and kaolinite. The ascending curve between 600°C and 700°C might indicate presence of feldspar. The calcite peak is very well defined. Shale Petr_E (Figure 4.17) has similar characteristics; however, the inflection below 100°C is less pronounced than for Petr_C (signalizing smaller amount of smectite), and it should have a similar smectite type as the one present in the Wyoming bentonite (Figure 4.15, observe peak around 120°C). Again, two peaks of dehydroxylation are observed, indicating some illite and kaolinite. Free water in this sample is greater than for Petr_C (observe height of the peak and weight lost); this can be an indication that sample Petr_C was not as well preserved as Petr_E, confirming information received from the time the cores were taken.

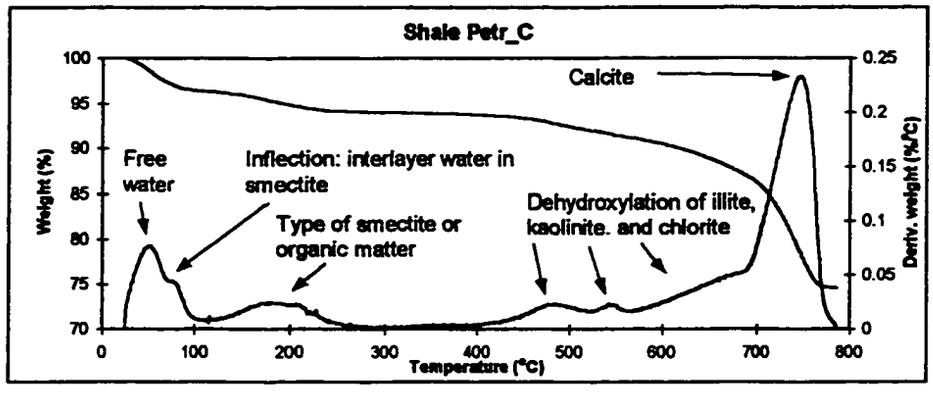


Figure 4.16: TGA of shale Petr_C. Observe free water and inflection due to interlayer water.

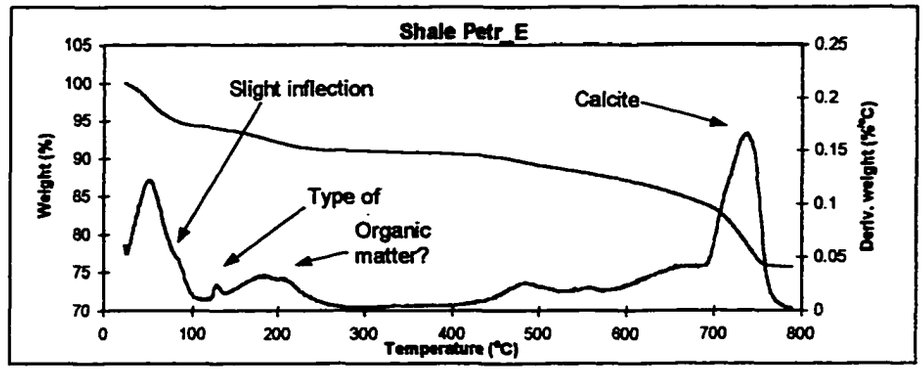


Figure 4.17: TGA of shale Petr_E. Smectite is similar to the one present in the Wyoming bentonite.

Shales B and D also show a high calcite content on the TGA test and a relatively small mount of clay minerals (Figure 4.18 and Figure 4.19). Shale B indicates a smaller amount of free water than shale D. This can be an indication that this shale has gone through some dryness process, at the rig, not strong though. The peak around 200°C found in shale D can be due to organic matter, as well as from clay minerals.

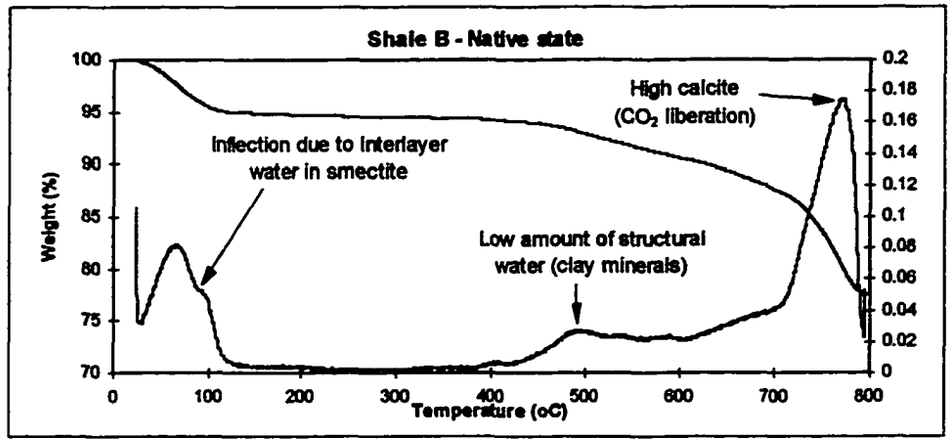


Figure 4.18: TGA (10°C/min.) of shale B - native state - high calcite content.

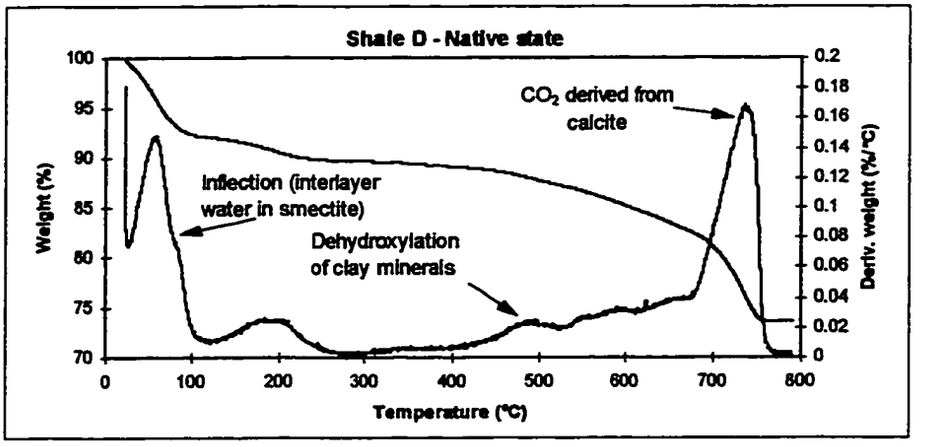


Figure 4.19: TGA (10°C/min.) of shale D - native state - high calcite content.

A more clear observation of different clay minerals is provided by Pem_1, Pem_2, Pem_7, and Pem_22 (Figure 4.20 to Figure 4.23). On one extreme are Pem_2 and Pem_7, with very low smectite content, observed with the quasi-complete absence of inflection on the derivative curve below 100°C. Pem_1 shows a clear inflection and also a peak, slightly above 500°C, indicating dehydroxylation of illite. Pem_22 is on the other extreme. Due to high smectite content, not an inflection, but a separate peak, was detected just below 100°C. The pronounced peak around 500°C indicates dehydroxylation of illite, in great quantity. Just by the shape and temperature of the peaks for dehydroxylation the difference in clay minerals present in these shales can be identified. Pem_2 and Pem_7 are very similar, with all characteristics almost the same. Pem_22 has no indication of calcite. The other three show a peak just below 700°C, that might be feldspar, or more probably a clay mineral, chlorite, another type of illite, or even dehydroxylation of smectite. If this is

the case, no calcite is found for these shales. Laboratory A was the only one to report close to zero values of calcite. In order to better characterize this peak, a reaction with acid should be observed to detect the presence of calcite in these shales. Smectite and illite content reported by laboratory A, however seem not adequate, comparing with the TGA results. Pem_22 shows more smectite than Pem_1. For illite this conclusion also applies, assuming the peak around 700°C is not due to illite dehydroxylation.

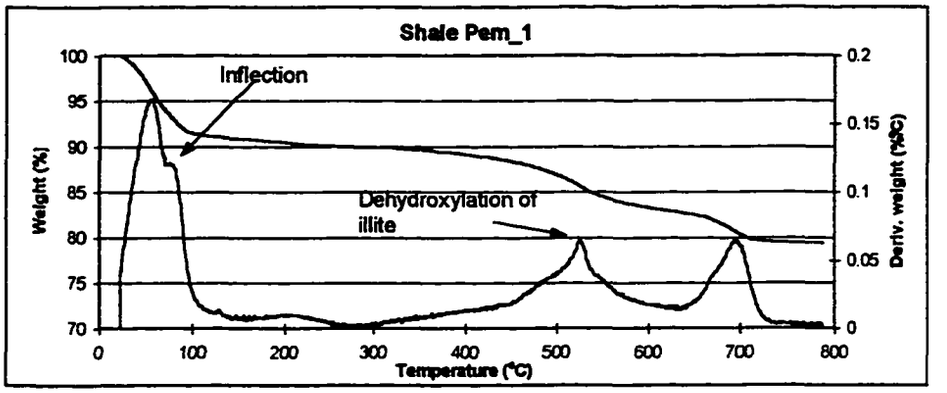


Figure 4.20: TGA of shale Pem_1. Isolated peak for illite, and no presence of calcite.

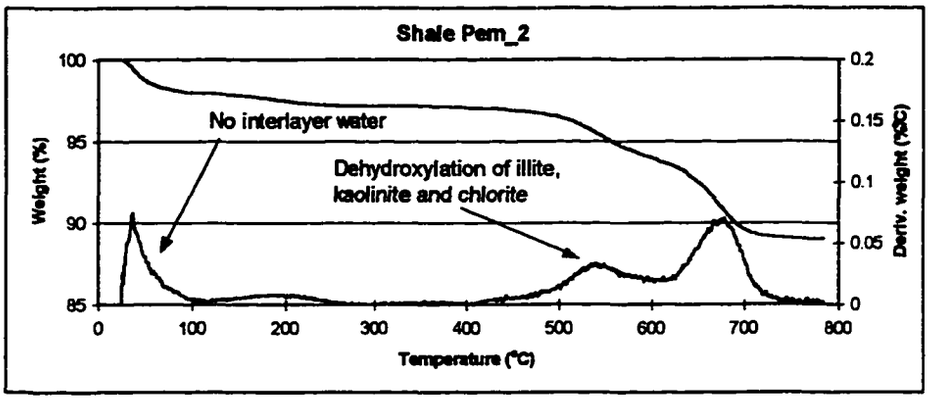


Figure 4.21: TGA of shale Pem_2. No interlayer water signals absence of smectite.

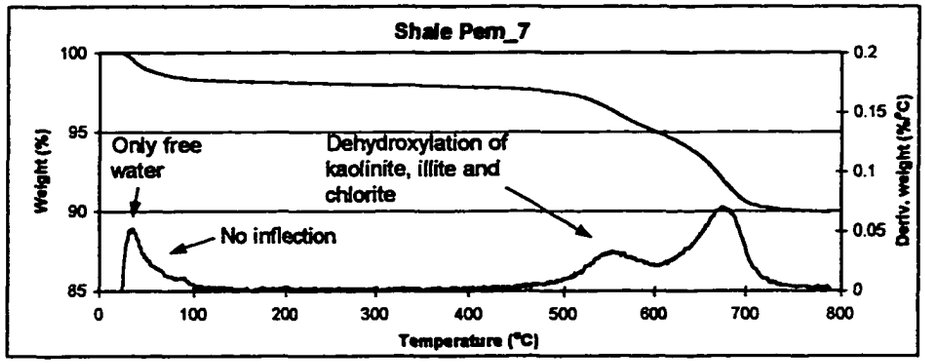


Figure 4.22: TGA of shale Pem_7. Similar to the previous one.

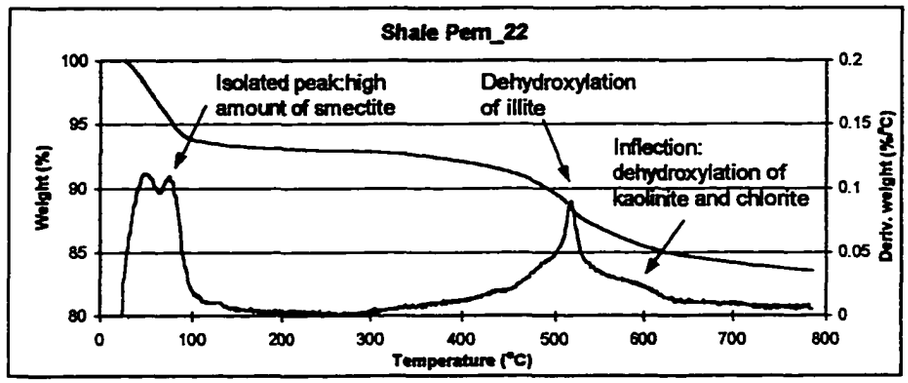


Figure 4.23: TGA of shale Pem_22. Isolated peak of interlayer water signals high amount of smectite. Even dried, this shale presents a high amount of "free" and interlayer water. This water cannot be considered totally free, being attached to the smectite, and does not evaporate at room temperature.

A different type of shale was also tested, the Speeton (Figure 4.24), from the North Sea. As it can be observed, it has high amount of smectite, illite, and kaolinite. Its clay content is very high, and no calcite is found. XRD results also indicate a 71% clay content with 6% of smectite for this type of shale (Amanullah & Chenevert, 1996). Nevertheless, XRD results indicate 12% of calcite, which is not observed from TGA. The same peak around 700°C

is observed in this shale, identical to the one observed for Pem_1, Pem_2, and Pem_7. An effort is underway to better characterize this peak, since it is appearing in shales with high clay content.

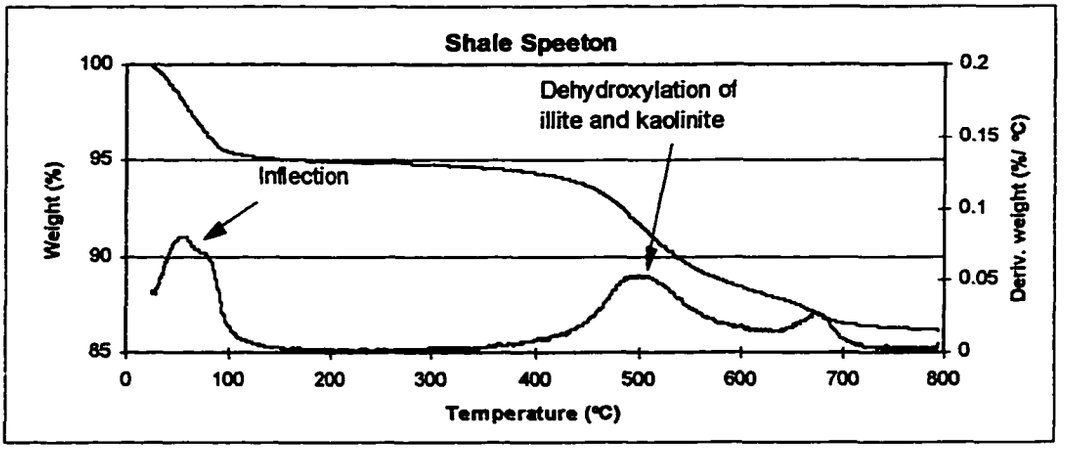


Figure 4.24: TGA of shale Speeton. High clay content, no calcite.

In order to show the capability of the methodology to characterize other sedimentary rocks, a chalk was tested (Figure 4.25). As expected, it is composed basically of calcite. An event was found with a peak around 200°C. Most probably, this is caused by the presence of some organic matter (Todor, 1976), even though the rock has been "cleaned" to remove all the hydrocarbons. This observation raised the possibility of the events observed in some shales (peak around 200°C) be due to the presence of some mineral oil, used for preservation, or some organic matter. Despite the fact that the samples are thoroughly wiped off to remove all excess oil on the surface, some amount might still be present. The organic matter is obviously not removed with this procedure.

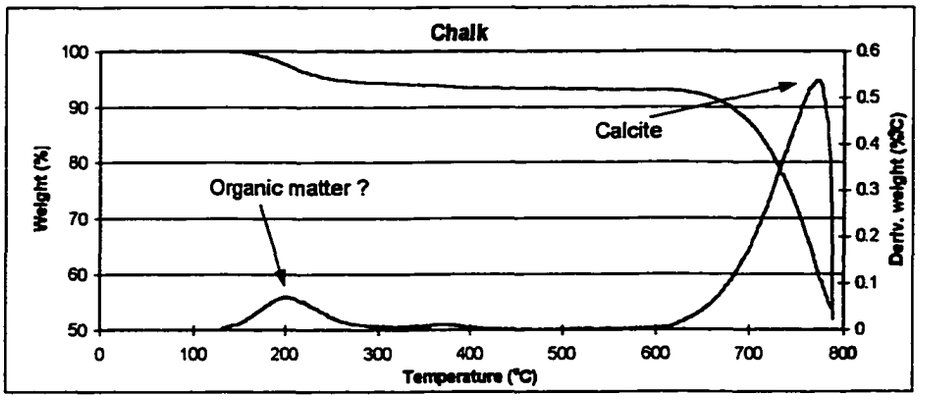


Figure 4.25: TGA of chalk. Peak at 200°C might indicate presence of organic matter in the rock.

Since water content and distribution was found to strongly influence shale behavior when immersed in water solutions, tests were also conducted with preserved and partially-dried samples. TGA is capable of detecting even slight changes of water content and type. Figure 4.26 shows the TGA result of Petr_D; the sample was taken by scratching the surface of a preserved core piece. Inflection is observed in the first peak, indicating the presence of some smectite. The amount, however, is not very large. Since not all the powder scratched from the sample surface was used for the TGA test, the remaining powder, left exposed to air for 3.5 hrs., dried, was also tested (Figure 4.27). Comparing to Figure 4.26, the original preserved sample, it can be noted that all free water has been removed just by air exposure. The only water left is a relatively low amount of interlayer water (no inflection), as expected from the

low amount of smectite. The remainder of the derivative curve remains almost the same. A third sample was tested, this time by scratching the surface of the same big piece of shale used for the first test (Figure 4.26) after being exposed to air for the same 3.5 hrs. (Figure 4.28). Again, except for the first peak, the derivative curve is almost the same. A close look at the first peak reveals an important observation: an inflection is still present, indicating the presence of both free and interlayer water. As the dried powder does not show any free water, the free water present on the surface of the big piece came from the still wet inner part, since it dehydrates slower than the surface. Water redistribution has been already demonstrated when shales are dehydrated, but using a different method for the temperature variation and terminology for the water types.

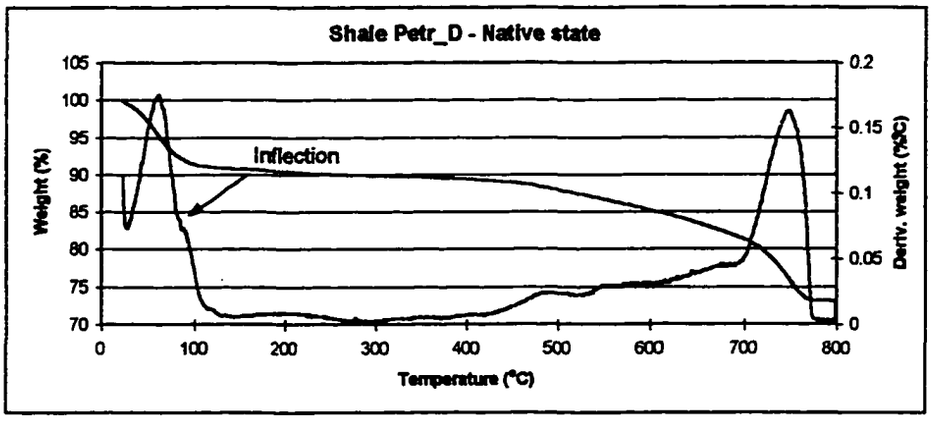


Figure 4.26: TGA of shale Petr_D - Native state.

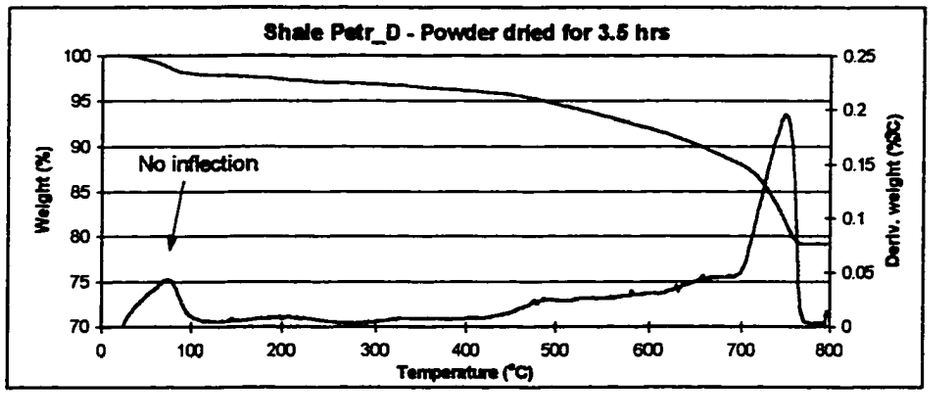


Figure 4.27: TGA of the remaining sample of the previous chart left exposed to air for 3.5 hrs. No free water, just interlayer water.

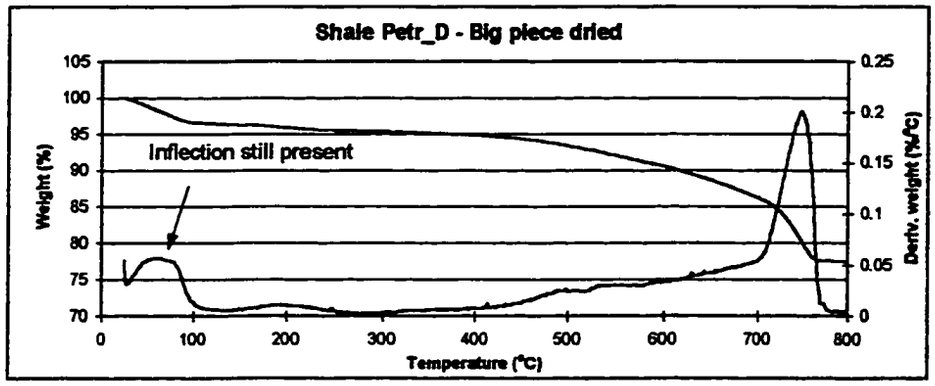


Figure 4.28: TGA of the sample from the surface of a big piece dried for 3.5 hrs. Free and interlayer water present in the sample.

4.5 Discussion

A first important conclusion can be drawn from the composition of the individual clay minerals. In the oil industry, shale water content is usually determined by heating a sample to 105°C in an oven until weight stabilization. Weight loss is assumed to derive from the water leaving the sample, and this water is normally called free water. As illustrated on the TGA chart of

montmorillonite, interlayer water in smectites is released at temperatures below 100°C. Shales with high smectite content, even though dried in air for one year, present a significant amount of "free" water (e.g. Pem_22). Even shales with almost no smectite (e.g. Pem_7), and dried for one year, present some "free" water, possibly from the illite (depending on the type it can have water bounded). Therefore, water content in a shale can be erroneously interpreted as free water. Depending on the amount of smectite (and/or illite) present in a shale, the majority of its "free" water is actually interlayer water from montmorillonite minerals.

Thermogravimetry has proven to be a powerful technique for detecting and identifying important shaly-rock characteristics, which are useful in various studies. Rock modification after exposure to a drilling fluid can be tracked, and the consequences of interaction observed. Tests exposing the same shale to different solutions are presented in Chapter 6, to evaluate the effects of each solution element on the rock structure. With this capability, TGA can be used to screen drilling and completion fluids, in order to improve their composition. TGA analyses can be performed periodically as the sample is exposed to a fluid. As it requires a very small sample, the same shale piece can be kept immersed and the surface periodically scratched and tested. Tests with both OBM and WBM are described in Chapter 6; shale structure changes are investigated with the technique described here.

Another advantage of the technique is the possibility of using cuttings, which abound (preservation since the rig site must be guaranteed) and are

cheaper to be obtained than cores. The only concern relates to any contamination the cuttings might have acquired (by interaction with the drilling fluid), which may be overcome by taking an inside sample rather than one on the surface. If the cutting is too small, this might be difficult to do, and some bias could be introduced. By carefully selecting the samples, this problem can be eliminated. It is also extremely important to guarantee complete preservation for the cuttings, by immediately rinsing them with mineral oil and paper towel to remove the drilling fluid, and immersing them in mineral oil. With this careful preservation procedure the water content of the rock is preserved as close as possible to its native values.

Even though not all the rock composition can be resolved with TGA, the main and important characteristics of a shaly rock are easily identified. Rather than presence of a certain mineral, it is absolutely necessary to observe how the rock changes, with the redistribution of free, interlayer, bound, and crystalline water. A deeper understanding of the interaction mechanisms is now possible, by observing the structure modification of the rock subjected to different solutions.

4.6 Summary

Most of the problems when drilling for oil and gas are attributed to shales and their interactions with the drilling fluids. Such interactions are dependent on the composition of drilling fluid and shales. Therefore, an accurate method for

shale characterization is essential for a better design of the drilling fluid and reduction of the problems. This chapter described a methodology based on thermal analysis which is able to characterize not only shaly rocks, but also any other sedimentary rock. The methodology is simple, inexpensive, and requires a small amount of sample. First, this chapter presented the limitations of the method usually used by the industry, X-Ray diffraction (XRD), and how it can lead to wrong decisions in the field. A description of the new methodology, its advantages and limitations, as well as results with several rocks are showed. The suggested methodology is capable of detecting important features such as interlayer, bound and crystalline water, that are essential components of the different clay minerals, and therefore it is able to analyze the effects of a given drilling fluid composition in contact with a shale, in great detail. The methodology is suggested for screening drilling fluids, in order to observe shale alteration when exposed to a solution, and, at least, as a quality control tool for XRD results.

Chapter 5

5. Shale-Reactivity Test: A Novel Approach to Evaluate Shale-Fluid Interaction

5.1 Introduction

In the oil industry most of the operations, if not all of them, need a fluid to be in contact with a rock, either by flowing through it or just in contact with it, as in the wellbore. This rock-fluid interaction can generate problems if the solution does not have affinity with the rock. Not only chemical but also physical disturbances can be created and several problems may arise. These problems increase when the rock has high clay content, known as having ability to absorb water and swell. Different additives and chemicals are added to water to create a solution that does not disturb the rock, either during the

drilling phase, or during completion, stimulation or even when water-flooding a shaly reservoir. In order to define the suitable fluid to be used, different tests were developed and are currently in use by the industry. Not only simple tests, in which samples are just immersed in the solution and visually inspected after some time, but also sophisticated tests to measure swelling pressures under triaxial stress conditions were proposed.

Even though a huge amount of work has already been done just in evaluating rock-fluid interaction, problems in the field indicate that the phenomena are not completely understood. Despite the fact that complex and sophisticated equipment have been used in some tests proposed in the past, interpretation of the data generated plays an important role. Another important point is to guarantee that the original rock condition is reproduced, trying to mimic the actual downhole environment. In this sense, a new approach and methodology to evaluate shale reactivity is proposed. Equipment setup is similar to the swelling pressure test proposed by Steiger (1993). The basic difference is on how to run the test, how to handle the shale samples, and how to interpret the results.

Water is believed to be driven in or out of shale by different driving forces: hydraulic pressure, electrical and chemical potential, and temperature (van Oort *et al.*, 1994). With the *shale-reactivity test* one can investigate separately the effect of the chemical potential, i.e., how the rock reacts when a chemical potential exists between the rock and the fluid. By isolating each effect (i.e., chemical potential and hydraulic potential), one can verify how important this

mechanism is and then use a strategy to minimize the consequences. Partially dried North Sea shale and preserved Campos Basin's (offshore Brazil) shale were tested, as well as an aluminum standard sample. Unique results and observations presented in the paper were made possible by the use of this new methodology. Being able to differentiate between a surface reaction and complete rock swelling is one of the major advantages of the test.

5.2 Previous works

Drilling fluid selection is often done with very simple (under atmospheric pressure) immersion tests, in which a shale sample (piece) is immersed in a certain solution. Reactivity between the rock and fluid can be evaluated by different means: sample weight loss, rock surface hardness index, and sometimes by using visual and tactile inspection. Limitations of this test are various. Probably the most important one is the lack of confining pressure. Due to its simplicity, immersion tests are still used by the industry to select drilling fluids. Sometimes, outcrop shale samples and/or old and dried cores are used. In other cases, reconstituted samples are made by grinding the original shale, and then adding some water and confining it. All these procedures give completely wrong results, because the samples have lost their original water content, as shown in Chapter 3. When partially-dried or outcrop samples are used, a strong swelling is usually observed when the shale is

exposed to fresh water. The slake durability test and the linear swelling test are 2 examples of what is called here simple immersion tests.

Another class of test is called *swelling pressure test*. In this case the rock is subject to confining and pore pressure, simulating downhole conditions. When the rock has reached an equilibrium, it is exposed to a test fluid. If the rock reacts with this fluid, it will usually swell, expanding its volume. As the test is conducted under constant volume, pressure variation from the initial condition is called the swelling pressure of that rock when exposed to such a fluid. The strongest the reaction, the bigger the swelling pressure. Steiger (1993) presented a test setup and procedure with several swelling pressure results. In those tests, the test fluid is circulated around the sample under a constant pressure. In this way, the rock is subject not only to a chemical potential but also to a hydraulic potential. It is difficult to isolate and quantify the effects of each potential separately. Shale samples were adjusted under equilibrium conditions to predetermined standard water contents and activities (Steiger & Leung, 1991). After equilibration, the sample is placed in the triaxial cell and the test is performed.

A different setup is proposed by Heidug & Wong (1996) in which they are interested in the pressure evolution on one side of the sample and the swelling of the shale when the rock is exposed to fluids of different chemistry. An important point to be emphasized here is that they equilibrate the sample under 30 bars of fluid pressure, using de-ionized water in direct contact with the sample. After pressure equilibration, the test fluid replaces the de-ionized

water. Swelling strains and fluid pressure are measured and compared to predicted theoretical results. The sample is subjected only to axial stress. In the radial direction, the sample is confined by a stiff ring. The test is conducted under constant axial stress, while axial strains are measured.

Shale swelling studies have also been conducted using different approaches, equipment, and procedures (Chenevert & Osisanya, 1992; Salisbury *et al.*, 1991; Onaisi *et al.*, 1994; Cook *et al.*, 1993; Mese, 1995). Most of these tests, if not all, use a sample handling procedure or test procedure that somehow disturbs the original water content of the rock. This disturbance happens either by equilibrating the samples in dessicators until they reach a desired value of water content, or by contacting the surface with some water-base solution prior to flowing the test fluid. It has been shown that even a small variation on the original water content can turn a shale into a strongly reactive rock. Therefore, the minimum requirement for a test which is intended to measure the swelling (reactivity) potential of a shale is to keep the sample preserved, i.e., with its original water content, until the rock is exposed to the test fluid.

5.3 Test description

The importance of the chemical potential in shale destabilization has been the subject of several publications (Hale *et al.*, 1992; van Oort *et al.*, 1994). Most of the experiments combine the effect of both the chemical and hydraulic

potential. In order to separate the effects and be able to quantify how the chemical potential is affecting the shale when the rock is exposed to a different chemical solutions the shale-reactivity test was designed. Quantification of the chemical potential impact on shale strength and integrity is crucial to understand the mechanisms of shale swelling. The tests presented in Chapter 3 suggest that the swelling of shales are due to the lack of original water, lost by dehydration at any stage since the core was retrieved. Those experiments, however, were performed under atmospheric pressure.

In order to closely represent the in-situ stress environment, it was decided to perform the experiments in a triaxial cell, where confining pressures can be applied. A schematic representation of the setup is shown in Figure 5.1. Radial and axial strains were measured during the test using extensometers and LVDT's (not shown in Figure 5.1).

5.3.1 Sample Preparation

The importance of sample handling on shale test results has been described and emphasized in Chapter 3. As a consequence, a careful and detailed handling procedure has been defined to avoid any dehydration. The tests conducted so far had a sample diameter of 1.5 in. In order to guarantee minimal sample dehydration, a coring box was built to immerse the samples in oil at all times during the coring operation. A description of the coring box and the procedure to cut the plugs without dehydrating them is presented in Appendix C. The

plugs were prepared without air exposure; this procedure is important and essential to certify good results.

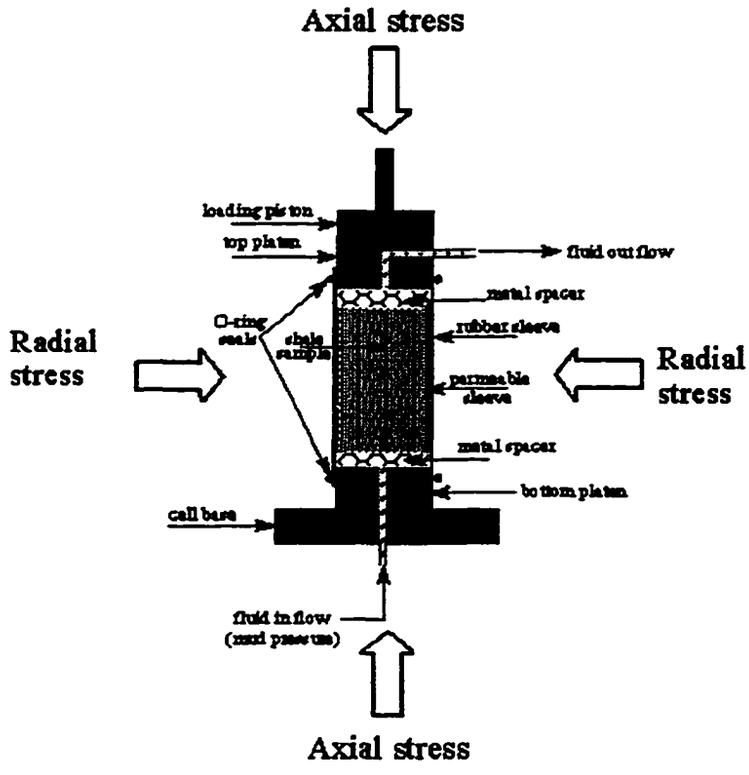


Figure 5.1: Schematic representation of the equipment for the shale-reactivity test.

The plug should be kept immersed in oil until the moment of testing. The metal screen and the jacket should be prepared in advance according to the dimensions of the plug (Figure 5.2 and Figure 5.3). Plug height can vary from 1.5 in. up to 3 in. Although shorter plugs can be used, the difficulty in measuring radial strains leads to samples of at least 1.5 in. in length. As the test will not measure the rock strength, the sample need not have to follow the

ISRM standards for triaxial tests (for example, height/diameter ratio > 2). When preparing plugs from downhole field cores, it is difficult sometimes to obtain long plugs. Another advantage of this test is that it can be conducted on broken pieces (due to presence of fractures or inappropriate handling) and are not suitable to be used for a standard rock mechanics test.

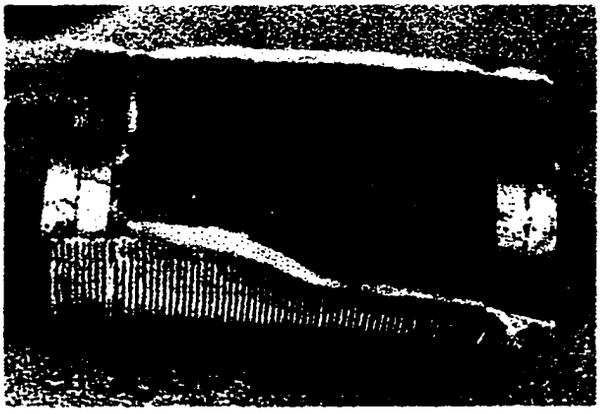


Figure 5.2: Sample after the test showing the metal screen around it.



Figure 5.3: Detail of the sample with the metal screen and jacket, with bottom and top caps.

The operation of mounting the sample on the base, heating and wiring the jacket should be done as fast as possible. After some practice, this step can be

done in less than 5 minutes. Although this time is enough to partially dry a shale, in our case the problem is minimized due to the film of oil surrounding the sample when it is removed from the container. Immediately after the wires to seal the jacket are in place, the sample should be placed on the base of the cell, and mineral oil flowed through the pore pressure system. At this point, the sample again is prevented from any further dehydration. The inlet and outlet valves are closed and the remaining preparation (installation and testing of strain measurement devices, closing the cell, application of pressure...) can be carried out without any worry with the sample integrity (moisture content). It is important to point out here that this final step, sometimes, can take more than 2 hours, if equipment fails, or adjustments in the extensometers or LVDT's need to be made. It is absolutely necessary, therefore, that the sample be surrounded with oil as soon as possible. It has been previously showed that the oil does not avoid the shale reaction with a water solution, and it is the best mean to prevent any dehydration. Figure 5.4 shows a sample instrumented, mounted on the cell, and ready to start the test.

It is obvious that none of these steps are necessary if one is testing a partially-dried or dried shale sample. The industry must, however, emphasize the tests with preserved downhole shale samples. These samples are the only ones that represent the actual downhole rock behavior and should be used in tests to understand rock-fluid interaction.

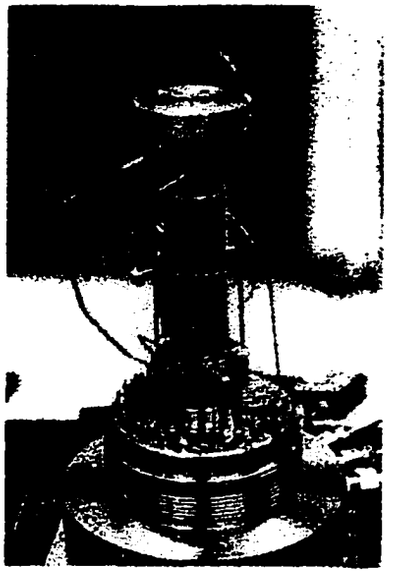


Figure 5.4: Sample ready to start the shale reactivity test. Preservation is provided by the oil surrounding the sample.

5.3.2 Test Procedure

Confining pressures are raised in steps of 1,000 psi. This value can be varied according to how slow one can run the test. The smaller the increase in confining pressure, the smaller the excess pore pressure generated. After each step the sample is allowed to equilibrate. Equilibrium is monitored by both radial and vertical strains. During the equilibration phase, mineral oil is circulated through the pore pressure system. At all times the pressure in this system is atmospheric, to keep the hydraulic pressure difference between the rock and the fluid equal to zero. Equilibration is achieved by allowing the excess pore-pressure generated by increasing the confining pressure to drain. When deformations are almost constant, the confining pressure is raised again

by 1,000 psi. This procedure is repeated until the test pressure is achieved. At each step it is important to check if the oil is flowing around the sample.

At the end of the equilibration period, test fluid is introduced in the pore-pressure system and displaces the mineral oil. The rock gets in contact with the test fluid and reactions are monitored via deformation measurements. The confining pressure is kept constant. To avoid introduction of complex stress distributions within the sample, a hydrostatic stress state was chosen to be applied on the sample. In this way, any reaction that is observed can be attributed to the chemical potential (the test fluid pressure is zero). The test fluid can be flowed at a different than zero pressure, creating a hydraulic pressure gradient. In this case, not only the chemical potential but also the hydraulic gradient will influence the reaction. In all the tests described here the test fluid pressure was chosen to be zero to isolate the effect of the chemical potential. De-ionized water was the test fluid of choice because it creates the worse scenario ($A_w = 1.0$) and does not affect the equipment. If the test equipment can handle corrosive solutions, any test fluid can be used. The same fluid will be used to test different shales. Testing the same shale with different fluids is another option.

5.4 Results

Three test results are presented here. The first test was conducted with a standard aluminum sample. The goal of this test was to measure all system

deformations and verify the performance of the metal screen and the jacket with the proposed procedure. The setup was exactly the same as a real test. In this way when de-ionized water is flowed, no reaction is expected. The screen and jacket deformation as a function of confining pressure and time were also recorded. Only the radial deformations are presented in this paper. Figure 5.5 shows the plot of circumferential length as a function of time. As can be seen, deformation stabilizes pretty quickly, after each increase in confining pressure. It is also obvious that no deformations are observed when water is pumped.

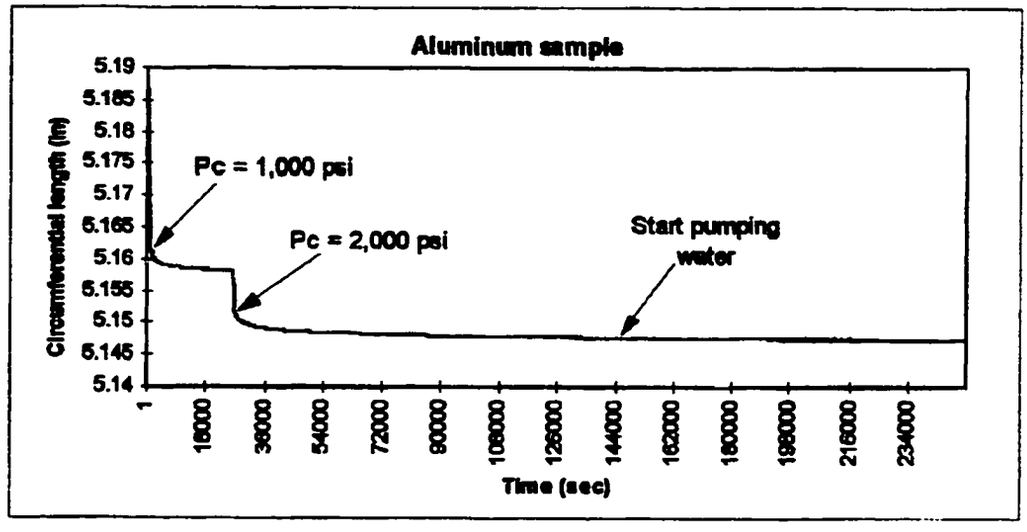


Figure 5.5: Circumferential length variation for the aluminum sample.

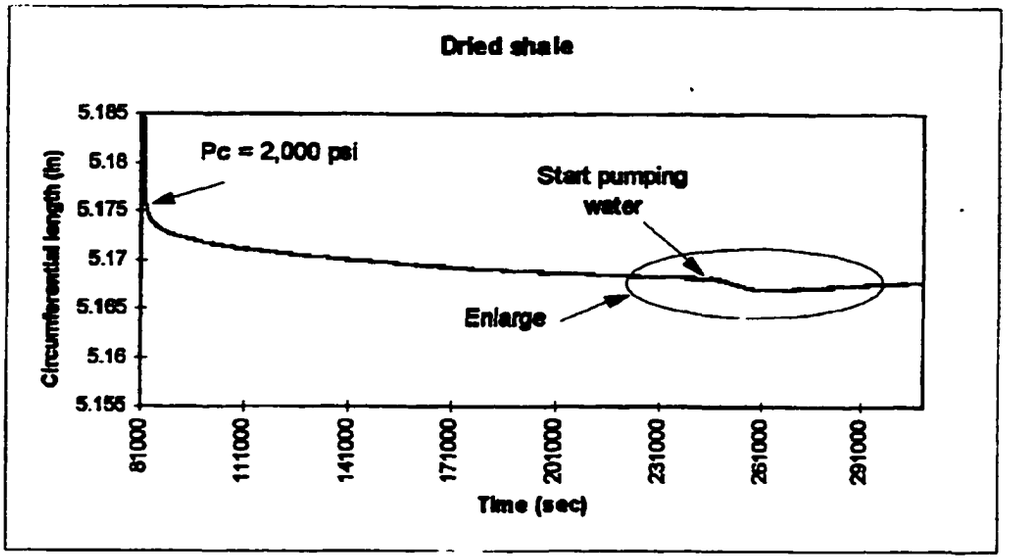


Figure 5.6: Circumferential length variation for a dried shale.

The second test was performed with a North Sea reddish shale, partially dried. This dried sample presented a strong reaction when immersed in de-ionized water under atmospheric pressure. This behavior is also seen under pressure (Figure 5.6). As soon as the water contacts the sample, the deformation rate starts to change: initially the sample shrinks, and after some time, it starts to expand.

In order to better visualize the reactions, only the time period of interest is plotted in Figure 5.7. It can be seen that the first reaction of the shale is to expand, due to the swelling pressures generated. However, as reaction proceeds, the rock weakens. This weakening (loss of strength) under confining pressure leads to a new consolidation of the sample, causing additional shrinkage. The swelling mechanisms are not enough to overcome the

contraction. Only after more than 3 hours consolidating will the sample start to expand.

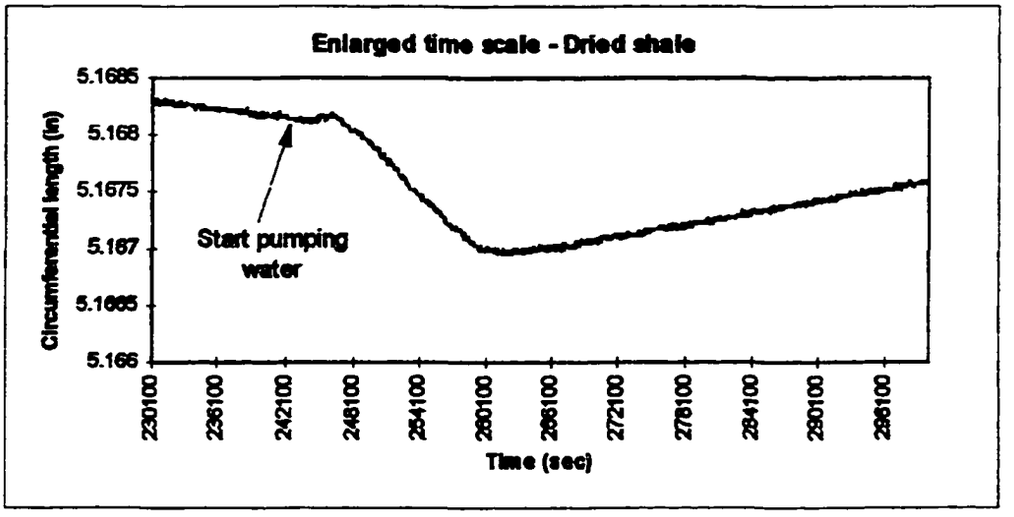


Figure 5.7: Enlarged time scale for the dried shale.

The third test was conducted with a preserved shale, from the Campos Basin, offshore Brazil. Even though this is a preserved sample, a reaction can be observed after the water contacts the shale (Figure 5.8). From this same figure, it can be seen that this shale takes much longer to dissipate all the excess pore-pressure generated when the confining pressure is increased. The ideal situation would have been to wait much longer for the deformations to stabilize. However, after 2 days, deformations were not varying strongly anymore and it was decided to displace the oil with the water.

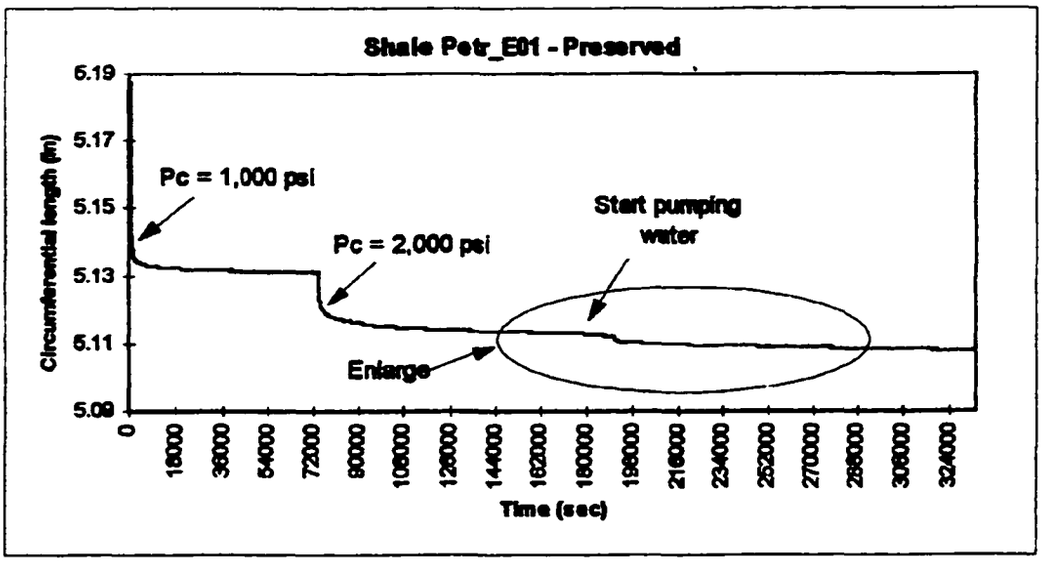


Figure 5.8: Circumferential length variation for a preserved shale.

A plot with an enlarged time scale is shown in Figure 5.9. A detailed investigation of the plot shows that the circumferential deformation changes immediately after water contacts the sample. This change in the circumferential deformation must be caused by some reaction. However, after a small period of time, reaction stops and the sample continues to consolidate with the same rate as before (note the projected slope with the same inclination as the curve after reaction takes place).

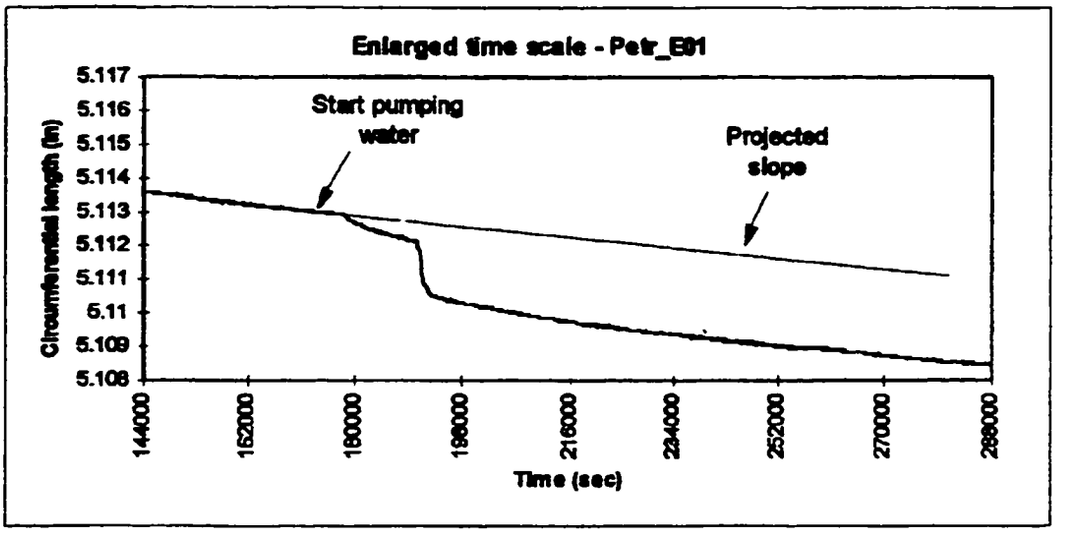


Figure 5.9: Enlarged time scale for the preserved sample.

It can also be observed that a short time after the reaction starts the circumferential deformation presents a sharp decline and then resumes its original trend. All the fluids that circulate around the sample are collected (Figure 5.10). A closer inspection of the output fluid helped the interpretation of this test. It has been showed in Chapter 3 that mechanical damage on the surface of the sample produced a thin powder as the surface reacts when the sample is immersed in de-ionized water. The same phenomenon happened here. As the plug was prepared by drilling a 3.5 in. core, mechanical damage was introduced on the sample surface. As soon as the water contacted the shale, a superficial reaction started, generating the powder. As the test fluid is being circulated around the sample, this thin powder is removed from the surface and the diameter reduces. The output fluid has the same color and aspect

(opaque) as when the sample is just immersed in de-ionized water. Also, sample consolidation proceeded normally as before, confirming that the reaction was just on the surface. The thickness of the layer affected by the mechanical damage can be estimated from the plot in Figure 5.9 as equal to 10^{-3} cm. Therefore, the mechanical damage produced by the drill bit can be considered of minor importance in wellbore stability studies.



Figure 5.10: Picture of the whole equipment during a test. A plastic beaker is used to collect the outlet fluid for future analysis.

5.5 Discussion

In all cases the first reaction of the rock has been to reduce its diameter. Therefore, if the tests were performed under constant volume, a decrease in pressure would have been observed and a negative swelling pressure (shrinking pressure) would have been recorded. With the dried shale, positive swelling pressures would have been recorded only after a long time, when the sample

expansion overcame the contraction. Nowhere in the literature has a negative swelling pressure been mentioned.

The results confirmed that just the dried shale presents reactions when in contact with water. In the preserved samples, only the surface of the sample, where the water content was completely disturbed by the mechanical action of the drill bit, reacts. After this reaction is finished, the sample remains intact. No change in deformations are recorded, indicating no swelling or contraction. This surface reaction can be interpreted as a reaction of the rock, and can lead to a wrong interpretation if the test is conducted under constant pressure, as the swelling pressure tests. Preliminary results indicate that the preserved shale tested has an activity of 0.84. As can be seen, just the effect of the chemical potential was not enough to cause reaction and failure of the shale.

It is important to emphasize, once more, that the procedure followed to prepare the samples and to run the test preserves, as close as possible, the original water content of the shale. Tests reporting positive swelling pressures on shales were conducted on samples that suffered, somehow, changes on the amount and/or distribution of the original water content. This disturbance might explain the swelling of shales, generated when the rock is exposed to a water solution. Some tests reported in the literature also flow more than one test fluid around the sample, one after the other. Each solution that contacts the rock will change to a different degree the rock water content. Depending on how long is the exposure, the whole sample or just an outside layer is

affected. When another solution contacts the rock, a reaction should take place to equilibrate the rock again.

5.6 Conclusions

The following conclusions can be derived from the results obtained with the shale-reactivity test:

A test to evaluate the effect of chemical potential on shale behavior is proposed. The test is run under constant pressure and with zero fluid pressure. The test gives much more detailed information about the rock behavior, and should replace the standard swelling pressure tests.

A detailed sample preparation and handling procedure are also presented. This procedure should be followed very close in order to preserve the shale moisture content until the rock contacts the test fluid.

Shale swelling was observed only with dried samples. However, the rock only started to expand after a big contraction took place, caused by the weakening due to the reaction of the rock with the water.

The surface reaction observed as a consequence of the mechanical damage during sample preparation can lead to a wrong interpretation in swelling pressure tests, conducted under constant volume.

Preservation of the shale moisture content until the test fluid contacts the rock is essential to provide reliable results.

The use of disturbed samples to evaluate the swelling of shales should be avoided. The test should be conducted in different undisturbed shale samples to provide a broad and generalized conclusion about the swelling mechanisms of shales when in contact with water-base solutions.

5.7 Summary

The oil industry has been studying rock-fluid interaction not only in the drilling phase but also in completion, stimulation, and in enhanced oil recovery projects. Correct evaluation on how the rock reacts when in contact with a certain fluid is crucial for the success of several operations. Shales are especially troublesome rocks and a great deal of attention has been devoted to these rocks. A new approach to evaluate rock-fluid interactions is proposed. The test evaluates the reactivity of a rock when in contact with a fluid using a triaxial cell to reproduce downhole in-situ stresses. Although used, so far, to test shale reactivity, the methodology can be used for any type of rock, with a significant clay content (shaly sandstones or limestones). This chapter described the test procedures, sample preparation, and results obtained with dried and well-preserved downhole cores. The results show that this test provides much more detailed information about the rock behavior than the standard swelling pressure tests already in use today by the industry. The test can be run to evaluate the effect of the chemical potential alone, or in conjunction with the hydraulic potential.

Chapter 6

6. Misconceptions Related to Shale-Fluid Interaction

6.1 Introduction

Preliminary immersion tests described in Chapter 3 identified the need for a more detailed and accurate rock characterization methodology and also for an improved reactivity test under stress. Some well established ideas in the industry today have been questioned, especially the hypothesis that shales (mainly the ones with high smectite content) are strongly reactive rocks when in contact with water.

In order to understand the most important shale-fluid interaction mechanisms, specific tests were designed. The steps taken in Chapter 3 were fundamental in the planning phase of these tests. The handling procedure described in Chapter 3 was also followed closely. The semi-permeable

membrane assumption in shales, the use of chemical potential difference to drive water in/out of shales, the influence of capillary effects on partially-dried shale samples, and shale swelling mechanisms were all investigated.

Both WBM and OBM fluids were used. A completely new understanding of shale-fluid interaction is proposed, based on the test results. It is shown that the presence of surfactants in OBM makes such fluid more effective than WBM, by changing the rock wettability. The established concept that water in the shale can be driven in or out by a chemical potential is proven to be unrealistic. Using the characterization methodology described in Chapter 4 it is shown that the shales exhibit a structural modification or redistribution of water after exposure to different solutions. A detailed analysis of the TGA results led to a new understanding of fluid flow in a shale, that has consequences on pore pressure and effective pressure, dissipation of the excess pore-pressure, and poro-elastic effects.

6.2 Concepts or Misconceptions?

Usage of dried shale samples and extrapolation of clay behavior to downhole shales have led to the belief that shales are very reactive rocks. Drilling fluid additives have been designed to minimize the reaction with dried shales at laboratory conditions. In all the tests described in this chapter, just one well preserved shale was used. By keeping the same rock type comparisons of interactions with different solutions can be made without other artifacts.

6.2.1 Swelling Clay Minerals

It has been shown in Chapters 3 and 4 that there is a lack correlation between the presence of smectite in a shale and its reactivity potential for the group of shales studied. The same shale, with the same smectite content, reacted differently according to its dryness. Actually, it is the water content, rather than the smectite content, that controls the shale reactivity. Inconsistent results from different laboratories indicate that quantification of smectite amount with XRD is subject to question. Therefore, this information cannot be used as the criterion to determine shale behavior.

The fact that dried smectite absorbs a large amount of water, increasing its volume in the process, does not imply that a downhole shale with high smectite content, which is saturated and in equilibrium, will swell when in contact with a water solution. The first hypothesis that needs to be challenged is that the presence of smectite in a shale is directly related to a strong reaction with water.

Actually, many years ago Grim (1968) has already mentioned that: "*A considerable body of evidence, largely unpublished, shows that smectite clays, when subjected for long periods of time to substantially uniform moisture conditions, develop hydration characteristics of considerable stability. Such materials resist change in the degree of hydration, but when the hydration is changed even to a very slight degree, the stability may be abruptly and completely lost. Thus a high-swelling bentonite sample carefully*

collected to preserve its natural hydration can be placed in water without any slaking, even when moderately stirred. However, if such a bentonite is dried only a very small amount, it will slake and swell immediately when placed in water."

The majority of smectite's water is retained in its interlayer, and is not released at room temperature even after a long period of exposure to air, as shown in Chapter 4 with shale Pem_22. The water content in a shale, then, is closely related to its moisture content as well as the clay type and amount present in it. The "free" water content determined by heating samples in an oven at 105°C actually includes both free and part of interlayer water from smectites. Laboratory procedures that include drying of shale samples in an oven before running tests (capillary suction test (CST), use of reconstituted shale samples in swelling pressure tests, and the hot-rolling test) are unacceptable, since they remove the interlayer water of smectite, causing it to be artificially more reactive.

6.2.2 Shale Swelling Mechanisms

It has been previously demonstrated that shale swelling is strongly related to both the amount and distribution of water within the rock. The water redistribution experiment presented in Chapter 3 showed that the amount of water at the surface changes, in order to always remain in equilibrium. Since dehydration in air is faster than the flow of water in shale, the inside portion of the sample, still wet, replenishes water to the mostly dried surface. After a

certain period of time an equilibrium must be achieved, and water flow inside the sample should stop. When equilibrium is reached, the sample becomes homogeneously dried. On the other hand, if equilibration is not allowed, the sample shows two distinct regions: a dried surface and a wet inner portion. In this case only the dried surface reacts with water. When a third situation is considered, a preserved sample of the same shale without any dehydration, no reaction was observed even after 1 year of immersion in water.

A long term experiment was also conducted to confirm the ideas presented above. A preserved sample was dehydrated in air for 3 hrs. and then immersed in mineral oil to allow water redistribution for 1 year. After this long period equilibrating, the sample was immersed in water. As the sample was more homogeneously dried after this long-term equilibration, surface reaction was minimal (the same behavior of the other samples with equilibration allowed, described previously). However, after 24 hours of immersion in de-ionized water, the sample presented fractures all over it (Figure 6.1). The swelling mechanisms described in Chapter 2 (crystalline and osmotic) are, most probably, a function of the dryness state of the clay minerals.

In other words, the same shale, with the same mineralogy, behaves differently when immersed in water. What should be questioned here is not the fact that shale swells, but whether downhole shales swell. What has been observed is that shale only swells if it loses some water, disturbing its equilibrium, i.e., the observed swelling is primarily an artifact of sample drying.



Figure 6.1: Immersion in de-ionized water of different sample conditions. All the samples are from the same shale, with pieces taken from the same core box. Top, from left to right: preserved sample after 3 days immersed in water; sample dried in air for 2 hrs., after 2 hrs. immersed in water; sample dried in air for 22 hrs., after 24 min. immersed in water. Bottom, from left to right: sample dehydrated in alcohol and immersed in water for 2 days; sample dried in air for 2 hrs., equilibrated in oil for 4 weeks, and immersed in water for 2 days; sample dried in air for 2 hrs., equilibrated in oil for 1 year, after immersion in water for 24 hours.

The intensity of swelling is proportional to the deficiency of water in the shale. Since loss of smectite's interlayer water might be the main fact that causes shale to swell in the laboratory, both smectite content and amount of air-exposure time will influence the swelling of a shale sample. Hence, a shale with a high smectite content might require smaller time exposed to air

(dehydrating) to present the same swelling as a shale with a small smectite content.

6.2.3 Capillary Effects

After the preliminary observations that the capillary effects might not explain all the swelling and breakage of samples in the laboratory (refer to Chapter 3), specific tests were designed and conducted to reach a final conclusion. By allowing the shale to dehydrate in air, the rock becomes both water and oil wet, depending on the fluid contacting the partially dried sample. Therefore, a dried shale absorbs water as well as oil, as can be seen in Figure 6.2, where the submersed weight in mineral oil is plotted as a function of time. The same mineral oil used for preservation, without additives, was used in all these tests to investigate the capillary effects. Even after weight stabilization, the rock remained intact, with no reaction (swelling) with the oil. The sample was then immersed in de-ionized water, reacting strongly. Absorption of oil somehow eliminates the suction (negative pressure) present in the dried shale. Only after water made a contact with the sample was a reaction observed. There is no certainty that all the capillary effects were eliminated by oil absorption. There must be another mechanism, besides the capillary effects, to explain these results. The reaction is strongly related to shale dehydration and subsequent contact with a water solution.

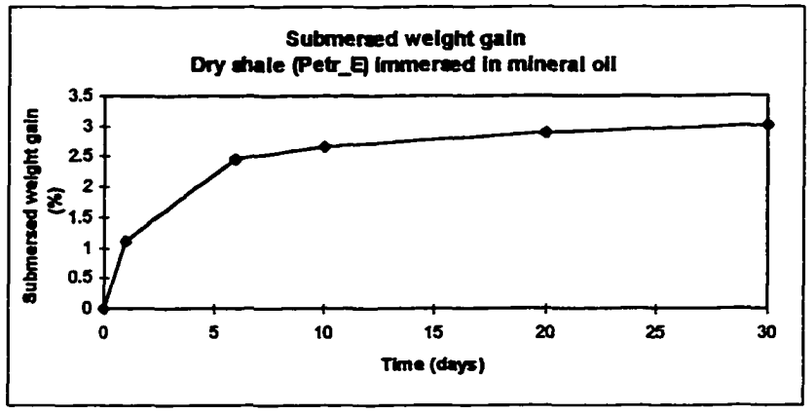


Figure 6.2: Immersion of dry shale in mineral oil: penetration into the rock indicated by gain in submersed weight.

Observations in both micro- and macro-scale were also conducted. Dried shale samples from an outcrop in Brazil (almost 100% smectite) were tested in the fluid-rock interaction loop (Martins *et al.*, 1996), flowing fresh water and oil through the central hole of a hollow cylinder sample. In the first case, reaction was intense and completely destroyed the rock (Figure 6.3). When oil was used, fluid penetration was observed, but no reaction happened (Figure 6.4). The hole remained in gauge, even with oil penetrating into the rock. Oil penetration is caused by the capillary pressure mentioned before, since the flow occurs under very low pressure.



Figure 6.3: Rock-fluid interaction loop: dried outcrop shale (100% smectite) with fresh water; reaction throughout the sample.

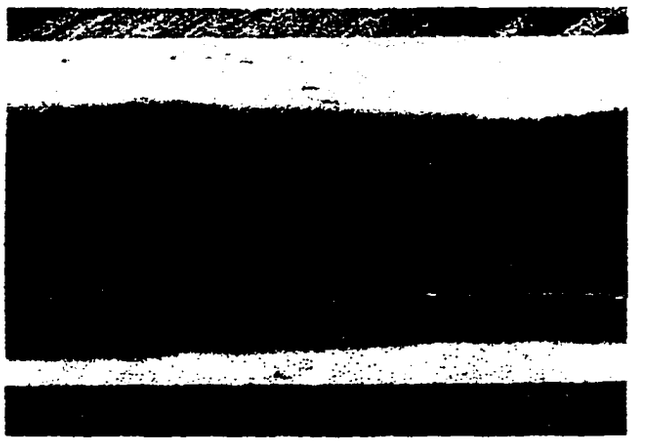


Figure 6.4: Rock-fluid interaction loop: dried outcrop shale (100% smectite) with oil; hole in gauge and no reaction whatsoever, despite penetration of oil into the shale (see dark shade around the horizontal hole).

The last test was done with dried pieces of shales and observed with the help of a microscope. Preserved shale samples were allowed to dehydrate in air. Development of fissures on the surface could be seen after a certain time of dehydration. After 24 hours of air exposure, the samples were almost completely dried. A small amount of oil was then dropped on the surface of the shale. Oil was strongly sucked into the shale and also spread on the surface (Figure 6.5 through Figure 6.7). Penetration was faster through the more permeable fissures. Again, even with the penetration, no swelling or reaction was observed; the shale remained intact.



Figure 6.5: Oil spreading on a dried shale: initial stage.



Figure 6.6: Same as Figure 6.5, minutes later: penetration is faster in the fracture than into the matrix.



Figure 6.7: Same as Figure 6.6, minutes later: front advance is seen on the left, as well as penetration into the rock around the fracture. Oil does not evaporate at room temperature and penetrates deeper into the rock. No reaction occurs.

Water was also dropped, but on another side of the same sample. Instead of spreading and being sucked into the sample, the drop of water remained stationary and penetrated slowly (this could give an indication that the shale was more oil wet than water wet) (Figure 6.8). After a few minutes the surface was dried again (both evaporation and penetration into the rock occurred) and the final surface was itself altered due to the reaction between the rock and water (Figure 6.9).

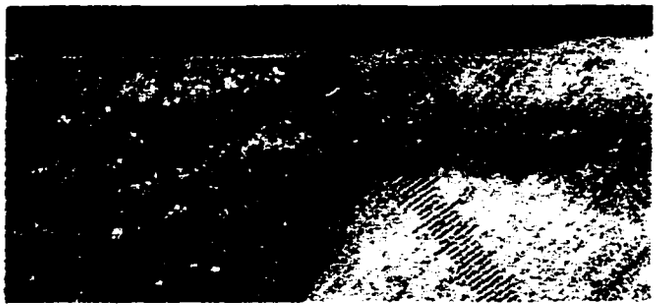


Figure 6.8: Water drop on a dried shale: penetration in the fracture, but most of the water remains steady.

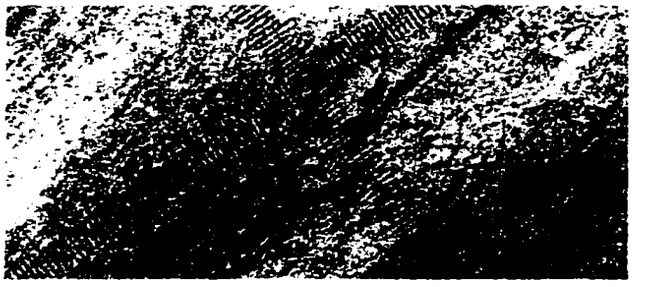


Figure 6.9: Shale surface after water has evaporated: signs of reaction visible on the surface, despite little penetration into the rock.

All these observations led to the conclusion that the reaction between a dried shale and water is not due to capillary effects alone. Although they are present, they are not responsible for the breakage of a partially dried shale. It has been previously shown that partially saturated samples, but well preserved (with no dehydration), did not react when contacted by water (refer to Chapter 3). In this case, desaturation occurred due to stress relief during coring and the two-phase system which was present in the rock. All these findings reinforce the previous conclusion that it is actually lack of water in the shale (clay minerals) that causes a partially dried shale to adsorb water and swell.

6.2.4 Swelling Pressure

A different approach to study swelling pressure is suggested in the shale reactivity test described in Chapter 5. Even though the test is run under constant confining pressure, it is possible to evaluate if swelling pressure could be developed by measuring the volumetric change. Associating with the swelling pressure test, in which the sample volume is maintained constant, if an increase in volume is experienced in the shale-reactivity test a swelling pressure would have developed; on the other hand, if the volume of the sample reduces, a shrinkage pressure would have been the result.

Following this careful procedure no sample expansion was observed with the preserved downhole shale (Petr_E) from the Campos Basin, Brazil (Chapter 5). In order to establish some comparison pattern, a preserved sample of a different shale (Petr_D) was intentionally allowed to dry. The partially dried sample expanded in the vertical and radial directions. In the radial direction, however, expansion occurred only after a reduction in diameter due to the strong reaction with de-ionized water in the mechanically damaged surface (Figure 6.10). The preserved sample of this shale Petr_D did not show any reaction, confirming what was expected (Figure 6.11). These carefully conducted tests show that shale swelling is highly influenced by shale dehydration, as also demonstrated by immersion tests under atmospheric conditions (Chapter 3). By experiencing volume reduction, the dried samples would have actually presented a final shrinkage pressure, rather than a

swelling pressure. However, this volume reduction should be carefully analyzed, since part of the reduction is due to loss of material dispersed in the test fluid flowing around the sample.

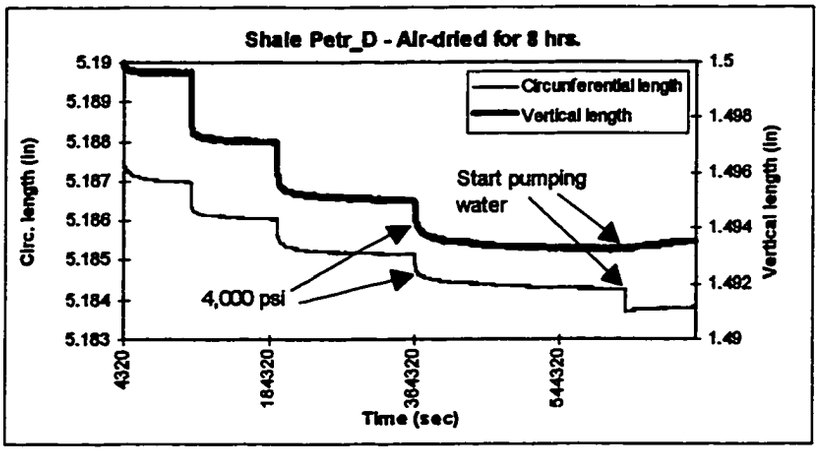


Figure 6.10: Shale reactivity test of an air-dried shale D sample: expansion in the vertical direction and contraction followed by expansion in the circumferential direction. Final volume smaller than the initial one.

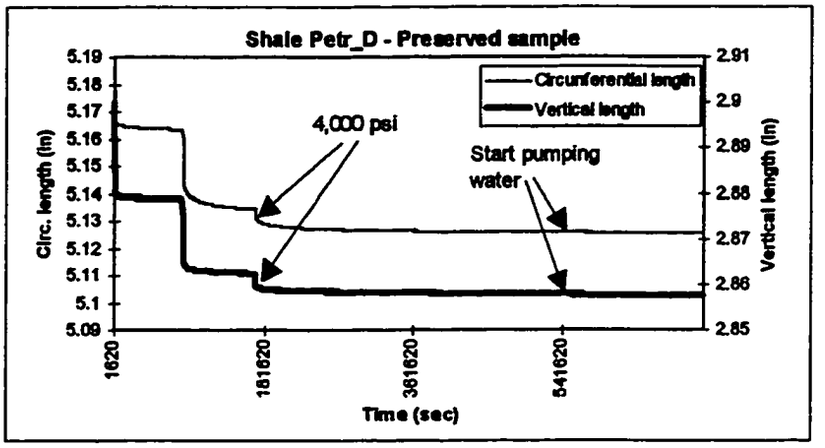


Figure 6.11: Shale reactivity test of a preserved shale D sample: no reaction was observed after pumping water.

Another shale reactivity test was conducted with a sample of shale Petr_E dried for 24 hrs. in air. The idea was to verify the generation of swelling pressures with an extremely dried sample. Only in this case contact with de-ionized water produced a final volume greater than the initial one (prior to the contact with water) (Figure 6.12). In this case, a swelling pressure would have been recorded in a swelling pressure test due to the expansion. This test was conducted with a confining pressure of 4,000 psi. The strong reaction observed can only be attributed to the dryness, rather than to the confining pressure, since under atmospheric pressure the behavior was the same.

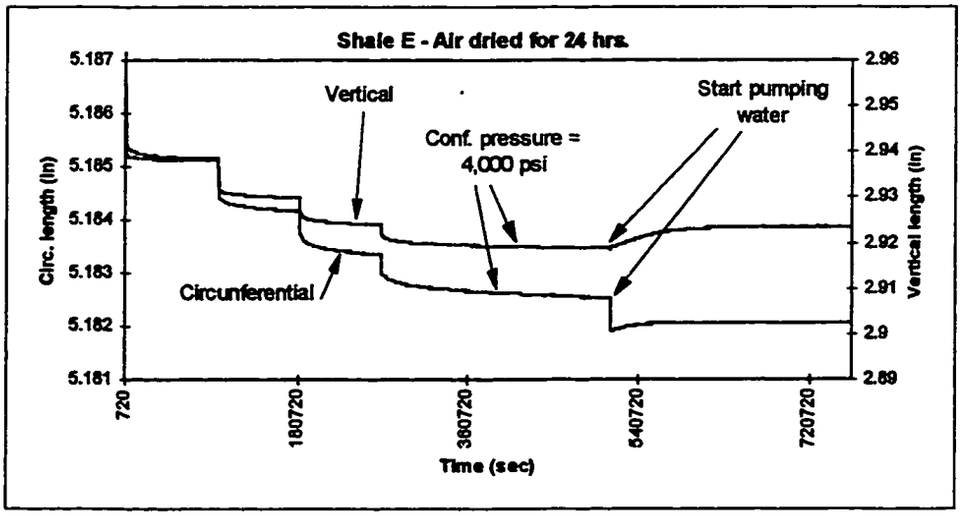


Figure 6.12: Shale reactivity test: shale Petr_E, dried for 24 hrs. with de-ionized water as the test fluid. Final sample volume greater than before water gets in contact.

It is clear that dried clay minerals, specially smectites, develop swelling pressures when in contact with water. However, extrapolation of this fact to downhole shales is very dangerous. At its in-situ conditions the shales are saturated and in equilibrium. It has been shown that the need for water occurs just when part of its water has been lost. Therefore, there is no support for the argument that even shales with a high content of smectite will significantly swell when in contact with water under downhole conditions. Such a phenomenon only occurs if the water equilibrium inside the rock is disturbed, being subsequently contacted by different fluids.

6.2.5 Chemical Potential as a Driving Force

In order to check the effectiveness of the chemical potential to drive water in or out of shales, various immersion tests under atmospheric pressure were conducted. The only potential in these tests was the chemical potential. Samples of the same well-preserved shale (Petr_D) were immersed in different water solutions, alcohol, and oil solutions. The submersed weight was continuously measured, and the samples were also weighted in air before and after the test. Although the volume change was not measured, the weight gives an indication of the flow of water in or out of the sample. Not only water is flowing in or out of the shale; however, water should be the most important component in the weight change. A parallel test for each solution was conducted in which the penetrometer index was measured (with a Rex Durometer H-1600 Type C) and water content and shale characterization

determined with thermogravimetry. A 10°C/min. method was used for the temperature variation with the same methodology as described in Chapter 4.

Quasi-saturated salt solutions were used: NaCl 24 % w/w (A_w = 0.78); KCl 25 % w/w (A_w = 0.85); $CaCl_2$ 36 % w/w (A_w = 0.50)[1]. Also, de-ionized water (A_w =1.0) and alcohol were used. For the oil solutions, the water phases were as follows: de-ionized water (A_w = 1.0) and saturated salt solutions (NaCl, A_w = 0.75; KCl, A_w = 0.84; $CaCl_2$, A_w = 0.39)[1]. In these oil solutions, only diesel oil, water, salt, and the emulsifier were present. The activity of the shale was 0.9, measured with a hygrometer. This information, though limited (Carminati *et al.*, 1997), is mentioned here to show that solutions with higher and lower activities, compared to the shale, were tested.

Immersed in water solutions, the samples increased their weight (both submersed and in air), regardless of the solution's activity (Figure 6.13). Immersion in alcohol was the only situation in which the weight decreased. What was less expected, however, was the fact that in the salt solutions the increase was bigger than in de-ionized water. A closer look at the beginning of the chart (first 2.5 hrs., Figure 6.14) shows that in calcium chloride the weight started to decrease, but that tendency was reversed less than 0.5 hour later. After 1 hour the weight was already greater than the initial one. In de-ionized water the weight increased monotonically. It can be seen that only in the very beginning were the samples behaving according to the chemical potential

[1] The solution's activity was determined from a table as a function of salt concentration found in Hale *et al.*, 1993.

concept. However, after an initial period in the salt solutions, the weight increased faster than in water. Even with a very low activity, the calcium chloride solution was not able to drive water from the shale, except for less than 30 min. After about 60 hrs., the weight started to decrease for all salt solutions, whereas in de-ionized water it remained constant. The KCl experiment was interrupted due to precipitation of salt crystals on the nylon wire hanging the sample (observe weight increase in Figure 6.13). Weight variation was also confirmed by the measurements in air, before and after immersion in the solutions (Figure 6.15). The test with KCl was interrupted after salt crystals started to be deposited in the wire hanging the sample (note the increase in weight for the KCl solution).

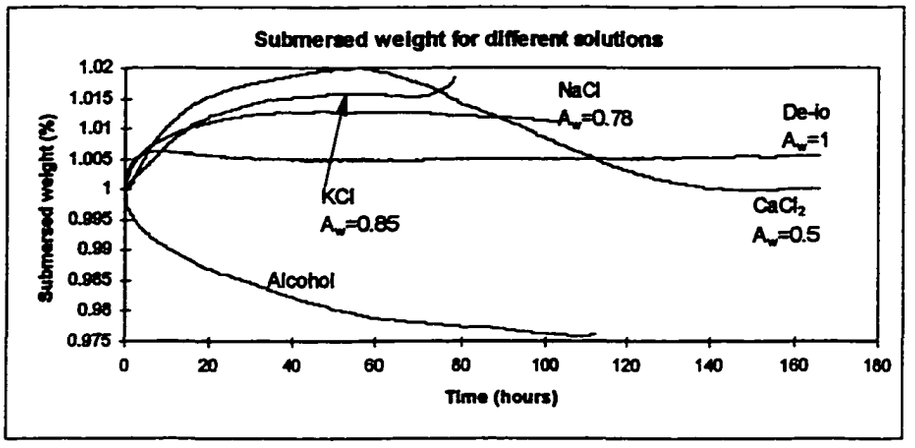


Figure 6.13: Submersed weight as a function of time in different solutions: all samples of shale D and well preserved.

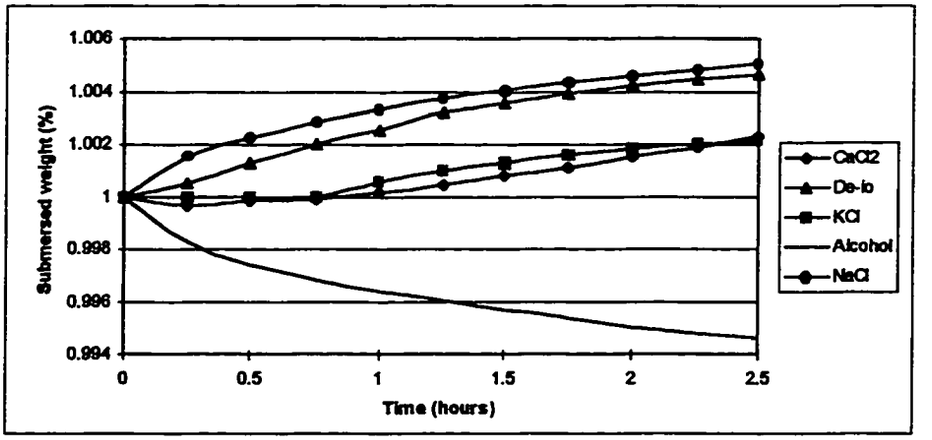


Figure 6.14: First 2.5 hrs. of the previous graph.

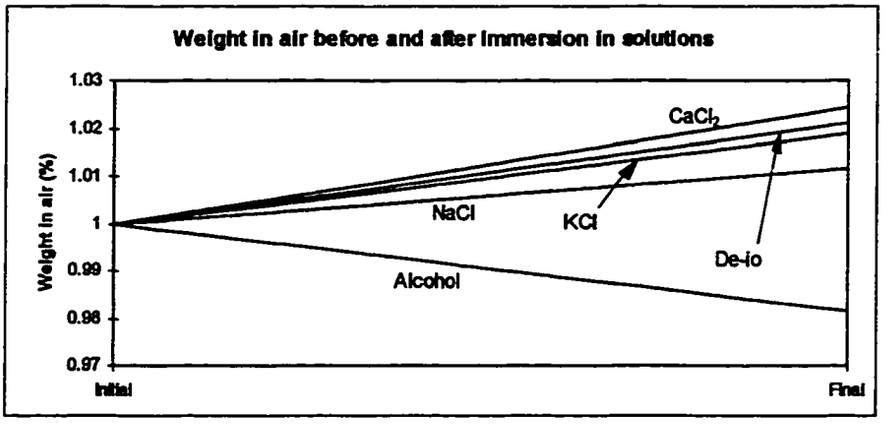


Figure 6.15: Weight in air before and after immersion in different solutions: samples and solutions are the same as in Figure 6.13.

The free water content (measured with TGA, weight loss up to 110°C) at the surface of the sample was determined with TGA. In all water solutions the values increased, despite some oscillations, whereas for the alcohol, a strong reduction was detected (Table 6.1). These results are in agreement with the measured submersed weight.

Table 6.1: Free water (%) as a function of time for the samples immersed in different solutions.

Solution	Original	1 day	2 days	3 days	4 days	5 days
De-ionized water	7.3	10.1	10.0	11.2	-	-
NaCl	7.1	-	8.9	8.4	9.2	-
$CaCl_2$	7.9	8.5	9.4	8.6	9.5	10.8
KCl	8.5	9.4	8.6	8.8	-	9.4
Alcohol	7.1	2.4	2.5	1.8	1.8	2.1

Dehydration with alcohol produced an increase in strength, as dehydration progressed (Figure 6.16). However, when immersed in water it rapidly lost resistance. Behavior in water solutions were essentially the same. Difference in salt type did not change significantly the test results. Only after immersing in water the sample that was previously immersed in the NaCl solution lost strength. During the immersion period in the salt solutions all the samples maintain their property. It is important to note also that slight differences among the samples might have introduced variation in the results. The worst situation was immersion in de-ionized water, with a continuous decrease in strength. This behavior raised suspicion that the sample was not well preserved. In Chapter 3, with a different well-preserved shale (Petr_E), no strength reduction was observed.

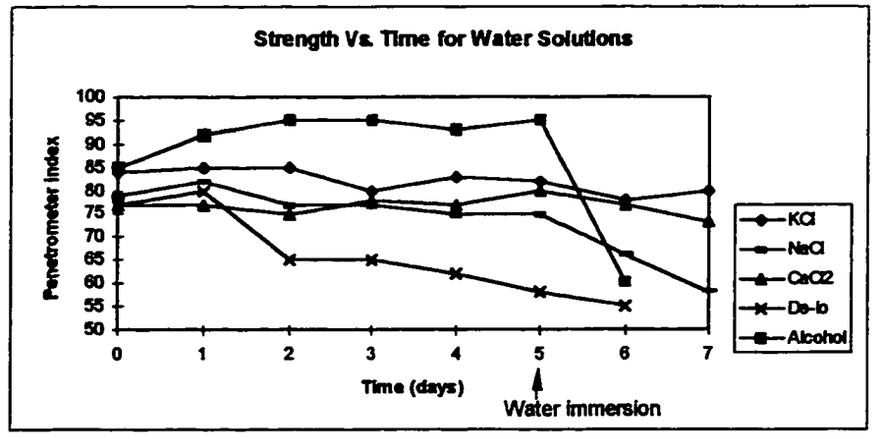


Figure 6.16: Penetrometer index as a function of time. Preserved samples immersed in quasi-saturated salt solutions, alcohol, and de-ionized water.

For the oil solutions the weight initially increased, for a short period of time, and subsequently decreased (Figure 6.17). This behavior was observed for all solutions, regardless the water phase's activity. Weight in air before and after immersion in the oil solutions showed the same behavior: decrease for all the solutions (Figure 6.18). TGA results also confirm a decrease in the free water content at the surface (Table 6.2). The water phase activity did not work driving water in or out of the shale, as assumed in several works (Hale *et al.*, 1993; van Oort *et al.*, 1996; Sherwood, 1993; Tan *et al.*, 1996; Chenevert & Osisanya, 1992). Change in the rock wettability is the only explanation for the observed behavior. After immersed in the oil solutions, the shales become oil wet, due to the presence of the emulsifier. This change in wettability, common to all the tested samples, forces water to leave the surface, dehydrating the shale. For all the OBM tested, the trend in the beginning of the test was the opposite of what was observed for the WBM. In the initial

stages of immersion, all the submersed weight increased, regardless of the activity of the water phase (Figure 6.19). This trend was reversed for all the solutions after some time. The intensity of this reversal was not equal for all the solutions tested. Interaction of the salt present in the water phase with the emulsifier might be playing an important role in this behavior. It will be necessary some more specific and dedicated tests to further investigate this point.

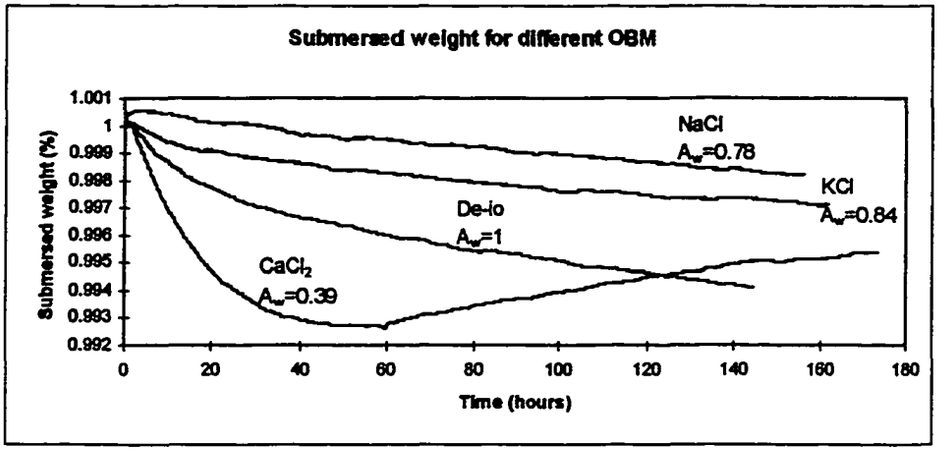


Figure 6.17: Submersed weight as a function of time in different oil solutions: all samples of shale D and well preserved.

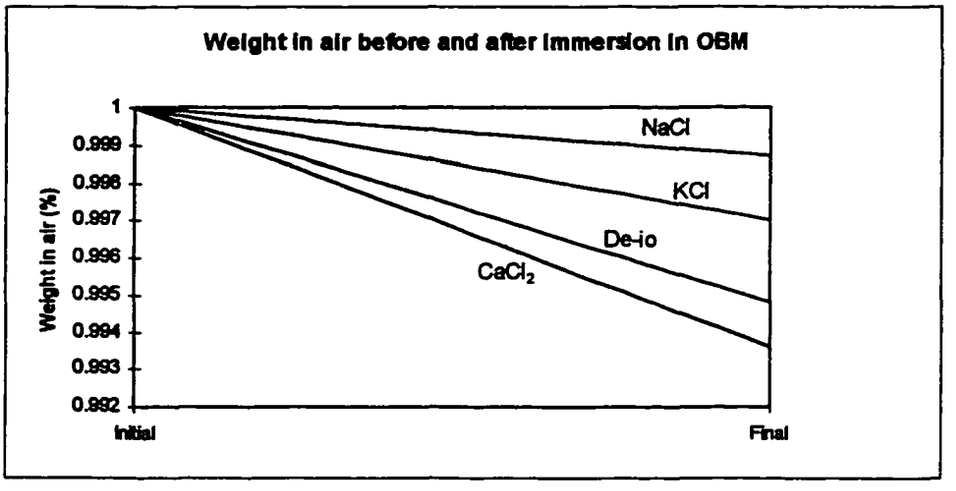


Figure 6.18: Weight in air before and after immersion in different oil solutions: samples and solutions the same as in Figure 6.17.

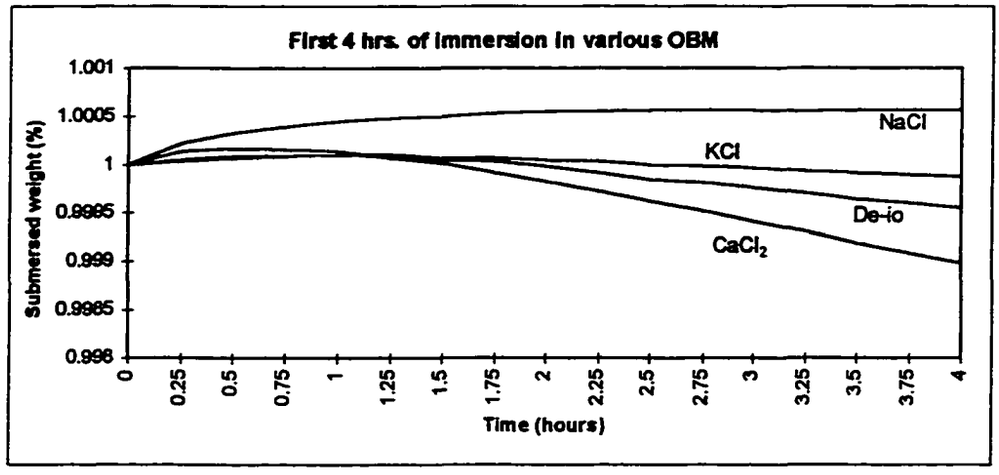


Figure 6.19: First 4 hrs. of Figure 6.17. Contrary to the immersion in the water-based solutions, all the samples increased the weight in the beginning. This trend was reversed after a few hours.

Table 6.2: Free water as a function of time for the samples immersed in OBM with different water-phase activities.

Water-phase	Original	1 day	2 days	3 days	4 days
De-ionized water	7.5	4.2	5.0	3.8	3.6
NaCl	7.6	3.3	3.8	3.7	3.0
$CaCl_2$	8.3	4.6	2.7	-	3.1
KCl	7.3	3.8	3.0	2.9	3.1

The wettability change was so intense that immersion in de-ionized water after 5 days immersed in the oil solutions did not modify the shale strength (Figure 6.20), even considering that the rock lost water. Wettability change avoids the contact of water with the dehydrated clay minerals, preventing them from reacting and swelling. Gieseking (1939) has described this mechanism reporting that smectite clays lost their tendency to swell by water sorption when saturated with a variety of organic cations. These cations are absorbed

on the basal plane surfaces of the smectite (Grim, 1968; Appendix B). Hendricks (1941) and Grim *et al.* (1947) also described this mechanism in kaolinite and smectite, emphasizing that the reduction in water sorption should not be exactly correlative with the size of organic ion, since the shape of the organic ion may be such as to destroy the configuration of water molecules in the adsorbed water layer.

This is not the case of samples dehydrated in alcohol and then immersed in de-ionized water, shown previously. Besides dehydration, immersion in OBM produced a strong surface alteration that impedes the clay minerals to react with water. Exposure to air and immersion in alcohol produced also dehydration, but the clay minerals maintained their ability to absorb water.

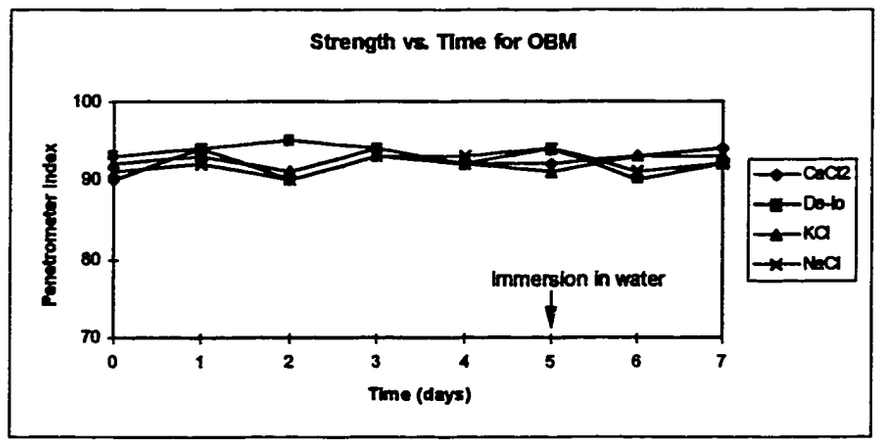


Figure 6.20: Strength (penetrometer index) as a function of immersion time. After 5 days immersed in different OBM, the samples were immersed in de-ionized water.

The increase in weight at the beginning of the test cannot be attributed to the difference in activity between the shale and the water phase, since it

occurred to all the tested solutions. Change in bound water can be explained by interaction with the salts, since the variation is different for each solution, as was the case for the water solutions. The presence of the emulsifier, however, impeded changes in the structural water, due to the wettability modification. It is seen, then, that besides the effect of the chemical potential, other mechanisms are stronger than this one, causing a totally unexpected behavior.

Even though the samples were not checked for saturation degrees, all of them had a reasonable value for the original free water content, as expected for this type of shale (see Chapter 3, Table 3.6). Two samples with values lower than 7% were discarded. The samples were all preserved in a similar way following the handling procedure described in Chapter 3, avoiding air exposure at all times. Being conducted under atmospheric pressure, the samples were probably not saturated. Also, running the experiments at room temperature did not reproduce downhole conditions. These facts could have introduced some artifacts, though difficult to be quantified. It should be clear that the only driving force present in these experiments was the chemical potential. Incorporation of temperature and pressure should be done after a complete understanding of the chemical potential effects, since other driving mechanisms will be added (hydraulic and thermal)

Temperature affects solubility of the chemical species, and, therefore, will change the final equilibrium of the shale exposed to a solution. Results in the TGA should show this variation as a function of temperature of the

solution/sample. Pressure sensitivity should be lower than temperature; however, an effort to quantify this parameter influence should also be pursued. An attempt to run similar experiments under more realistic conditions (high pressure and temperature) should be made, so that an understanding of the actual downhole mechanisms can be developed.

6.2.6 Analysis of Shale Structure Alteration with TGA

For each solution TGA tests were conducted on the shale sample before immersion and after each 24 hrs. periods of immersion. Typically, the samples remained immersed in the solutions for 5 days, and then immersed in de-ionized water until no further variation of structure was seen. The aim was to observe the change in structure as a function of immersion time, and then check the effects of immersing the samples in a higher activity solution. In the field it is very difficult to keep exactly the same mud properties all the time, and immersing the sample in de-ionized water after some time in a solution creates the worst situation.

TGA results for each solution is presented so that a comparison and observation of the alteration can be easily done. For the sake of simplicity, when just the salt type is mentioned, it means that a water solution is used. For the OBM solutions, differentiation is on the water phase. In these cases, it is mentioned the salt type followed by OBM.

6.2.6.1 Immersion in $CaCl_2$ 36% w/w (A_w = 0.50)

Immersion in $CaCl_2$ water solution produced a strong alteration in bound and structural water as well as the elimination of the inflection observed in the derivative curve below 100°C. This inflection elimination is associated with the change in the interlayer water of the smectite. The calcite content does not indicate a significant change. Another interesting point to mention here is that no major change is observed after the first 24 hrs. of immersion. The sample remained practically with the same structure up to 6 days of immersion.

Immersion in de-ionized water produced a surprising result: the structural water recovered almost the same shape as in its native state. The bound water, however, was not recovered. Adsorption of water is clearly seen by the increase in the first peak of the derivative curve. The calcite content also remained almost the same as in the native state. Even with a very low activity, this solution could not drive water out of the shale.

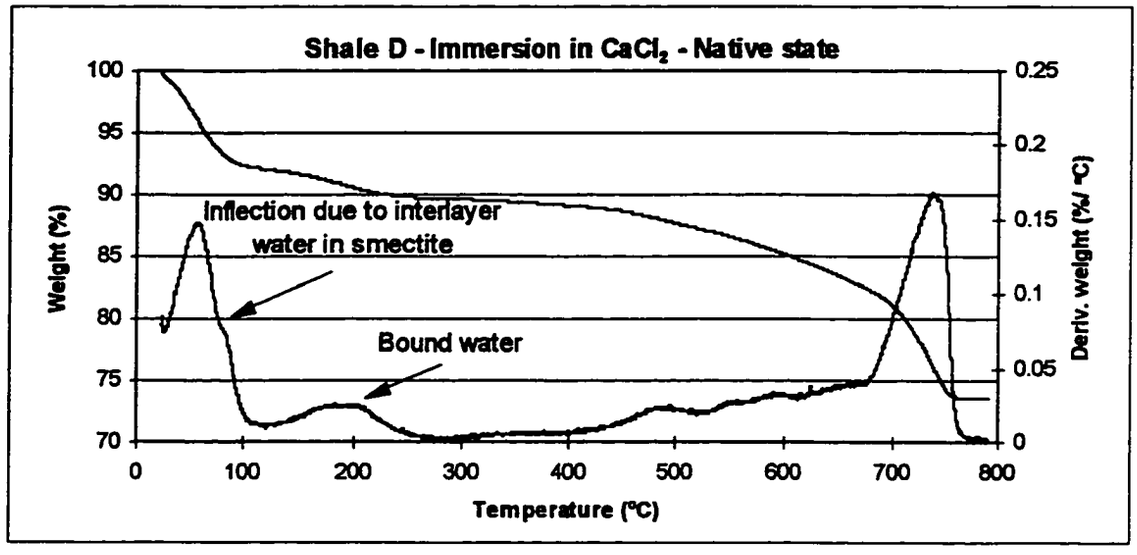


Figure 6.21: TGA (10°C/min.) of shale D - Native state - Immersion in $CaCl_2$.

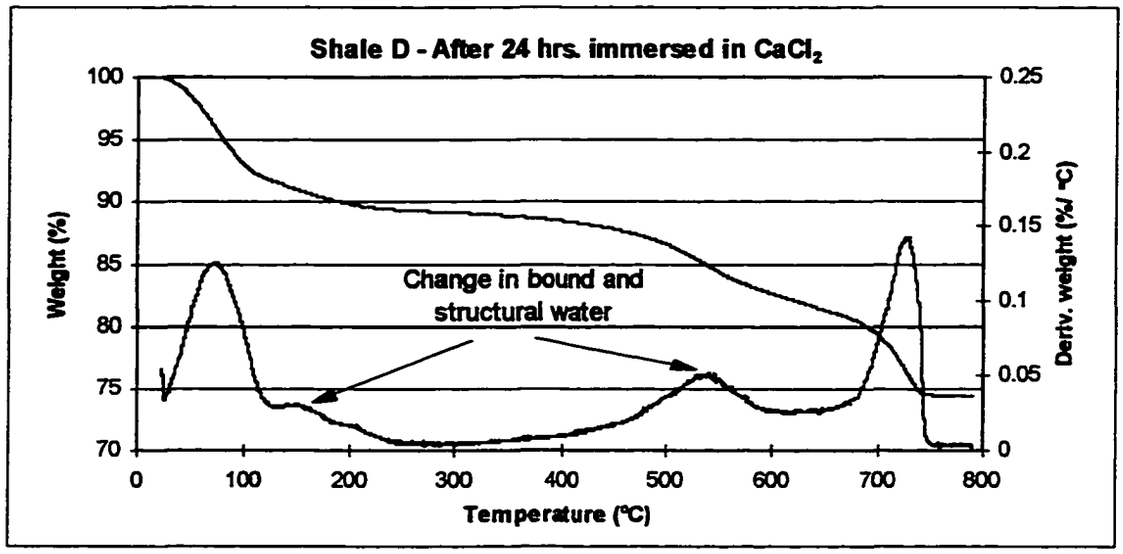


Figure 6.22: TGA (10°C/min.) of shale D after 24 hrs. immersed in $CaCl_2$ 35% w/w (A_w = 0.50).

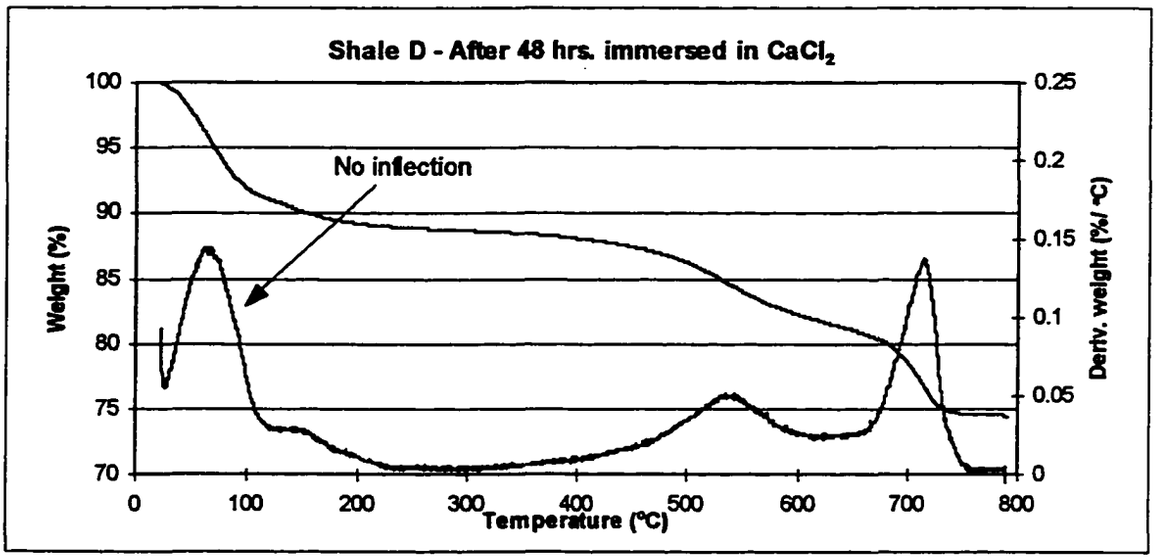


Figure 6.23: TGA (10°C/min.) of shale D after 48 hrs. immersed in $CaCl_2$ 35% w/w (A_w = 0.50).

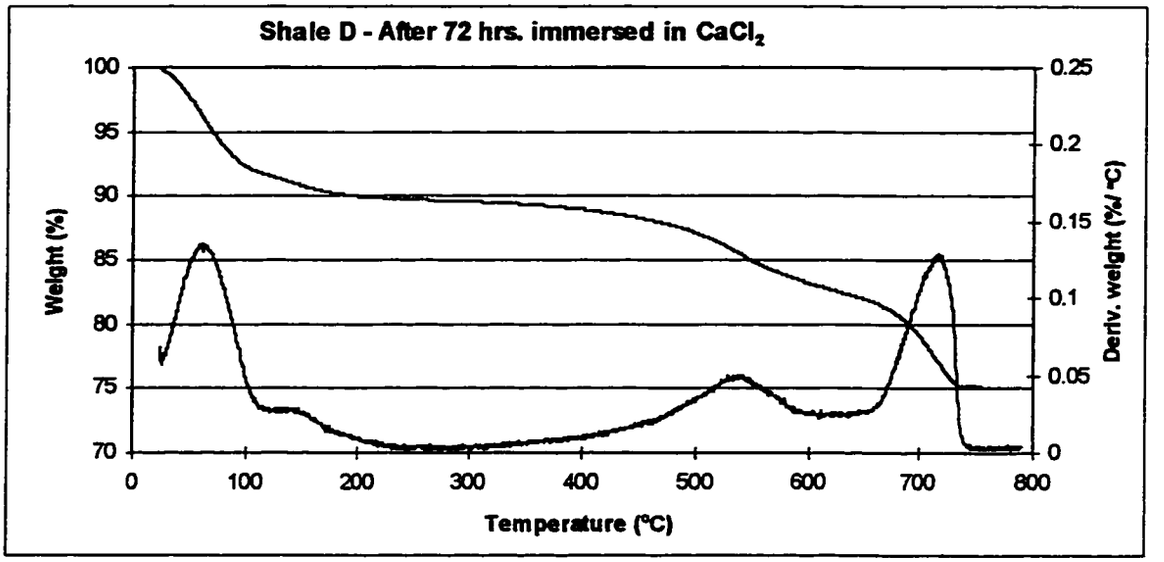


Figure 6.24: TGA (10°C/min.) of shale D after 72 hrs. immersed in $CaCl_2$ 35% w/w (A_w = 0.50).

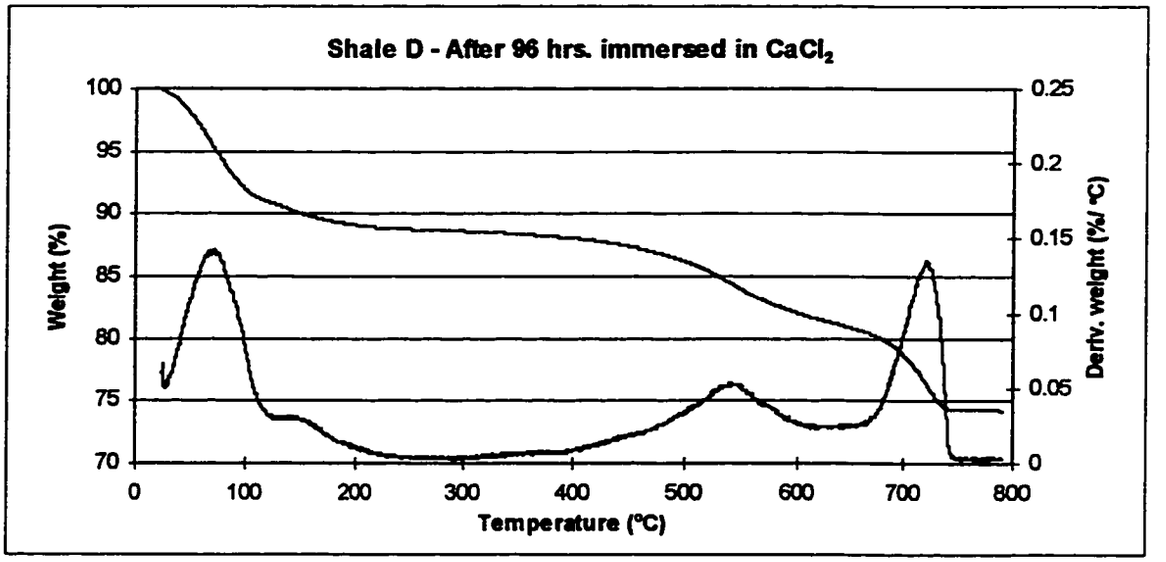


Figure 6.25: TGA (10°C/min.) of shale D after 96 hrs. immersed in $CaCl_2$ 35% w/w (A_w = 0.50).

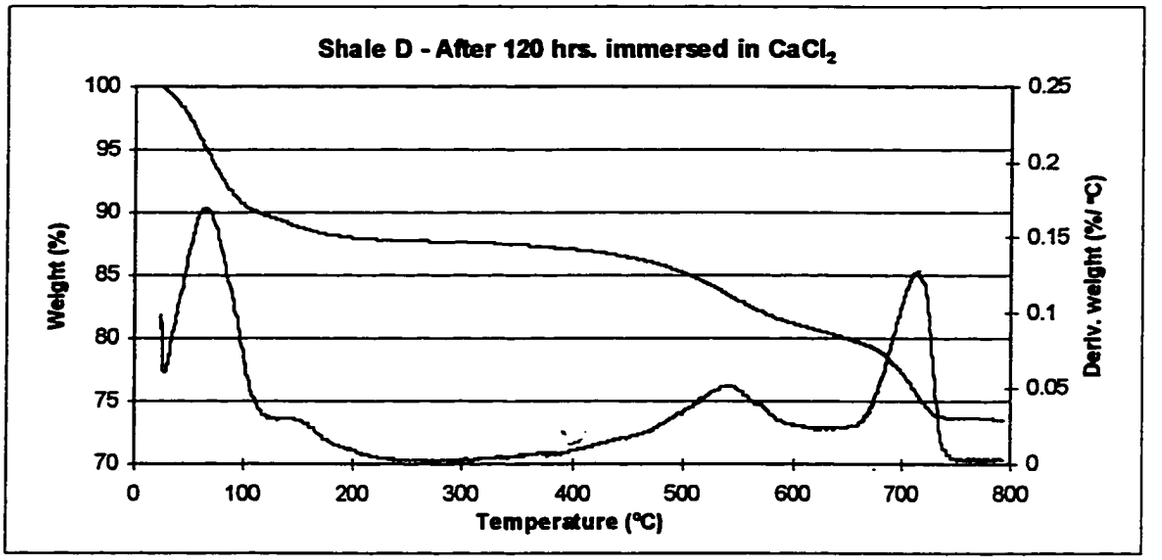


Figure 6.26: TGA (10°C/min.) of shale D after 120 hrs. immersed in $CaCl_2$ 35% w/w (A_w = 0.50).

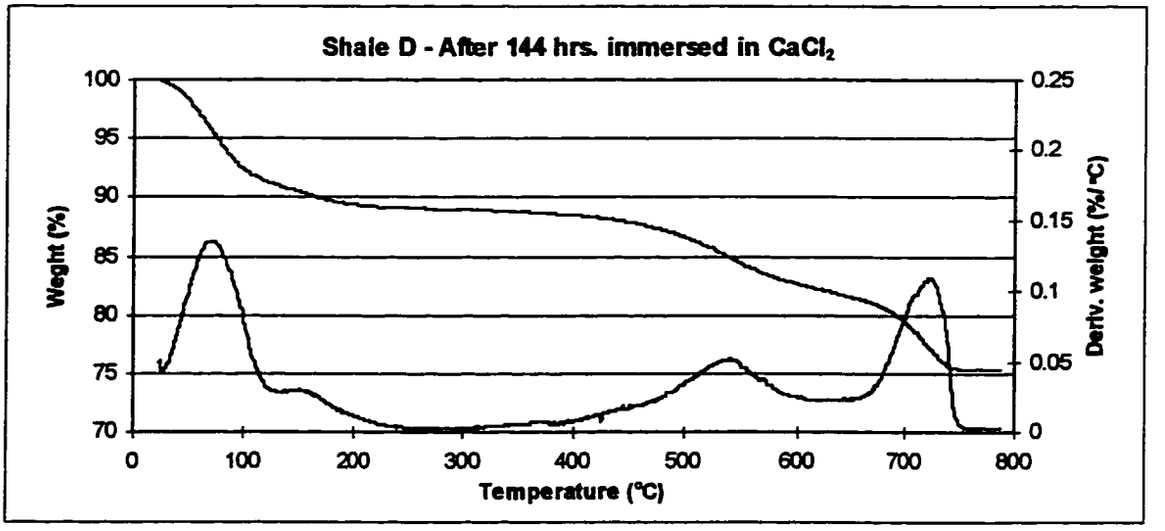


Figure 6.27: TGA (10°C/min.) of shale D after 144 hrs. immersed in $CaCl_2$ 35% w/w (A_w = 0.50).

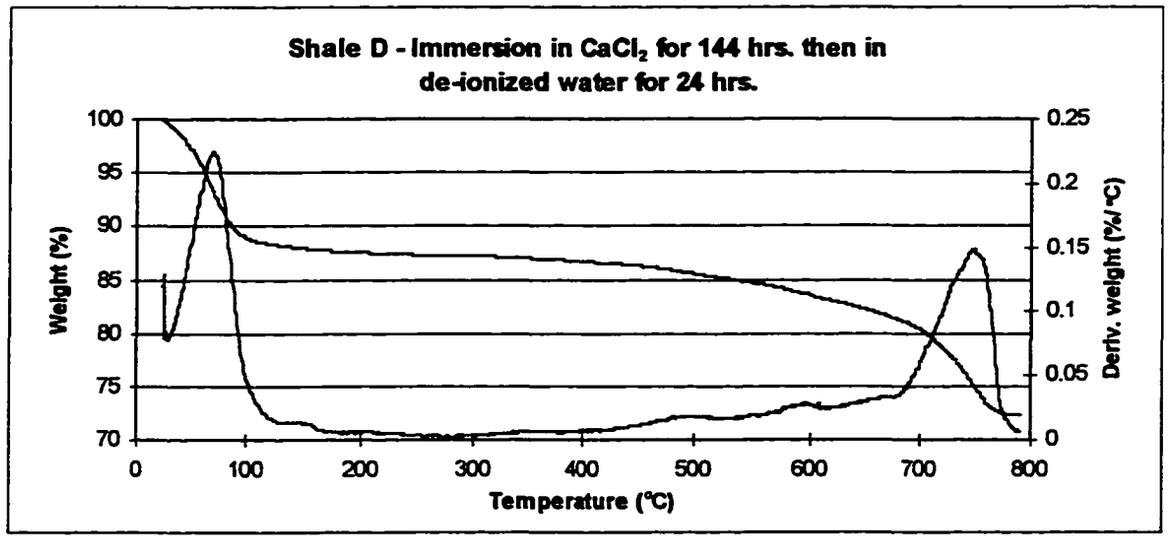


Figure 6.28: TGA (10°C/min.) of shale D after 144 hrs. immersed in $CaCl_2$ 35% w/w (A_w = 0.50), then immersed in de-ionized water for 24 hrs.

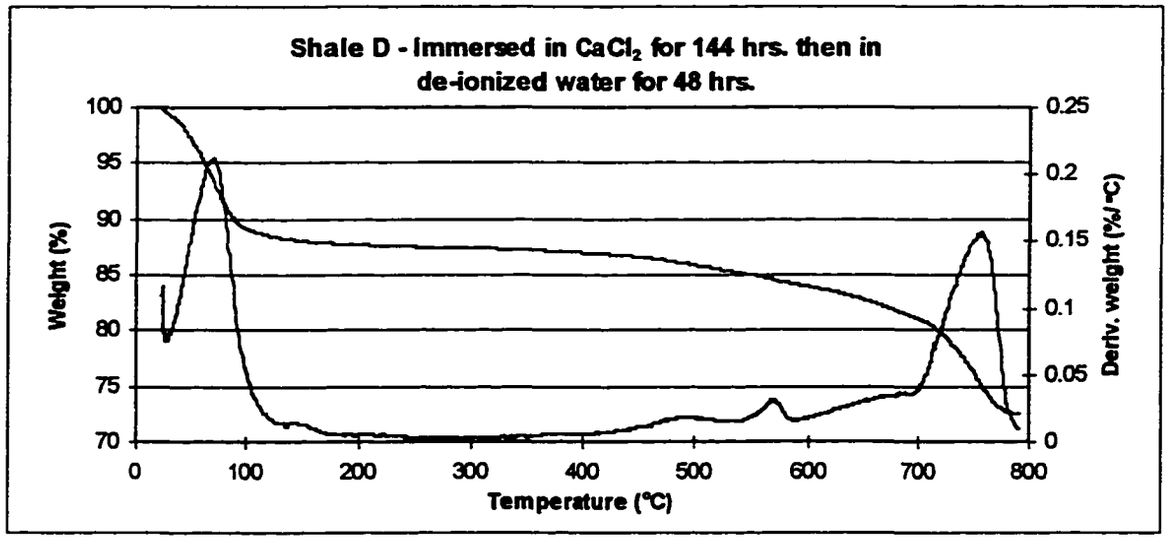


Figure 6.29: TGA (10°C/min.) of shale D after 144 hrs. immersed in $CaCl_2$ 35% w/w (A_w = 0.50), then immersed in de-ionized water for 48 hrs.

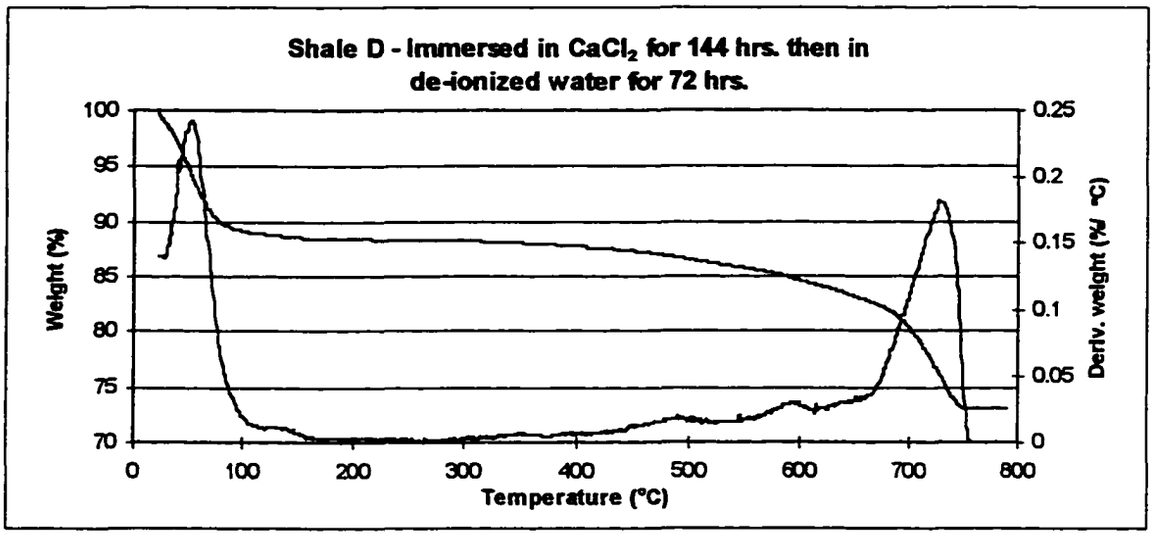


Figure 6.30: TGA (10°C/min.) of shale D after 144 hrs. immersed in $CaCl_2$ 35% w/w (A_w = 0.50), then immersed in de-ionized water for 72 hrs.

6.2.6.2 Immersion in NaCl 24% w/w (A_w = 0.78)

The same shale presented a completely different behavior when immersed in the NaCl solution. The inflection was also eliminated in the first portion of the derivative curve, indicating that the smectite was somehow affected. The structure water was also affected, but in a different way than when the shale was exposed to $CaCl_2$. In addition, a reduction in calcite content is consistently seen. As in the previous case, after the first 24 hrs. of exposure, there is no significant change in the shale structure. Immersion in de-ionized water produced a recovery in the structural water to the same shape as in the native state. Also, the calcite content increased, going back to the same original level.

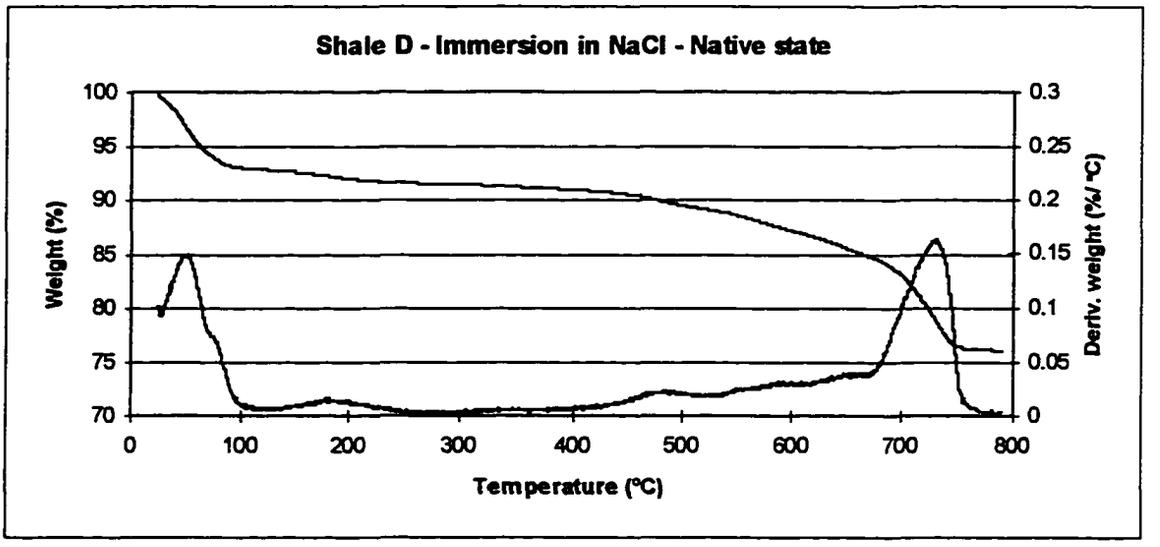


Figure 6.31: TGA (10°C/min.) of shale D - Native state - Immersion in NaCl.

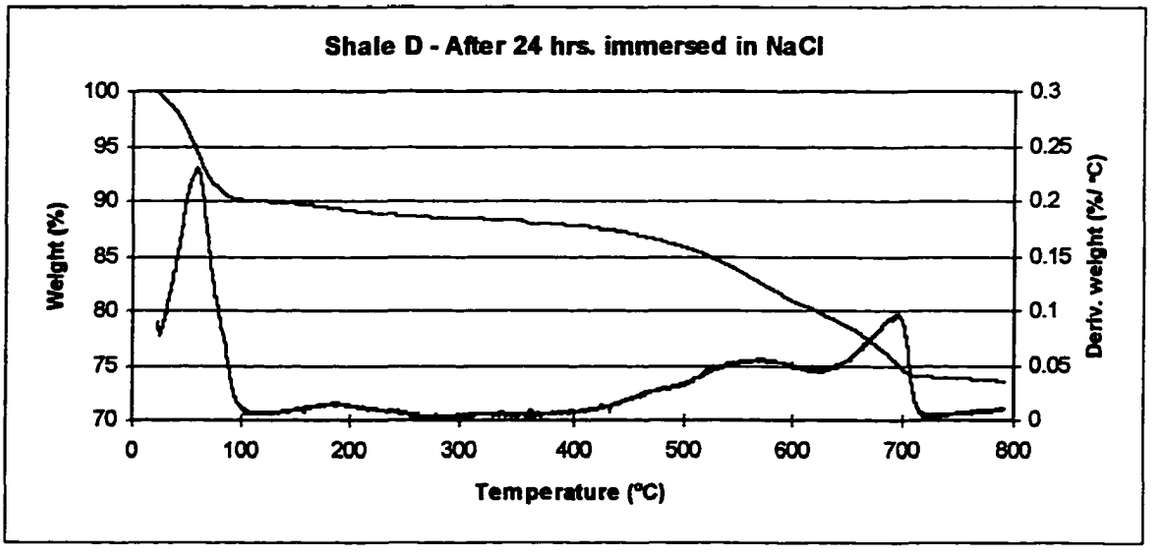


Figure 6.32: TGA (10°C/min.) of shale D after 24 hrs. immersed in NaCl 24% w/w (A_w = 0.78).

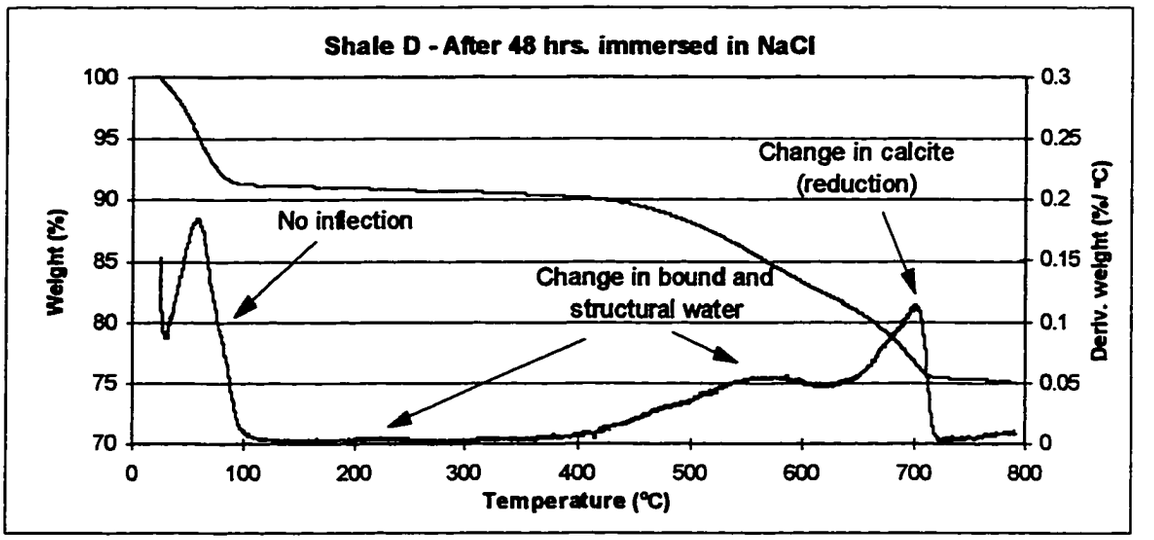


Figure 6.33: TGA (10°C/min.) of shale D after 48 hrs. immersed in NaCl 24% w/w (A_w = 0.78).

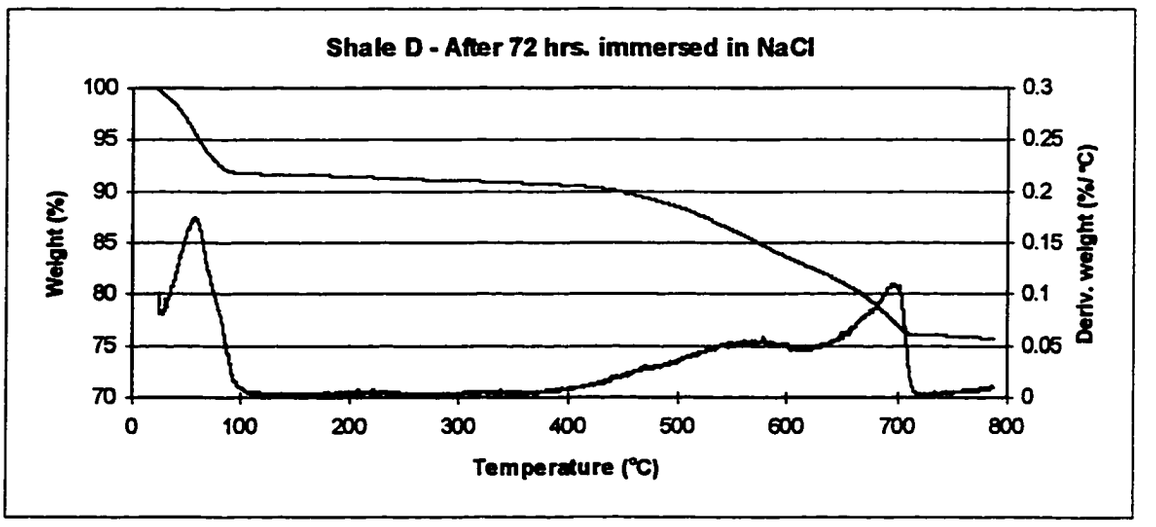


Figure 6.34: TGA (10°C/min.) of shale D after 72 hrs. immersed in NaCl 24% w/w (A_w = 0.78).

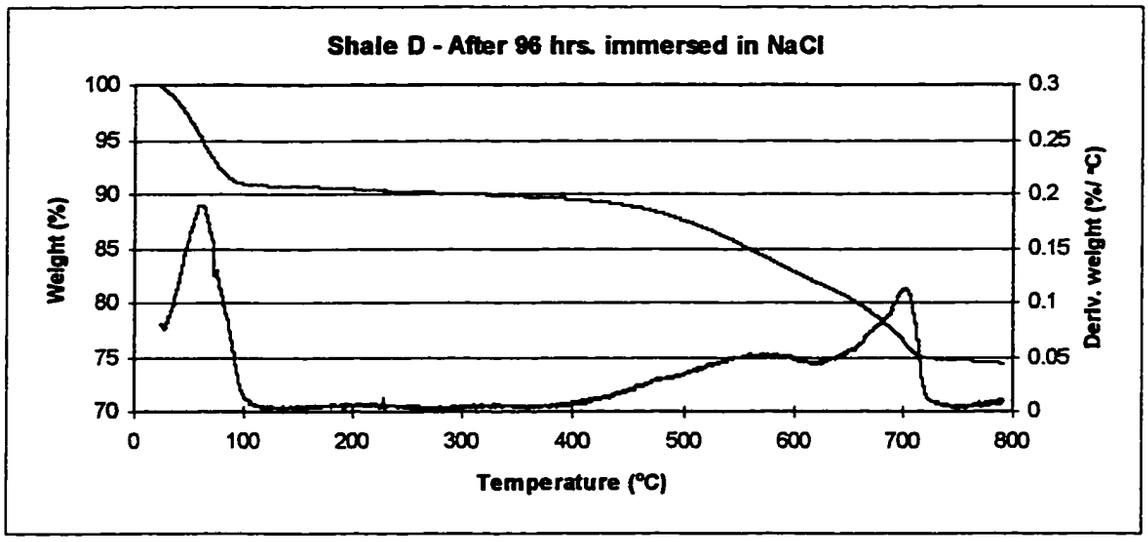


Figure 6.35: TGA (10°C/min.) of shale D after 96 hrs. immersed in NaCl 24 % w/w (A_w = 0.78).

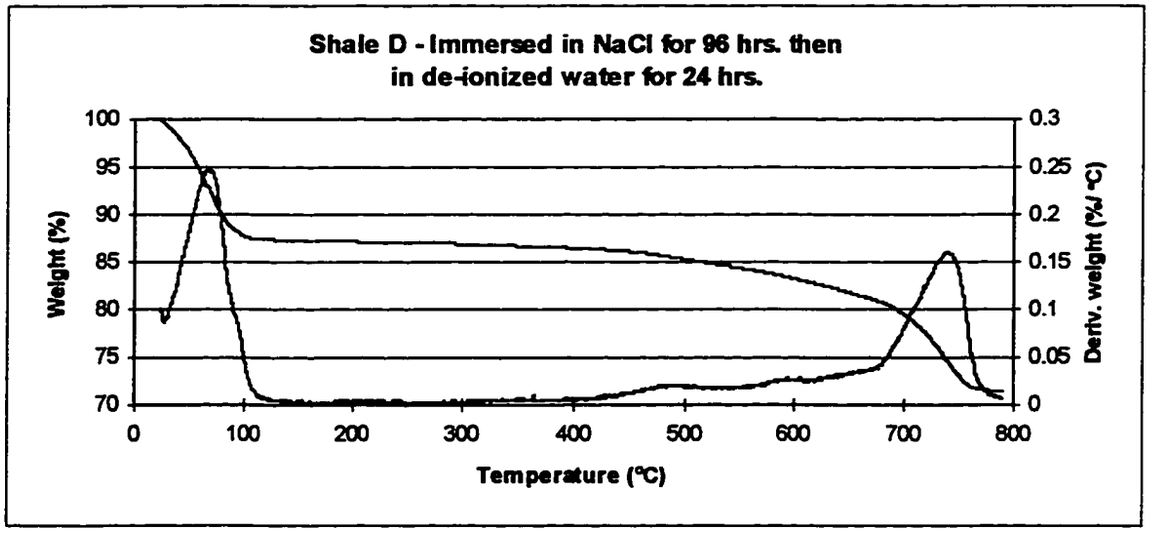


Figure 6.36: TGA (10°C/min.) of shale D after 96 hrs. immersed in NaCl 24% w/w (A_w = 0.78), then in de-ionized water for 24 hrs.

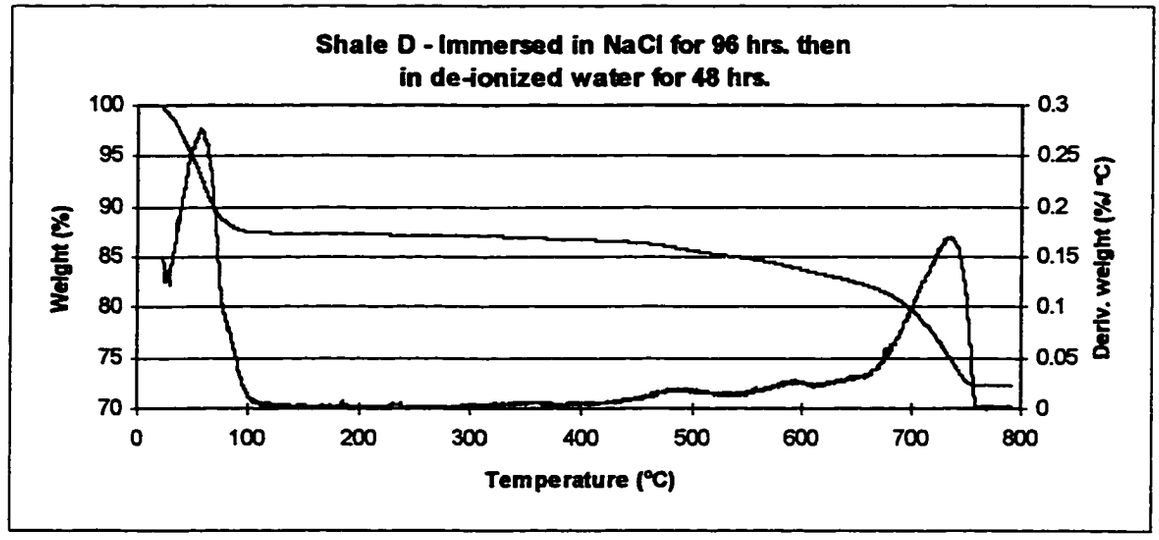


Figure 6.37: TGA (10°C/min.) of shale D after 96 hrs. immersed in NaCl 24% w/w (A_w = 0.78), then in de-ionized water for 48 hrs.

6.2.6.3 Immersion in KCl 25% w/w (A_w = 0.85)

Immersion in KCl produced a similar change as NaCl. The change in the bound water took longer, but a flat derivative was also the result. The structural water modified in a slightly different way from what was seen with NaCl, but far from the alteration produced by $CaCl_2$. A reduction in calcite can be observed. Despite the fact that the bound water took longer to change, all the remaining alteration observed took place in the first 24 hrs. of exposure, as in the previous salt solutions. Immersion in de-ionized water restored the shape of structural water, but not the bound water. Calcite content also increased after immersion in de-ionized water, recovering its original value. This same behavior was observed for the immersion in NaCl.

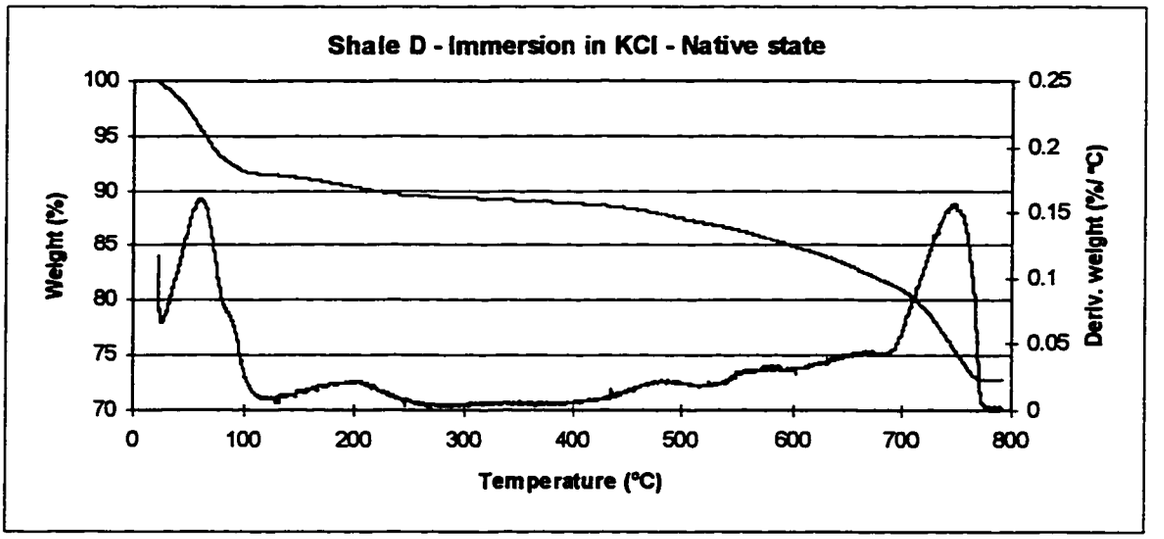


Figure 6.38: TGA (10°C/min.) of shale D - Native state - Immersion in KCl.

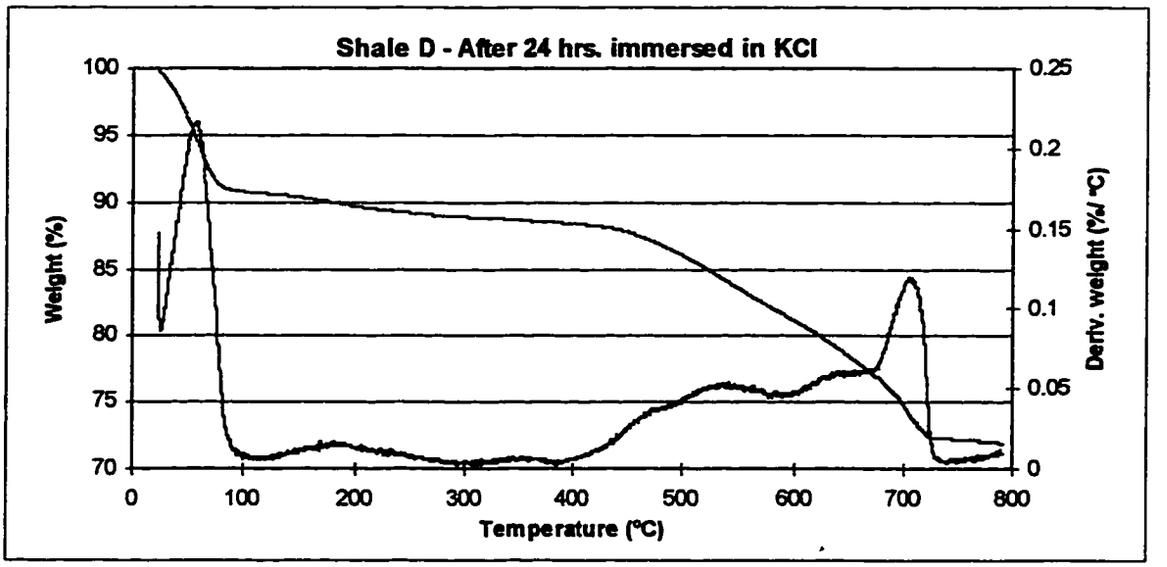


Figure 6.39: TGA (10°C/min.) of shale D after 24 hrs. immersed in KCl 26% w/w (A_w = 0.85).

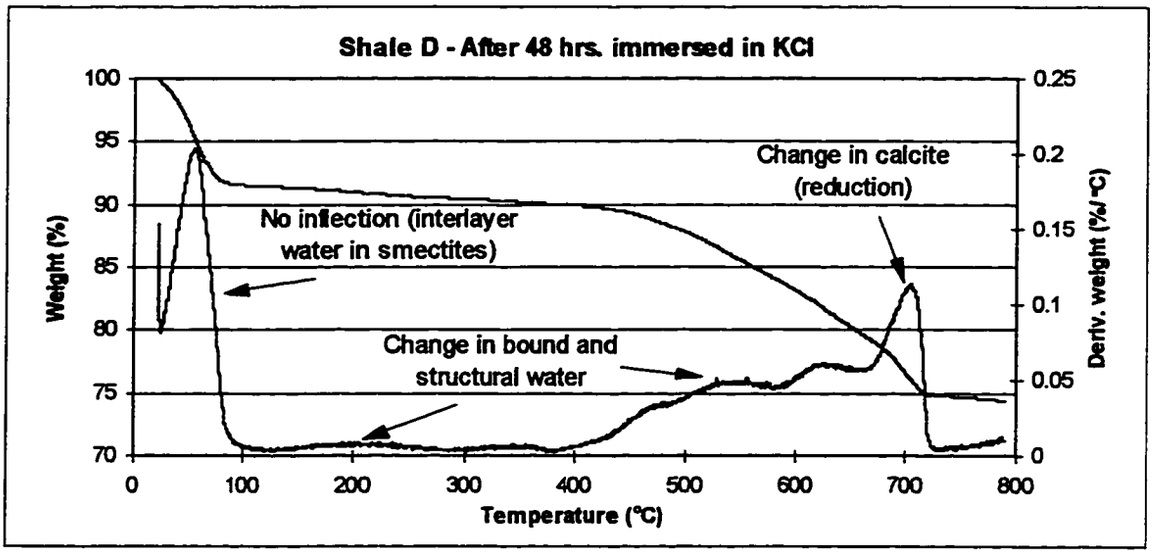


Figure 6.40: TGA (10°C/min.) of shale D after 48 hrs. immersed in KCl 26% w/w (A_w = 0.85).

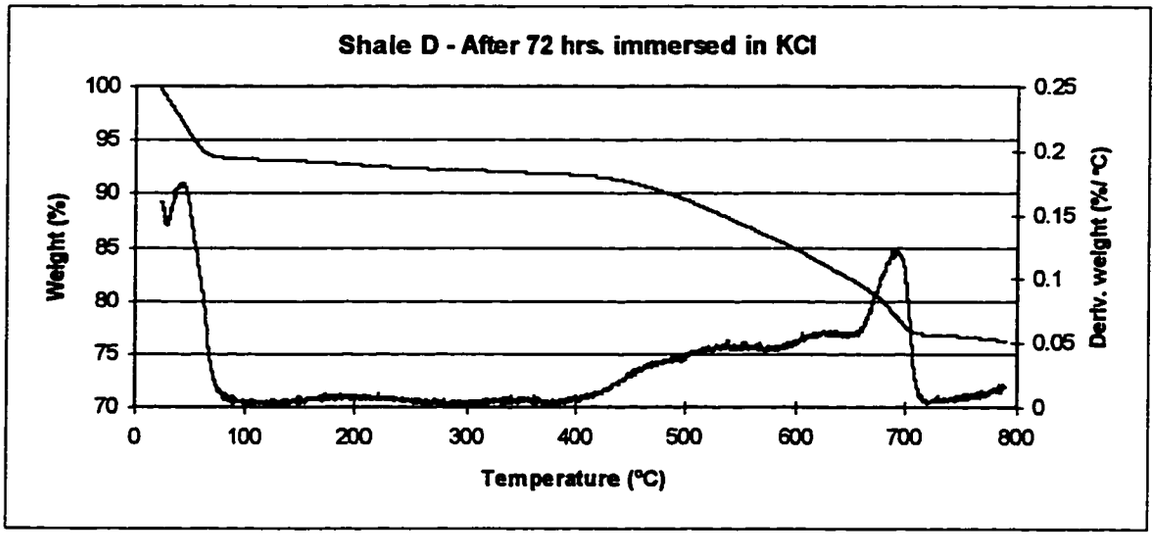


Figure 6.41: TGA (10°C/min.) of shale D after 72 hrs. immersed in KCl 26% w/w (A_w = 0.85).

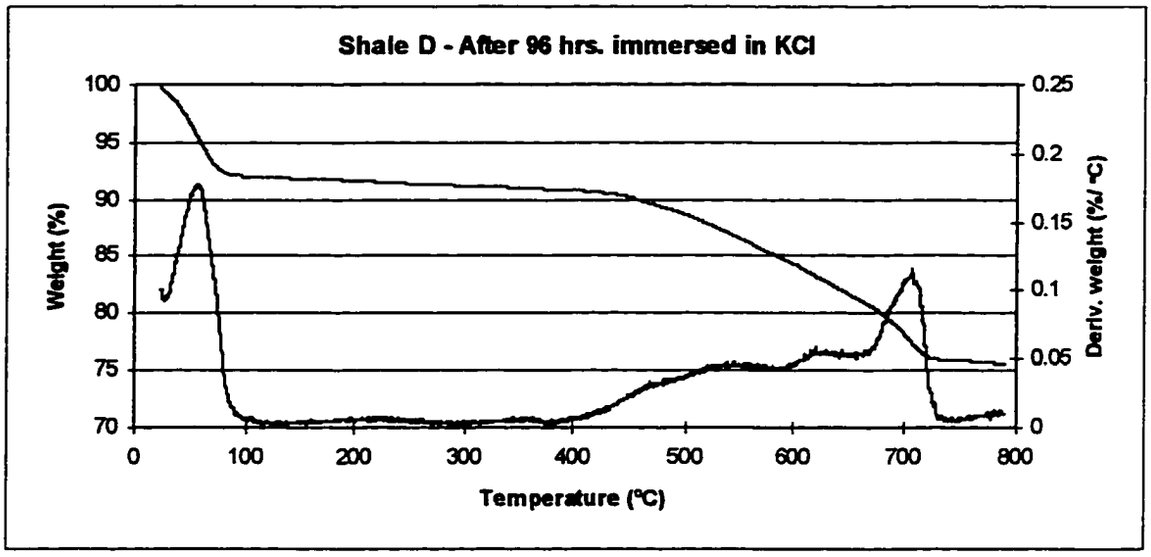


Figure 6.42: TGA (10°C/min.) of shale D after 96 hrs. immersed in KCl 26% w/w (A_w = 0.85).

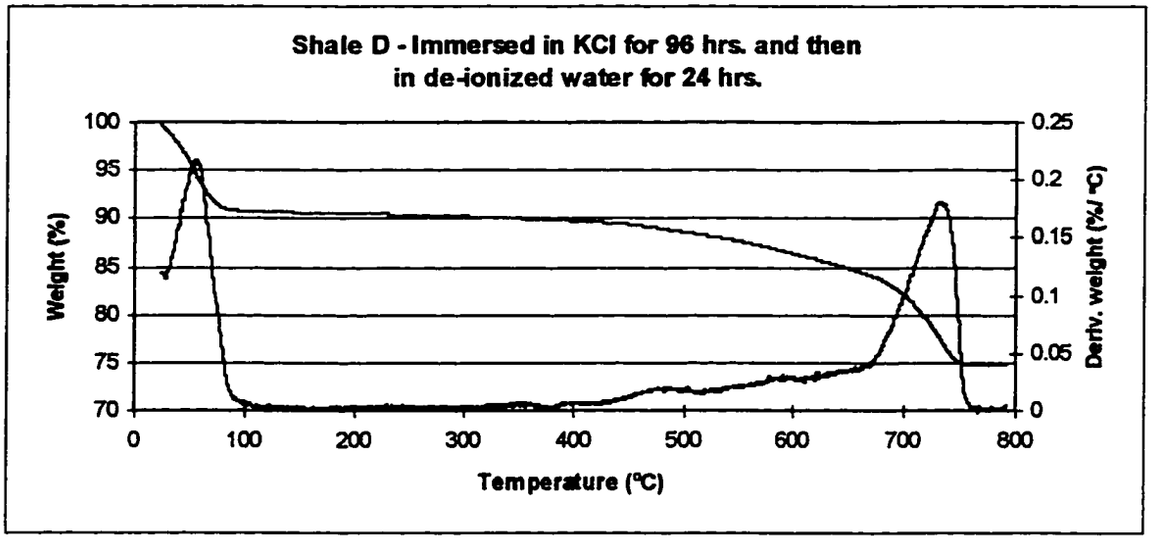


Figure 6.43: TGA (10°C/min.) of shale D after 96 hrs. immersed in KCl 26% w/w (A_w = 0.85), then in de-ionized water for 24 hrs.

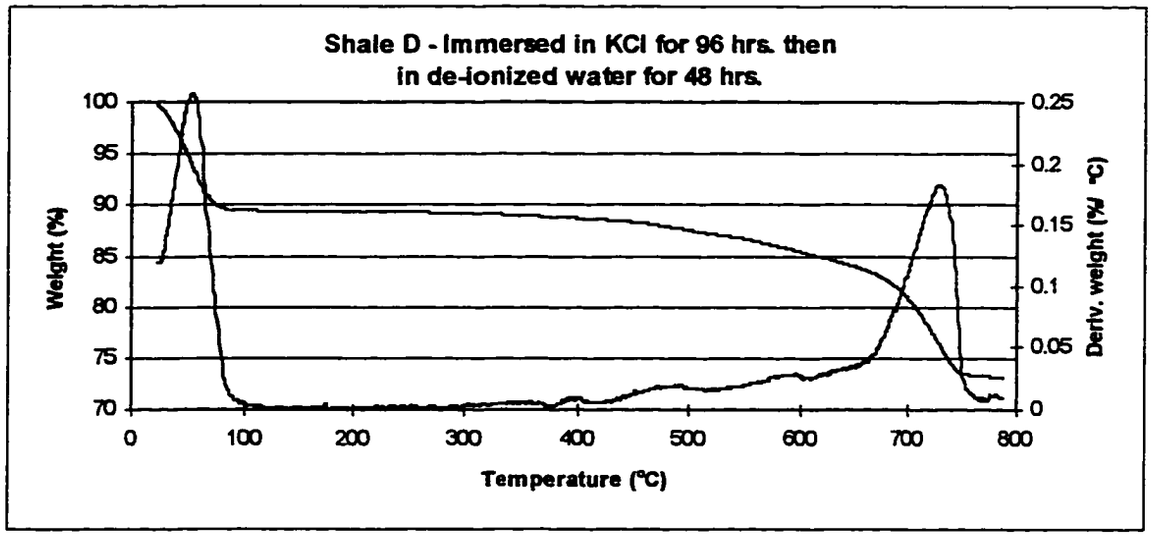


Figure 6.44: TGA (10°C/min.) of shale D after 96 hrs. immersed in KCl 26% w/w (A_w = 0.85), then in de-ionized water for 48 hrs.

6.2.6.4 Immersion in de-ionized water (A_w = 1.00)

Only the free and bound water presented some alteration when shale Petr_D was immersed in de-ionized water. Structural water and calcite content remained the same throughout the duration of the test. Absorption of water is clear, with a direct consequence on the strength of the rock. Change in the bound water took some time, reproducing the same behavior as when immersed in KCl. Essentially, all the other features of the shale remained constant.

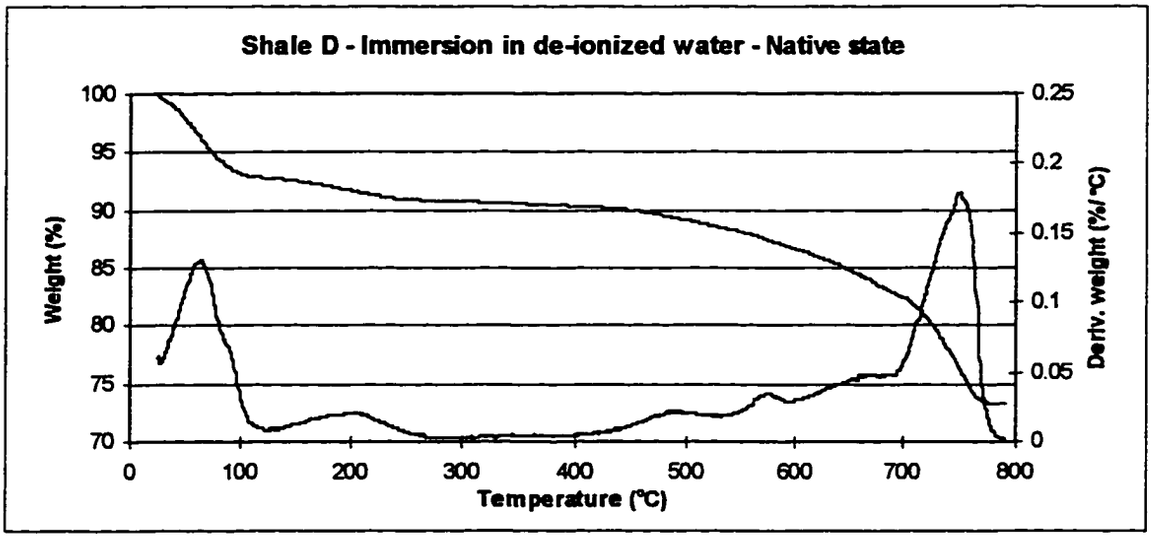


Figure 6.45: TGA (10°C/min.) of shale D - Native state - Immersion in de-ionized water.

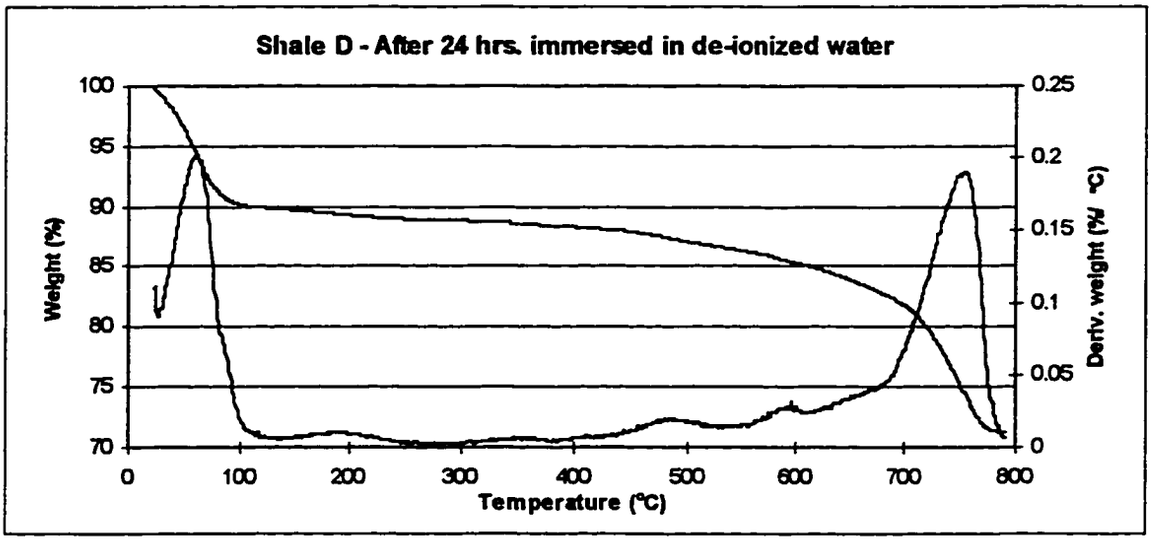


Figure 6.46: TGA (10°C/min.) of shale D after 24 hrs. immersed in de-ionized water.

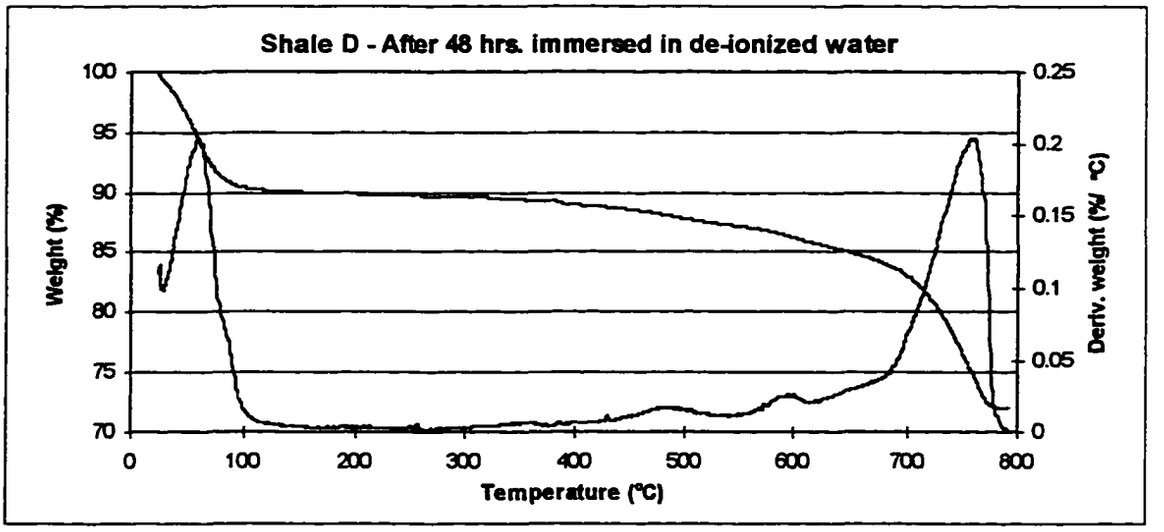


Figure 6.47: TGA (10°C/min.) of shale D after 48 hrs. immersed in de-ionized water.

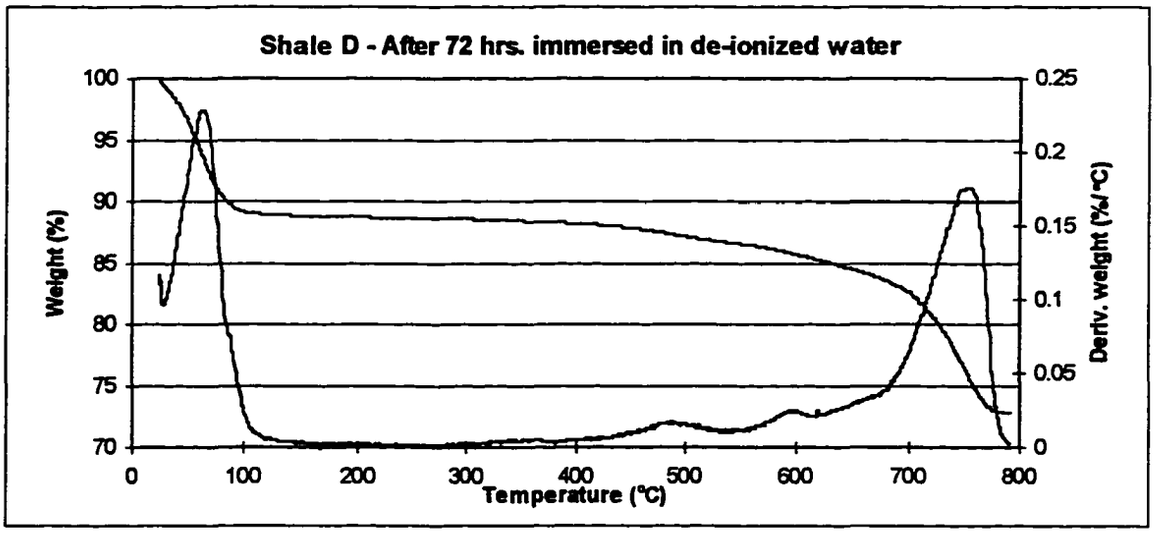


Figure 6.48: TGA (10°C/min.) of shale D after 72 hrs. immersed in de-ionized water.

6.2.6.5 Immersion in alcohol

Shale dehydration is clear when immersed in alcohol. A huge reduction of the first peak in the derivative curve shows that the free water reduced significantly from the original level. Bound water was also modified, as well as an increase in calcite can be seen. Even though a change in structural water did happen, this modification was not as strong as observed for the salt solutions. It is important to note the presence of the inflection in the derivative curve after some dehydration has taken place. This is an indication that the interlayer water of the smectite was not strongly affected, as in the case of the salt solutions mentioned previously.

Due to its dried stage, immersion in de-ionized water produced a huge increase in the free water content. However, all the remaining characteristics remained the same, except for a slight change in the bound water. The adsorption of a great amount of water led the sample to completely lose its strength after only 24 hrs. of immersion in de-ionized water.

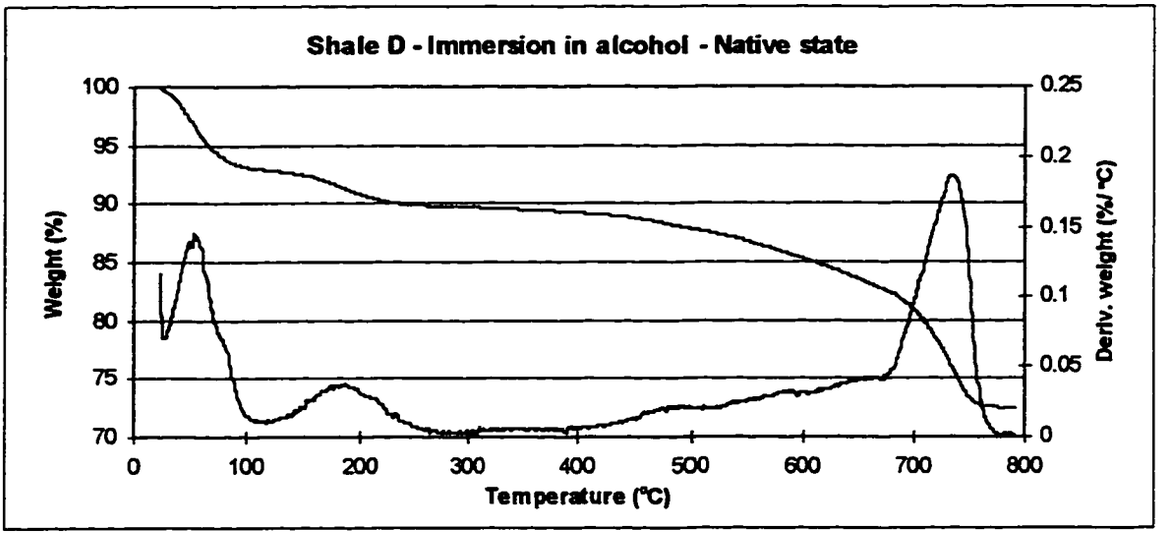


Figure 6.49: TGA (10°C/min.) of shale D - Native state - Immersion in alcohol.

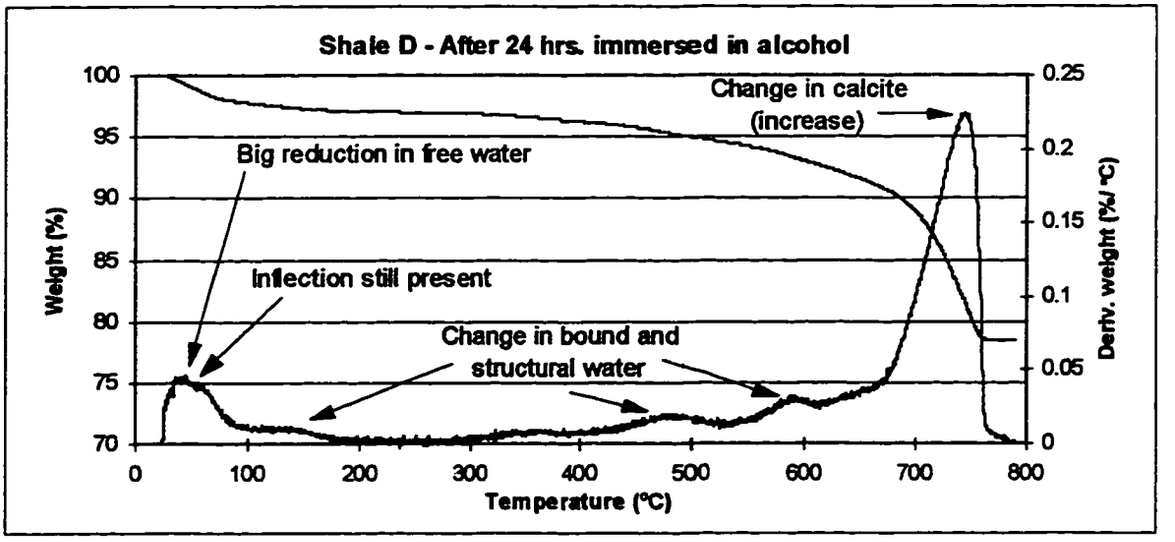


Figure 6.50: TGA (10°C/min.) of shale D after 24 hrs. immersed in alcohol.

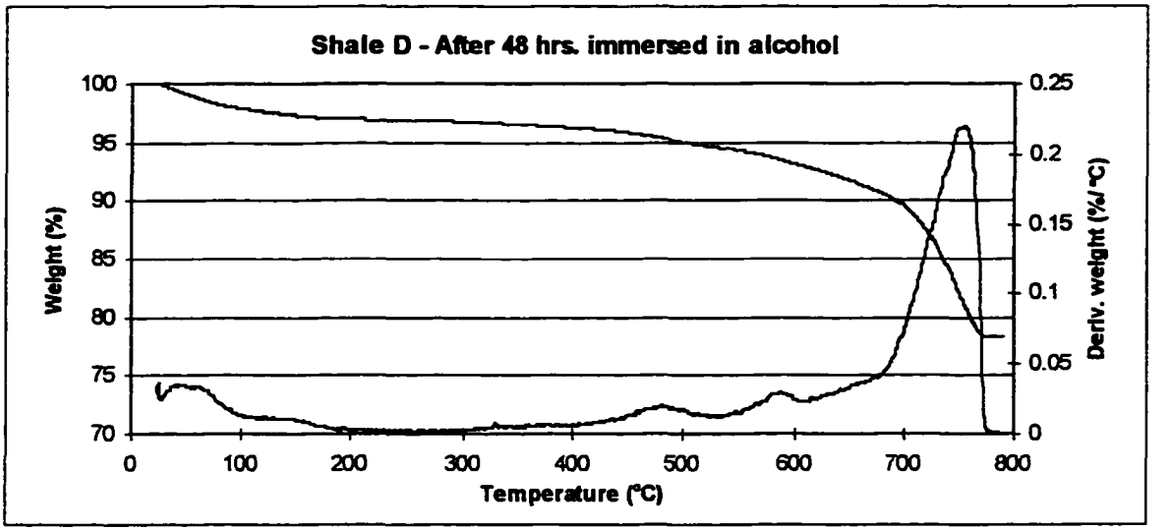


Figure 6.51: TGA (10°C/min.) of shale D after 48 hrs. immersed in alcohol.

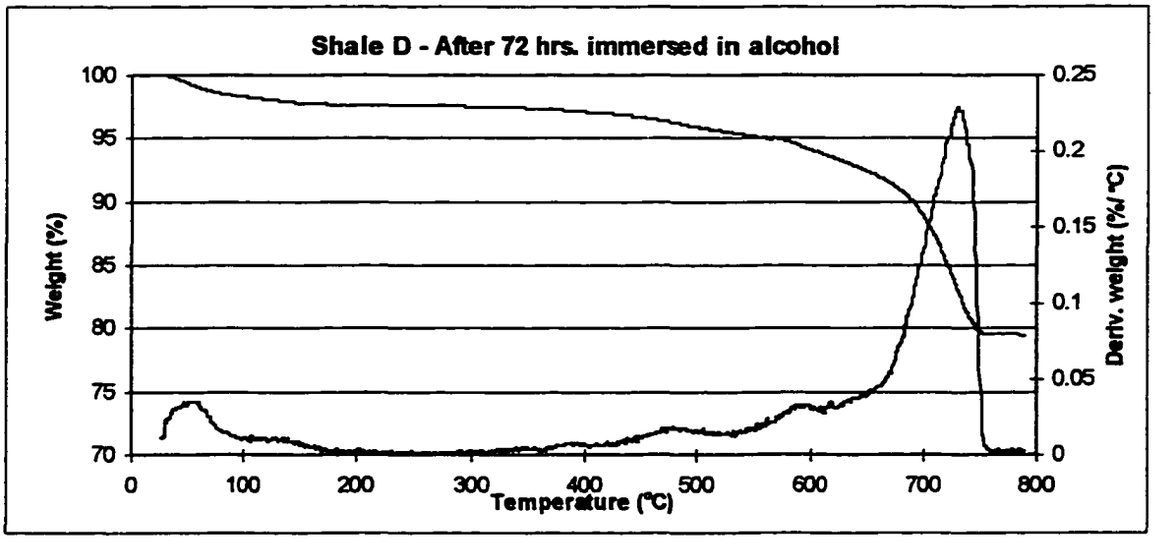


Figure 6.52: TGA (10°C/min.) of shale D after 72 hrs. immersed in alcohol.

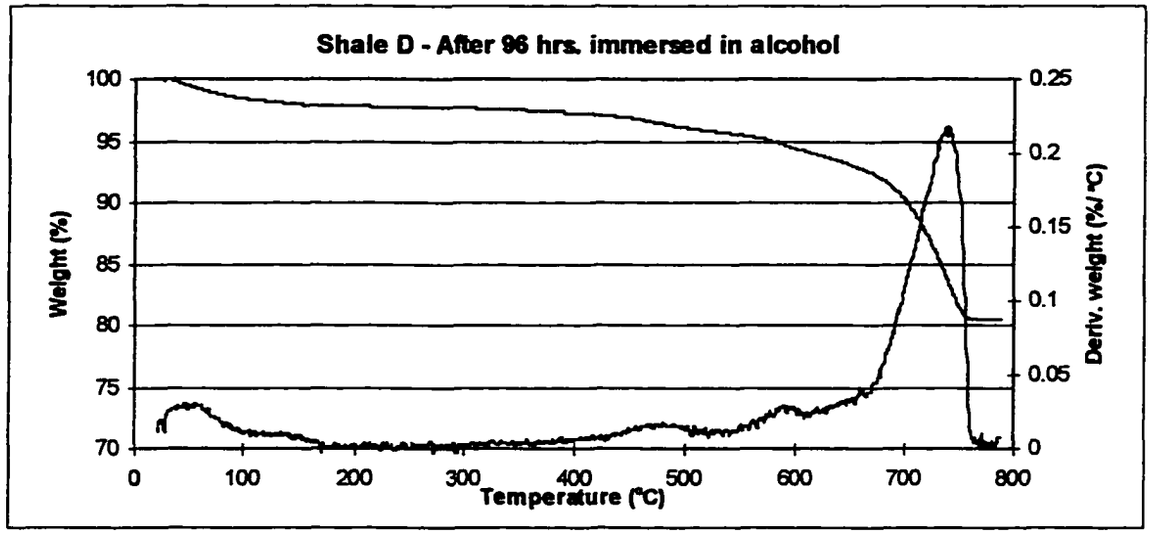


Figure 6.53: TGA (10°C/min.) of shale D after 96 hrs. immersed in alcohol.

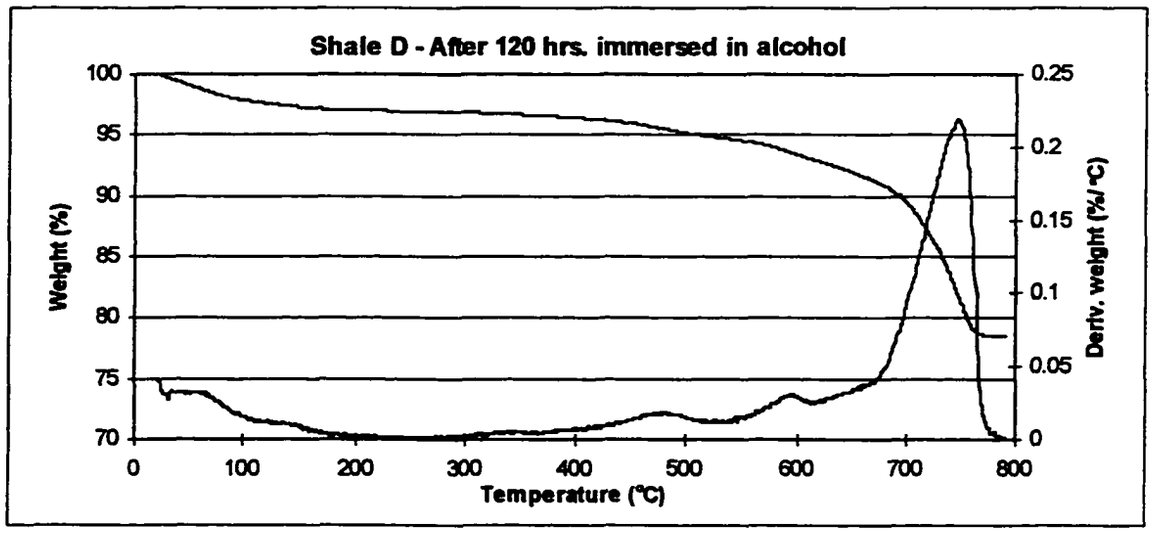


Figure 6.54: TGA (10°C/min.) of shale D after 120 hrs. immersed in alcohol.

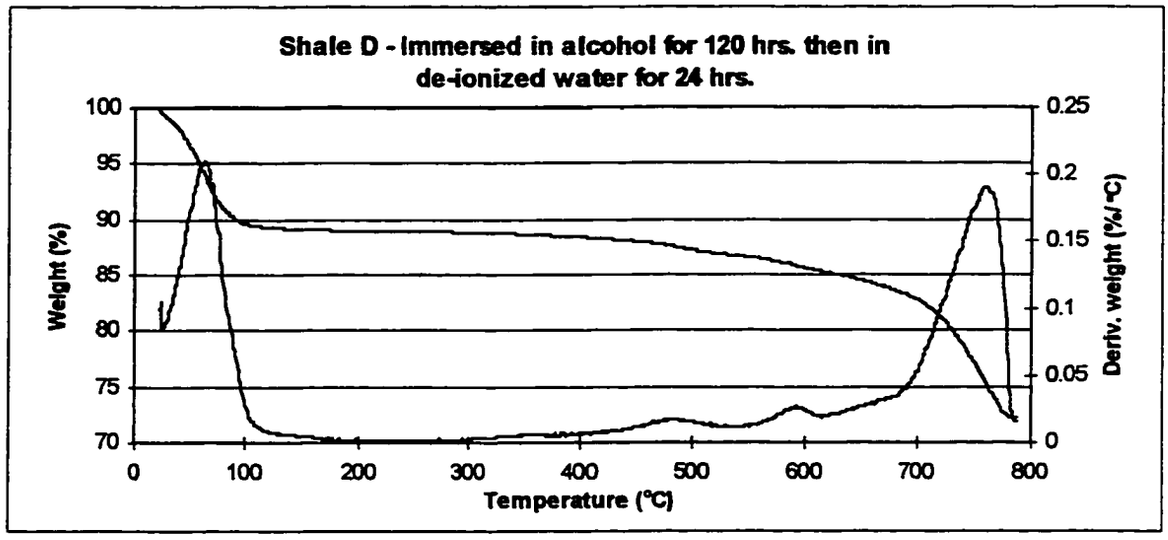


Figure 6.55: TGA (10°C/min.) of shale D after 120 hrs. immersed in alcohol, then in de-ionized water.

6.2.6.6 Discussion and analysis of the results for the water solutions

Since the tests were conducted with just one type of well-preserved shale, a comparison among the results is possible. It was observed that a simple immersion in salt solutions produced a profound change in the shale, affecting even its structure. Not only free water is moving in or out of the shale, but cations and anions must be exchanging between the solution and the pore fluid in order to alter the shale structure. This conclusion derives from the observation that each salt imposed a different alteration in the structure.

The exchange of cations and anions was expected since the so called semi-permeable membrane is assumed to be very weak when a shale is immersed in a water solution (Hale & Mody, 1992). One important observation was the change in calcite content. Immersion in $CaCl_2$ did not produce a significant

change, but immersion in both NaCl and KCl presented a reduction in calcite. The reaction of calcite in water is given by the following equations:

$$CaCO_3\,(s) \leftrightarrow Ca^{2+}\,(aq) + CO_3^{2-}\,(aq) \qquad (6.1)$$

$$CaCO_3 + H_2O \leftrightarrow Ca^{2+} + HCO_3^- + OH^- \qquad (6.2)$$

When exposed to the quasi-saturated calcium solution there is no more calcium possible to be dissolved. Immersion in sodium and potassium chloride required a dissolution of some calcite, so that the chemical equilibrium can be reached.

Salt solutions:

$$NaCl + H_2O \leftrightarrow Na^+ + Cl^- + H^+ + OH^- \qquad (6.3)$$

$$CaCl_2 + H_2O \leftrightarrow Ca^{2+} + 2\,Cl^- + H^+ + OH^- \qquad (6.4)$$

$$KCl + H_2O \leftrightarrow K^+ + Cl^- + H^+ + OH^- \qquad (6.5)$$

Some sodium, calcium, and potassium should have gone inside the shale, exchanging with other cations, but at this point it was not possible to detect them. The different changes in structural water in the clay minerals when

exposed to the calcium, potassium, and sodium chloride support this assumption.

The fact that all the change in the shale structure was observed in the first 24 hrs. (for the majority of the cases) does not support the argument that instabilities in the field are a consequence of shale-mud interaction. Time-delayed failures in shales cannot be explained with the argument that the interaction changes the rock, weakening it. In some situations, these changes might be even beneficial to strengthen the rock. No reduction in strength was observed by immersing the samples in the salt solutions, even though swelling was observed (by increase in sample weight due to fluid adsorption). Only when de-ionized water was used did the rock lost some strength.

6.2.6.7 Immersion in $CaCl_2$ (A_w = 0.39) OBM

Changes in calcite content and in structural water is not significant when immersed in OBM with calcium chloride. However, reduction in free water is obvious, and also a modification in bound water. Again, these changes occur predominantly in the first 24 hrs. of exposure. An increase in free water content is observed when the sample is immersed in de-ionized water. The remaining features remained practically the same, with a small change in the bound water. The interlayer water in the smectite is preserved, as can be noted by the inflection in the derivative curve. The inflection is present even after the sample is contacted by de-ionized water.

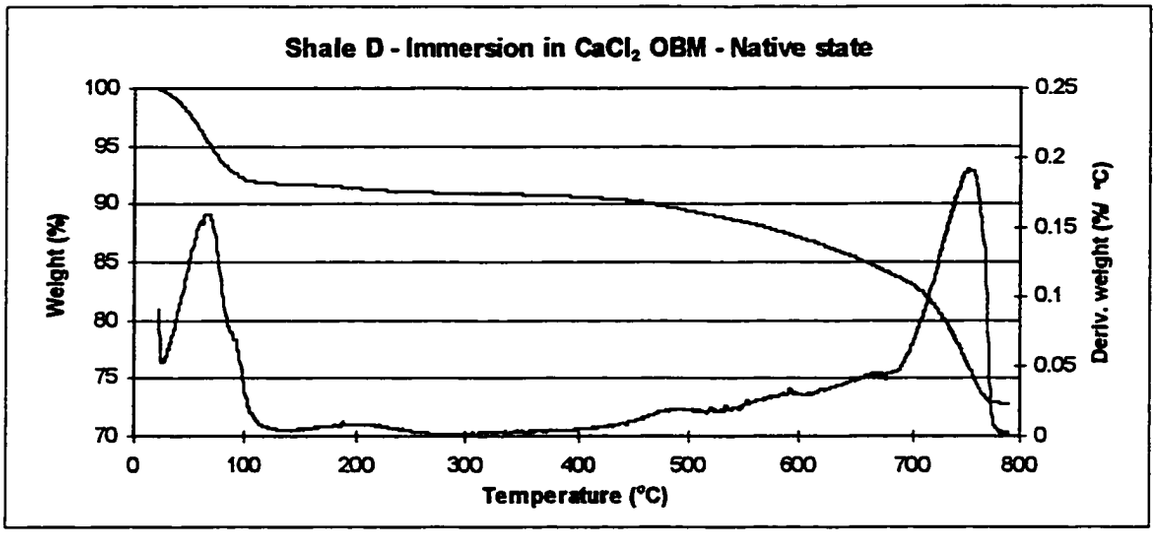


Figure 6.56: TGA (10°C/min.) of shale D - Native state - Immersion in OBM with $CaCl_2$ (A_w = 0.39) as water phase.

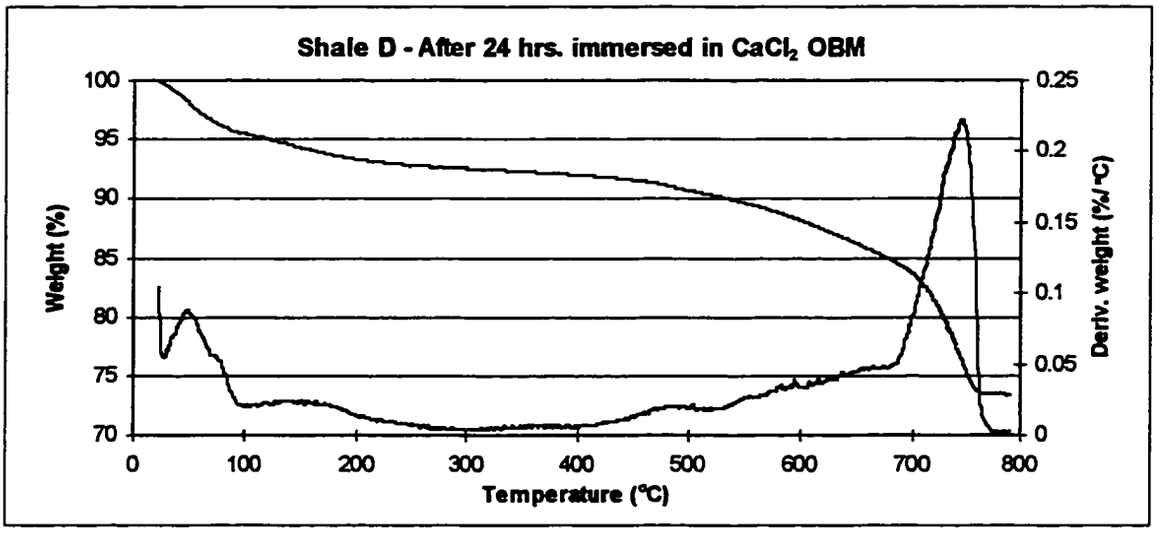


Figure 6.57: TGA (10°C/min.) of shale D after 24 hrs. immersed in OBM with $CaCl_2$ (A_w = 0.39) as water phase.

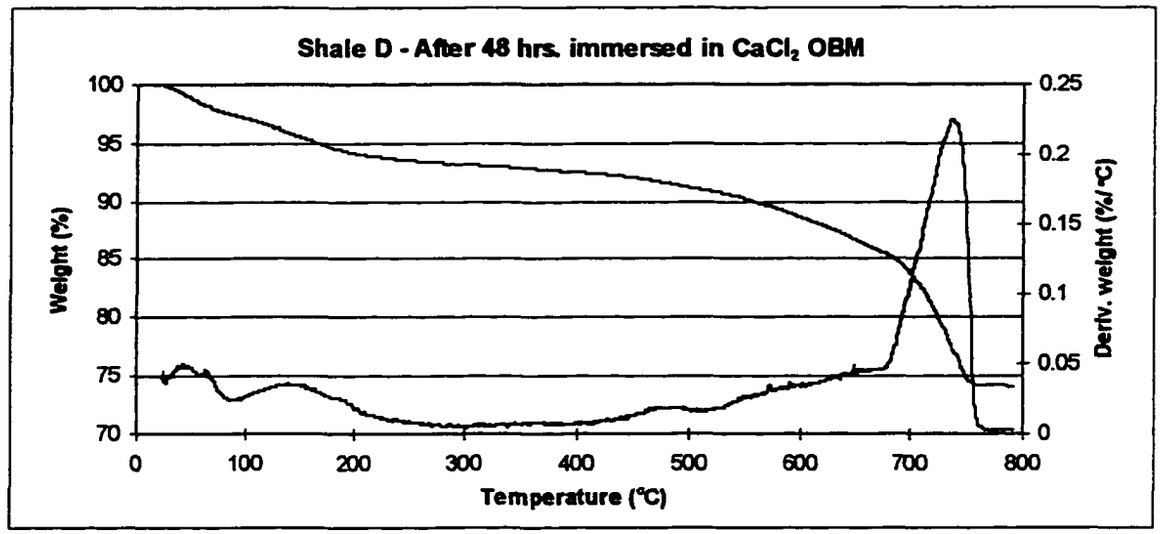


Figure 6.58: TGA (10°C/min.) of shale D after 48 hrs. immersed in OBM with $CaCl_2$ (A_w = 0.39) as water phase.

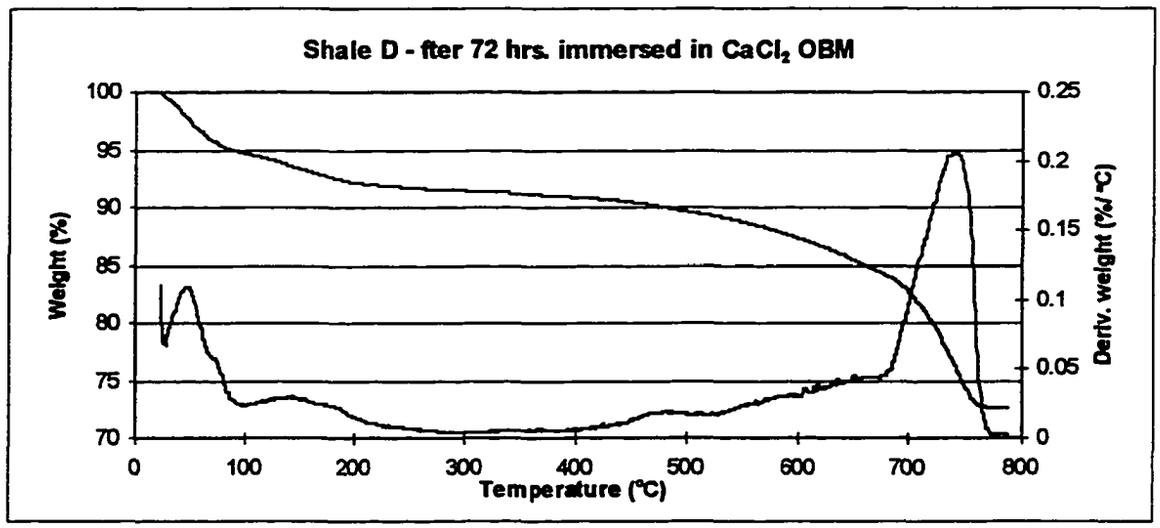


Figure 6.59: TGA (10°C/min.) of shale D after 72 hrs. immersed in OBM with $CaCl_2$ (A_w = 0.39) as water phase.

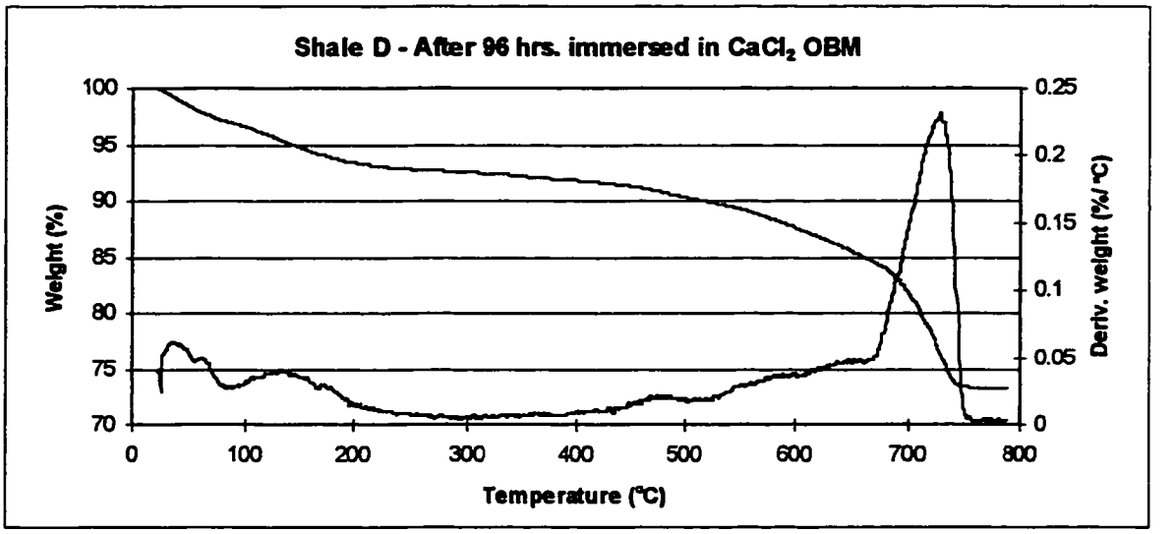


Figure 6.60: TGA (10°C/min.) of shale D after 96 hrs. immersed in OBM with $CaCl_2$ (A_w = 0.39) as water phase.

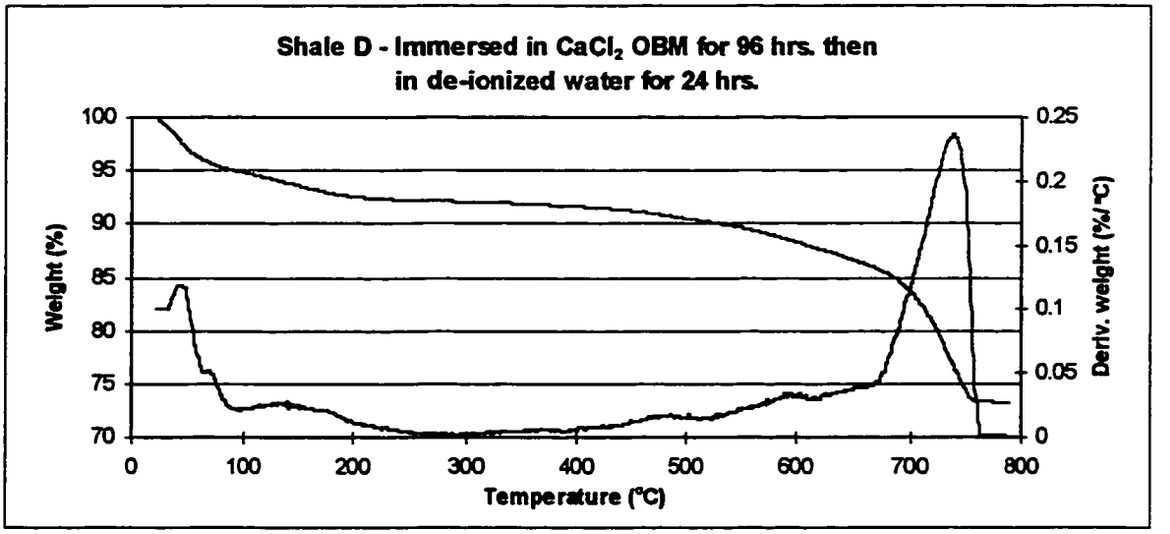


Figure 6.61: TGA (10°C/min.) of shale D after 96 hrs. immersed in OBM with $CaCl_2$ (A_w = 0.39) as water phase, then in de-ionized water for 24 hrs.

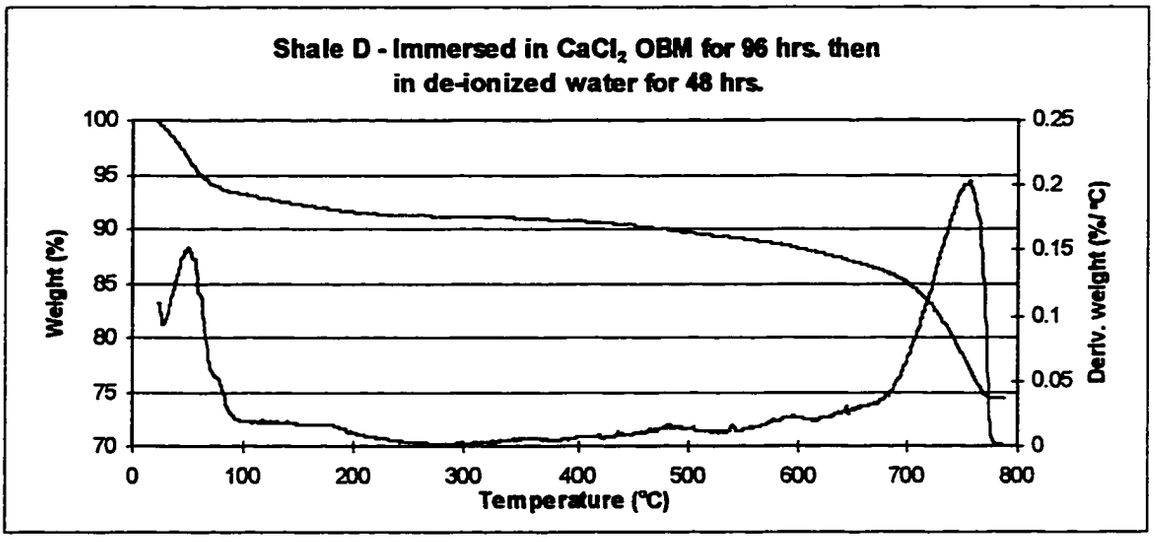


Figure 6.62: TGA (10°C/min.) of shale D after 96 hrs. immersed in OBM with $CaCl_2$ (A_w = 0.39) as water phase, then in de-ionized water for 48 hrs.

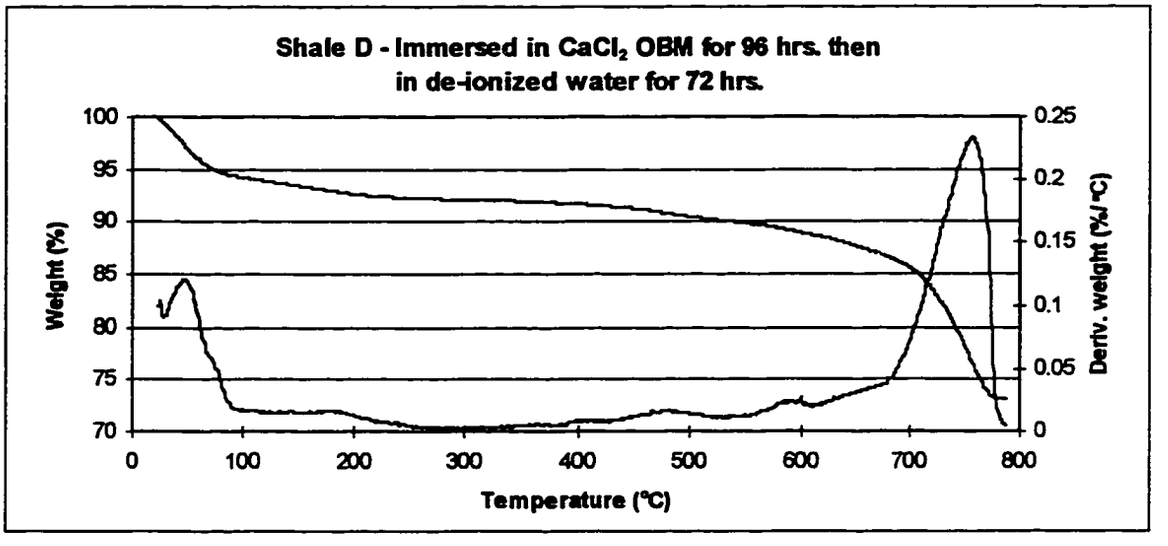


Figure 6.63: TGA (10°C/min.) of shale D after 96 hrs. immersed in OBM with $CaCl_2$ (A_w = 0.39) as water phase, then in de-ionized water for 72 hrs.

6.2.6.8 Immersion in KCl (A_w = 0.84) OBM

A very similar behavior is seen with the OBM and KCl. Reduction in free water preserves the inflection, and changes are mainly limited to bound water. Close observation of the charts indicate that the change in bound water is slightly different from the observed with the calcium chloride OBM. This might be an indication that the different cations might be playing an important role even when an OBM is used. Both free and bound water changed after immersion in de-ionized water.

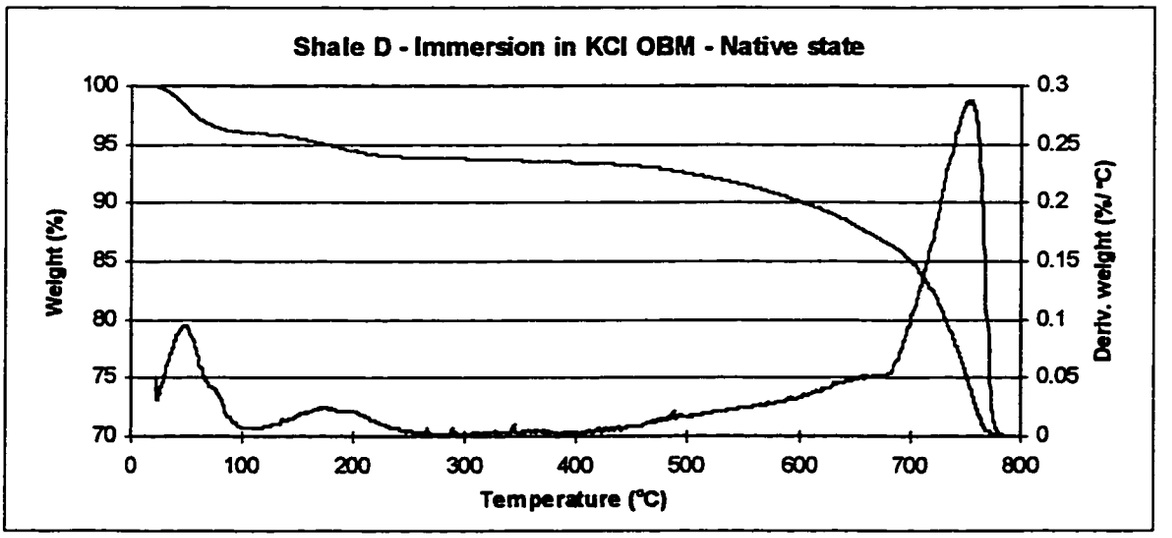


Figure 6.64: TGA (10°C/min.) of shale D - Native state - Immersion in OBM with KCl (A_w = 0.84) as water phase.

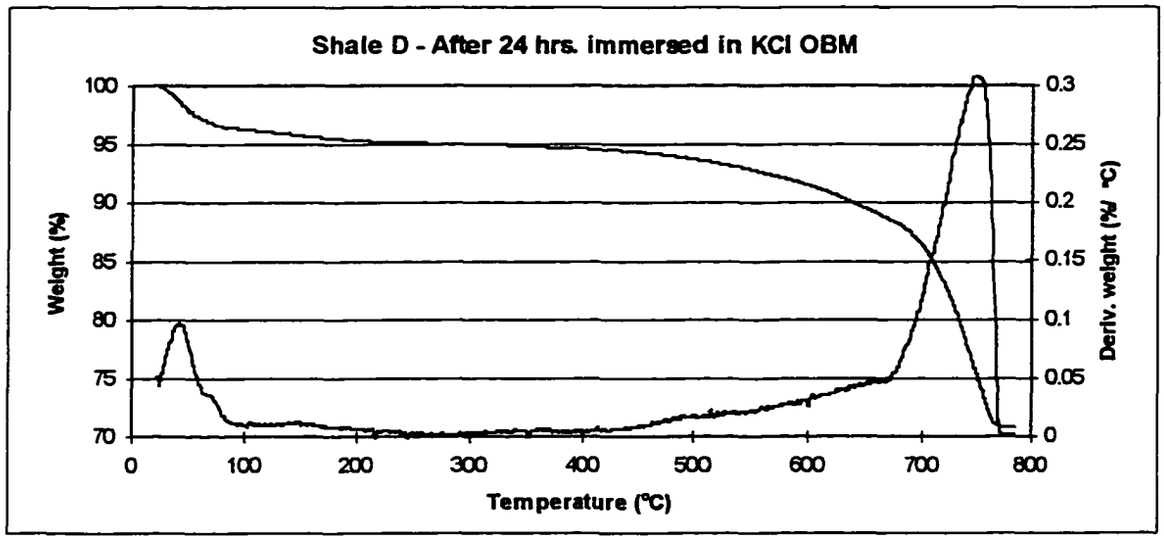


Figure 6.65: TGA (10°C/min.) of shale D after 24 hrs. immersed in OBM with KCl (A_w = 0.84) as water phase.

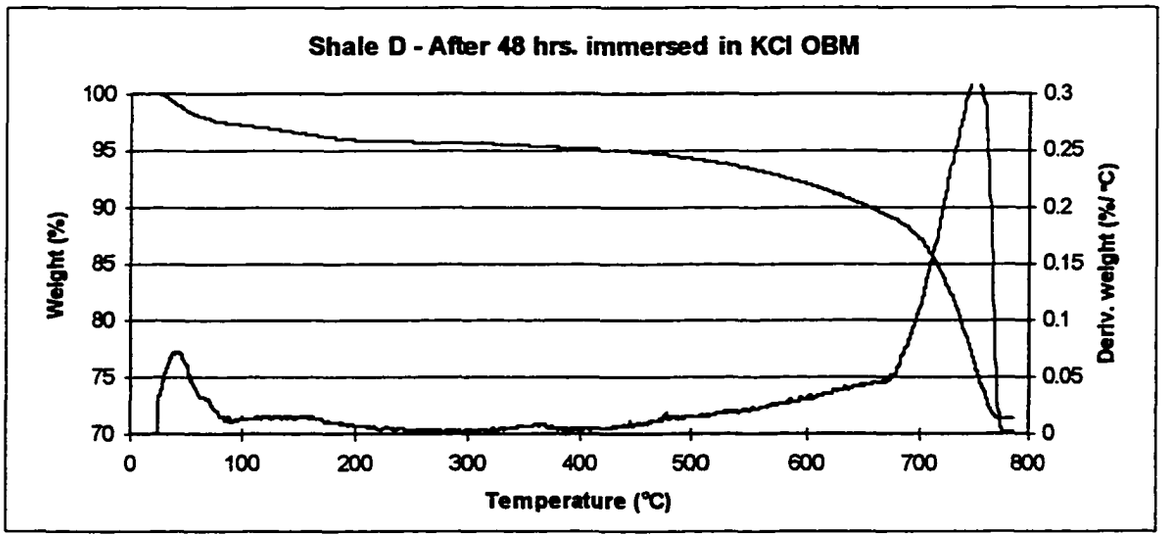


Figure 6.66: TGA (10°C/min.) of shale D after 48 hrs. immersed in OBM with KCl (A_w = 0.84) as water phase.

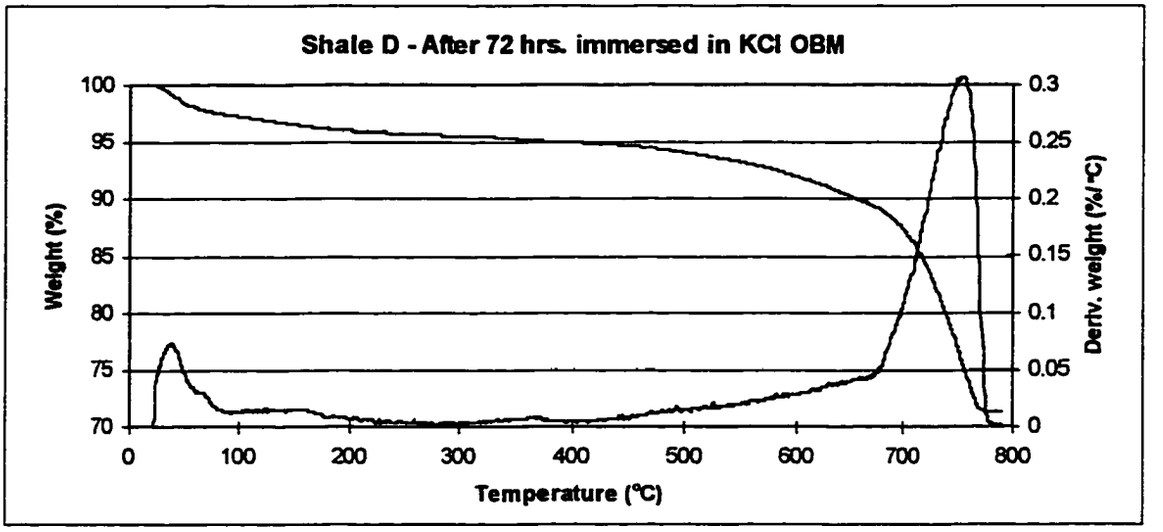


Figure 6.67: TGA (10°C/min.) of shale D after 72 hrs. immersed in OBM with KCl (A_w = 0.84) as water phase.

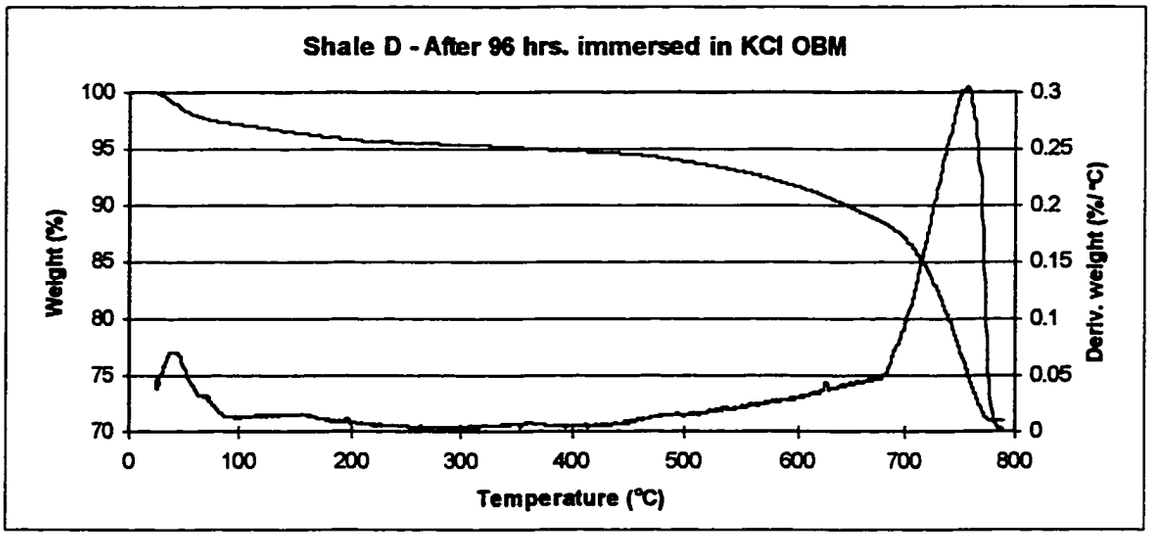


Figure 6.68: TGA (10°C/min.) of shale D after 96 hrs. immersed in OBM with KCl (A_w = 0.84) as water phase.

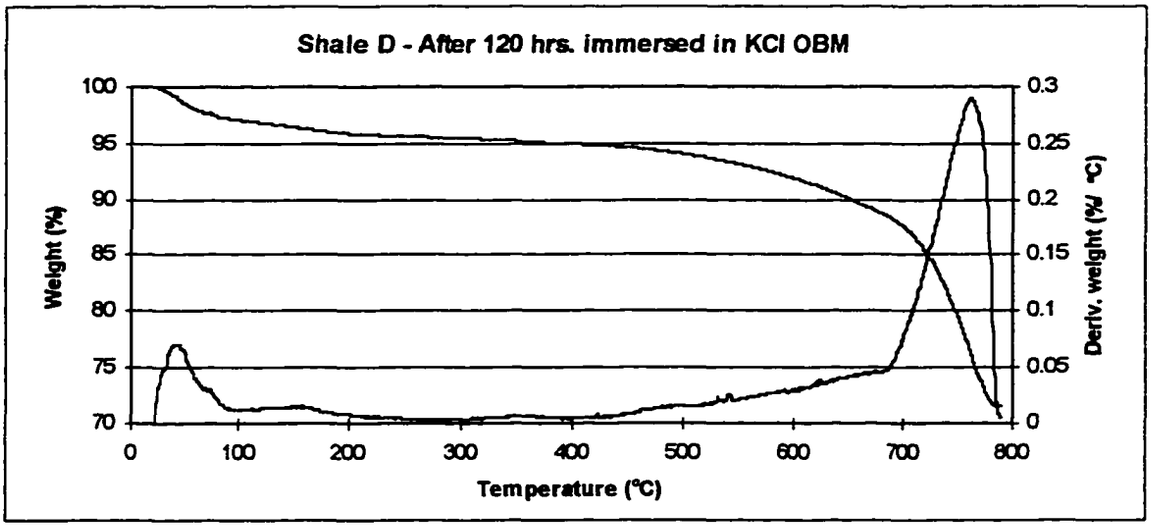


Figure 6.69: TGA (10°C/min.) of shale D after 120 hrs. immersed in OBM with KCl (A_w = 0.84) as water phase.

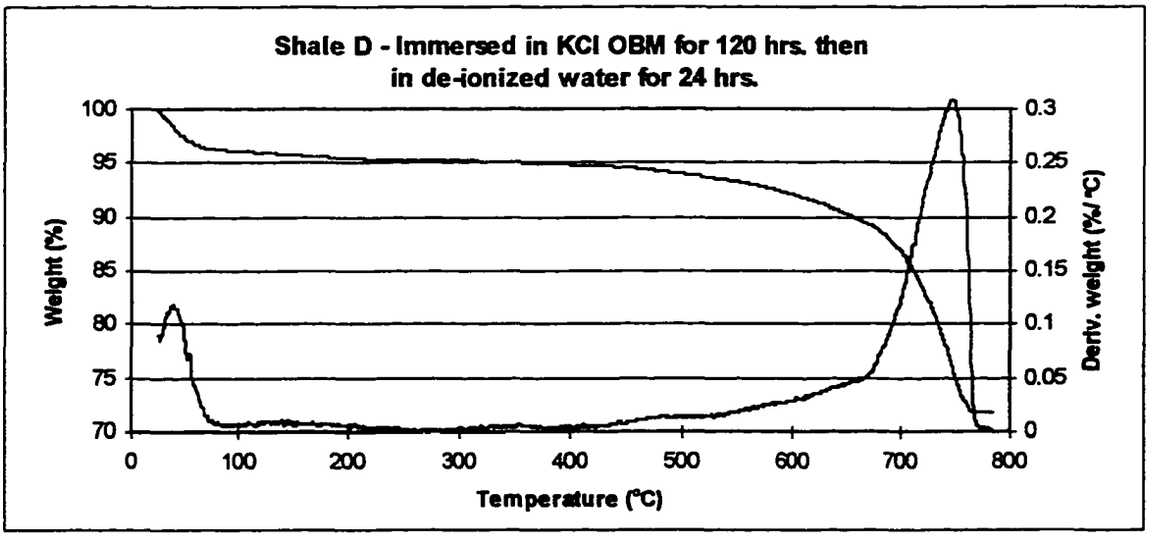


Figure 6.70: TGA (10°C/min.) of shale D after 120 hrs. immersed in OBM with KCl (A_w = 0.84) as water phase, then in de-ionized water for 24 hrs.

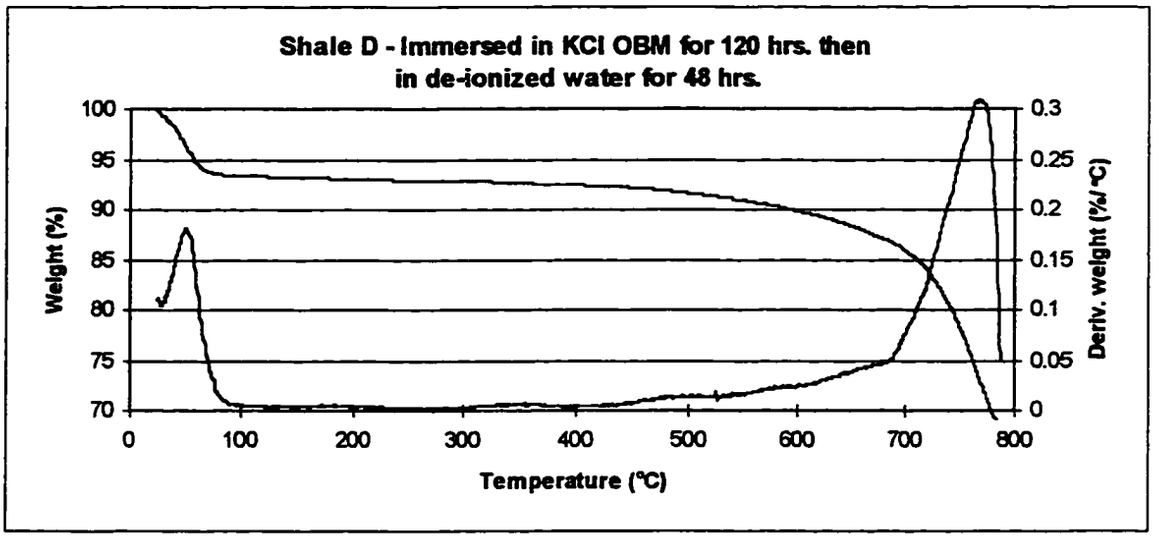


Figure 6.71: TGA (10°C/min.) of shale D after 120 hrs. immersed in OBM with KCl (A_w = 0.84) as water phase, then in de-ionized water for 48 hrs.

6.2.6.9 Immersion in NaCl (A_w = 0.75) OBM

Again, a very similar behavior is observed when the water phase contains sodium chloride. Reduction in free water and change in bound water, repeating almost exactly what was seen with the potassium chloride OBM. The inflection in the derivative curve is also present at all times. Besides an increase in free water, only the bound water was slightly affected after the sample has been exposed to de-ionized water.

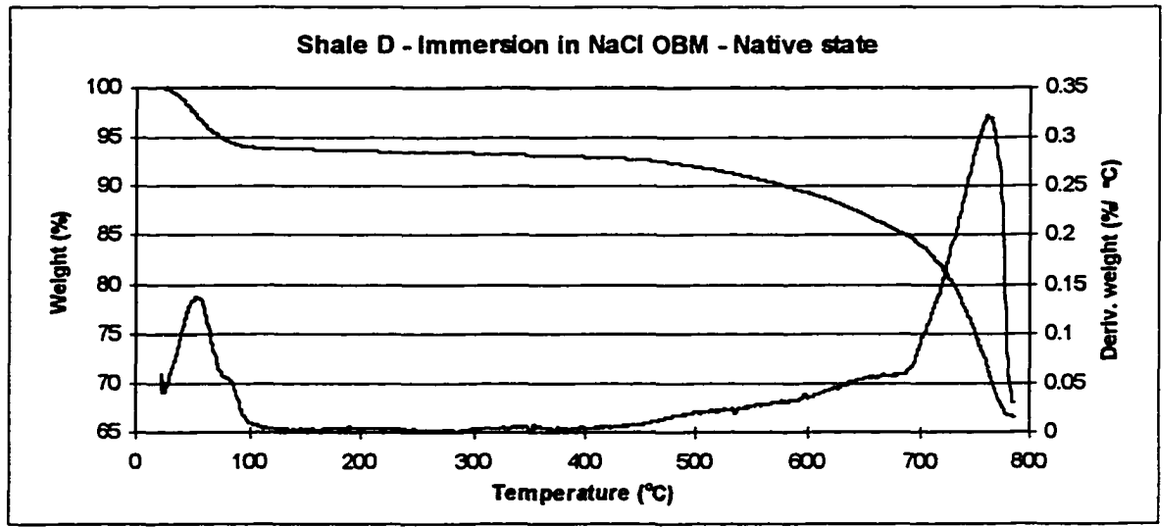


Figure 6.72: TGA (10°C/min.) of shale D - Native state - Immersion in OBM with NaCl (A_w = 0.75) as water phase.

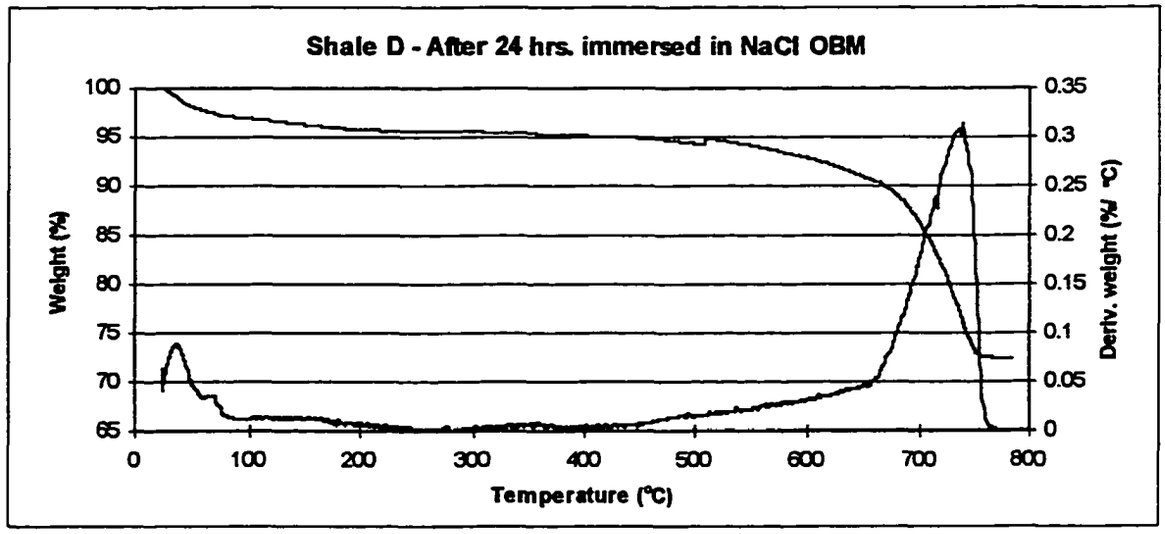


Figure 6.73: TGA (10°C/min.) of shale D after 24 hrs. immersed in OBM with NaCl (A_w = 0.75) as water phase.

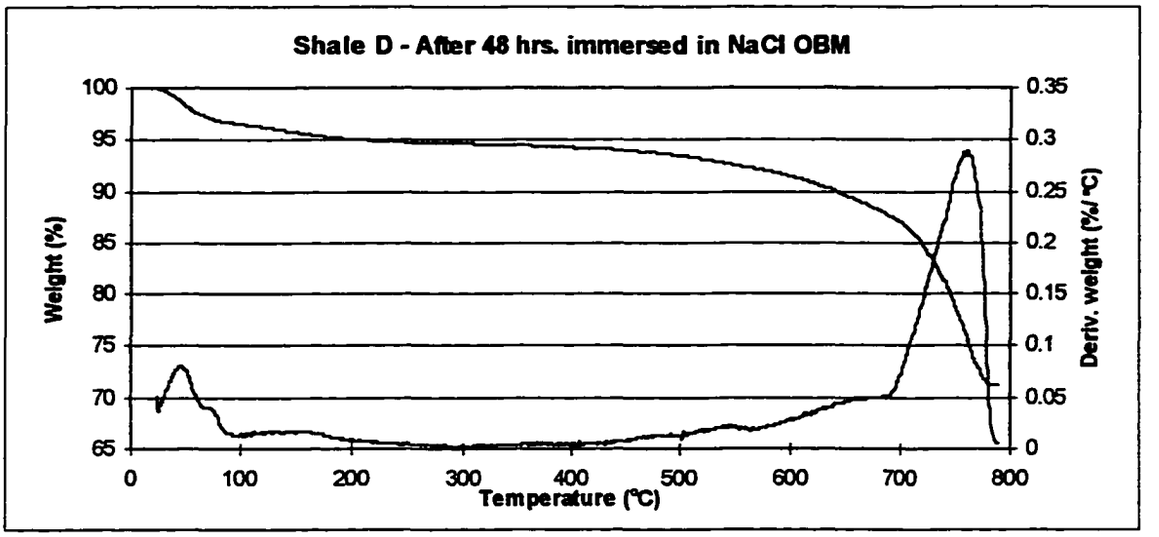


Figure 6.74: TGA (10°C/min.) of shale D after 48 hrs. immersed in OBM with NaCl (A_w = 0.75) as water phase.

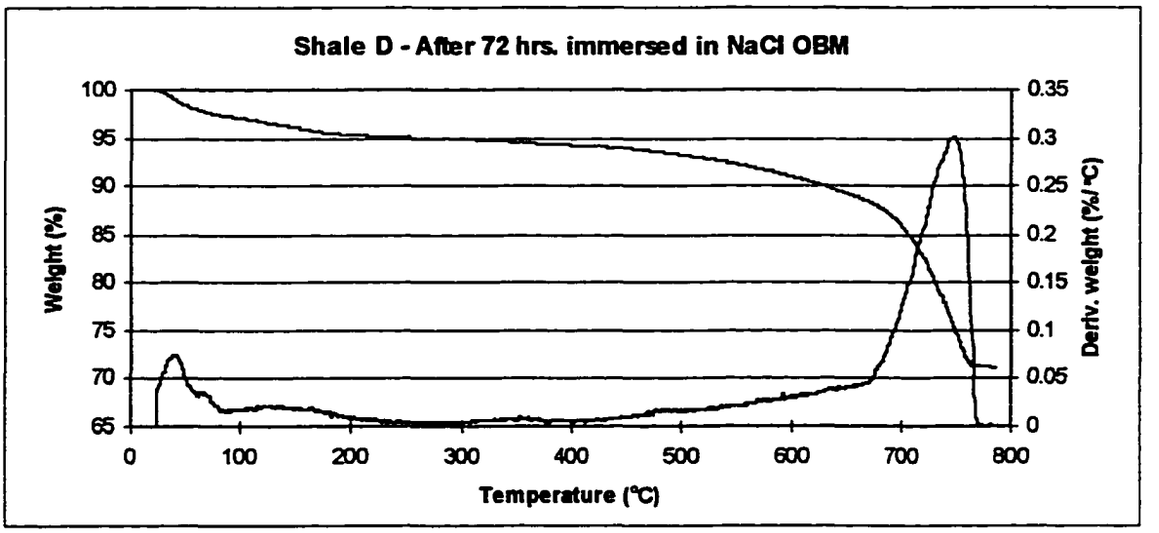


Figure 6.75: TGA (10°C/min.) of shale D after 72 hrs. immersed in OBM with NaCl (A_w = 0.75) as water phase.

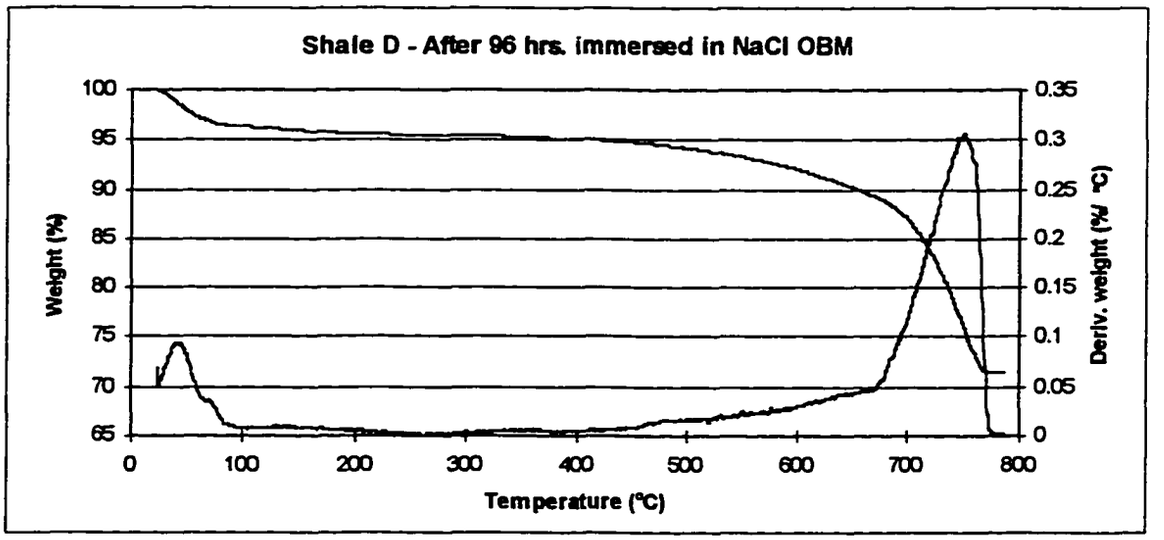


Figure 6.76: TGA (10°C/min.) of shale D after 96 hrs. immersed in OBM with NaCl (A_w = 0.75) as water phase.

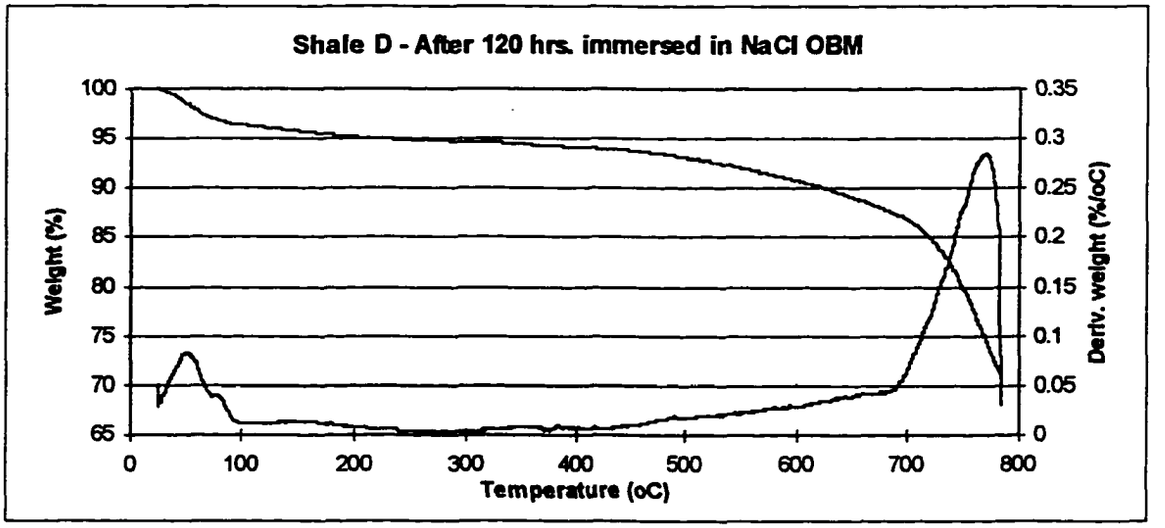


Figure 6.77: TGA (10°C/min.) of shale D after 120 hrs. immersed in OBM with NaCl (A_w = 0.75) as water phase.

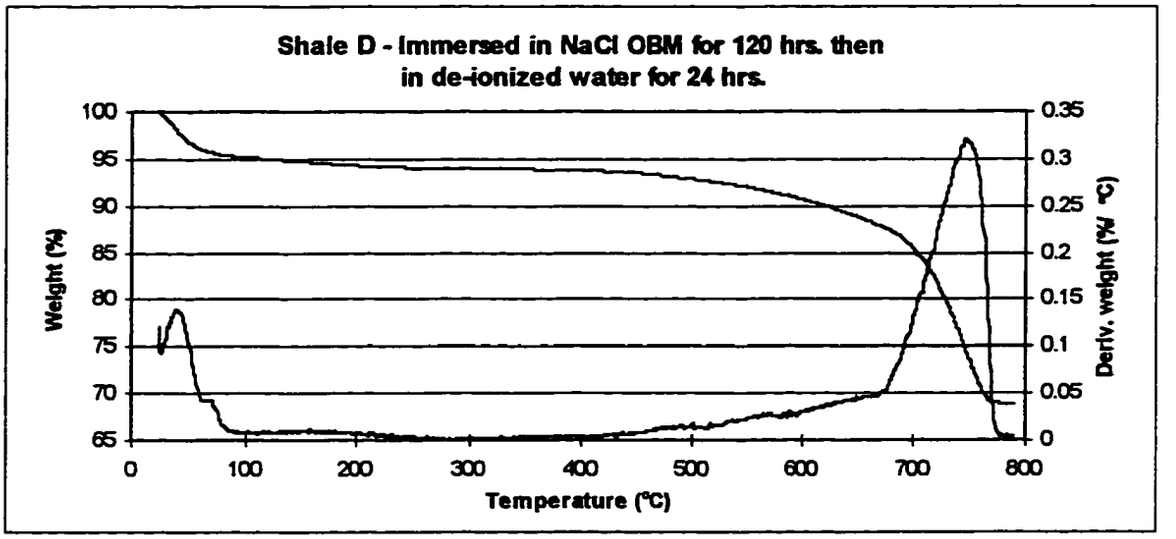


Figure 6.78: TGA (10°C/min.) of shale D after 120 hrs. immersed in OBM with NaCl (A_w = 0.75) as water phase, then in de-ionized water for 24 hrs.

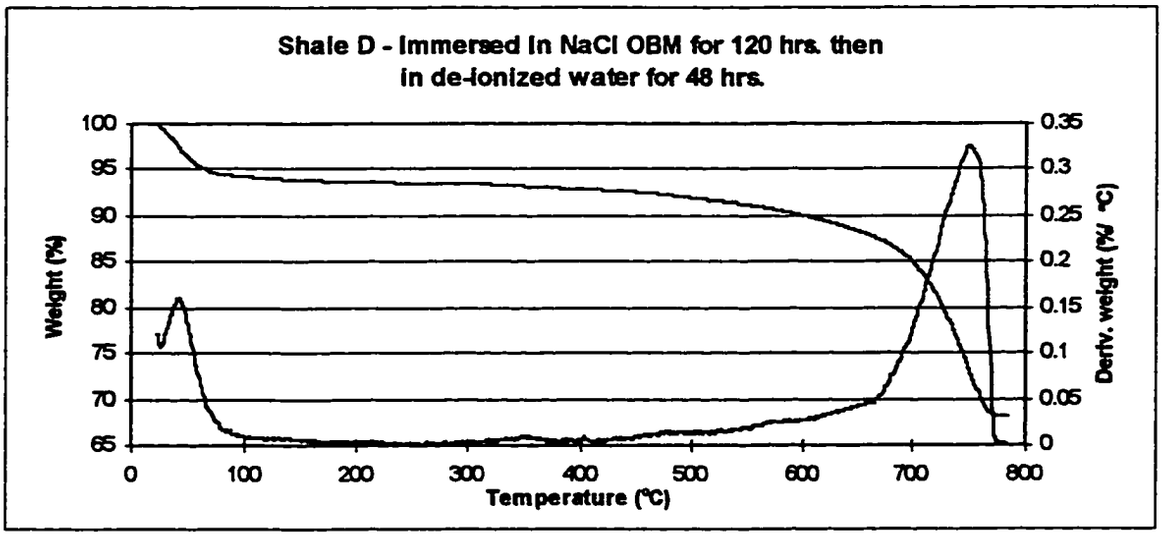


Figure 6.79: TGA (10°C/min.) of shale D after 120 hrs. immersed in OBM with NaCl (A_w = 0.75) as water phase, then in de-ionized water for 48 hrs.

6.2.6.10 Immersion in fresh water (A_w = 0.99) OBM

Immersion in fresh water OBM shows the most surprising result. The change observed in the rock is almost identical as the ones observed with salted water. Reduction in free water with maintenance of the inflection in the derivative, unaltered calcite content and structural water, and a change in bound water, in a very similar way than observed for the other OBM used. Also, immersion in de-ionized produced the same change: a slight modification in bound water.

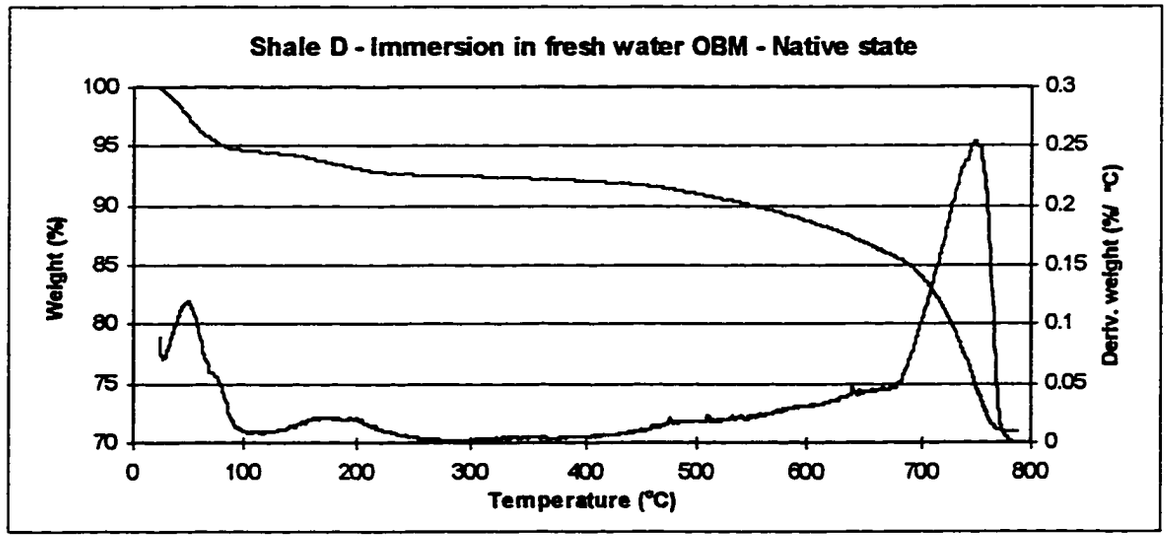


Figure 6.80: TGA (10°C/min.) of shale D - Native state - Immersion in OBM with fresh water (A_w = 0.99) as water phase.

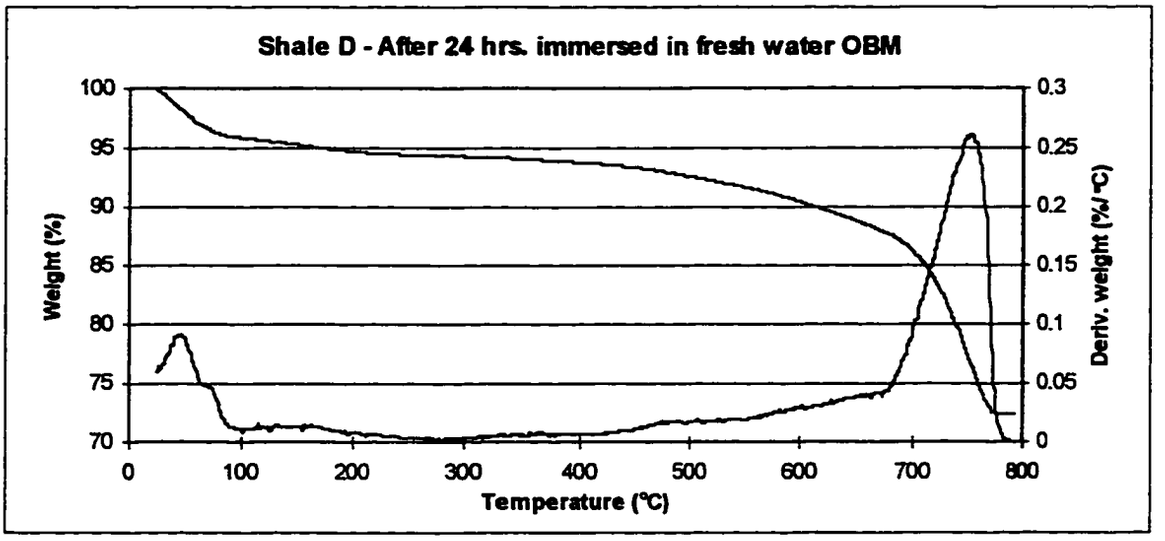


Figure 6.81: TGA (10°C/min.) of shale D after 24 hrs. immersed in OBM with fresh water (A_w = 0.99) as water phase.

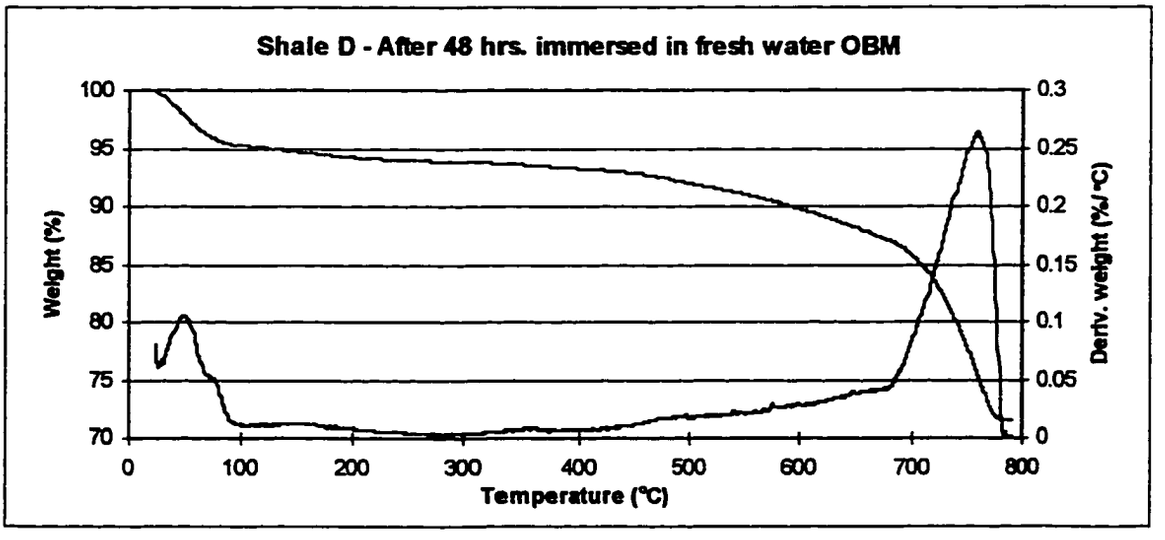


Figure 6.82: TGA (10°C/min.) of shale D after 48 hrs. immersed in OBM with fresh water (A_w = 0.99) as water phase.

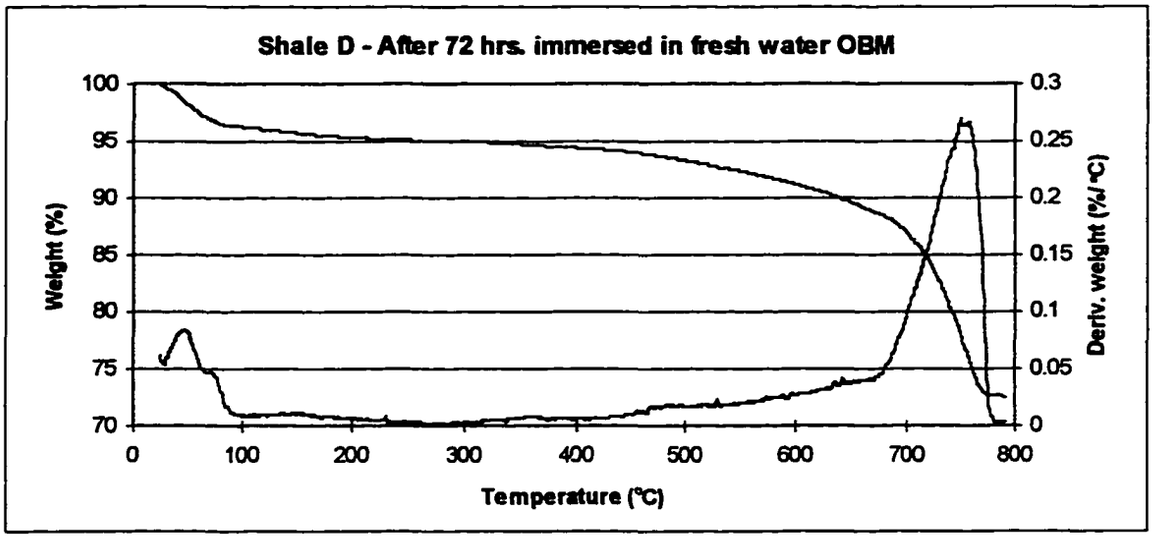


Figure 6.83: TGA (10°C/min.) of shale D after 72 hrs. immersed in OBM with fresh water (A_w = 0.99) as water phase.

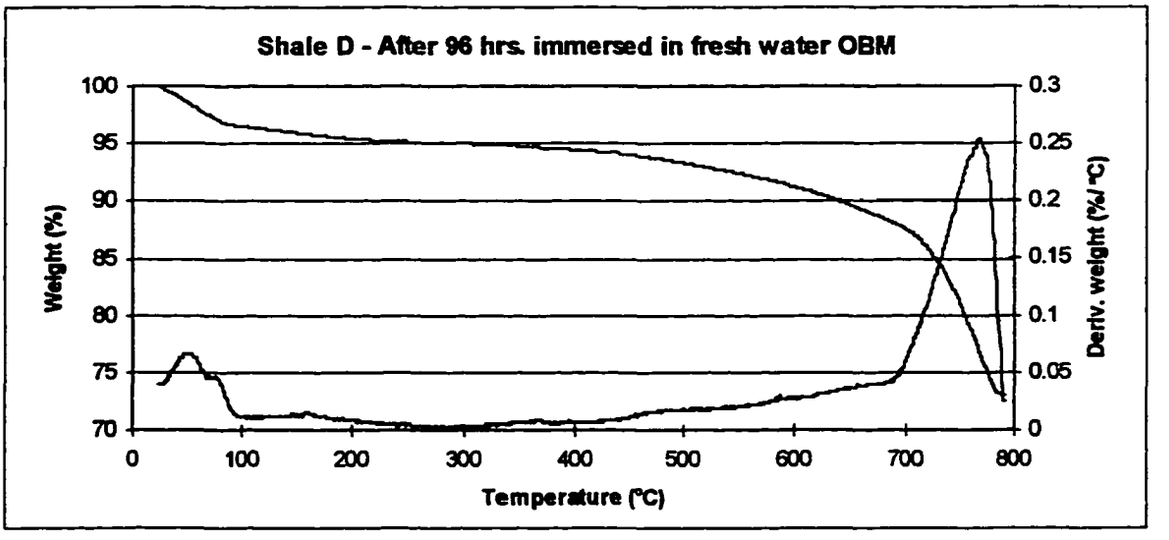


Figure 6.84: TGA (10°C/min.) of shale D after 96 hrs. immersed in OBM with fresh water (A_w = 0.99) as water phase.

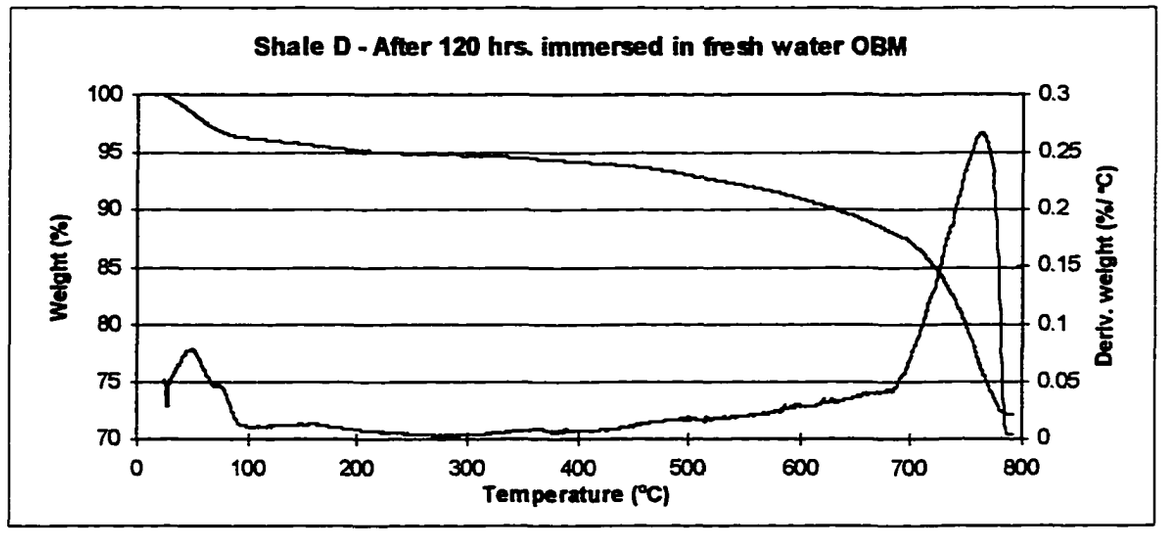


Figure 6.85: TGA (10°C/min.) of shale D after 120 hrs. immersed in OBM with fresh water (A_w = 0.99) as water phase.

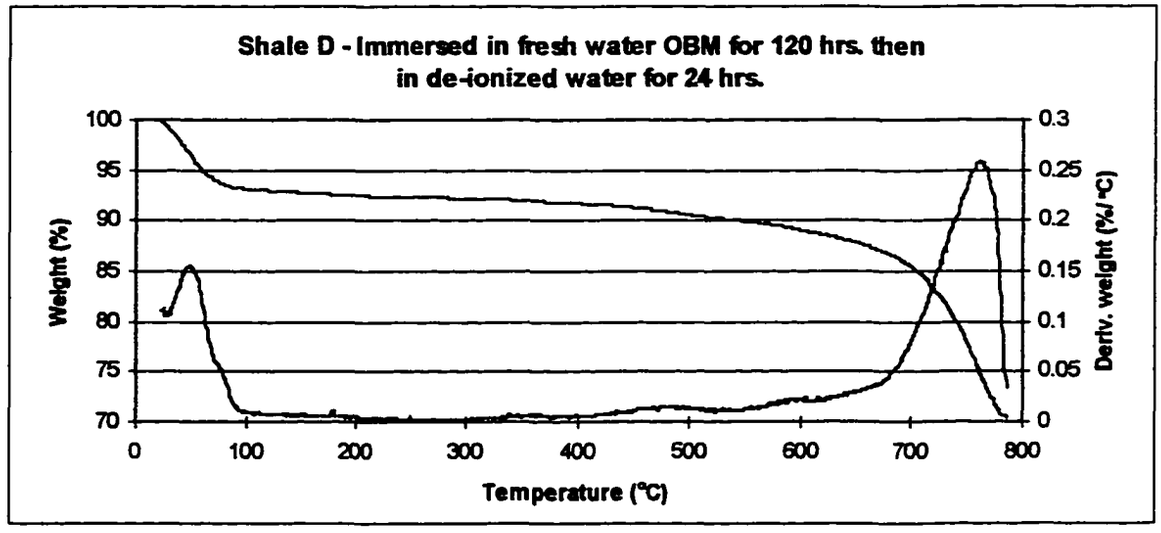


Figure 6.86: TGA (10°C/min.) of shale D after 120 hrs. immersed in OBM with fresh water (A_w = 0.99) as water phase, then in de-ionized water for 24 hrs.

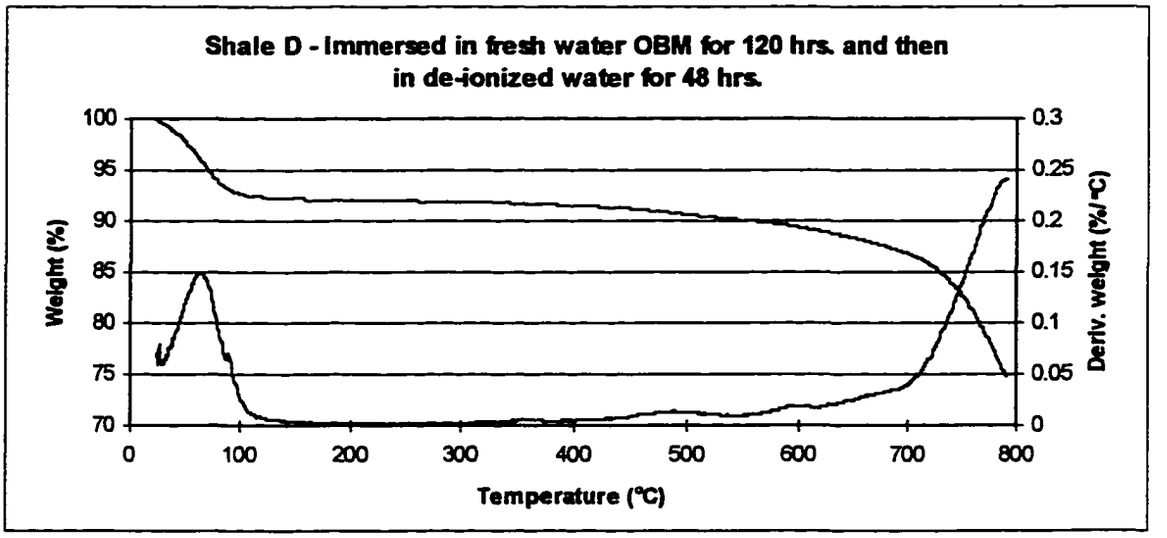


Figure 6.87: TGA (10°C/min.) of shale D after 120 hrs. immersed in OBM with fresh water (A_w = 0.99) as water phase, then in de-ionized water for 48 hrs.

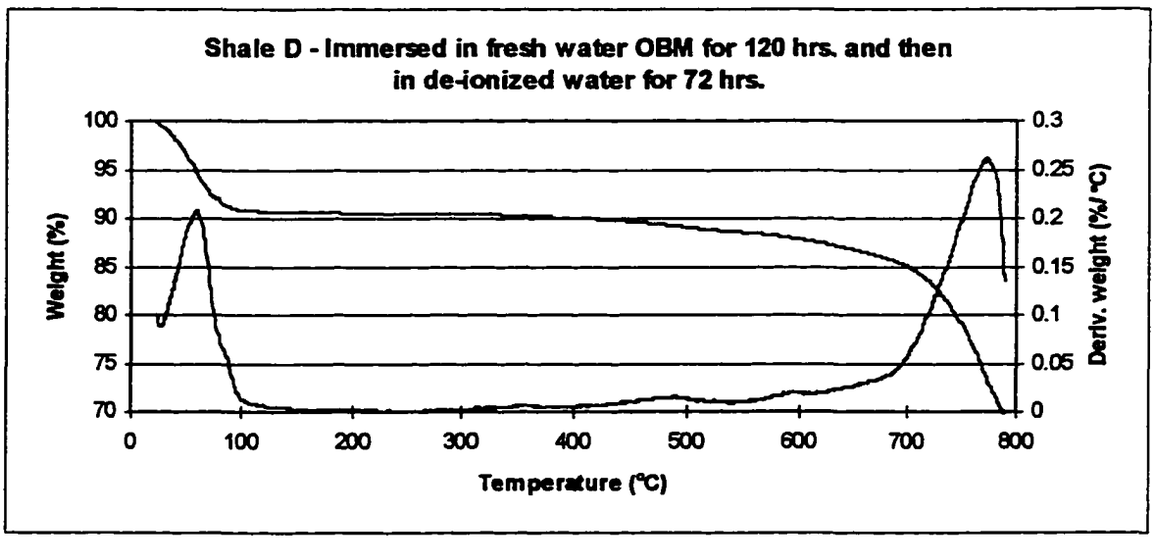


Figure 6.88: TGA (10°C/min.) of shale D after 120 hrs. immersed in OBM with fresh water (A_w = 0.99) as water phase, then in de-ionized water for 72 hrs.

6.2.6.11 Discussion and analysis of the results for OBM

The almost identical behavior for the different OBM tested can only be attributed to the presence of the emulsifier in the fluid. It was clear that different salts had no effect on the shale. Rather than difference in the water phase activity, it was the presence of the emulsifier that caused the alteration in the shale. All the samples presented an inversion in wettability, becoming not water wet as before immersing in the OBM.

The calcium chloride OBM produced a similar modification in the bound water as the water solution with calcium chloride. The similarity can only be attributed to the presence of the same cation in both the water and the oil solution. The potassium and sodium solutions presented different changes. This observation shows that the cation and/or the anions might have exchanged with the ones inside the shale.

Similarities among all the TGA results (in both bound and structural water) must have been caused by the common emulsifier used. All these OBM were prepared with the same composition, differing just in the type and amount of salts used in the water phase. It can be observed that even the original samples that did not present any curvature in the derivative between 100°C and 200°C, did so after immersion in the OBM (immersion in $CaCl_2$ and NaCl OBM). There is almost no experience with TGA experiment in the case of surfactant-impregnated shale surfaces; hence, no comparisons can be made.

Because the emulsifier is common to all the OBM used, it must be its presence that produced this change.

6.2.7 Semi-Permeable Membrane and Osmotic Pressure.

The hypothesis that shale behaves as an ideal semi-permeable membrane when an OBM is used is highly questionable at this point. From the TGA results, it can be seen that the calcium chloride affected the shale in a different way than the potassium and sodium chloride solution in the water phase. Actually, the modifications in bound water, considering the same salt, were very similar in both the water and oil solutions. Therefore, even regarding the oil solution, it is reasonable to admit at this point that cations and/or anions moved into/out of the shale, together with water. Water movement only cannot explain such modifications in the bound water.

Another important point to be emphasized is the wettability change of the shale. As mentioned before, the concept of a semi-permeable membrane, an ideal one in the case of OBM, assumes that only water moves in or out of the shale. Since the rock is no longer water wet after being in contact with the emulsifier present in the OBM, it is hard to admit that water flow will still occur in/out of the shale. This assumption might be valid only in the early stages of interaction between the rock and the drilling fluid, when the wettability has not yet been modified. Even in this period, the results of immersion tests do not support this concept, since the weight of samples

immersed in OBM with different water phase solutions had almost the same behavior.

When a shale is immersed in a water solution, the presence of a non-ideal semi-permeable membrane is assumed. The absence of a perfect membrane is clear when analyzing the solution composition after shale samples have been immersed in de-ionized water for 5 hrs. (Table 6.3). The 3-hour air-dried sample showed all values, except the bicarbonate, greater than for the preserved sample. Appearance of bicarbonate (HCO_3^-) in solution was due to dissolution of calcite, as shown in Eq. (6.2). The change in calcite content was also detected in the TGA results presented earlier (immersion in KCl and NaCl, for example).

Table 6.3: Solution composition after 5 hrs. immersed in de-ionized water (mg/l) (ND = not detected).

Element	Preserved sample	3-hr. air-dried sample
Sodium	36	43
Potassium	4	5.5
Calcium	3.7	13
Magnesium	ND	1.1
Silicon	4.1	16.3
Iron	0.61	2.7
Aluminum	0.68	4.1
Bicarbonate	47	5
Sulfate	ND	ND
Chloride	63	73

Several works tried to incorporate an effectiveness coefficient for the semi-permeable membrane in a shale-water system. Tan *et al.* (1996) suggested a reflection coefficient in the osmotic pressure equation:

$$\pi = \alpha \frac{RT}{V} \ln\left(\frac{A_w}{A^o_w}\right) \tag{6.6}$$

where α is the reflection coefficient, which describes the osmotic efficiency or solute leakage through the membrane system. In a shale-OBM system this coefficient is assumed to be 1. Values for α as low as 5% have been reported in the literature (van Oort *et al.*, 1994), signaling the weakness of this semi-permeable membrane in water-based solutions. Difference in activity between the mud and shale (with the consequent generation of osmotic pressure) have been proposed to counterbalance the hydraulic potential (van Oort *et al.*, 1996; Tan *et al.* 1996; Hale *et al.*, 1993). What the results of the tests presented here showed was that regardless of the salted solutions' activity, the flow of water was into the shale, for the WBM. The opposite behavior was observed for the OBM. The osmosis mechanism in shales has already been questioned before (Gazaniol *et al.* 1995; Santarelli & Carminati, 1995; Onaisi *et al.*, 1994), and the results herein provide further support for some of the doubts previously raised.

It was clear from the immersion tests conducted that other mechanisms are stronger to drive water than the osmotic pressure generated. This happened in both OBM and WBM. In OBM, the assumption that an osmotic pressure is generated derives from the idea that a semi-permeable membrane is present.

As described above, this is highly questioned at this point, raising serious doubts about the effective generation of an osmotic pressure when drilling with OBM. When WBM is being used, other stronger mechanisms are driving water into the shale, instead of out. Even though the cation exchange mechanism is well known (see Appendix B), other possible forces should be investigated, since the water is actually the responsible for the weight increase. The difference in cations used in the salt is the only explanation for the variation in behavior.

It was not possible to determine the solution composition for the water solutions due to the high concentrations used. Solution composition determination for the oil solutions had not been done yet. If this determination is possible, at least for the fresh water phase, an estimation of how efficient the semi-permeable membrane is can be done.

6.2.8 Shale Structure

The concept that water flow can occur freely into or out of the rock implies the assumption of a relatively simple structure, such as the one of a sandstone (Figure 6.89). It is reasonable, in the case of sandstone, to assume that the rock is composed of a matrix (grains + cementation) and pore space. In the case of shale, however, the structure is far from being simple, as suggested earlier (van Oort, 1997). Interaction among all the components, besides the fact that water is present in not just a free state, tremendously increases the complexity. Figure 6.90 shows a schematic representation of all the items that

interact and modify throughout the equilibration process. The TGA results show how the structure of the rock changed by contact with a water solution. The modification of the relative amount of each species present in the shale causes also a change in water distribution, depending on the salt used.

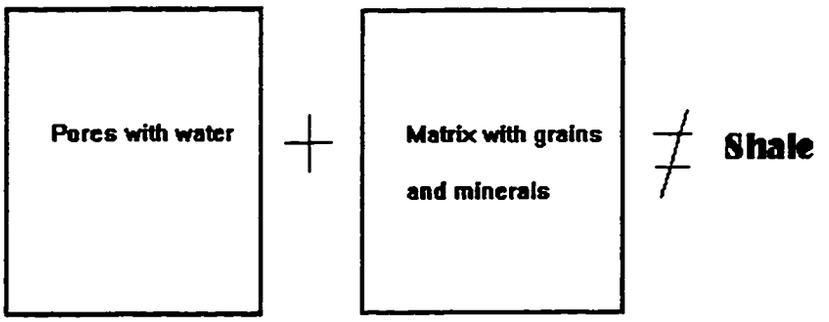


Figure 6.89: Idealized structure for a granular material: pores and matrix. Shale structure cannot be represented by means of this simplified view.

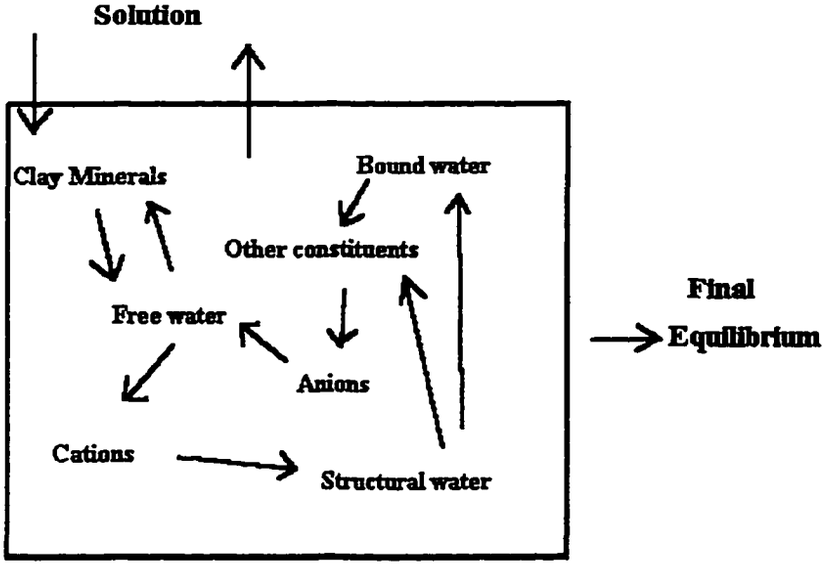


Figure 6.90: More realistic structure representing a shale. When exposed to a water solution, interaction among all the components leads to a different structure when the final equilibrium is reached.

The effects of physical changes, such as pressure, have not been investigated yet. Surface effects are strong when dealing with clays and different kinds of forces are present in the shale: electrical double layer repulsion, van der Waals, ion-ion correlation attraction, and hydration forces, just to name a few (see Appendix B for more details). The equilibrium of all the forces that interact on the micro-scale is affected when pressure (either fluid pressure or total pressure) is changed (Diek & Santos, 1996). New equilibrium will be reached by movement and redistribution of water and ions dissolved in the fluid. Some bound water can become free, or even structural. Structure rearrangement, as it can be imagined, is a complex issue involving several parameters.

It is not reasonable to assume, at this point, that just by imposing a difference in potential fluid flow will occur in shales according to Darcy's law. The experiments described here demonstrate that other phenomena might be more important than these potentials to induce a change in the shale structure. Any flow of a water solution through a shale will disturb the equilibrium and will induce a rearrangement of the structure, in order to reach a new equilibrium.

6.2.9 Pore Pressure in Shales

From the discussion presented above, one might question the pore pressure concept in shale. A simple definition is not possible, due to its complex

structure, different types of water present, modifications in these waters when exposed to a solution, and all types of forces and interactions. The pore-pressure concept derived from granular material, in which pores are connected and have a considerable size, should be reviewed in order to be applied in a material with predominant surface interactions, due to electrical and physico-chemical phenomena.

Fluid flow in shales are unlikely to follow Darcy's law. By contacting a water solution, a change in structure is observed. Therefore, the sizes and arrangements of "pore channels" in the shale will be under constant modification. It is also expected that under pressure variation (either total pressure or fluid pressure), a new equilibrium will be achieved but with a different rearrangement of the water. A direct consequence on the effective stress concept follows this pore-pressure debate. Wellbore stability models usually compare the effective stresses and the rock strength. In shales, this approach should be carefully taken into consideration, since the effective stresses are directly calculated using pore pressure values. Also, Darcy's law is often applied to estimate pore-pressure dissipation.

Another important aspect is related to pore pressure dissipation in shales. The poro-elasticity theory assumes pore-pressure dissipation according to Darcy's law (Cheng & Detournay, 1988). Based on this assumption the effect of an excess pore pressure generated by an external load or any other event can be estimated and quantified. In low permeability formations, the influence of excess pore pressure is more pronounced than in high permeability

formations, in which the dissipation takes place almost instantaneously. Nevertheless, the use of Darcy's law to estimate the excess pore pressure dissipation in shales can introduce a misleading interpretation and evaluation of the actual consequences. TGA results show clearly a different change in shale structure when the rock contacts various solutions. It is obvious that a change in structure will also take place if a solution flows through a shale; in addition, just by changing an external or fluid pressure rearrangement of the shale structure will occur. Having the clay minerals water in their structure a flow of a water solution in a shale is expected to significantly modify the flow pattern. Another important consideration is that Darcy's law is a macro-scale law. Since the micro-scale interactions and phenomena are much more relevant in shales, it might not be reasonable to apply Darcy's law to fluid flow in shales.

Poro-elasticity effects have been suggested to explain the delayed-failures in shales. However, with the aid of a computer code (Ekbote et al., 1997) to estimate the dissipation of the excess pore-pressure, it was found that for a formation with 20 x 10^{-9} D permeability, the dissipation lasts less than 1 day. Instabilities in shales are usually observed after some days of open hole. Obviously the poro-elastic effects are responsible for changes in pore pressure; these effects alone, however, cannot be responsible, but only contribute, to explain the problems.

6.2.10 Pore-Pressure Induced by Chemical Potential

The idea of increasing mud salinity to stabilize shales should be revised. Downhole shale swelling is not likely the best mechanism to explain wellbore instability. In some wells drilled in the North Sea (Bratli, 1993) problems actually increased when saturated muds were used. Water flow induced by chemical potential (activity difference) should also be reevaluated. The tests described in this paper indicated an opposite than expected variation in (free) water content in the shale, and also a change in bound and structural water. The effects were different depending on the salt used, and just the solution activity is not enough to estimate the consequences.

The absence of a semi-permeable membrane (very low efficiency) shows that other processes are modifying the shale structure. Water is not the only element flowing in or out of the rock. The movement of water follows the chemical potential concept only in the early stages, and with very low activity solutions. The increase in weight observed in the samples shows that water is actually going inside the shale. Instead of reducing the pore-pressure, as assumed by some models (van Oort *et al.*, 1994; Sherwood, 1993; Tan *et al.*, 1996), the chemical potential would induce an increase in pore-pressure since the free water content increases.

In the case of OBM, pore-pressure change due to chemical potential is quite unlikely to happen. Due to a strong change in wettability, flow through the rock is completely different. After the wettability has changed, the concept

of a semi-permeable membrane cannot be used anymore. Therefore, the chemical potential will not be effective. Even before the wettability alteration, water and/or oil plus salts (cations and anions) entered the rock (increase in weight in the beginning of the test), regardless the water phase's activity, contrary to what the chemical potential would assume.

6.3 Suggested Interaction Mechanisms for WBM and OBM

It is clear from TGA results that all water solutions produced some kind of change on the shale. Similar activity solutions, but with different salt, affected the shale in a different way. It can be seen that not only free water, but also structural water, bound water, interlayer water in the smectites, and even calcite content, have changed. A new equilibrium is achieved by dissolution and precipitation of elements, and it will be a function of the composition of both solution and shale. If one wants to investigate the final equilibrium of the rock, a complete chemical balance, considering all species present in the rock and in the solution, should be done. For example; decomposition of calcite will be a function of the solubility of calcium and bicarbonate in the rock and in the solution. In a saturated calcium chloride solution, calcite will not be decomposed. In sodium or potassium chloride solutions, a dissolution and transformation of calcite is observed. Only with a very detailed characterization technique, such as TGA, it is possible to detect these

variations. In order to conclude which salt and which concentration is better to minimize modifications of the shale, immersion tests should be conducted with varying salinity.

It has been suggested in Chapter 3 that the wettability change could actually be the most important factor in OBM's effectiveness. The results presented here are in agreement with these findings. However, type and amount of emulsifiers, and the salt in the water phase will change OBM's success, as well as the type and composition of the shaly formation being drilled. Although very limited (restricted to just one type of shale), the results herein presented show that the salinity of the water phase has no influence on the rock's water modification. Other shales (well-preserved downhole cores) should be tested so that the interaction mechanisms with OBM become more clear. In the beginning of the 80's, addition of oil and emulsifier to WBM was the common practice in the northeast of Brazil when wellbore instabilities became serious. It is important to emphasize that the salinity of the mud remained the same, but the stability of the borehole improved tremendously. By reversing the wettability of the rock, the WBM becomes actually a non-penetrating fluid, providing an extra support and improving the stability. It also has been observed that excessive quantity of emulsifier in OBM avoids stability problems, in fields prone in wellbore instability (Brignoli, 1997).

In addition to the action of the emulsifier, in water-wet shales the capillary threshold pressure plays an important role. When the drilling fluid has an oily continuous phase, the fact that the rock is water-wet will require an excess

pressure to the fluid penetrate into the pores. This process is similar to the one described above when the emulsifier changed the wettability of the shale, and WBM was used. This extra support provided by this capillary threshold pressure is completely lost if micro-cracks or fractures are created in the rock. This point has been mentioned by Dusseault & Gray (1992), and it will be recalled later in Chapter 7.

6.4 Conclusions

Even though the tests presented herein were conducted with limited types of shales, and at room temperature, some conclusions can be drawn. The tests should be repeated with other shale types in order to increase the understanding of shale-fluid interaction mechanisms, and to make possible a generalization of the knowledge gained:

1. It is shown that the capillary effects in a partially saturated shale are not the only responsible mechanism explaining the interaction and breakage of the rock when in contact with water.

2. Shale swelling is a consequence of the affinity of water by the clay minerals, when part of its water (interlayer) is removed.

3. Wettability change is the most predominant phenomenon causing dehydration when OBM contacts a shale, rather than chemical potential.

4. Due to this change in wettability, a semi-permeable membrane cannot be assumed to exist when shale is exposed to an OBM.

5. Chemical potential did not act according to an osmotic assumption. Water was driven into the shale regardless of the water solution's activity. For the oil solutions, water was driven out of the shale in all the cases, due to the wettability change caused by the emulsifier.

6. The idea of increasing the drilling fluid salinity to dehydrate the shale and increase its strength should be seriously reevaluated, as well as the induced change in pore pressure. A low salinity should be enough to avoid any reaction (swelling) of the shale.

7. Due to its highly complex structure and interactions, fluid (mainly water) flow in shales does not follow Darcy's law. Also, a reevaluation of the pore pressure concept (and its dissipation) in shales should be done, since it affects the effective stresses usually used to estimate wellbore stability.

6.5 Summary

Problems when drilling through shales are usually attributed to inadequate weight and/or composition of the drilling fluid. Drilling fluid is most often selected based on experience (after trial and error attempts), based on screen tests with available samples, and finally based on some concepts developed in the past. In this chapter, some of the most important concepts used by the industry to select the appropriate drilling fluid, such as semi-permeable membrane, use of chemical potential (due to difference in activity) as a driving force, shale swelling mechanisms, and the capillary effects in the laboratory

were checked. Specifically designed laboratory tests conducted with downhole preserved shale cores show that these concepts cannot explain shale-fluid interaction. Most of these misconceptions were originated from inadequate laboratory practices. Based on the results obtained from the carefully conducted experiments, it was described new interaction mechanisms between shale and water and oil-based solutions. The idea that shales react and swell was found to be not representative of the downhole behavior. It is not reasonable to assume that the majority of instability problems has chemical origin. As a consequence, a totally new approach to analyze wellbore stability, based on energetic processes, was developed and is presented in the next chapter.

Chapter 7

7. An Energy Approach to Wellbore Stability Analysis

7.1 Introduction

Wellbore instabilities experienced in the field have been attributed, mainly, to the chemical interactions between the drilling fluids and the shaly formations. However, the laboratory results presented in this dissertation demonstrated that downhole shales do not appreciably react with water and swell. Therefore, the tests conducted with the preserved samples do not support the thesis that the chemical reaction of rocks with the drilling fluids gradually reduce the rock strength or the effective stresses. Whereas, the standard stress vs. strain analyses can explain the rock failures. Drilling operations involve mud flow, string rotation, string vibration, and string movement up or down. As a consequence, the wellbore wall is constantly subjected to continuously-

changing conditions. Therefore, only a comprehensive energy analysis of the near wellbore phenomena, considering the major effects all together, can explain the causes of the wellbore instabilities. Whereas, the wellbore instability has been considered to occur as a result of a series of isolated events in terms of stress, and only a few attempts to couple the governing phenomena have been made (Coussy, 1995), but the important and relevant events have not been simultaneously considered in these attempts.

In this chapter, the wellbore stability phenomenon is analyzed, based on the conservation of energy principle. A conceptual model and simple method to quantify the energy associated with each event, are proposed here. However, evaluation of the consequences in terms of damage to the rock requires specially designed tests to determine the response of the rock in terms of energy. This approach can explain the failure mechanism in the laboratory tests and in most of the problems faced in the field. In view of this new approach, adequate solutions to effectively alleviate the instability problems are discussed. Successful field cases are described, demonstrating the validity of the suggested failure mechanisms.

7.2 Distribution of the Excess Energy during Rock Fracture Failure

Energy can be stored in and released from a stressed body. If the internal energy exceeds the limit that a particular material can carry, a release

mechanism is triggered to release the excess energy and to bring the energy content to an acceptable level. Griffith (1921 &1924) was the first to introduce that one potential mechanism is the creation of microfracture surfaces. Cook (1965) pointed out that Griffith (1921) originally defined the low tensile strength of brittle materials in terms of an inequality between the rate at which elastic energy is released and the rate at which surface energy is absorbed, as a flaw or crack extends within the material. The general basis of Griffith's theory is that elastic potential energy is converted to surface energy during rock failure. In this way, the excess energy, large in relation to the stored elastic strain energy, is dissipated during the failure of rock (Cook, 1965). Thus, the rock failure process is well recognized as originated by mini fractures. Under a compressive stress state, the failure process starts with the creation of microcracks, that eventually evolves into a damage zone. With the coalescence of those cracks, the specimen cannot further sustain the applied load, and failure occurs (Roegiers, 1997). Evolution of the failure process during a triaxial test clearly shows an increase in crack density in the center of the specimen (Figure 7.1). It is observed that the cracking process is started at low stress levels, far from the maximum stress recorded for the rock. Even when a material (including rock) is subjected to a great impact, the material cracks completely. The impact, in this case, compresses the material, but the consequence is fracturing.

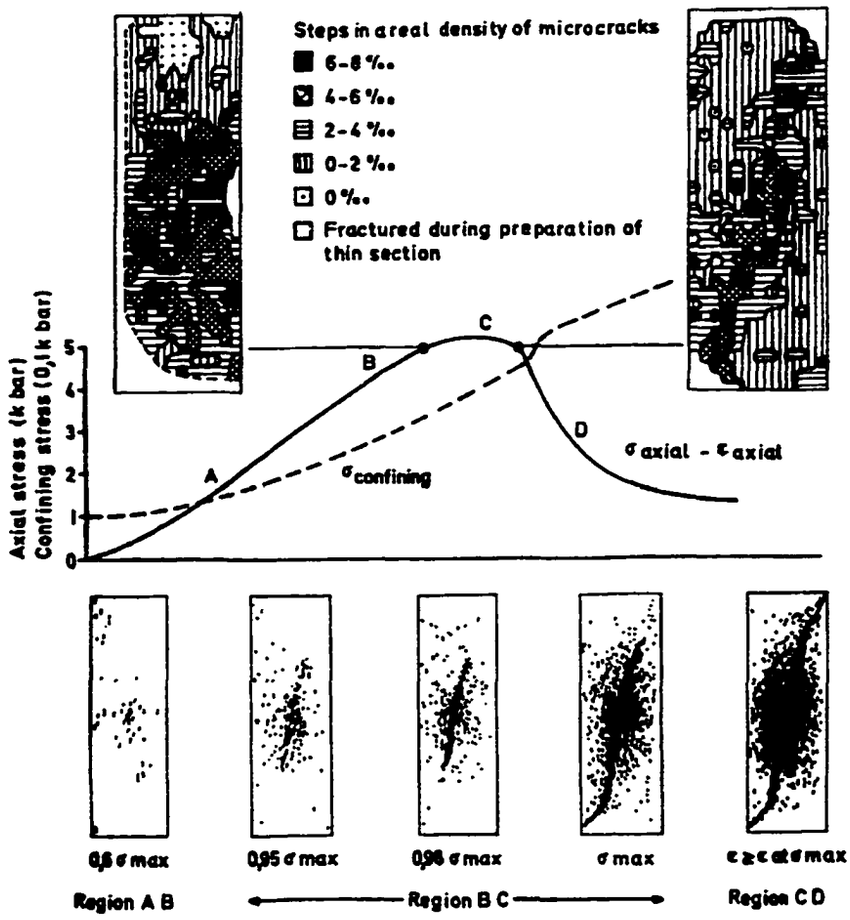


Figure 7.1: A composite representation of the complete stress-strain curve and the incremental radial stress-axial strain curve for a suite of triaxial compression tests done in a stiff-testing machine and in a stiff, sealed triaxial cell, using specimens of argillaceous quartzite prepared from a single piece of rock. The axial sections through specimens stopped at various stages of compression show the structural changes associated with the complete stress-strain curve and associated dilatancy (Jaeger & Cook, 1979).

Another clear evidence of this fracturing process comes from the laboratory experiments conducted with an acoustic sensor. By loading the sample, the stress-strain curve, as well as the seismic events are recorded. It

can be seen that before the rock failed, the acoustic emissions increased, due to fracture creation. These acoustic events are plotted as a function of strain (micro-seismic envelope, Figure 7.2 and Figure 7.3). Not only the stress-strain curve, but also the amount and moment of fracturing are functions of both the rock type and the loading rate. These experiments are the evidence that the energy release mechanism is fracturing. Besides fracture creation, heat is also exchanged with the surroundings, if the rock temperature is allowed to equilibrate with the ambient condition. However, this mechanism is not enough to restore the original internal energy of the specimen when its internal energy is increased due to the axial load applied, as will be seen later (Langhaar, 1962).

From the micro-seismic plot given in Figure 7.2, it can be seen that the first event is equivalent to the final one. The event is so severe that a direct influence on the stress-strain curve is clear, with a break exactly aligned with the strong seismic signal. The rock, however, did not completely loose its strength, and with further energy stored, more fractures were created until the specimen failed.

A closer look at the seismic chart shows that the events are discrete. This means that after a fracture is created, an increase in the internal energy is again required before the next fracture is created. Thus, the work done on the sample by the external force is converted into internal strain energy. After some more deformation, the internal energy level reaches a critical value and fractures should be created.

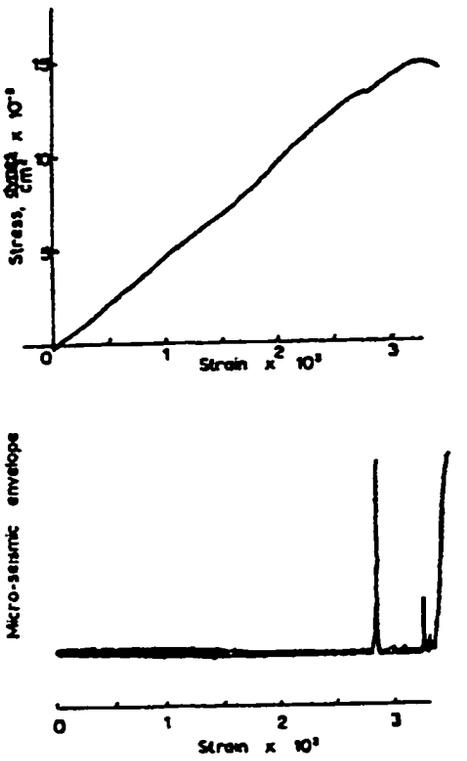


Figure 7.2: The stress-strain characteristics and the envelope of micro-seismic activity for Tennessee marble loaded to fracture in compression (Cook, 1965).

In contrast to the previous result, the stress-strain curve in Figure 7.3 did not show any alteration or influence during the creation of fractures prior to the final one. The plot of micro-seismic activity indicates smaller events in the beginning, compared to the final state, and the stress-strain curve is a straight line until the rock attains its ultimate strength.

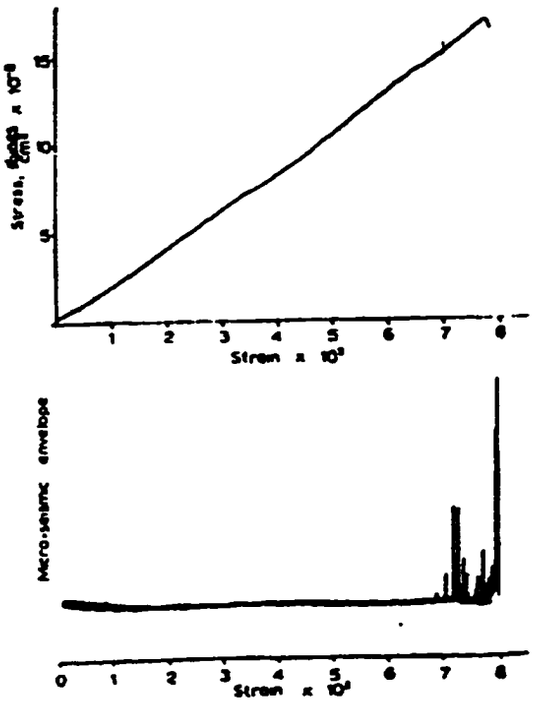


Figure 7.3: The stress-strain characteristics and the envelope of micro-seismic activity for St. Cloud granite loaded to fracture in compression (Cook, 1965).

Because fracture initiation always results in a decrease in the internal energy, the fracture energy term is negative. The other terms can be positive or negative, depending on their interactions with the surroundings. The change in internal energy associated with the phenomena occurring in a borehole is given by:

$$\Delta U = E_m + E_s + E_t + E_c - E_f \qquad (7.1)$$

where E_m, E_s, E_t, and E_c represent the mechanical energy, strain energy, thermal energy, and chemical energy, respectively, and E_f is the fracture surface energy, given by:

$$E_f = \gamma . F_s \tag{7.2}$$

where γ is the specific surface energy and F_s is the area of the fracture created. According to Eq. 7.1, the internal energy is modified by five energy terms. When the internal energy reaches a limit value, this level should decrease by one or more release mechanisms. The most dominant mechanism is the fracture creation.

7.3 Most Relevant Energetic Processes in a Wellbore

The operations carried out during drilling of wells contribute to change in the energetic level of the formation. Only the most important energetic contributions and simple ways to quantify them are mentioned in this chapter. However, further studies are needed to better understand each effect and to determine the maximum acceptable energy levels.

7.3.1 Drill String Vibration (Mechanical Energy)

Field observations, in the form of downhole and surface vibration measurements, have clearly indicated that drillstrings, particularly bottomhole assemblies (BHA's), are generally subjected to severe vibrations (Dykstra *et al.*, 1995; Dunayevsky *et al.*, 1993). The two primary excitation sources induced by these vibrations are the bit/formation and drillstring/borehole interactions (Dunayevsky *et al.* 1993). As a consequence, the drillstring can

vibrate axially, laterally, torsionally, or more often, by a combination of these three basic modes. According to Dunayevsky *et al.* (1993), this makes the drillstring vibration problem fairly complex to investigate and makes the full simulation of the dynamic events impractical. Individual vibration mechanisms have, therefore, been studied by a number of authors (Dykstra *et al.*, 1995; Besalsow & Payne, 1988; Dunayewsky *et al.*, 1993); especially the severe lateral vibrations induced by axial excitations caused by bit/formation interactions. As emphasized by these authors, accelerated fatigue failure in the drillstring, borehole enlargement, and poor directional control can usually occur.

Operating at or close to resonance can create vibration leading to the rapid destruction of the BHA. At rotating speeds that reinforce the natural vibration of the BHA, the destructive harmonics can generate stresses as high as 80,000 psi (Mitchell & Allen, 1987), shortening the fatigue life. According to Mitchell & Allen (1987), a significant percentage of field failures are due to lateral harmonic vibrations.

Drillstring vibrations have been studied mainly to minimize failure of the pipes due to fatigue. Several models of vibration analysis taking into account the composition of the drill string, weight-on-bit, size of hole, distance from the bit, borehole geometry, rotary speed, and mud weight have been developed (Aadnoy, 1986; Besalsow & Payne, 1988; Aarrestad & Kyllingstad, 1989; Dykstra *et al.*, 1995). These models estimate the stresses on the pipe and the lateral displacement and the frequency of the vibration. These studies suggest

that rotary speeds generating resonance should be avoided. At high speeds the stresses in the pipe (Figure 7.4) and the lateral displacements (Figure 7.5) are high. Therefore, problems with the drillstring and the integrity of the wellbore can frequently arise. Lateral displacements of more than 1 in. were predicted by modeling the effect of the component mass imbalance on downhole vibrations and also measured with experiments (Dykstra *et al.*, 1995). This displacement, as reported by the authors, is enough for the 6.25 in. collar to hit an 8.50 in. hole.

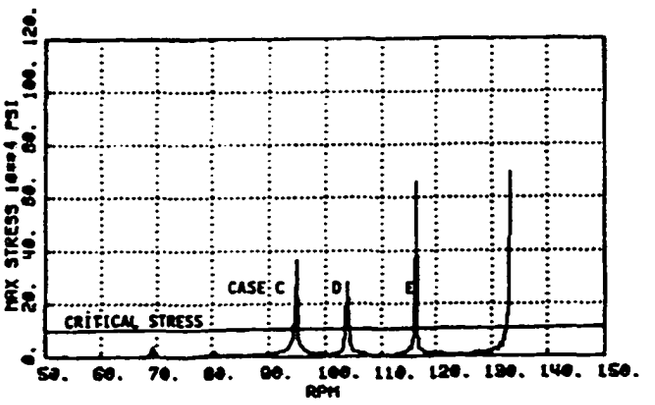


Figure 7.4: Peak stress vs. RPM. Resonances are indicated by high stresses, above the critical stress (Mitchell & Allen, 1987).

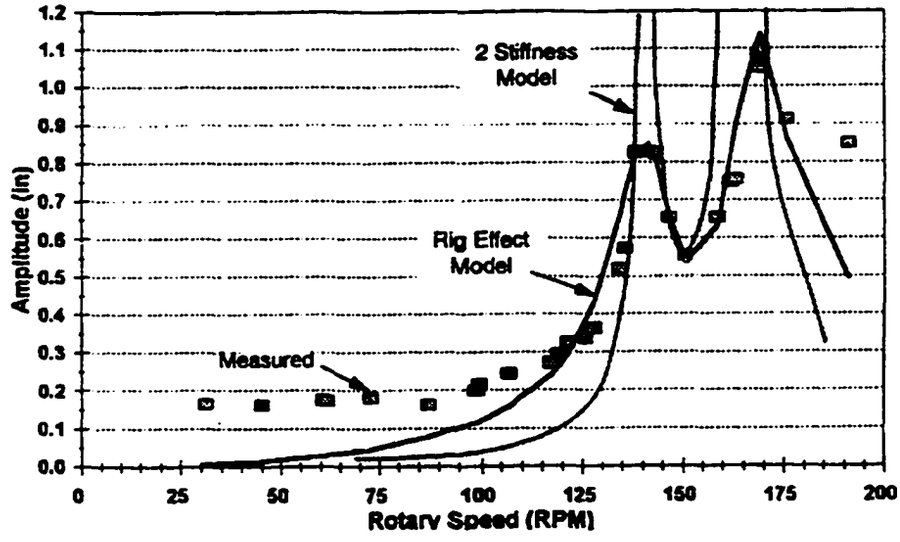


Figure 7.5: Displacement vs. rotary speed due to mass imbalance on the drill string. Both models predicted accurately the range of RPM in which resonance occurs. The magnitude of displacements is accurately predicted by the rig effect model (Dykstra *et al.*, 1995).

Even though the effects of vibration on the enlargement of boreholes are well-known, studies of vibration consequences on the integrity of the wellbore walls are very limited. Two interesting field cases are reported by Field *et al.* (1993), correlating the string vibration with hole enlargement. Substantial lateral displacements within the first 45 feet of the BHA were induced by a large resonant peak at a speed of 170 RPM. This analysis was performed after the failure of a MWD tool, while drilling at 175 RPM. The caliper log showed that most of this hole section was in excess of 3" over gauge. In another case, drilling proceeded at 130 RPM and the MWD tool failed almost immediately after drilling commenced. The analysis indicated that large lateral displacements and bending stresses were induced at around 170 RPM, which

was above the operating range of the assembly for "in gauge" hole. However, the caliper showed 1-2 1/2" over gauge for this particular section. When the analysis was conducted considering this new hole diameter, a critical speed of 135 RPM was found, coinciding with the operating range for the failure.

Replacement of tricone bits by PDC-type can also reduce the drill string vibration, because the rock bit interaction is one of the sources. By adopting this strategy, wellbore stability was greatly improved in the completion of wells drilled in the Campos Basin (Maia, 1994).

The roller cone bit fulfills its task of destroying rock by means of successive percussions. Part of this energy term destroys the rock; another part is reflected in the drillstring (vibrations) and is partly conveyed to the surface, and the remaining part is dissipated. The excessive development of resonance or other more complex forms of dynamic behavior is detrimental to the efficient transfer of energy from the surface to the bottomhole (Henneuse, 1992). The kinetic energy of the drill string due to this dynamic behavior, can be dissipated by heat or by impact on the borehole wall. However, the impact on the wellbore causes the most borehole damage.

Excessive drillstring vibrations can cause borehole enlargements. However, vibration is only analyzed during the failure of the drill string. Such analyses are usually done for special wells, such as horizontal or extended-reach wells. The impact energy of the drill string on the wellbore wall can provide an estimate of the "amount" of damage produced.

A simplistic approach to quantifying this kinetic energy is based on the knowledge of the lateral force of the drillstring. The acceleration of the string can be found from Newton's law:

$$F = ma \tag{7.3}$$

where m is the mass, and a the acceleration. Some models directly give the lateral acceleration of the string. Knowing the maximum displacement of the drillstring (annular space), the velocity (v) of the drillstring immediately before hitting the wellbore wall can be calculated, by integrating the acceleration. The kinetic energy is, then, given by:

$$K = 0.5\ mv^2 \tag{7.4}$$

This kinetic energy of the drillstring is considered as the mechanical energy in the energy balance equation.

Downhole lateral acceleration can be measured with sensors placed in the BHA, and according to Field *et al.* (1993), its values range between 20-30 g, where g = 9.81 m/s^2, under smooth drilling conditions. However, values up to 80 g were also reported by Field *et al.* (1993) and up to 150 g by Dykstra *et al.* (1995). A 12 1/4" hole with an 8" OD drill collar was drilled in the former case. The mass of this drill collar was 150 lb/ft. Here, it is assumed that only one foot of drill collar hits the wellbore. The lateral force exerted by the drillstring can be estimated as following:

$$m = 150 \text{ lbm/ft} \times 1 \text{ ft} = 150 \text{ lbm} \tag{7.5}$$

$$F = ma = 150 \text{ lbm} \times 0.454 \text{ kg/lbm} \times 9.8 \text{ m/s}^2 \times 80 = 53{,}390 \text{ N} =$$

$$= 11{,}917 \text{ lbf} = 5{,}410 \text{ ton} \tag{7.6}$$

For the estimation of the kinetic energy, a 2 in. distance between the drill collar and the wellbore wall is assumed, as indicated by the geometry described by Field *et al.* (1993) . With the acceleration of 80 g, the time for the string to cover this 2 in.-distance is given by:

$$d = 0.5 \, at^2 \tag{7.7}$$

where d is the distance and t the time. Solving the above equation for time yields:

$$t^2 = 2 \times 0.05 \text{ m} / 784 \text{ m/s}^2 = 12.94 \times 10^{-5} \text{ s}^2 \tag{7.8}$$

$$t = 0.0113 \text{ s} \tag{7.9}$$

The velocity at a constant acceleration is given by:

$$v = at \tag{7.10}$$

Thus, solving for velocity yields:

$$v = 784 \text{ m/s}^2 \times 0.0113 \text{ s} = 8.91 \text{ m/s} \tag{7.11}$$

Then, the kinetic energy each time the drillstring hits the wellbore wall can be estimated, in Joules, as:

$$k = 0.5 \times 150 \text{ lbm} \times 0.454 \text{ kg/lbm} \times 8.91^2 \text{ m}^2/\text{s}^2 =$$

$$= 2{,}703 \text{ J} = 2.7 \text{ KJ} \qquad (7.12)$$

As can be seen, when the lateral displacement is sufficiently high for the drillstring to hit the wellbore wall, the large force generated as a result will cause a significant increase in the internal energy of the rock.

7.3.2 Rock Deformation (Strain Energy)

In a wellbore, the walls are constantly subjected to a certain pressure, exerted by the drilling fluid, in addition to the in-situ stresses. If rock deformation occurs, it is reasonable to assume that displacement occurs only in the radial direction, because the rock is confined both laterally and axially. A zero axial deformation and the plane strain hypothesis are usually assumed in many wellbore stability models. For simplicity, only the radial displacement is considered in the following analysis.

Variation of the stress state around a wellbore can easily be calculated (Hsiao, 1987; Santos, 1989; Ong, 1994). However, the deformation of the rock is the most important contribution for the consideration of energy. When a deformation occurs under the application of a force, the associated strain energy is given by:

$$E_s = 0.5\ \sigma\varepsilon \qquad (7.13)$$

where E_s is the strain energy per unit volume, σ is the stress, and ε is the deformation (in the same direction of the stress) produced by the applied stress.

According to Langhaar (1962), the internal energy for an elastic body is determined by the strain and the temperature. Whereas, the internal energy of inelastic bodies depends on other factors than configuration and temperature (Langhaar, 1962). For example, by slow extension and compression of an inelastic rod, an hysteresis loop on a stress-strain chart (Figure 7.6) may be present. The external work supplied for one cycle is represented by the area enclosed by the loop. If no heat escapes, this work is equal to the increase ΔU of internal energy during the cycle. The temperature may be changed by the cycle, but the heat that must be extracted to restore the initial temperature is not equal to ΔU, because some energy is locked up in the rod by residual stresses at the microscopic level. Consequently, by leading the rod around a hysteresis loop and then restoring the initial temperature, the internal energy of the rod is altered without changing the macroscopic strain or the temperature.

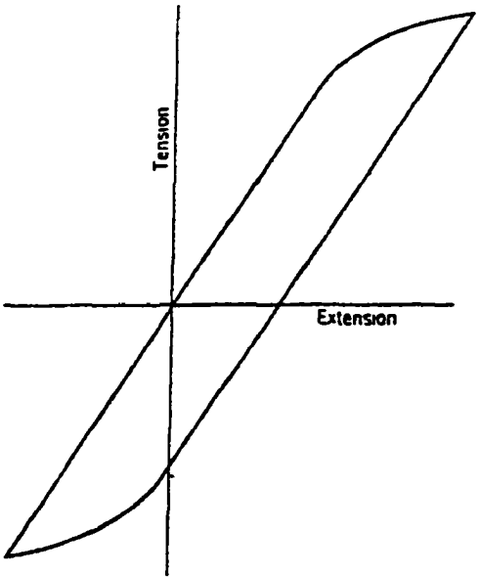


Figure 7.6: Hysteresis loop due to loading-unloading of an inelastic material. The area inside the loop gives the amount of internal energy stored in the material for this cycle (Langhaar, 1962).

Hysteresis in the loading-unloading experiments have been observed for several rock types, and also in different laboratory tests. The plastic deformation and the shape of the loop are functions of the rock type and experiment conducted. Figure 7.7 shows a triaxial test with a confining pressure of 3,000 psi, with a pronounced loop, but a relatively small plastic deformation after each unloading cycle.

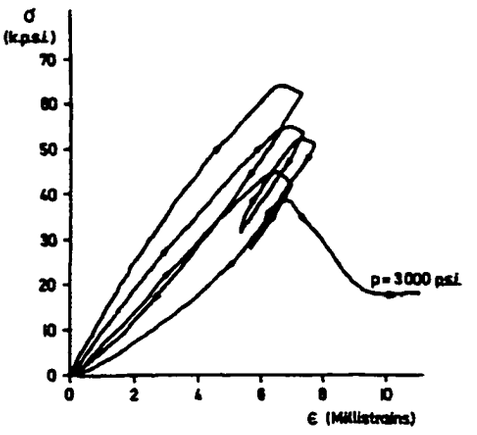


Figure 7.7: Complete stress-strain curves for a specimen of norite loaded and unloaded through several cycles at a confining stress of 3,000 psi (Jaeger & Cook, 1979).

The same process described by Langhaar (1962) for a metal rod applies to rocks. The loading curve is always at the top of the unloading curve. This means that the amount of energy corresponding to the area enclosed by the loop was absorbed by the specimen. By definition, strain energy is equivalent to mechanical energy.

In a wellbore, the fluid pressure various continuously. The hydrostatic pressure provided by the mud weight is modified by several factors:

1) mud circulation increases the bottom hole pressure due to pressure drop in the annulus;

2) surge and swab pressures are generated when the drill string is tripped in or out of the hole;

3) turning the mud pumps on to break the mud gel increases the bottom hole pressure; and,

4) sudden variations due to instabilities of the wellbore wall. An increase in bottom hole pressure occurs when the annulus is full of cuttings and a drop occurs when a severe loss of circulation occurs.

The bottom hole pressure is commonly estimated by using the concept of equivalent mud weight (EMW[1]). When the mud is circulating, equivalent circulation density (ECD[2]) is also used. The EMW and ECD can be higher or lower than the static mud weight, depending on the operation and the wellbore conditions (e.g., in gauge or enlarged hole, full of cuttings). Some models are available to estimate the ECD in order to check if the pressure does not exceed the fracturing gradient. In slim holes, this is extremely important because the pressure drop in the annulus is much higher than in normal-size wells. Models to estimate surge and swab pressures during casing and drillstring movements are also available (Campos, 1986).

Downhole sensors and equipment enable the observation of the effective change in the bottom hole pressure. Ward & Andreassen (1997) show several measurements of EMW during various operations in the wellbore. The effect of pipe rotation, tripping in the hole, breaking gels, cuttings load in the annulus, reaming, can be seen in Figure 7.8 to Figure 7.15. Oscillation of the EMW is sometimes large enough to provoke fracturing of the formation (Figure 7.14). This event is clearly observed at the surface, because the mud

[1] The equivalent mud weight is calculated by dividing the fluid pressure at a given depth by the depth.
[2] The equivalent circulation density is calculated by dividing the dynamic fluid pressure, including all the pressure drop due to fluid flow in the annulus, by the corresponding depth.

volume immediately decreases. However, the most important observation is the oscillations on the EMW during the various operations, especially tripping in/out, reaming, and restarting circulation. As rocks are not perfectly elastic, each cycle of bottom hole pressure variation imposes an additional deformation cycle with a hysteresis similar to the one showed in Figure 7.7. The consequence of each cycle is to further increase the internal energy of the rock. Even if each cycle produces only a slight increase in internal energy the amount of accumulated internal energy can reach a significant level. Therefore, after a period of drilling, the upper open hole formations will have been subjected to a large number of cycles, in the order of thousands. As the completion of the phase delays, and more operations need to be done in the well, the situation only gets worse. The stored internal energy increases as the number of cycles increases.

The difference between the swab and surge peak values can reach 0.16 sg[3]. This is equivalent to almost 700 psi at a depth of 3,000 m. The typical cyclic load is around 400 psi, for tripping in the hole. This value is highly influenced by the speed of running the drill string, which can generate excessive swab/surge values. Also, mud properties (gel and yield point) contribute to increase or decrease the swab/surge pressures. Because the rock is subjected to a stress state at the borehole wall, the cyclic load of a few hundred psi can be enough to take the rock beyond the elastic limit and create permanent damage in the form of fractures.

---

[3] Specifig gravity. Pure water has sg = 1.

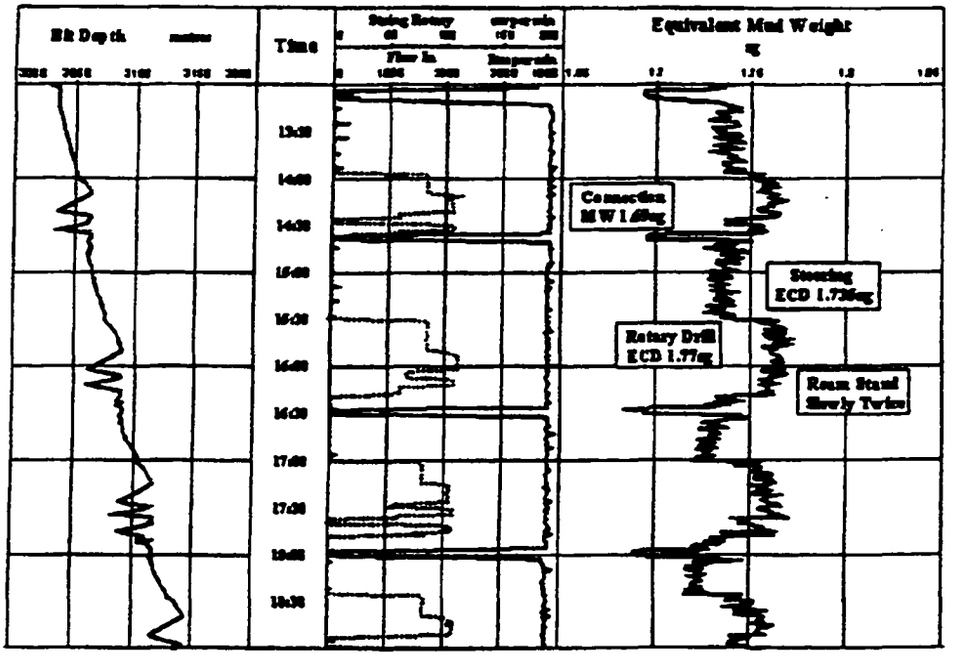


Figure 7.8: Effect of pipe rotation. Gullfaks B-32. 12 1/4" section. Water-based KCl/Polymer mud. PWD sensor 14 m behind the bit (Ward & Andreassen, 1997).

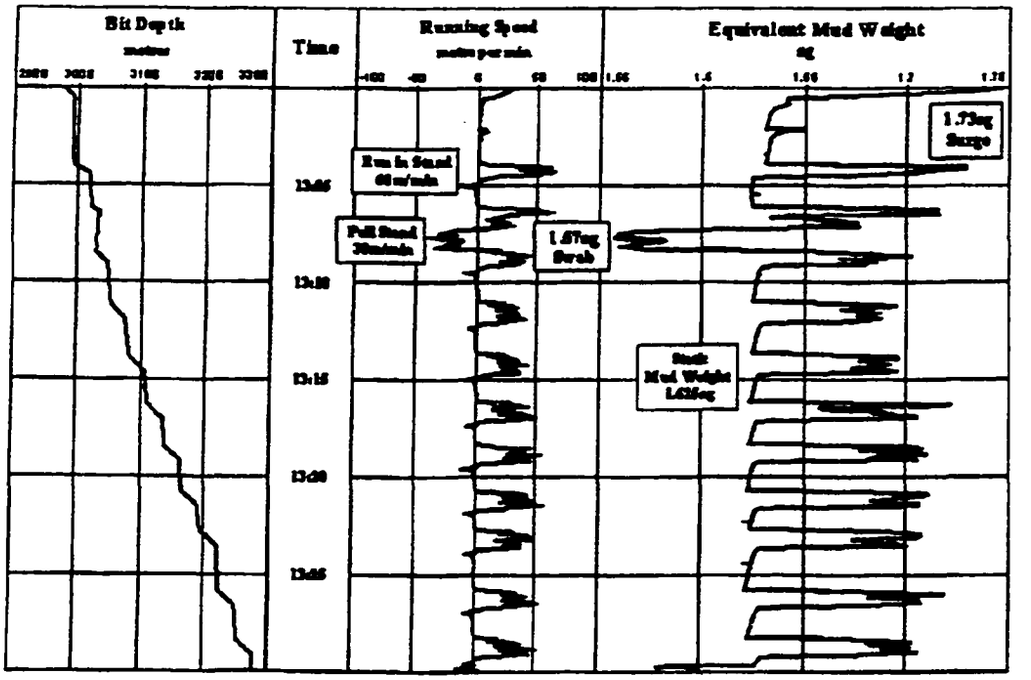


Figure 7.9: Swab/surge pressures. Statfjord C-22. 8 1/2" section. Synthetic Oil-based mud. PWD sensor 34.5 m behind the bit. (Ward & Andreassen, 1997).

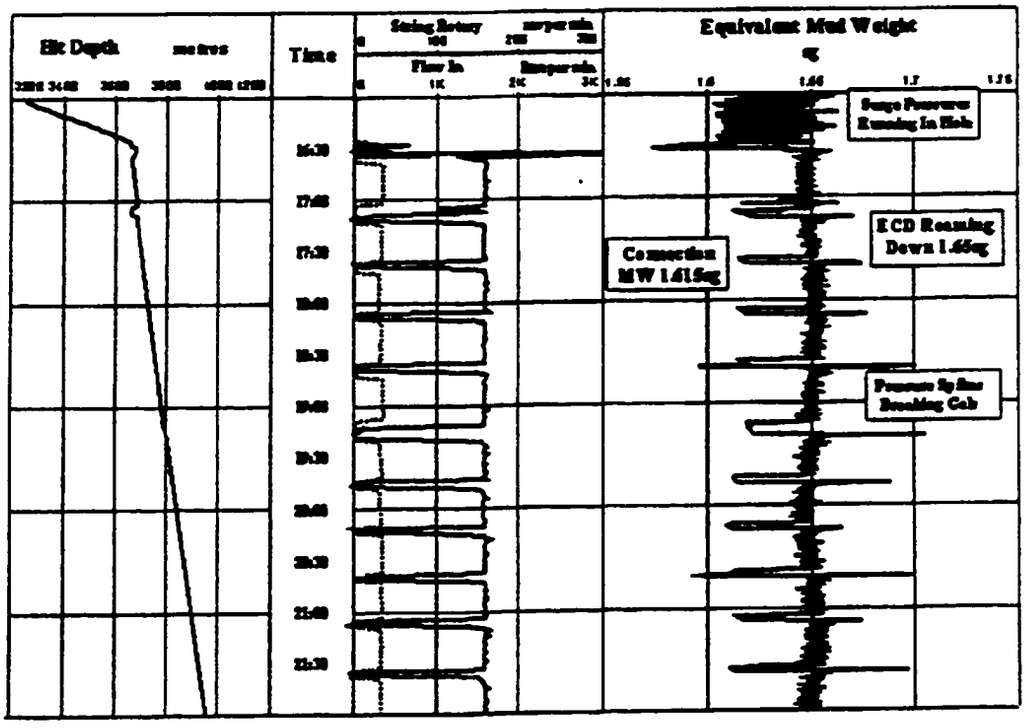


Figure 7.10: Breaking gels. Gullfaks B-32. 9.4" section. Normal Oil-based mud. PWD sensor 27 m behind the bit. (Ward & Andreassen, 1997).

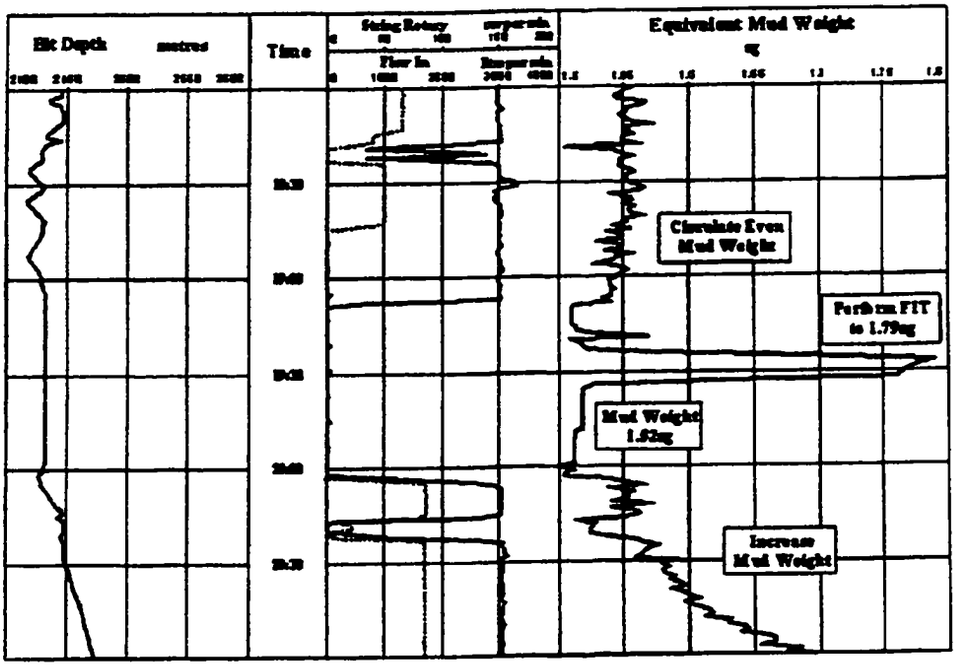


Figure 7.11: Leak-off test/Formation integrity test (FIT). Gullfaks B-32. 12 1/4" section. KCl/Polymer mud. PWD sensor 14 m behind the bit. (Ward & Andreassen, 1997).

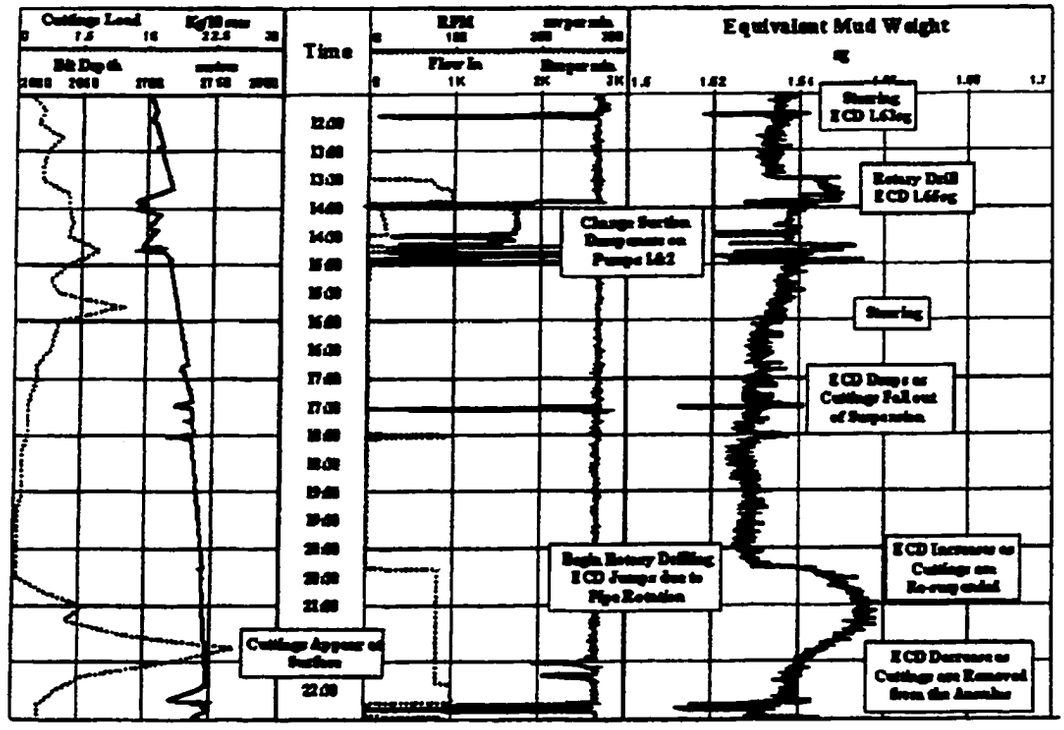


Figure 7.12: Cuttings load. Statfjord A15 A. 12 1/4" section. Synthetic Oil-based mud. PWD sensor 27 m behind the bit. (Ward & Andreassen, 1997).

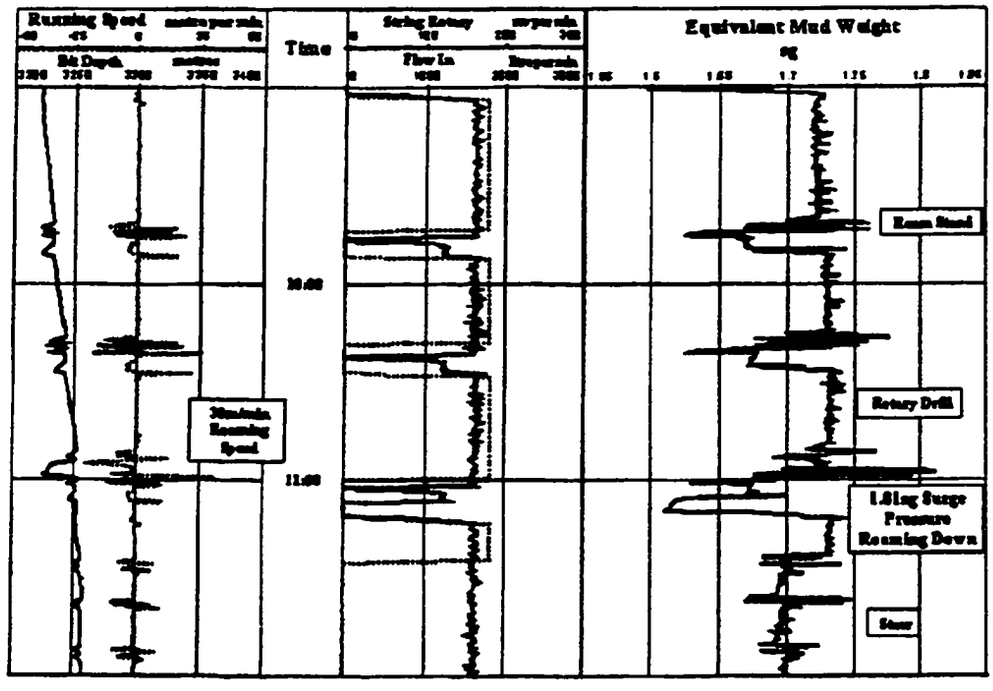


Figure 7.13: Reaming down. Statfjord C-22. 8 1/2" section. Synthetic Oil-based mud. PWD sensor 34.5 m behind the bit. (Ward & Andreassen, 1997).

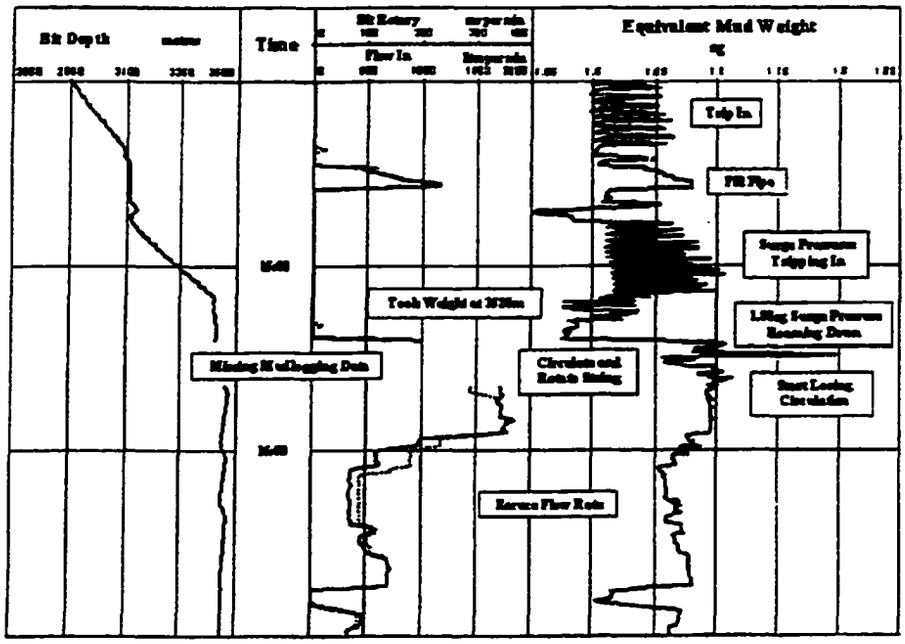


Figure 7.14: Lost circulation. Statfjord A-6 A. 8 1/2" section. Synthetic Oil-based mud. PWD sensor 8 m behind the bit. (Ward & Andreassen, 1997).

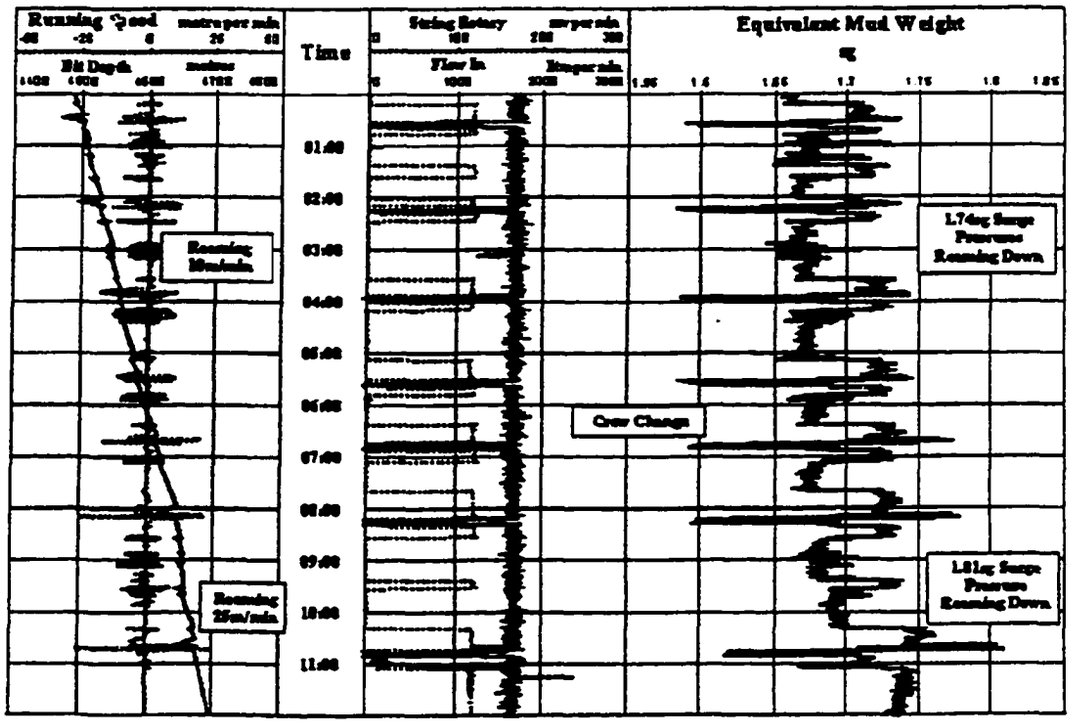


Figure 7.15: One driller still reaming fast. Statfjord A-35 A. 8 1/2" section. Synthetic Oil-based mud. PWD sensor 28.5 m behind the bit. (Ward & Andreassen, 1997).

The importance of cyclic loads is well recognized in fatigue studies. In 1913, Inglis has explained the relevance of cracking and cyclic loads in brittle materials: *"a small loading tending to open the crack will produce overstrain at its ends. On reversing the load the crack closes again, but not before it has set up some reversed stress at the ends of the crack. In this manner a small alternating load may produce in the material an alternating stress far in excess of its elastic range, and under these circumstances, if a crack has once fairly started, no amount of ductility will prevent it spreading through the substance"*.

Fatigue studies in rocks are not common, but there are evidences that fractures propagate in rocks when subjected to cyclic loads. Based on linear elastic fracture mechanics, crack propagation is governed by the stress concentration factor, K_f, and the fracture toughness γ. If $K_f < \gamma$, creep or fatigue failures could not take place. However, according to Celestino *et al.* (1995), there are abundant evidence against this fact. The same authors pointed out that the mechanisms most probably responsible for fatigue in rocks are decreased shielding at the crack tip (consequently increasing K_f), modifications of the microstructure in the crack tip region, and stress corrosion. Celestino *et al.* (1995) reported that some experiments conducted with ceramics showed that crack propagates under fatigue, regardless of stress corrosion action (Dauskardt *et al.*, 1987; Sylva & Suresh, 1989; Reece *et al.*, 1989; Dauskardt *et al.*, 1990). Experimental evidence of rock failure under fatigue is given by Celestino *et al.* (1995), with Brazilian tests conducted on

granite. After the first three cycles (stage 1), in which fracture propagates and fracture toughness was measured, a cyclic loading condition corresponding to 50 and 90 % of the maximum load was applied. As shown in Figure 7.16, the specimen failed after several cycles, although $K_f < \gamma$ during the cyclic loading.

Quantification of the amount of internal energy given to the rock in each cycle requires the knowledge of the stress-strain behavior of the material. Depending on the hysteresis, more or less energy will be added in each cycle. It is important to emphasize that not only the difference in the maximum and minimum load of each cycle, but also the stress state that is applied to the rock are important in determining whether and when the rock will fail. If the rock is under a very low stress state, and the cyclic load is of low magnitude, very little damage is produced during each cycle, due to the low amount of energy given in each cycle. The hysteresis in these situations is not detectable.

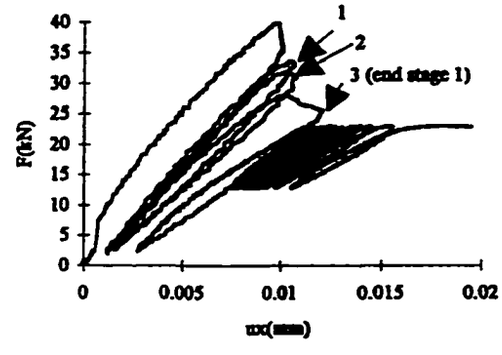


Figure 7.16: Fatigue test on a medium-grained granite from the Socorro Granitic Complex, Sao Paulo, Brazil (Celestino *et al.*, 1995).

A quick estimate of the amount of internal energy stored in the rock in each cycle can be done considering the period at the end of stage 1. A rough estimate indicates an amount 15 x 10^{-3} J accumulated in each cycle. Even though this value is small the amount of energy stored after a large number of cycles is significant, and enough to lead the specimen to failure.

7.3.3 Heat (Thermal Energy)

When a difference in temperature between two bodies exists, heat flows from the body with the higher temperature to the body with the lower temperature until the two temperatures become identical. In the wellbore, heat flow occurs between the drilling fluid and the rock formation throughout the drilling phase.

Mud temperature has been considered as a second order parameter in drilling for a long time. In order to explain some problems in the field, the temperature profile inside the wellbore and the associated stresses were investigated by some authors (Guenot & Santarelli, 1989; Maury & Idelovici, 1995; Maury & Guenot, 1995; Coussy, 1995). According to Guenot & Santarelli (1989). Temperature change affects the behavior of the rock at the borehole wall in several ways:

1) modification of rock properties, stiffness, strength, toughness;

2) cyclic variations of temperature contribute to rock properties change;

3) generation of thermal stresses due to difference in temperature between the drilling fluid and the rock; and,

4) the associated volume change of the porous skeleton, and also of the fluid itself, have an effect on the pore pressure.

When drilling starts, immediately below the casing shoe, the mud is cooler than the formation. As drilling proceeds deeper, the bottom hole mud is still cooler than the formation, but the mud reaches the top of the open hole section which is warmer than the rock at that depth. The temperature profile along the well can be estimated by the available models. Use of MWD tools contributed to an improved access to bottom hole temperature values. A typical temperature profile for the circulating mud for different drilling phases is shown in Figure 7.17. Figure 7.18 presents the mud temperature in the annulus and also the borehole wall temperature variation during each phase.

Difference in temperature between the mud and the rock produces a stress distribution at the wall equivalent to (Guenot & Santarelli, 1989):

$$\Delta\sigma_\theta = \Delta\sigma_z = \frac{\alpha\Delta T.E}{(1-\nu)} \qquad (7.14)$$
$$\Delta\sigma_r = 0$$

where α is the coefficient of linear thermal expansion ($^\circ C^{-1}$), ΔT is the temperature drop between the wall and the far field, E and ν are the Young's modulus and Poisson's coefficient, and $\Delta\sigma_\theta$, $\Delta\sigma_z$, and $\Delta\sigma_r$ are the change in tangential, axial, and radial stress, respectively. A downhole cooling of 20°C produces a reduction of 10 MPa (1,450 psi) in the tangential stress,

considering the following estimated characteristics for a limestone (Guenot & Santarelli, 1989):

$E = 40{,}000$ MPa

$\nu = 0.2$

$\alpha = 1 \times 10^{-5}\ ^{\circ}C^{-1}$

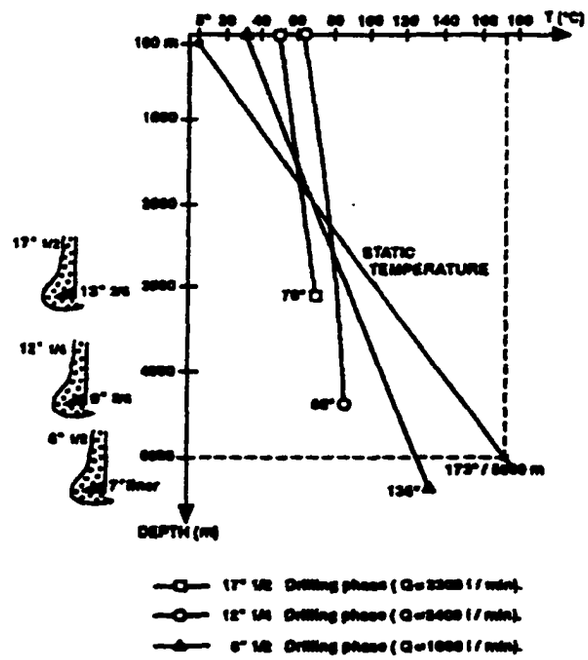


Figure 7.17: Typical profile for the circulating mud for different drilling phases (Maury & Guenot, 1995).

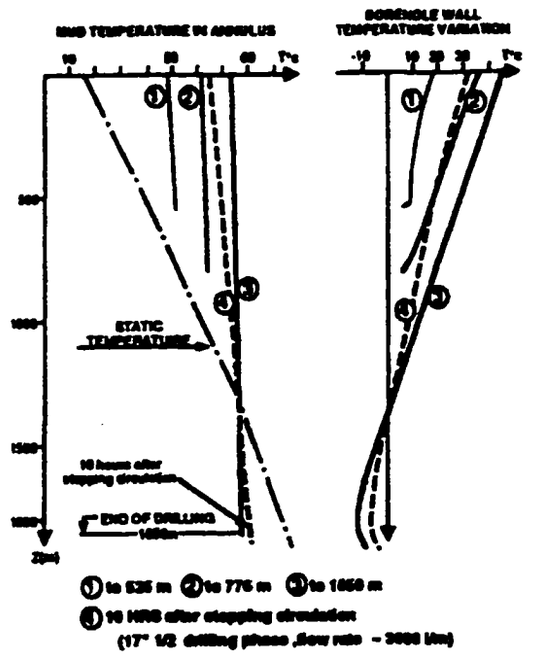


Figure 7.18: Mud and borehole wall temperature evolution when deepening (Maury & Guenot, 1995).

Thermally-induced fractures have been observed in several situations, due to reduction in tangential stress. In general, reduction in tangential stress increases the overall stability of the hole (considering shear failure). As this cooling effect turns into a warming effect, as drilling proceeds deeper, the stresses at the borehole wall increases and instability may result. A raise in mud weight should be considered to compensate the effect of the increased tangential stress due to the warming of the mud.

Influence of drill pipe rotation on mud temperature was investigated by Guenot & Santarelli (1989) with a special downhole tool. With the data acquired, the influence of drill pipe rotation was incorporated into a computer code. The results of a typical simulation indicate a strong influence of the drill

pipe rotation on mud temperature (Figure 7.19). Downhole temperature increases with rotation, because friction is transformed into heat. By stopping the drill pipe rotation alone, can reduce the downhole temperature by more than 20°C. This example shows the importance of the mud temperature. In some extreme situations, a decision to drill with mud motor (the drillstring does not rotate), instead of with a traditional rotary system, may be the key to reduce the instability problems.

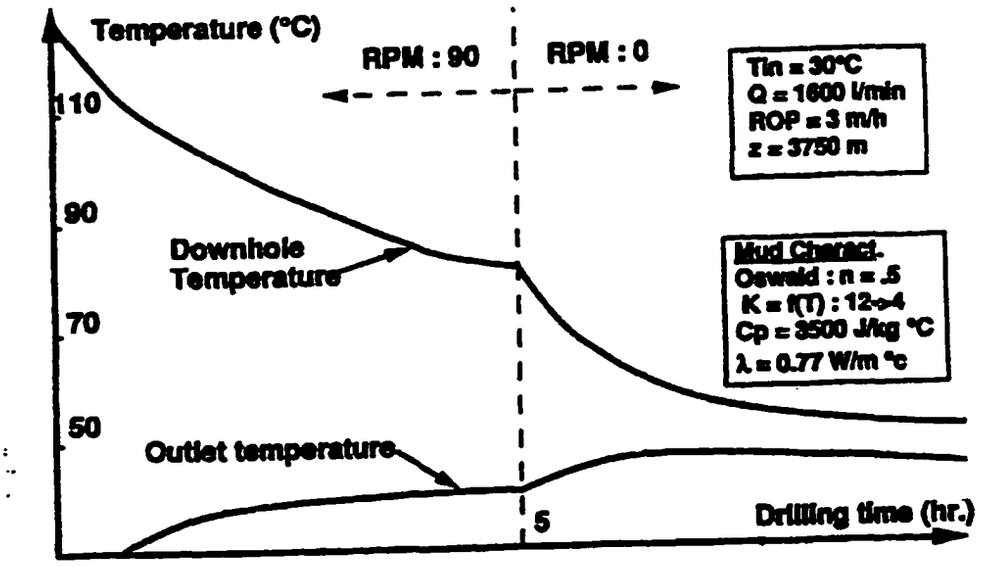


Figure 7.19: Effect of pipe rotation on downhole and outlet (measured on the surface) temperature (Guenot & Santarelli, 1989).

The cyclic effect is also extremely important when considering temperature. The thermal and pressure regimes of the well during drilling and mud circulation interruptions consist of alternate cooling and reheating. According to Maury & Idelovici (1995), borehole stress evaluation shows that

the near wellbore fracture gradient can be exceeded, when cooling is combined with ECD, inducing small cracks. Upon reheating, these cracks close, being responsible for transient pressure build-up. A cyclic load exists even without the creation of fractures, and fractures can be created by the fatigue mechanism without necessarily exceeding the tensile strength.

Even though instabilities can be better explained and understood with a stress thermal analysis, the temperature difference leads to an important contribution in terms of the cyclic phenomenon and the energy. At the beginning of the phase, the internal energy of the rock is reduced due to lower mud temperatures. As drilling proceeds, and if the mud at the top of the open hole section is warmer than the formation, energy is transferred from the mud to the rock, increasing the internal energy of the formation. Energy transfer is also a function of time, as heat flow is allowed. Every time drilling is stopped, the temperature in the wellbore and in the rock tend to equilibrate. When drilling is reinitiated, this process is interrupted, and a thermal gradient again exists.

Laboratory experiments show that the rock strength is inversely proportional to temperature, keeping the confining pressure constant (Figure 7.20). These results become evident if an energetic analysis is done. By heating the rock, the internal energy of the specimen is increased (heat is being given by the surroundings); because the rock failure occurs by creation of microcracks (when the internal energy reaches a critical level), the amount of mechanical energy (strain energy due to the applied axial load) necessary to

produce failure is smaller, compared to the amount required when the test is conducted at a lower temperature. Assuming that a critical amount of internal energy needs to be transferred to the rock in order to reach failure, in this experiment only thermal and strain energy is being transferred from the surroundings. Therefore, the change in internal energy is:

$$\Delta U = E_t + E_s \tag{7.15}$$

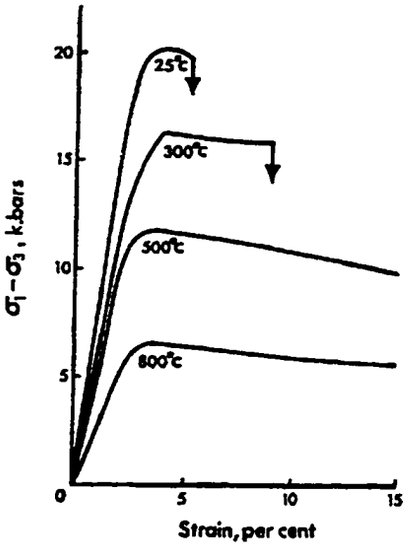


Figure 7.20: Stress-strain curves for granite at a confining pressure of 5 kilobars and various temperatures (Jaeger & Cook, 1979).

Because only the change in energy can be measured, the test conducted at 25°C will be considered as the baseline for the thermal energy. The strain energy released by the specimen due to radial deformation is not computed

due to the absence of such a curve. All the energy values below are per unit volume. For this test, $E_t = 0$, and then,

$$\Delta U = E_s = 0.5\ \sigma\varepsilon = 0.5 \times 25 \times 0.045 = 56.25\ J/cm^3 \qquad (7.16)$$

For the test conducted at 300°C, the strain energy required to produce failure was:

$$E_s = 0.5 \times 21 \times 0.045 = 47.25\ J/cm^3 \qquad (7.17)$$

The need for less amount of strain energy can only be attributed to the internal energy increase due to heat. As temperature increases, the amount of heat also increases and less strain energy (from the axial load) is required to cause failure, as shown in Figure 7.20. The maximum load is reduced and the strain at the time of failure is smaller compared to the test conducted at room conditions. By keeping the rock at a constant stress state, lower than its strength, temperature increase alone can fail the specimen. The increase in internal energy due to the raise in temperature is more important than the stress state due to thermal oscillations (in the case of the laboratory experiment). If the specific heat of the rock is known, the exact change in internal energy due to raise in temperature can be evaluated.

A simple example for a shale is given here. Somerton (1992) gives the heat capacity and thermal conductivity properties of several sedimentary rocks. A typical value for heat capacity of shale is 0.218 cal/g-K. Because thermal

conductivity of rocks is very small, compared to metals or liquids, for example, the effect of temperature is expected to be restricted to a region near the borehole wall. Assuming a positive change of 20°C on the rock temperature, the internal energy of the rock increases 18.24 J/g.

The same energetic analysis can be done for triaxial tests conducted at the room temperature, but with different confining pressure (Figure 7.21). As the confining stress increases, the axial stress required to produce failure also increases. In these tests, only mechanical (strain) energy is exchanged by the system with the surroundings. As the specimen is compressed in the axial direction, an expansion in the radial direction is observed, due to the effect of Poisson's ratio. The energy given to the system by the axial load should be subtracted by the energy released by the specimen due to its expansion in the radial direction. Both energy terms are calculated using the same equation, that is stress x strain. For the test conducted with zero confining stress, the amount of energy released by the specimen is zero. Therefore, the energy required for failure can be calculated simply by the axial load and strain. When the confining stress is different from zero, the specimen releases mechanical energy as the radial deformation increases (Figure 7.21). Therefore, the energy given by the surroundings to produce failure is greater than in the previous case, to compensate for the release of radial strain energy. Therefore, greater axial load and deformation are needed as a bigger confining stress is applied.

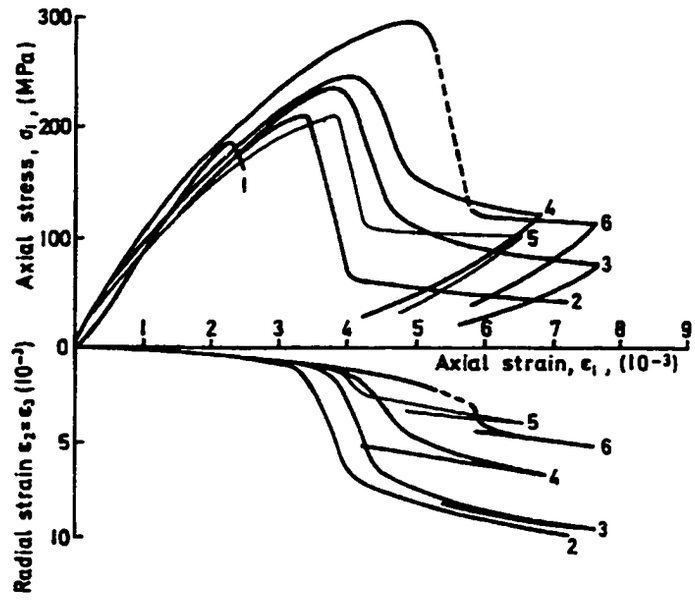


Figure 7.21: Complete axial stress-strain and radial strain-axial strain curves at different confining pressures for a suite of specimens prepared from a single piece of argillaceous quartzite. Uniaxial compression: curve 1. Triaxial compression: curves; (2) $\sigma_2 = \sigma_3 = 3.45$ MPa; (3) $\sigma_2 = \sigma_3 = 6.9$ MPa; (4) $\sigma_2 = \sigma_3 = 13.8$ MPa; (5) $\sigma_2 = \sigma_3 = 27.6$ MPa, cracked specimen; (6) $\sigma_2 = \sigma_3 = 27.6$ MPa (Jaeger & Cook, 1979).

7.3.4 Chemical Rock Alteration

The last important energetic process undergoing in a wellbore is the chemical alteration of the formation due to its contact with the drilling fluid. Some formations are more prone for chemical alteration than others. An unconsolidated sandstone, for example, with just quartz in its composition and almost no cement, has a very small degree of chemical interaction with any fluid. On the other hand, carbonates and shaly formations react vigorously with some fluids. Carbonates are dissolved in the presence of acid, and shales react chemically with fluids, both WBM and OBM, as shown in Chapter 6.

Any alteration in the rock structure by a chemical reaction implies a change in the total original volume and in the internal energy. It is rare to have a reaction in which the final volume is equal to the volume of the reagents. Due to the structure modification, the internal energy of the material is also changed. Therefore, depending on the reaction, the internal energy is increased or decreased.

Every chemical reaction obeys two fundamental laws: (i) the law of conservation of mass; and, (ii) the law of conservation of energy. Almost all reactions absorb or produce energy. As a general rule, energy is released when a change leads to a more stable state (that is, less stable molecules are converted to more stable molecules); and energy is absorbed if the change leads to a less stable state. Heat is the form of energy that is most commonly absorbed or released in a chemical reaction. When a reaction produces energy, and heat is transferred to the surroundings as is the case of the combustion of oxygen and hydrogen (Eq. 7.18), this process is called exothermic. The reverse process is called endothermic.

$$2H_2\,(g) + O_2\,(g) \rightarrow 2H_2O\,(l) + \text{heat} \qquad (7.18)$$

Enthalpy (H), or heat content, is the quantity used by chemists to measure the heat change of any process (Chang, 1984). Only the processes that occur under constant pressure are considered here, because the reactions

undergoing at constant volume are rare. The reaction enthalpy is the difference between the enthalpies of the products and the reactants:

$$\Delta H = H \text{ (products)} - H \text{ (reactants)} \qquad (7.19)$$

For an endothermic process ΔH is positive, and for an exothermic process ΔH is negative. The combustion of methane is an example of an exothermic process:

$$CH_4\,(g) + 2O_2\,(g) \rightarrow CO_2\,(g) + 2H_2O\,(l) \quad \Delta H = -890.4\ kJ \qquad (7.20)$$

The above equation is called a thermochemical equation, because it satisfies not only the mass balance, but also shows enthalpy changes. Specification of the physical states of the reactants and products is essential, because the enthalpy changes depend on them. Another important point is that the enthalpy of a substance increases with temperature. Hence, the enthalpy change of a reaction must also depend on temperature.

If a reaction is run at constant volume no work will result from these changes. Therefore, the first law of thermodynamics states:

$$\Delta U = Q + W = Q \qquad (7.21)$$

Even though constant-volume conditions are sometimes impossible to achieve, such an assumption will be made here for the sake of simplicity. For a chemical reaction, then, the amount of energy released or absorbed is equal to the change in internal energy. If a volume change occurs, part of this energy is consumed to work. Assuming the constant-volume simplification:

$$\Delta U = Q = \Delta H \tag{7.22}$$

Two quantities should be introduced in order to quantify the amount of energy of a reaction: (i) specific heat (ρ) of a substance, which is the amount of heat energy required to raise the temperature of one gram of the substance by one degree Celsius; and, (ii) the heat capacity (C) of a substance, which is the amount of heat required to raise the temperature of a given quantity of the substance by one degree Celsius. Therefore, from the knowledge of the specific heat or the heat capacity, it is possible to calculate the heat change (heat absorbed or released) of a system in a given process by using the following equations:

$$q = m\rho\Delta T \tag{7.23}$$

$$q = C\Delta T \tag{7.24}$$

where q is the heat change, m is the mass of the system, and ΔT is the temperature change. Eqs. (7.23) and (7.24) can also be combined:

$$C = m\rho \tag{7.25}$$

Quantification of the amount of energy of any reaction can be done with a calorimeter. Different types of calorimeters are available (constant pressure and constant volume) to measure the heat capacity of a substance. For the purpose of obtaining the energy change due to the interaction between the drilling fluid and the rock, measurements should be made before and after the reaction. One of the modern calorimeters available is the differential scanning calorimeter (DSC). The change in internal energy due to the reaction of the rock with a fluid can be estimated by running a test on the virgin sample, and then running another test after the rock has been exposed to the test fluid.

Figure 7.22 shows the result of a DSC run with shale D, before and after immersion in a solution with NaCl 24% w/w; the difference between the two curves is small. The integration of a DSC signal over the caloric zero line yields the enthalpy function of the sample. By integrating the whole curve, a balance from the exothermic and endothermic reactions can be made, and the final enthalpy for the entire temperature interval is calculated. For the native sample, with the peak at 319.1°C:

$$H_{native} = 1395.6 \text{ J/g} \tag{7.26}$$

For the sample immersed for 24 hrs. in the NaCl solution the peak was at 308°C and the enthalpy:

$$H_{NaCl\ (24hrs.)} = 1515.8\ J/g \tag{7.27}$$

The change in internal energy on the rock due to chemical alteration is:

$$\Delta H = 120.2\ J/g \tag{7.28}$$

Unfortunately, problems with the DSC equipment prevented further investigation of the energetic changes of the rock due to interaction with different solutions[4]. With this single example, it is expected that interaction with salt solution would not impact the rock as much as the strain and thermal effects. Even though a better evaluation needs to be done, the chemical interaction seems to be the less important phenomenon in terms of energetic changes. The TGA results presented in Chapter 6 indicate that there is not much alteration of the rock structure after the first 24 hrs. of immersion.

[4] After several tests the calorimeter response started to be the inverse of what it was supposed to be. Evaporation of free water is an endothermic reaction, characterized by a curve with an upward concavity, as shown in Figure 7.22 for temperatures up to 120°C. The poor results generated by the equipment showed the curve in this region with a downward concavity, indicating an exothermic reaction, which is unrealistic. The manufacturer suspected of a problem with the differential sensors, which cannot be solved easily.

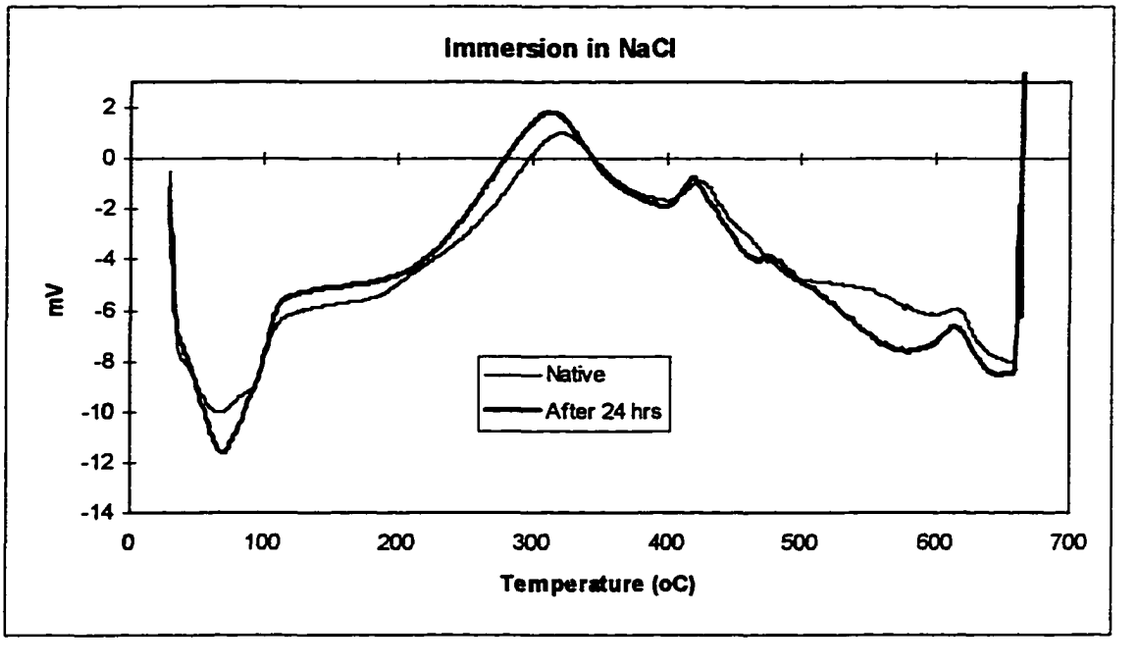


Figure 7.22: DSC result of shale D, before and after 24 hrs. immersed in NaCl 24% w/w.

7.4 Proposed Instability Mechanism

Based on the hypothesis that fractures are created to release some internal energy stored in the rock, and recalling that all the important operations in the wellbore in one way or another impact the energy balance, the wellbore instability starts by fracture initiation at or in the neighborhood of the rock walls.

The initiation of fractures due to the release of excess internal energy does not occur immediately after drilling. An energy balance should be done, taking into account all the events described previously. Most of these events contribute to the increase of the internally stored energy as the drilling

proceeds. Therefore, as the drilling operations continue, the internal energy level of the open hole section tends to increase, mainly in the upper part of the hole, which is exposed longer. Hence, the probability of instability increases as drilling operations take longer.

After the rock has been fractured, its strength decreases and it might not be able to resist the applied stresses, reaching failure immediately. Another important factor is the fluid penetration. If the fluid penetrates into the fractures, an instability mechanism can be triggered because the support provided by the difference between the pore pressure and the mud pressure diminishes.

The suggested fatigue mechanism has been observed in several civil engineering structures. Appearance of micro-fractures in railroad bridges and stadiums around the world has been observed lately (Machado, 1997). The mechanism that caused these fractures is cyclic loading. The internal energy level of the structure increases and fractures are created to reduce the energy level. This phenomenon is not commonly observed in highway bridges. The main difference between a highway and a railroad bridge is the applied load level. The bigger the cyclic load, the higher the energy accumulated in each cycle. In sports stadiums, a similar phenomenon happens. During a game, the structure is subjected to an excessive cyclic load. The appearance of fractures is detected by an excessive deformation of the structure, usually long after its construction was completed.

By analogy, in the wellbore fracturing should start slowly, and an excessive deformation of the wall should be the first symptom (increased torque and drag). Also, if the rock is ductile, a large deformation (compared to a brittle rock) is tolerated by the rock, before failure. Depending on the type of formation, brittle or ductile, the consequences observed in the well will be different.

The fracturing mechanism in a wellbore has been studied for quite a long time, and has been well addressed by Dusseault & Gray (1992). However, all the analyses done so far explained the fracturing process via stress analyses. This dissertation, on the other hand, suggests an energetic failure criterion.

Wellbore stability analysis still can be done by comparing the stress level with the strength. However, the analysis should be conducted with a certain safety factor, in order to guarantee that the stresses applied are well below the level to create cracking. This level is not known; hence, in many situations fracturing might be induced immediately, due to an excessive stress state applied to the wellbore walls with inadequate (either high or low) mud weight.

Field observations clearly show that shales are more prone to hole enlargement than sandstones or carbonates. Even though a deeper investigation is necessary, the low permeability of shales associated with strong micro-scale interactions explain this different behavior. Most of the energy events described previously have a direct effect on the pore pressure. In high-permeability rocks pore pressure equilibrium is quickly restored by fluid flow. However, as flow is severely restricted in shales, fluid pressure

imbalance causes the matrix to deform, creating micro-cracks. Understanding the process of cracking in a micro-scale can better explain the fundamental difference among these rocks. Low-permeable carbonates usually have low porosity, and therefore pore pressure has only a minor effect on these rock types.

7.5 Need for Laboratory Tests to Determine the Required Parameters

Quantification of the various energetic contributions described previously is essential to predict the relative importance of the various phenomena. The effect is also dependent on the rock type. Laboratory tests should be specifically designed to obtain the most relevant parameters to be used in a model.

The first parameter to be measured is the amount of internal energy a rock can absorb without cracking. Laboratory tests should be run with acoustic emission sensors, so that the seismic events can be mapped and detected as a function of temperature, strain, and stress applied to the specimen. Also, the influence of temperature, e.g., internal energy level, should be investigated. Cyclic loads should be applied in order to reproduce the oscillations observed in the bottomhole pressure. Different levels of cycles should be employed with varying magnitudes of the average load. The maximum load should not only be limited to the elastic and undamaged region, but some of the cycles should be

conducted at load levels reaching cracking. The ultimate strength of the rock can be obtained at the end of each test, by taking the specimen to failure.

The *shale-reactivity test* should be used to measure the effects of fluid-rock interaction. Because such a test is run under pressure, a combined effect of pressure, temperature, cyclic load, and chemical interaction can be achieved.

Hollow-cylinder geometry should also be used as it closely mimics the field geometry. The fluid pressure and the temperature gradient between the specimen and the fluid in the wellbore should be varied. An impermeable membrane can be used to guarantee a non-penetrating condition to the fluid in the wellbore. Therefore, only the mechanical effects will be contributing to the damage of the rock. In another stage, a penetrating condition can be tested, adding the effect of rock-fluid interaction. Constant monitoring with acoustic sensors is essential to observe the cracking of the rock.

7.6 Effective Minimization of the Wellbore Stability Problems

As shown in this dissertation, the shale swelling is not the main mechanism responsible for the wellbore instability problems. The main cause is the creation of a cracked zone in the vicinity of the wellbore, as a consequence of either excess stored energy or excess stress (Figure 7.23). According to Growcock (1997), increasingly the oil industry believes that most shales are

naturally fractured, therefore increasing the risks of instability problems. This confirms that even if the rock is not naturally fractured, it will become fractured as drilling goes on. Shale cores taken from offshore wells in the Campos Basin show that the rocks are not naturally fractured. Even in this case, instability problems were encountered, supporting the argument that the fracturing, in this particularly case, might develop with time.

In order to minimize the damage to the rock, operational procedures should be adjusted. For example, mud cooling is being used in some fields to reduce the temperature gradient between the drilling fluid and the rock, with great improvement of the overall wellbore stability (Maury, 1996; Maury & Guenot, 1995). Reduction of drillstring vibrations have proven to be a great contributor to keep the integrity of the borehole walls. Even simple operations, such as tripping in/out of the hole, are extremely important. Inadequate procedures can lead to high surge/swab pressures, causing irreversible damages to the rock.

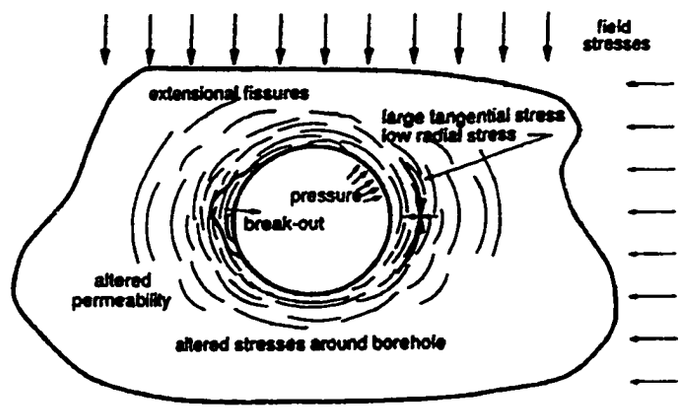


Figure 7.23: Extensional fissures around a borehole due to insufficient mud pressure (Dusseault & Gray, 1992).

Even though cracking itself can be a serious mechanism leading to failure, mud penetration also triggers the instability in the fractures. With fluid penetration, all the support provided by the difference between the mud pressure and pore pressure is lost, and the finite-sized piece created by the fractures, therefore, falls into the wellbore. The best way to reduce instability problems is, then, to use effectively non-penetrating fluids (sometimes these fluids are called non-invasive). Dusseault & Gray (1992) illustrates the case of using gilsonite to prevent pressure penetration into fractures (Figure 7.24).

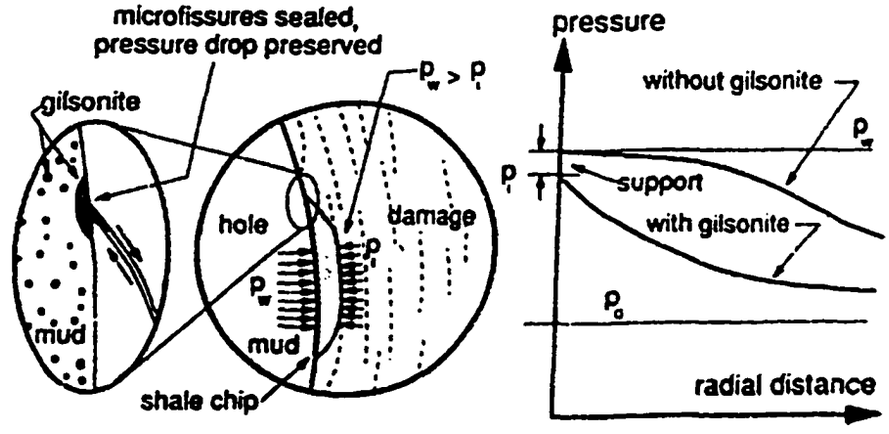


Figure 7.24: Pressure penetration into fractures blocked by gilsonite. Mud pressure greater than pore pressure guarantees wellbore stability (Dusseault & Gray, 1992).

When OBM is being used, this non-penetrating characteristic is given by the capillary threshold pressure in the case of a water-wet shale, as described in Chapter 6. However, this threshold pressure vanishes if fractures or cracks

(natural or induced) are present in the rock. This is probably the situation in which wellbore stability problems are faced, even when OBM is used.

Several additives have been developed to give a non-penetrating property to WBM. Silicate muds, thermal activated additives (van Oort, 1997; Downs *et al.*, 1993), and several polymers (Estes, 1986) have been developed and are currently used to minimize mud penetration into the formation. Increasing field cases are being reported (Estes, 1997), emphasizing the success of a non-penetrating drilling fluid to solve stability problems, which confirms the hypothesis that the main cause is not the reaction of the shale with the mud. Non-penetrating fluids have been used to drill formations which were thought to be reactive. Drilling has been highly successful even when using fresh water to drill problematic gumbo shales (Estes, 1997). As can be seen, the inhibitive nature of the drilling fluid has been substituted by the non-penetrating characteristic with a high degree of success. These field cases strongly support all the ideas described in this dissertation.

One of the biggest problems with muds, known as non-invasive, is that most of them have serious side effects. Silicate mud, for example, imposes a severe formation damage, dramatically decreasing the reservoir productivity. Gilsonite, on the other hand, affects the formation evaluation through by logging. So far, the best product is a mixture of varying solubility polymers, extremely efficient in reducing invasion, not causing formation damage, which are also environmentally safe (EDTI, 1997).

7.7 Relevance of the Various Energy Terms in the Overall Energy Balance

In this section, an overall energy balance involved in the creation of cracks is presented using the parameter values typical to drilling of wells in reservoirs. For this analysis, a cubic shaped representative elementary volume (REV) of 1 cm^3 is taken at the wall of the well (Figure 7.25).

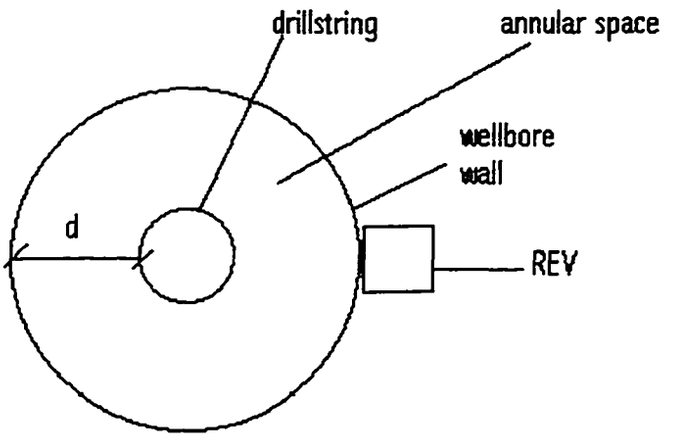


Figure 7.25: Schematic of a wellbore with a drillstring and the REV at the wellbore wall (not in scale).

Because the details of the calculations have been described in preceding sections, only the main equations are listed in Table 7.1. For the calculations, a density of 2.5 for typical shaly rocks was assumed. The mass of the REV is, then, 2.5g. The energy contributions of the various terms are presented in Table 7.1.

Table 7.1: Evaluation of the various energy contributions for a 2.5g sample in the microfracturing process of rocks.

Energy Term	Origin	Method of calculation	Parameters used	Energy Change
Mechanical	String impact on the wall	$d = 0.5at^2$ $v = at$ $K = 0.5mv^2$	d = 5 cm (annular space) $a = 784\ m/s^2$ m = 2.2 kg[a]	88.5 J
	Wall deformation	$\sigma = E\varepsilon$ $E_s = 0.5\sigma\varepsilon\Delta v$	E = 50 GPa $\varepsilon = 1\%$ $\Delta v = 1 cm^3$	2.5 J
	Cyclic loading	$E_{cyc} = \Delta\int\sigma\varepsilon$	20,000 cycles[b]	300 J
Thermal	Temperature change	$E_t = m.Cp.\Delta T$	Cp = 0.912 J/g-K[c] $\Delta T = 20°K$ m = 2.5 g (mass of the REV)	45.6 J
Chemical	Immersion in saturated NaCl solution	ΔH[d]	-	300 J[e]
Fracture	Opening of 1 cm^2 of fracture surfaces	$E_f = \gamma S$	γ[f] = 4000 J/m^2	0.4 J

[a] mass correspondent to 1 cm of drill collar (150 lb/ft)
[b] source Celestino *et al.* (1995)
[c] source Somerton (1992)
[d] the enthalpy change was directly measured with a differential scanning calorimeter
[e] this value should be taken with reserve due to problems with the equipment and no experience with the effect of enthalpy change on fracture creation
[f] value for limestone, source Labuz & Biolzi (1991)

Note that the specific surface energy (γ) values reported in the literature varies within an order of 4 magnitudes. Therefore, for a conservative estimate of the energy required for creation of fracture surfaces, an upper limit of γ was considered. Most of the tests to determine the specific surface energy of a rock were conducted with the application of strain energy only. The relatively high values calculated for the chemical and thermal energy terms clearly

indicate that these two effects should be investigated in the experiments so that γ is measured directly. This parameter is usually obtained from the propagation of one macro-fracture. Because the failure mechanism proposed here considers the generation of multiple, randomly oriented cracks in various dimensions (Figure 7.26), the values of γ determined under the current conditions may be different from those to be obtained from the suggested laboratory tests.

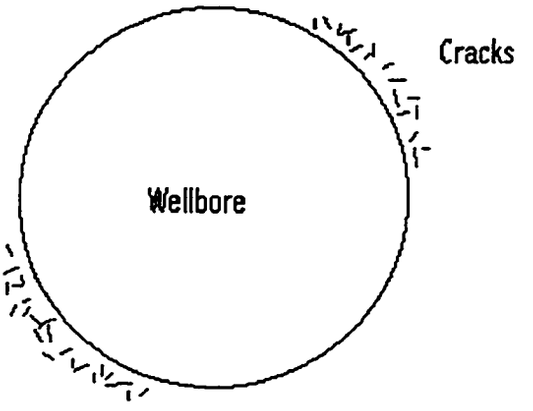


Figure 7.26: Schematic of multiple, randomly distributed cracks around the wellbore due to the excess energy stored in the rock (not in scale).

7.8 Summary

This chapter described a new way to analyze wellbore stability based on the energy distribution. It has been shown that when the internal energy level of the rock reaches a value that cannot be sustained by the rock, a fracturing

process starts in order to reduce the energetic level of the rock to an acceptable limit. Fracturing of the downhole rock occurs when the internal energy level increases beyond the acceptable level for that material. Then, the energy is converted into surface energy, by creation of micro-fractures. The most energetic processes during drilling were described to be vibration of the drillstring, deformation of the wellbore walls due to oscillation of the mud pressure, temperature difference between the drilling fluid and the rock formation, and the chemical alteration of the rock. Cyclic loads due to temperature difference and mud pressure oscillations cause the internal energy to increase. Fatigue phenomena are well known for metal, but not widespread known in rock. Subsequent fluid penetration into the fractures causes immediately instability of the wellbore. If fracturing cannot be completely avoided, use of effective non-penetrating fluids will minimize, and sometimes, completely eliminate the stability problems. Successful field operations has provided support for this proposed instability mechanism, as well as for the suggested remediation method. Specific laboratory tests were also proposed in order to obtain some of the parameters essential to quantify and develop a quantitative model, so that the rock fracturing can be predicted and field operations can be carried out to minimize the onset of the problem.

Chapter 8

8. Conclusions and Recommendations

8.1 Conclusions

Even though the laboratory program conducted was limited to shales from the Campos Basin, important conclusions can be drawn. However, it is too early to generalize the conclusions to all shales.

1. It has been shown that shale in contact with water reacts according to its dryness state. A detailed and careful preservation and laboratory handling procedures have been proposed for all shaly rocks to guarantee a close to original moisture content at all times.

2. A new characterization methodology based on thermogravimetric analysis was developed to overcome the limitations of X-Ray diffraction with clay-rich rocks.

3. The results shown in this dissertation demonstrate that shale swelling is unlikely to occur under downhole conditions, even when water based muds are used. Note that this conclusion contradicts conventional belief.

4. The new shale-reactivity test was designed in order to study shale-fluid interaction simulating wellbore conditions. Chemical and hydraulic potential, as well as temperature effects on the shale can be studied with this test.

5. The traditional assumption of an ideal semi-permeable membrane when OBM is used is not likely to be correct because the emulsifier changes the wettability of the rock.

6. Interpretation of the results of immersion tests with varying activity solutions suggests that the belief that chemical potential is the main mechanism that drives water in/out of subsurface shale may not be true.

7. Tests in both macro- and micro-scale were conducted and the results showed that lack of water in smectite is the main cause of partially-dried shale swelling in the laboratory, rather than presence of air inside the sample.

8. Chemical interaction of in-situ shales with the drilling fluid is minimal and does not produce significant changes in the rock structure to explain all wellbore instability problems.

9. An innovative conceptual approach based on an energy balance was developed and explains the time-delayed failures often encountered in the field.

10. The energy approach used to analyze wellbore stability implies a size-dependent effect (smaller holes are more stable), whereas all wellbore stability analysis based on stress is size-independent.

11. To reduce wellbore stability problems, one can reduce damage to the rock by cooling the mud to reduce the temperature gradient, reducing drillstring vibration, and reducing surge/swab pressure during tripping in and out of the wellbore.

12. Use of non-invasive drilling fluids almost guarantees a problem-free wellbore and it is the best option available today.

8.2 Recommendations

1. To generalize the conclusions, immersion tests with varying solution activities and other shale types should be conducted.

2. Only well-preserved downhole shale cores should be used in tests to understand interaction mechanisms.

3. To improve both characterization and quantification of rocks with TGA, a better understanding of the thermal reactions undergone by clay minerals is required. If this is accomplished, clay mineral modifications due to shale-fluid interaction can be studied using this methodology.

4. Rock fatigue studies should be conducted. Triaxial tests with hollow-cylinder geometries should be used to understand rock failure when subjected to cyclic loads. Because cyclic loading is a potential source of cracking, reducing fatigue consequences can directly reduce wellbore stability problems.

5. The size-dependent aspect of wellbore stability should be investigated. Field evidence indicates fewer stability problems with smaller holes. However, a conclusion has not been possible because of the large number of variables that change during drilling. With the proposed energy approach this issue can be studied in greater depth.

Nomenclature

a = acceleration
a_{df} = activity of the drilling fluid
a_{sh} = activity of the shale
a_w = activity of a water solution
C = heat capacity
c_1 = concentration of the monovalent cation in the bulk solution
c_2 = concentration of the divalent cation in the bulk solution
E = electrical potential and Young's modulus
E_f = fracture surface energy
E_m = mechanical energy
E_s = strain energy
E_t = thermal energy
F_s = area of the fracture
G_{total} = free energy per unit area
H = enthalpy
h = surface separation
I = flow of current
J_d = diffusive flow of solute relative to the volume flow
J_v = flow of total solution
K = kinetic energy
L = empirical constant denoting the contribution of a certain gradient to a specific flow
M = mechanical energy
m = mass
P = pressure
p_s = swelling pressure
p_w = partial pressure of the water vapor
p^0_w = vapor pressure of pure water
p/p_0 = relative water vapor pressure at equilibrium
Q = heat
R = universal gas constant
R.H. = relative humidity
T = temperature
t = time
U = internal energy
U_{sys} = internal energy of a system

U_{surr} = internal energy of the surroundings
V_w = partial molar volume of water (liters/mole)
v = velocity
W = work

Greek

α = coefficient of linear thermal expansion
ε = strain and dielectric constant of the medium
ϕ_m = electric potential at the midway plane between two surfaces
γ = specific surface energy
κ = Boltzmann constant
μ_c = chemical potential
ν = Poisson's coefficient
π = osmotic pressure
ρ = specific heat
σ = stress
Δ = symbol denoting difference
∇ = gradient
Γ = surface charge density

Subscripts

θ = tangential
r = radial
z = axial

References

Aadnoy, B. S. (1986). "Transversal vibrations in stabilized drilling assemblies," Energy Sources, vol. 8, no. 4, pp. 305-329.

Aarrestad, T. V. & Kyllingstad, A. (1989). "Measurements and theoretical models on rig suspension and the effect on drillstring vibrations," 64th SPE Annual Technical Conference and Exhibition, San Antonio, October 8-11, Paper SPE 19553.

Abousleiman, Y., Cui, L., Cheng, A. H.-D., & Roegiers, J.-C. (1995). "Poroelastic solution of an inclined borehole in a transversely isotropic medium," Proc. 35th US Rock Mechanics Symposium, In: Rock Mechanics, Daemen & Schultz (eds), Balkema, Rotterdam.

Amanullah, M. & Chenevert, M. E. (1996). "Atmospheric swelling of Speeton shale," Mid-Year Meeting, Drilling Research Program, University of Texas at Austin, August 21.

Bailey, S.W. (1966). "The status of clay mineral structures," Proceedings, 14th National Conf. on Clays and Clay Minerals, Pergamon Press, New York, pp. 1-23.

Barrer, R.M. & Perry, G.S. (1961). "Sorption of mixtures and selectivity in alkylammonium montmorillonite, Part II, Tetramethylammonium montmorillonite," *J. Chem. Soc.*, 850-858.

Barshad, I. (1949). "The nature of lattice expansion and its relation to hydration in montmorillonite and vermiculite," *Am. Mineralogist*, **34**:675-684.

Bates, T.F., Hildebrand, F. A., & Swineford, A. (1950). "Morphology and structure of Endellite and Halloysite," *Am. Mineralogist*, **35**, 463-484.

Berend, I. (1991). Les mechanisms d'hydratation de montmorillonites homoioniques pour les pressions relatives inferieures a 0.95, Thesis INPL, Nancy.

Besalsow, A. A. & Payne, M. L. (1988). "A study of excitation mechanisms and resonances inducing bottomhole assembly vibrations," SPE Drilling Engineering, March, pp. 93-101.

Biolzi, L. & Labuz, J. F. (1993). "Global instability and bifurcation in beams composed of rock-like materials," *Int. J. Solids Structures*, **30-3**, 359-370.

Bish, D. L. & Duffy, C. J. (1990). "Thermogravimetric analysis of minerals," in: Thermal Analysis in Clay Science, vol. 3, CMS Workshop Lectures, Stucki & Bish (eds.), The Clay Minerals Society, Boulder, CO.

Bohn, H., McNeal, B. L., & O'Connor, G. (1979). *Soil Chemistry*, John Wiley & Sons, New York.

Bol, G.M. (1986). "The effect of various polymers and salts on borehole stability and cutting stability in water-based drilling fluids," IADC/SPE Drilling Conf., Dallas, Feb. 10-12, Paper SPE 14802.

Bol, G. M., Wong, S-W., Davidson, C. J., & Woodland, D. C. (1994). "Borehole stability in shales," SPE Drilling & Completion, June, pp. 87-94.

Bolt, G. H. (1955). "Ion adsorption by clays," *Soil Sci.*, 79:267-276.

Bourgoyne Jr., A. T., Millheim, K. K., Chenevert, M. E., & Young Jr. F. S. (1991). Applied Drilling Engineering, Second Printing, Society of Petroleum Engineers, Richardson, TX.

Boyd, S.A., Lee, J. F., & Mortland, M. M. (1988a). "Attenuating organic contaminant mobility by soil modification," Nature, 333:345-347.

Boyd, S.A., Mortland, M.M., & Chiou, C.T. (1988b). "Sorption characteristics of organic compounds on hexadecyltrimethylammonium-smectite," *Soil Sci. Soc. Amer. J.*, **52**:652-657.

Bradley, W.F., Grim, R. E., & Clark, G. F. (1937). "A study of the behavior of montmorillonite on wetting," *Z. Kristallogr.*, **97**:260-270.

Bradley, W.F. (1940). "The structural scheme of attapulgite," *Am. Mineralogist*, **25**, 405.

Bradley, W.F. & Grim, R. E. (1947). "Colloid properties of layer lattices," *J. Phys. Chem.*, **52**:1404-1413.

Bradley, W. B. (1979). "Failure of inclined boreholes," *Journal of Energy Res. Tech.*, **101**, 232-239.

Bratli, R. (1993). Personal communication.

Brignoli, M. (1997). Personal communication.

Brindley, G.W. (1961). "Kaolin, serpentine, and kindred minerals," In: The X-ray Identification and Crystal Structures of Clay Minerals, G. Brown ed., Mineralogical Society, London, pp. 51-131.

Brindley, G.W. (1980). "Order-disorder in clay mineral structures," In: Crystal Structures of Clay Minerals and their X-Ray Identification, Brindley G.W. and Brown, G. eds., Monograph No.5, Mineralogical Society, London, pp. 125-195.

Brindley, G.W. & Robinson, K. (1951). "The Chlorite Minerals," In: The X-ray Identification and Crystal Structures of Clay Minerals, G. Brown ed., Mineralogical Society, London, pp. 172-198.

Campos, W. (1986). "Surge and swab pressures in oilwells due to drillstring movement," M. Sc. Thesis, Federal University of Ouro Preto, Ouro Preto, MG, Brazil (in Portuguese).

Carminati, S., Brignoli, M., Di Marco, A. & Santarelli, F. J. (1997). "The activity concept applied to shales: consequences for oil, tunneling and civil engineering operations," *Int. J. Rock Mech. & Min. Sci.*, **34:3-4**, Paper No. 00038.

Carpinteri, A. (1989). "Decrease of apparent tensile and bending strength with specimen size: two different explanation based on fracture mechanics," *Int. J. Solids Structure*, **25-4**, 407-429.

Celestino, T. B., Bortolucci, A. A., & Nobrega, C. A. (1995). "Determination of rock fracture toughness under creep and fatigue," Proc. 35th US Rock Mechanics Symposium, In: Rock Mechanics, Daemen & Schultz (eds.), Balkema, Roterdam.

Chang, R. (1984). *Chemistry*, Second Edition, Random House, New York.

Chenevert, M. E. (1969). "Adsorptive pressures of argilaceous rocks," 11th Symp. Rock Mech., Berkeley, Calif., pp. 16-19.

Chenevert, M. E. (1970a). "Shale alteration by water adsorption," *J. Petr. Tech.*, September, pp. 1141-1148.

Chenevert, M. E. (1970b). "Shale control with balanced-activity oil-continuous muds," *J. Petr. Tech.*, October, pp. 1309-1316.

Chenevert, M. E. (1995). Personal communication.

Chenevert, M. E. & Osisanya, S. O. (1990). "Shale testing procedures for the prevention of borehole collapse", Energy-sources Technology Conference & Exhibition, Proceedings, New Orleans, 14-17 January.

Chenevert, M. E. & Osisanya, S. O. (1992). "Shale swelling at elevated temperature and pressure," Rock Mechanics, Tillerson & Wawersik (eds), pp. 869-878, Balkema, Rotterdam.

Chilingarian, G. V., Donaldson, E. C. & Yen, T. F. (ed.) (1995). Subsidence due to fluid withdrawal, Elsevier Science.

Chiou, C.T. & Shoup, T. D. (1985). "Soil sorption of organic vapors and effects of humidity on sorptive mechanism and capacity," *Environ. Sci. Technol.*, **19**:1196-1200.

Cook, J. M., Goldsmith, G., Geeham, T. M., Audibert, A. M., Bieber, M. T. & Lecoutier, J. (1993). "Mud/shale interaction: model wellbore studies using X-Ray tomography", SPE/IADC Drilling Conference, Amsterdam, Feb. 23-25, Paper SPE 25729.

Cook, N. G. W. (1965). "The failure of rock," *Int. J. Rock Mech. Min. Sci.*, **2**, 389-403.

Coussy, O. (1995). *Mechanics of Porous Continua*, John Wiley & Sons, New York.

Cui, L., Abousleiman, Y., Cheng, A. H.-D., Leshchinsky, D., & Roegiers, J.-C. (1995). "Stability analysis of an inclined borehole in an isotropic poroelastic medium," Proc. 35th US Rock Mechanics Symposium, In: Rock Mechanics, Daemen & Schultz (eds), Balkema, Rotterdam.

da Fontoura, S. A. B. & Rego, L. F. B. (1995). "Shale characterization, physico-chemical, and mechanical properties," 2nd Quarter Report GTEP-003/95, PUC-Rio, in Portuguese.

Daniels, T. (1973). *Thermal analysis*. New York: John Wiley & Sons.

Daneshy, A. A. (1973). "A study of inclined hydraulic fractures," *Society of Petroleum Engineers Journal*, **13-2**, 61-68.

Darley, H. C. H. & Gray, G. R. (1991). *Composition and properties of drilling and completion fluids*, Fifth Edition, Houston, Texas: Gulf Publishing Company.

Derjaguin, B. V., Churaev, N. V., & Mueller, V. M. (1987). *Surface Forces*, Plenum Publishing Corporation, New York.

Detournay, E. & Cheng, A. H.-D. (1991). Fundamentals of poroelasticity, In: Rock Mechanics Continuum Modeling, Chapter 5.

Diek, A. & Santos, H. (1996). "Surface forces in clay/electroyte interactions," Rock Mechanics Institute report, RMC-96-04, University of Oklahoma, Norman, Oklahoma.

Diek, A., Santos, H. & Varela, A. (1996). "Determinants of shale and clay fabric features: structure and properties (a critical review)," Rock Mechanics Institute Report RMC-96-05, University of Oklahoma, Norman, Oklahoma.

Downs, J. D., van Oort, E., Redman, D. I., Ripley, D. & Rothmann, B. (1993). "TAME: a new concept in water-based drilling fluids for shales," Offshore European Conf., Aberdeen, 7-10 Sept, Paper SPE 26699.

Dunayevsky, V. A., Abbassian, F., & Judzis, A. (1993). "Dynamic stability of drillstrings under fluctuating weight on bit," SPE Drilling & Completion, June, pp. 84-92.

Dusseault, M. B. & Gray, K. E. (1992). "Mechanisms of stress-induced wellbore damage," SPE Int. Symposium on Formation Damage Control, Lafayette, Lousiana, February, 26-27, Paper SPE 23825.

Dykstra, M. W., Chen, D. C-K., Warren, T. M., & Azar, J. J. (1995). "Drillstring component mass imbalance: a major source of downhole vibrations", SPE/IADC Drilling Conference, Amsterdan, 28 February-2 March, Paper SPE/IADC 29350.

EDTI (1997). Environmental Drilling Technology Inc., Product Bulletin: DWC™, FLC™, LCP™, Tulsa, OK.

Ekbote, S., Cui, L., & Abousleiman, Y. (1997). "PBore-3D for Windows Version 1.02," Rock Mechanics Consortium Internal Report, Rock Mechanics Institute, The Univesity of Oklahoma, Norman, Oklahoma.

Eriksson, E. (1952). "Cation exchange equilibria on clay minerals," *Soil Sci.*, **74**:103-113.

Estes, J. C. (1986). "Role of water-soluble polymers in oil well drilling muds," American Chemical Society, 0065-2393/86/0213-0155.

Estes, J. C. (1997). Personal communication.

Field, D. J., Swarbrick, A. J., & Haduch, G. A. (1993). "Techniques for successful application of dynamic analysis in the prevention of field-induced vibration damage in MWD tools," SPE/IADC Drilling Conference, Amsterdam, 23-25 February, Paper SPE/IADC 25773.

Fisk, J. (1995). Personal communication.

Fisk, J. (1996). Personal communication.

Fletcher, P. (1993). *Chemical Thermodynamics for Earth Scientists*, Longman Scientific & Technical, Harlow, Essex, England.

Fooks, J. C. & Dusseault, M. B. (1996). "Strength of Pierre I shale as function of moisture content," Proc. Eurock'96, Barla (ed.), Balkema, Rotterdam.

Forsans, T. M. & Schmitt, L. (1994). "Capillary forces: the neglected factor in shale instability studies?," Eurock '94 Symp., Proc. Balkema, Rotterdam.

Frydman, M. & da Fontoura, S. (1997). "Numerical modeling of borehole pressurization," *Int. J. Rock Mech. & Min. Sci.*, **34:3-4**, Paper No. 082.

Gapon, Y. N. (1933). "On the theory of exchange adsorption in soils," *J. Gen. Chem. USSR* (English translation), **3**:144-160.

Gazaniol, D., Forsans, T., Boisson, M. J. F. & Piau, J-M. (1995). "Wellbore failure mechanisms in shales: Prediction and prevention," *J. Petr. Tech.*, July, pp. 589-595.

Germanovich, L. N., Galybin, A. N., Dyskin, A. V., Mokhel, A. N., & Dunayevsky, V. (1996). "Borehole stability in laminated rock," Eurock 96, Proc., Barla (ed.), Balkema, Rotterdam.

Gieseking, J. E. (1939). "Mechanism of cation exchange in the montmorillonite-beidelite-nontronite type of clay minerals," *Soil Sci.*, **47**: 1-14.

Greene-Kelly, R. (1973). "The preparation of clay soils for determination of structure," *J. Soil Science*, **24**, 277-283.

Grim, R. E., Allaway, W. H., & Cuthbert, F. L. (1947). "Reaction of different

clay minerals with some organic cations," *J. Am. Ceram. Soc.*, **30**, 137-142.

Grim, R. E., Bradley, W. F., & Brown, G. (1951). "The mica clay minerals," In: The X-ray Identification and Crystal Structures of Clay Minerals, G. Brown ed., Mineralogical Society, London, pp. 138-172.

Grim, R. E. (1968). *Clay mineralogy*, Second Edition, McGraw-Hill Book Company, New York.

Growcock, F. (1997). Personal communication.

Gruner. J.W. (1932) "The crystal structure of kaolinite," *Z. Krist.*, **83**, 75-88.

Guenot, A. (1987). "Contraintes et ruptures autour des forages petroliers," In: G. Herget & S. Vongpaisal (eds.), Proc. 6th ISRM Congress, vol. 1, pp. 109-118, Balkema, Rotterdam.

Guenot, A. & Santarelli, F. J. (1989). "Influence of mud temperature on deep borehole behaviour," In: Rock at Great Depth, Maury & Fourmaintraux (eds)., Balkema, Rotterdam, pp. 809-817.

Hale, A. H. & Mody, F. K. (1992). "Experimental investigation of the influence of chemical potential on wellbore stability," IADC/SPE Drilling Conference, New Orleans, Paper IADC/SPE 23885.

Hale, A. H., Mody, F. K. & Salisbury, D. P. (1993). "The influence of chemical potential on wellbore stability," SPE Drilling & Completion, Sept., pp. 207-216.

Heidug, W. K. & Wong, S. (1996). "Hydration swelling of water-absorbing rocks: a constitutive model," *Intern. J. for Numerical and Analytical Methods in Geomechanics*, **vol. 20**, 403-430.

Hendricks, S.B. (1938). "On the structure of the clay minerals: dickite, halloysite, and hydrated halloysite," *Am. Minerologist*, **23**, 295-301.

Hendricks, S.B. & Jefferson, M. E. (1938). "Crystal structure of vermiculites and mixed vermiculite-chlorites," *Am. Mineralogist*, **23**:863-875.

Hendricks, S.B. (1941). "Base-exchange of the clay mineral montmorillonite for organic cations and its dependence upon adsorption due to van der Waals forces," *J. Phys. Chem.*, **45**: 65-81.

Hendricks, S.B. & Teller, E. (1942). "X-ray interference in partially ordered layer lattices," *J. Chem. Phys.*, **10**:147-167.

Henneuse, H. (1992). "Surface detection of vibrations and drilling optimization: field experience," SPE/IADC Drilling Conference, New Orleans, 18-21 February, Paper SPE/IADC 23888.

Hojka, K. & Dusseault, M. B. (1991). "An analytical solution for transient temperature and stress field around a borehole during fluid injection into permeable media," CIM/AOSTRA Tech. Meeting, Banff, Alberta, 59-159-15, April 21-24.

Hsiao, C. (1987). "A study of horizontal wellbore failure," 62nd SPE Annual Technical Conference and Exhibition, Dallas, Paper SPE 16927.

Iimura, K. (1966). "Acidic properties and cation exchange of allophane and volcanic ash soils," *Bull. Nat. Inst. Agric. Sci.*, **17**:101-157.

Inglis, C. E. (1913). "Stresses in a plate due to the presence of cracks and sharp corners," Transactions of the Instiution of Naval Architects, **55**:219-230.

Israelachvili, J.N. (1991). *Intermolecular & Surface Forces*, 2nd edition, Academic Press, New York.

Jackson, W.W. & West, J. (1930). "The crystacl structure of muscovite," *Z. Krist.*, *76*, 211-227.

Jaeger, J. C. & Cook, N. G. W. (1979). "Fundamentals of Rock Mechanics," third ed., Chapman and Hall Ltd., New York.

Joesten, M.D. & Schaad, L. J. (1974). *Hydrogen Bonding*, Dekker, New York.

Jordan, J.W. (1949). "Organophilic bentonites I: Swelling in organic liquids," *J. Phys. Colloid Chem.*, **53**: 294-306.

Kjellander, R., Marcelja, S., Pashley, R. M., & Quirk, J. P. (1988). "Attractive double-layer interactions between calcium clay particles," *J. Chem. Phys.*, **92**, 6489-6492.

Labuz, J. F. & Biolzi, L. (1991). "Class I vs. Class II stability: a demonstration of size effect," *Int. J. Rock Mech. Min. Sci. & Geomech. Abstr.*, **28-2/3**, 199-205.

Lagaly, G., Witter, R., & Sander, H. (1983). In adsorption from solution (ed. R.H. Ottewill, C.H. Rochester, A.L. Smith), pp. 65-77,Academic Press, London.

Langhaar, H. L. (1962). Energy Methods in Applied Mechanics, John Wiley and Sons, Inc., New York.

Lee, J.F., Mortland, M.M., Chiou, C.T., & Boyd, S.A. (1989). "Shape selective adsorption of aromatic molecules from water by tetramethylammonium-smectite," *J. Chem. Soc. Faraday Trans. I.*, **85**:2953-2962.

Low, P. F. (1961). "Physical chemistry of clay-water interaction," *Advan. Agron.*, **13**, 323.

Lubetkin, S.D., Middleton, S. R., & Ottewill, R. H. (1984). "Some properties of clay-water dispersions," *Phil. Trans. R. Soc. Lond.*, **311**, 353-368.

Machado, C. F. (1997). Personal communication.

Mackenzie, R.C. (1965). Nomenclature sub-commitee of CIPEA, *Clay Min.*, **6**, 123.

Mackenzie, R.C. & Mitchell, B. D. (1966). "Clay mineralogy," Earth-Sci. Magazine, **2**, 47.

Maia, H. (1994). Personal communication.

Marshall, C.E. & Garcia, G. (1959). "Exchange equilibria in a carboxilic resin and in attapulgite clay," *J. Phys. Chem.*, **63**:1663-1668.

Martins, A. L., Soares, A. C., Sa, C. H. M., Rego, L. F. B. & Oliveira, J. E. (1996). "Drilling high-angle wells in unconsolidated sandstones and unstable shales," PROCAP 2000, Project #2, Final Report, Petrobras, Rio de Janeiro (in Portuguese).

Maury, V. (1997). Personal communication.

Maury, V. & Guenot, A. (1995). "Practical advantages of mud cooling systems for drilling," SPE Drilling & Completion, March, pp. 42-48.

Maury, V. & Idelovici, J. L. (1995). "Safe drilling of HP/HT wells, the role of the thermal regime in loss and gain phenomenon," SPE/IADC Drilling Conference, Amsterdam, 28 February-2 March, Paper SPE/IADC 29428.

McAtee, J.L., Jr. (1958). "Random interstratification in organophilic bentonite," *Natl. Acad. Sci.*, Publ. 566, pp. 308-317.

McBride, M.B., Pinnavaia, T. J., & Mortland, M. M. (1977). "Adsorption of aromatic molecules by clays in aqueous suspension," In: Fate of Pollutants

in the Air and Water Environments, part I, Vol. 8, I.H. Suffet, ed., Wiley, New York, 145-154.

McLean, M. R. & Addis, M. A. (1990). "Wellbore stability: the effect of strength criteria on mud weight rcommendations," 65th SPE Annual Technical Conference and Exhibition, New Orleans, Paper SPE 20405.

McMurchy, R.C. (1934). "Crystal structure of chlorites," *Z. Krist.*, **88**, 420-432.

Mese, A. (1995). "Effects of fluid saturation and stress state on the mechanical and chemical properties of shale," Ph.D. Dissertation, University of Texas at Austin.

Mitchell, R. F. & Allen, M. B. (1987). "Case studies of BHA vibration failure," 62nd SPE Annual Technical Conference and Exhibition, Dallas, September 27-30, Paper SPE 16675.

Mody, F. K. (1995). Personal communication.

Mody, F. K. & Hale, A. H. (1993). "A borehole stability model to couple the mechanics and chemistry of drilling fluid shale interaction", Paper SPE/IADC 25728, SPE/IADC Drilling Conference, Amsterdam, 23-25 Feb.

Mondshine, T. C. & Kercheville, J. D. (1966). "Successful gumbo shale drilling," *Oil Gas J.* (March 28), pp. 194-203.

Moore, D.M. & Hower, J. (1986). "Ordered interstratification of dehydrated and hydrated Na-smectite," *Clays and Clay Minerals*, **34**:379-384.

Nordstrom, D. K. & Munoz, J. L. (1994). *Geochemical thermodynamics*, Second ed., Blackwell Scientific Publications, Inc., Cambridge, Massachusetts, USA.

O'Brien, D. E. & Chenevert, M. E. (1973). "Stabilization of sensitive shales using inhibited potassium-based drilling fluids," *J. Petr. Tech.*, **25-9**, pp. 1089-1100.

Onaisi, A. Durand, C. & Audibert, A. (1994). "Role of hydration state of shales in borehole stability studies," Eurock'94, Proc., pp. 275-284, Balkema, Rotterdam.

Ong, S. H. (1994). "Borehole stability," Ph.D. Dissertation, School of Petroleum & Geological Engineering, The University of Oklahoma, Norman, Oklahoma.

Orowan, E. (1949). "Fracture and strength of solids," *Rep. Progr. Phys.*, **12**:185-232, The Physics Society, London.

Osisanya, S. O. & Chenevert, M. E. (1987). "Rigsite shale evaluation techniques for control of shale-related wellbore instability problems," Paper SPE/IADC 16054, SPE/IADC Drilling Conf., March 15-18, New Orleans.

Pashley, R. M. & Israelachvili, J. N. (1984). "DLVO and hydration forces between mica surfaces in Mg^{2+}, Ca^{2+}, Si^{2+}, and Ba^{2+} chloride solutions," *J. Colloid Interface Sci.*, **97**, 446-455.

Pusch, R. & Guven, N. (1990). "Electron microscopic examination of hydrothermally treated bentonite clay," *Engineering Geol.*, **28**, 303-314.

Quirk, J.P. (1968). "Particle interaction and soil swelling," *Israel Journal of Chemistry*, **6**:213-234.

Roegiers, J.-C. (1997). "Introduction to Rock Mechanics," in preparation.

Salisbury, D., Ramos, G. G. & Wilson, B. S. (1991). "Wellbore instability of shales using a downhole simulation test cell," In: Rock Mechanics as a Multidisciplinary Science, Roegiers (ed.), pp. 1015-1024, Balkema, Rotterdam.

Santarelli, F. J., Chenevert, M. E., & Osisanya, S. O. (1992). "On the permeability of shales and its consequences in terms of swelling and borehole stability," IADC/SPE Drilling Conference, New Orleans, Paper IADC/SPE 23886.

Santarelli, F. J. & Carminati, S. (1995). "Do shales swell? A critical review of available evidences," SPE/IADC Drilling Conference, Amsterdam, Paper SPE 29421.

Santos, H. (1989). "Inclined wellbore stability analisys", M.Sc. Thesis, Department of Civil Engineering, Pontifical Catholic University of Rio de Janeiro, Brazil (in Portuguese).

Santos, H. & da Fontoura, S. A. B. (1991). "Inclined wellbore stability analysis in anisotropic formations," Petrobras Research Center, Internal Report, June, Rio de Janeiro, Brazil (in Portuguese).

Santos, H., Rego, L. F. B. & da Fontoura, S. A. B. (1997). "Integrated study of shale stability in deepwater, Brazil," 5th Latin American and Caribbean Petroleum Engineering Conference, Rio de Janeiro, 30 August-03 September, Paper SPE 38961.

Schmidt, G. W. (1973). "Interstitial water composition and geochemistry of deep Gulf coast shales and sandstones", *American Association of Petroleum Geologists Bulletin*, **57(2)**: 321-337, Tulsa, OK.

Schmitt, L., Forsans, T. & Santarelli, F. J. (1994). "Shale testing and capillary phenomena", *Int. J. Rock Mech. Min. Sci. & Geochem. Abstr.*, **31**, pp. 411-427.

Sherwood, J. D. (1993). "Biot poroelasticity of chemically active shale," Proc. R. Soc. Lond. A., 440, 365-377.

Somerton, W. H. (1992). *Thermal properties and temperature-related behavior of rock/fluid systems*, Elsevier, NY.

Sostebo, E. F. & Horsrud, P. (1996). "Effects of brines on mechanical properties of shales under different test conditions," Proc. Eurock '96, Barla (ed.), Balkema, Rotterdam.

Steiger, R.P. (1981). "Fundamentals and use of potassium/polymer drilling fluids to minimize drilling and completion problems with hydratable clays," Paper SPE 10100.

Steiger, R. P. & Leung, P. K. (1991). "Consolidated undrained triaxial test procedure for shales," In: Rock Mechanics as a Multidisciplinary Science, Roegiers (ed.), pp. 637-646, Balkema, Rotterdam.

Steiger, R. P. (1993). "Advanced triaxial swelling tests on preserved shale cores," *Int. J. Rock Mech. Min. Sci. & Geomech. Abstr.*, **30:7**, 681-685.

Stokke, M. (1995). Personal communication.

Swindale, L.W. (1975). "Crystallography of kaolin minerals," In: Soil Components, vol. 2, p. 123., J.E. Gieseking ed., Spriger-Verlag, New York.

Tan, C. H., Richards, B. G. & Rahman, S. S. (1996). "Managing physico-chemical wellbore instability in shales with the chemical potential mechanism,", Asia Pacific Oil and Gas Conference, Adelaide, 28 October, Paper SPE 36971.

Tardy, Y. and Touret, O. (1987). "Hydration energies of smectites: a model for glauconite, illite and corrensite formation," In: Proc. Int. Clay Conf. Denver, L.G. Schultz, H. Van Olphen and H. Mumpton eds., The Clay Mineral Society, Bloomington, Indiana. pp. 46-52.

Todor, D. N. (1976). *Thermal analysis of minerals*. Tunbridge Wells, England: Abacus Press.

Touret, O., Pons, C-H., Tessier, D. and Tardy, Y. (1990). "Etude de la repartition de l'eau dans lesargiles saturee Mg^{2+} aux fortes teneurs en eau," *Clay Min.*, **25**, 217-233.

U.S. Salinity Laboratory Staff (1954). Diagnosis and improvement of saline and alkali soils. U.S. Departament of Agriculture Handbook 60.

van Oort, E., Hale, A. H., Mody, F. K. & Roy, S. (1994). "Critical parameters in modelling the chemical aspects of borehole stability in shales and in designing improved water- based shale drilling fluids," 69th Annual Technical Conference and Exhibition of the SPE, New Orleans, 25-28 Sept., paper SPE 28309.

van Oort, E., Hale, A.H. & Mody, F.K. (1996). "Transport in shales and the design of improved water-based shale drilling fluids", SPE Drilling & Completion, (Sept.), 137-146.

van Oort, E. (1997). "Physico-chemical stabilization of shales," SPE Int. Symposium on Oilfield Chemistry, Houston, Texas, 18-21 Feb., Paper SPE 37263.

Wada, K. (1959). "Oriented Penetration of Ionic Compounds between the Silicate Layers of Halloysite," *Am. Mineralogist*, **44**, 153-165.

Wang, Y. & Dusseault, M. B. (1995). "Response of a circular opening in a friable low-permeabilitymedium to temperature and pore pressure changes," *Int. J. Anal. Num. Meth. Geomech.*, **19**, 157-179.

Wang, Y., Papamichos, E., & Dusseault, M. B. (1996). "Thermal stresses and borehole stablity," In: Rock Mechanics Tools and Techniques, Proc. of 2nd North American Rock Mechanics Symposium, Montreal, 19-21 June, Aubertin, Hassani & Mitri (eds), Balkema, Rotterdam

Ward, C. D. & Andreassen, E. (1997). "Pressure while drilling data improves reservoir drilling performance," SPE/IADC Drilling Conference, Amsterdam, 4-6 March, Paper SPE/IADC 37588.

Wendlandt, W. WM. (1986). *Thermal analysis*. New York: John Wiley & Sons.

Weiss, A. (1963). "Organic derivatives of mica-type layer-silicates," *Angew. Chem.*, **2**:134-143.

White, D. & Cowan, C. T. (1958). "The sorption properties of dimethyldioctadecylammonium bentonite using gas chromatography," *Trans. Faraday Soc.*, **54**:557-561.

Yuan, Y. G., Abousleiman, Y., & Roegiers, J.-C. (1995). "Fluid penetration around a borehole under coupled hydro-electro-chemico-thermal potentials," 46th Annual Technical Meeting of The Petroleum Society of CIM, Banff, Alberta, May 14-17, Paper 95-72.

Zausa, F., Civolani, L., Brignoli, M. & Santarelli, F.J. (1997). "Real time wellbore stability analysis at the rig site," 1997 SPE/IADC Drilling Conf., Amsterdam, 4-6 March, Paper SPE/IADC 37670.

Appendix A

Structure of Clay Minerals - Literature Review

Introduction

This Appendix describes the structure of the most important clay minerals present in shales. Even though there are several clay minerals known, the ones that appear in significant amount in shaly rocks are: kaolinite, smectite, illite, and chlorite. The clay minerals are hydrous alumino-silicates and may broadly be defined as those minerals which dominantly make up the colloidal fraction of soils, sediments, and rocks. The term clay or clay fraction denotes a textural class of minerals with dimensions < 2 nm, which may consist of crystalline (ordered) and non-crystalline (disordered) parts. The majority of clay minerals belong to the class of layer silicates or phyllosilicates because their structural framework is basically made of layers containing silica and alumina sheets joined together and stacked on top of each other in a variety of ways. There is considerable variation in chemical and physical properties within this family of minerals, but most have in common platy morphology and perfect basal plane (001) cleavage, a consequence of their layered atomic

structures. The classification scheme for the phyllosilicates proposed by Mackenzie and Mitchell (1966) has been adopted instead of the one suggested by the Nomenclature Committee of the Clay Minerals Society because it seems more appropriate in characterizing clays in shales, clay-water interactions, and clay-polymer interactions. The scheme includes the pseudo-layer silicates, illite or hydromica, an important group as adsorbent of organic polymer, and halloysite, a disordered specie of kaolinites that adsorbs a water layer on the basal plane.

Structural Features

All layer silicates are constructed from two modular units: a sheet of corner-linked tetrahedra and a sheet of edge-linked octahedra.

Tetrahedral Sheets

The first unit is built of silica tetrahedrons. In each tetrahedron, a silicon atom is equidistant from four oxygens, or hydroxyls arranged in the form of a tetrahedron with the silicon atom at the center (Figure A.1 (a)). The tetrahedrons are arranged so that the tips of all of them point in the same direction, and the bases of all tetrahedrons are in the same plane (some of the tetrahedrons may be inverted). Each tetrahedron rests on a triangular face in the extending two-dimensional plane and shares the oxygens at all three corners with three other tetrahedra. The fourth, or apical, oxygen or the hydroxyl ion points upward in the direction normal to the base. Without

distortions, the silica tetrahedral groups are arranged to form a hexagonal network, which is repeated indefinitely to form a sheet of the composition $Si_4O_6(OH)_4$ (Figures A.1 (b) and A.2 (a)). However, in practice the arrangement of the surface oxygens of the silica sheet is more ditrigonal than hexagonal (Brindley, 1961). This is due to the opposed rotation of alternate silica tetrahedra which may be also slightly tilted with respect to the plane of oxygens (Figure A.2 (b)). The extent of rotation and tilting is influenced by the geometric fit between the tetrahedral and octahedral sheets, the amount and site of isomorphic substitution, and the nature of the charge-balancing cation. The Si-O bond distance is about 1.62 Å and the O-O distance is about 2.64 Å . The space available for the atom in tetrahedral coordination is about 0.55 Å and the thickness of the unit is 4.93 Å in clay mineral structures. The dominant cation in the tetrahedral sheet is Si^{4+} but substitution of Al^{3+} and Fe^{3+} are possible. The aluminum (Al) may replace up to half of the Si, and when it does the dimensions of the sheet increase because the Al-O distance is about 1.77 Å.

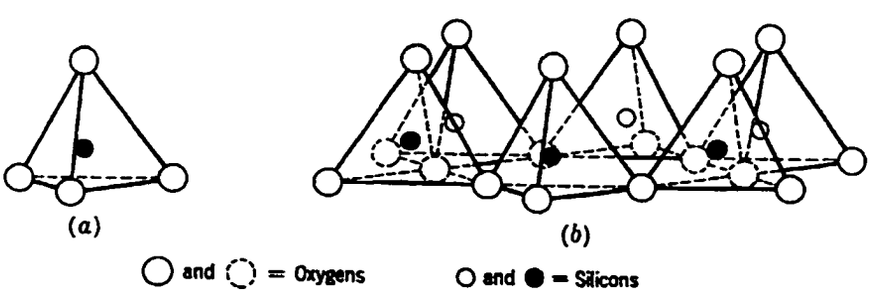


Figure A.1: Diagrammatic sketch showing (a) single silica tetrahedron and (b) the sheet structure of silica tetrahedrons arranged in an hexagonal network (Brindley, 1961).

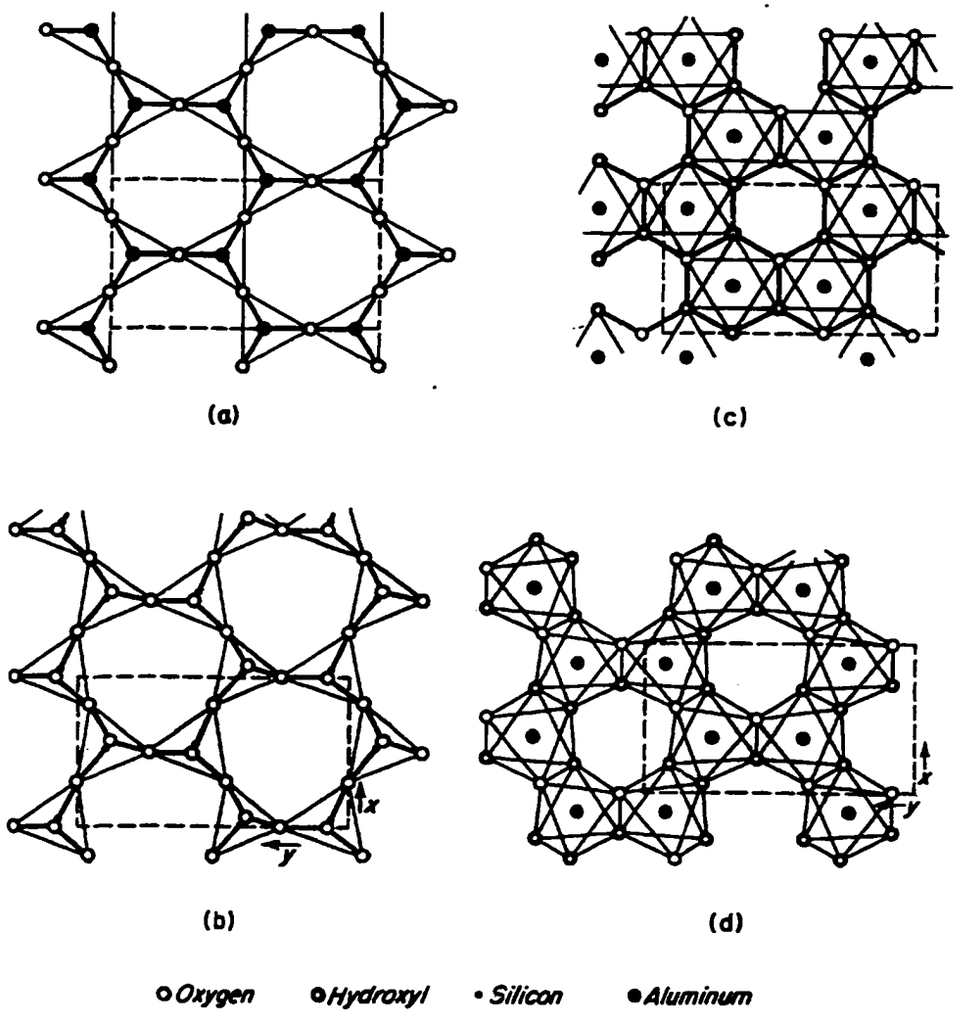


Figure A.2: Tetrahedral and octahedral configurations in kaolin minerals. Broken lines represent the unit-cell boundary (Brindley, 1961).

Octahedral Sheets

The octahedral sheet is made of two planes of closest-packed oxygen (or hydroxyl) ions with cations occupying the resulting octahedral sites between the two planes. An octahedron is formed by connecting the centers of the six

oxygen or hydroxyl ions packed around an octahedral cation site (Figure A.3 (a)). Connections from these to neighboring oxygen or hydroxyl ions form a sheet of edge-linked octahedra, extending in two dimensions (Figures A.3 (a) and (c)). Departure from the ideal symmetry takes the form of distortions, mainly in the form of a shortening of the shared edges of Al-O (OH) octahedrons (Figure A.2 (d)). The cations are usually Al^{3+}, Mg^{2+}, Fe^{2+}, or Fe^{3+}, but other transition elements and Li^{+} are possible. The O-O distance is 2.60 Å , OH-OH distance is about 3 Å and the space available for the atom in octahedral coordination is about 0.61 Å. The thickness of the unit is 5.05 Å in clay mineral structures.

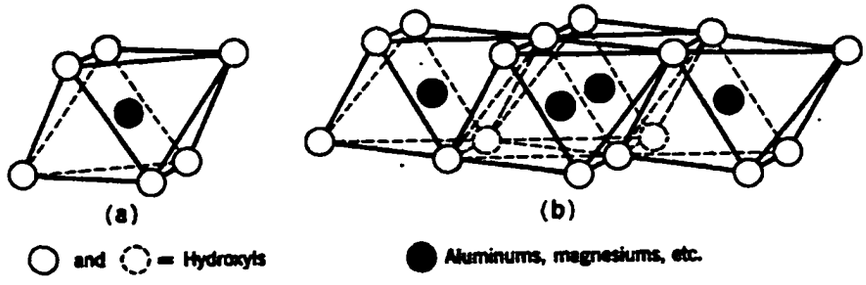


Figure A.3: Diagrammatic sketch showing (a) single octahedral unit and (b) the sheet structure of the octahedral unit.

Dioctahedral and Trioctahedral

In layer silicates, octahedral sheets are either gibbsite-like (i.e., $Al_2(OH)_6$) or brucite-like (i.e., $Mg_3(OH)_6$). In the brucite-like sheet the cation-to-anion ratio is 1:2. In a plane of closest-packed hydroxyls (Figure A.4), each

hydroxyl ion has six nearest neighbors making six "dimples" around each hydroxyl ion. When the next plane of closest-packed hydroxyls is fitted onto the top of this first plane of hydroxyls, the six dimples will become three octahedrally coordinated and three tetrahedrally coordinated cation sites. For the brucite-like sheet with divalent cations, all three octahedral sites around each hydroxyl must be filled to have electrical neutrality. Layer silicates with this arrangement are called *trioctahedral*. In layer silicates with gibbsite-like octahedral sheets, the cation-to-anion ratio in the sheet is 1:3. Only two Al^{3+} cations are needed instead of three Mg^{2+} ions to achieve electrical neutrality. Therefore only two of every three octahedral sites around each hydroxyl need to be filled. Layer silicates with this arrangement are called *dioctahedral*.

Joining the Tetrahedral and Octahedral sheets

The assemblage of one tetrahedral sheet and one octahedral sheet is called a 1:1 layer silicate structure. The apical oxygens of the tetrahedral replace two out of three of the hydroxyl ions in the lower plane of the octahedral sheet since the oxygen-to-oxygen or hydroxyl-to-hydroxyl ionic dimensions of the octahedral and tetrahedral sheets are approximately the same (Figure A.5). The remaining one-third of the hydroxyl ions are not replaced but fit into the ideal hexagonal pattern of the tetrahedral sheets, the middle of the hexagonal ring made by the apical oxygens of the tetrahedral sheet. A 2:1 layer silicate, one octahedral sheet sandwiched between two tetrahedral sheets, is formed by

inverting a tetrahedral sheet, bringing it down on top of the 1:1 layer in Figure A.5, and again replacing two-thirds of the hydroxyls with apical oxygen ions. The lateral dimensions of the tetrahedral sheet are usually larger than those of the octahedral sheet because the larger Al^{3+}, or sometimes Fe^{3+}, has been substituted for the smaller Si^{4+}.

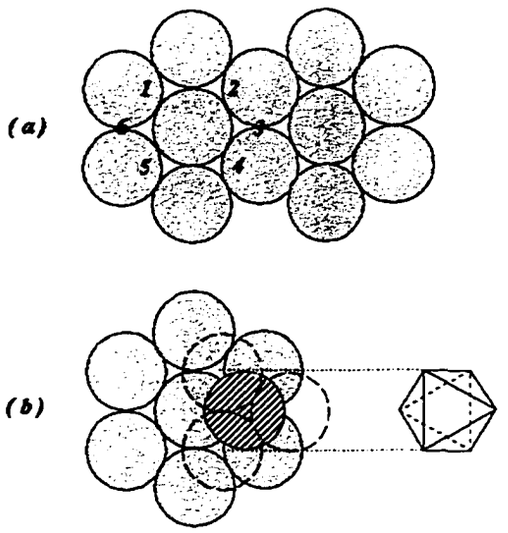


Figure A.4: Coordination in the octahedral sheet. (a) The six dimples in the plane of oxygen and hydroxyl ions make two sets of sites e.g., 1,3,5 (octahedral) and 2,4,6 (tetrahedral). (b) An octahedral site formed by cation in dimple 3 surrounded by six oxygens or hydroxyls, three above and three below.

Therefore, distortions or adjustments in one or both sheets occur whenever they combine at a common plane or junction. In trioctahedral sheets, distortion from the ideal results from the anion being pulled along the direction of three

shared edges toward the cation plane (Figure A.6). The result is a thinner sheet with larger lateral dimensions. In dioctahedral sheets, cations occupy only two of the three possible octahedral sites so that every third cation site is vacant (Figure A.7). Because of the repulsion between these cations, a pair of upper and lower anions between any two cations are drawn together to provide an electronic shield.

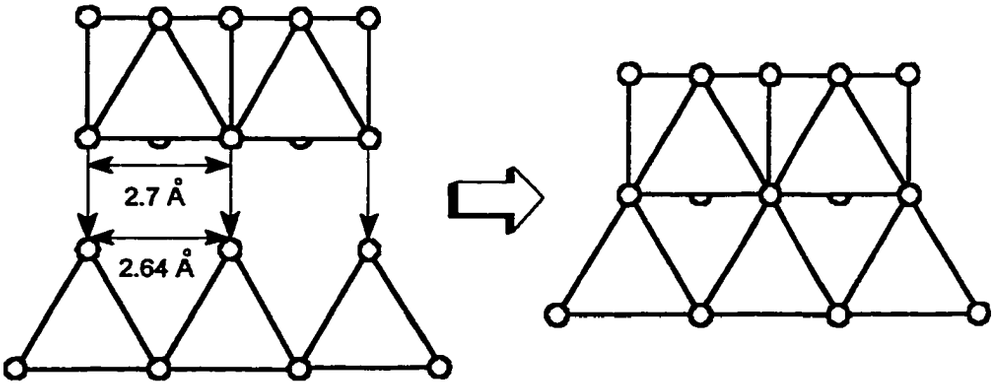


Figure A.5: Joining an octahedral sheet and a tetrahedral sheet into 1:1 layer silicate (general case).

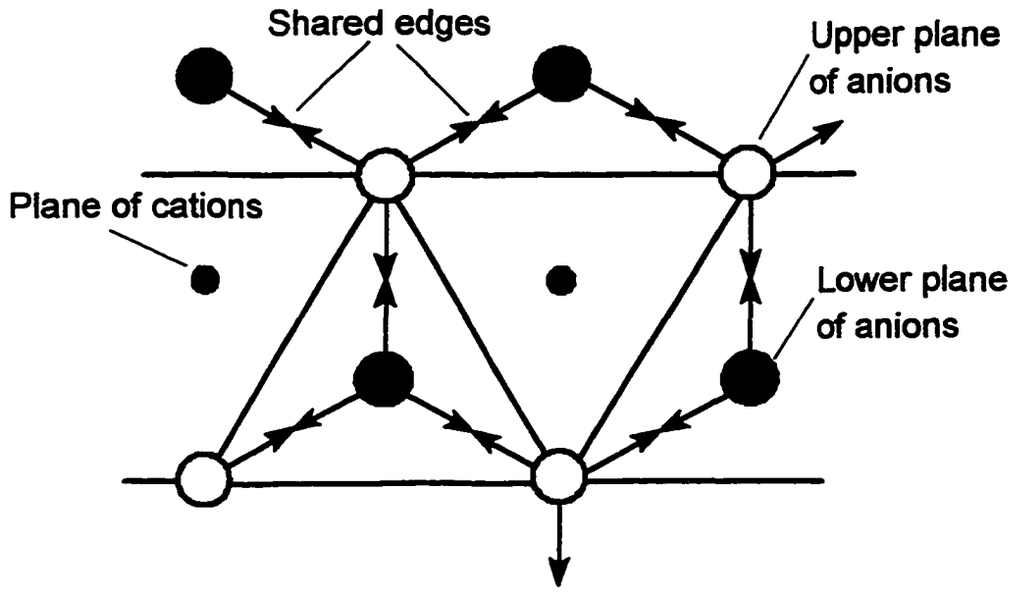


Figure A.6: Thinning of trioctahedral sheet.

This attraction produces the following distortions: (1) the upper and lower triangular faces of an octahedron rotate in opposite directions, the upper face rotates counterclockwise and is pulled downward, while the lower face rotates clockwise and is pulled upward (Figure A.7 (B) and (C)). The shared octahedral edges are shortened compared to unshared edges, (e.g., in kaolinite: OH-OH and O-OH ~ 2.5 Å compared to ~ 2.9 Å), (2) the six anions around a vacant site all move away from one another increasing the edge length of the octahedra around the vacant site from ~ 2.7 Å to ~ 3.3 Å . The combination of these distortions decreases the sheet thickness from that of an ideal sheet about 2.6 Å to 2.04 Å and increases somewhat the lateral dimensions.

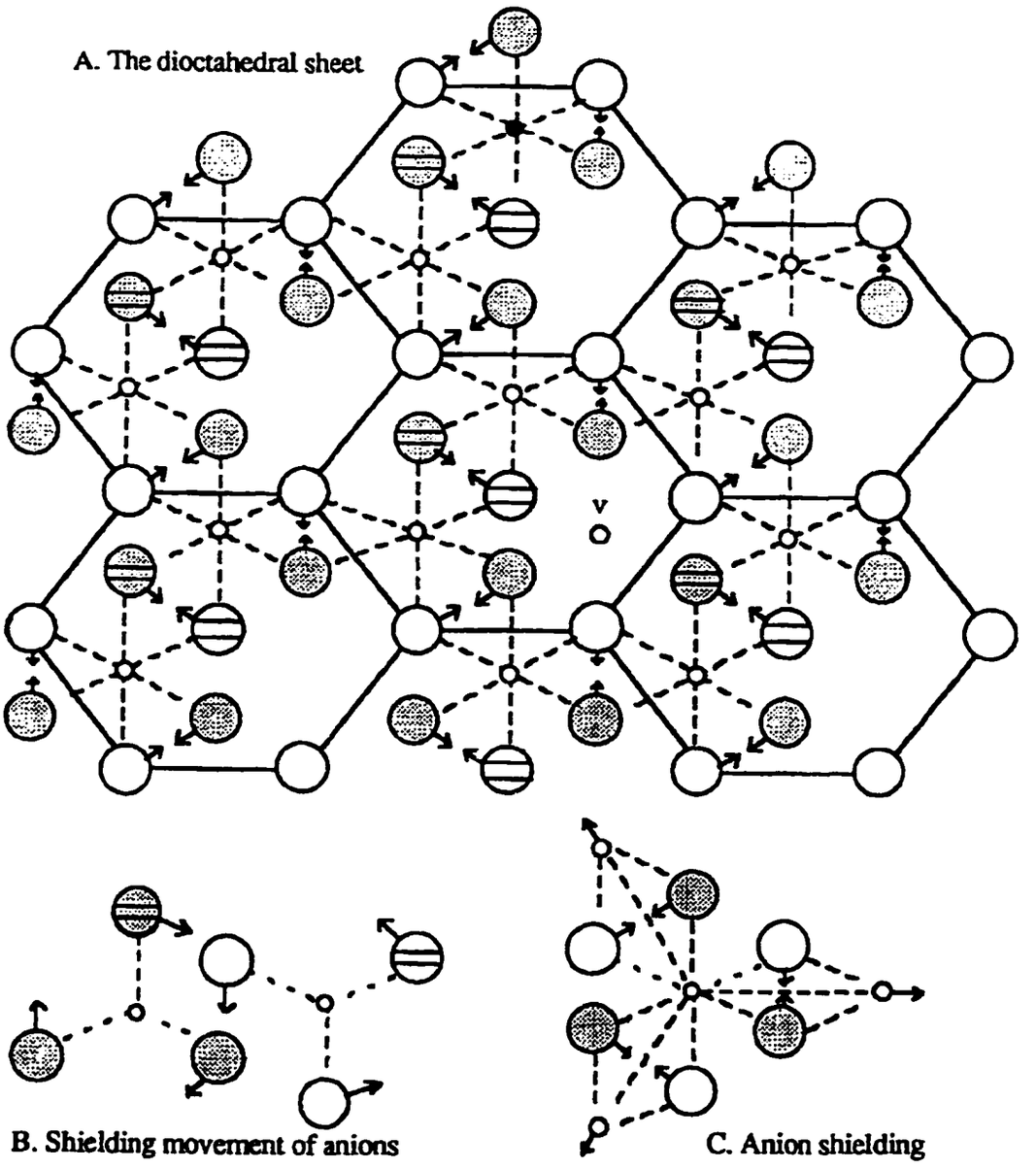


Figure A.7: Dioctahedral sheet showing ion shifts that occur to minimize cation-cation repulsion. Dark circles are anions in the basal octahedral layer, while light circles are anions in the upper octahedral layer. The ones with bars are hydroxyls. Small circles are aluminum cations and v marks a vacant octahedral site. B) Shielding movement of anions causes rotation of upper and lower layers in opposite directions around triad axis. C) Anion shielding shortens shared edges (Bailey, 1966).

Layer Charge

When the tetrahedral and octahedral sheets are assembled into layers, they may be electrically neutral or they may be negatively charged. Electrical neutrality exists if an octahedral sheet contains trivalent cations in two out of three octahedral sites, or divalent cations in all octahedral sites, combined with the tetrahedral sheets containing Si^{4+} in all tetrahedral sites. A net negative layer charge is formed if Al^{3+} is substituted for Si^{4+} in the tetrahedral sheet or Mg^{2+} is substituted for Al^{3+} in a dioctahedral sheet. The maximum layer charge for most 2:1 clay minerals is about 1.00 based on 4 tetrahedral cations and 10 oxygens. Neutrality is restored by having either single ions or ionic groups in the space between the layers called the interlayer-space. Potassium, as in muscovite and biotite, sodium, and calcium are the most common single cations. Complete and incomplete hydroxyl sheets occupy the interlayer space in chlorite and vermiculite. These sheets seem to be a consequence of hydrated, divalent cations that organize OH ions in the same configuration as the oxygen in a hydroxyl sheet. Ammonium ions, organic molecules, and water may enter this space also, and if the bonds are electrostatic they neutralize the negative charge on the silicate part of the clay mineral.

Classification

The majority of clay minerals belong to the class of phyllosilicates that are based on sheets with six-membered rings SiO_4 tetrahedra having the formula

Si_2O_5. The basic structures (Figure A.8) may be regarded essentially as formed by the condensation of sheets of SiO_4 tetrahedra with sheets of alumina or magnesia octahedra (as in gibbsite and brucite), and the major types are designated 1:1 (or diphormic), 2:1 (triphormic), and 2:2 or 2:1:1 (tetraphormic), depending on the ratio of tetrahedral to octahedral sheets in one repetitive layer. Thus, kaolinite (Figure A.8 (a)) belongs to the 1:1 type, montmorillonite (Figure A.8 (b)) and mica (Figure A.8 (c)) to the 2:1 type, and chlorites (Figure A.8 (d)) to the 2:1:1 type; palygorskite and sepiolite (Figure A.8 (e)) also have a basic 2:1 layer, although this is sharply limited in one direction with inversion of the sheet around an oxygen atom, resulting in a chainlike structure with channels along the fiber length.

Much isomorphous substitution occurs in some of these minerals, frequently leading (e.g., when Al^{+3} is replaced by Mg^{2+}) to a charge on the sheet surface satisfied by cations external to the layer, which may or may not be readily exchangeable with others from solution. The variation in the magnitude of the charge density on the sheet surface leads to minerals with different properties (e.g., as regards swelling in water or other polar liquids). Therefore, the charge should be considered as a principle in defining groups.

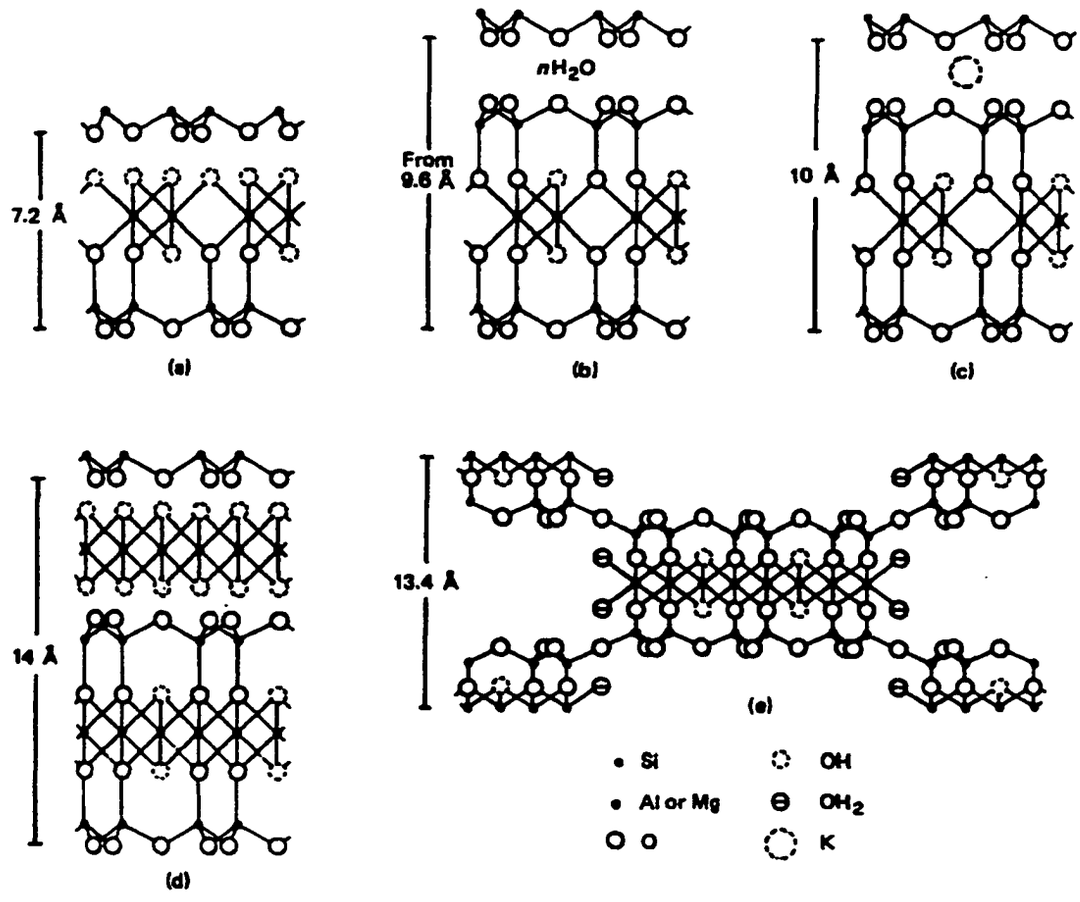


Figure A.8: Diagrammatic projections of the structure of clay minerals. (a) Kaolinite; (b) montmorillonite; (c) mica; (d) chlorite; (e) sepiolite (Mackenzie & Mitchell, 1966).

The electron charge per layer-unit-cell[1] in the 2:1 type varies from 0 to 4. At a charge of 0, there are no substitutions, no extraneous ions, and no swelling in polar liquids; at a charge of about 0.5 to 1, the cation-exchange capacity (CEC) is about 100meq/100g, and swelling in water is such that complete separation of layers can occur; at a charge of about 1 to 1.5, the

[1] In some minerals the unit cell comprises several layers, but it is convenient here to consider only one layer; hence the term layer-unit-cell. If charge per formula unit is employed, these values would be halved.

CEC is about 150meq/100g, and swelling is limited; at a charge of about 2 and higher, there is essentially no CEC (apart from some ions on exposed surfaces) and no swelling. It is generally undesirable to use external properties such as swelling for classification purposes (although this has been done in the past), but the use of fundamental attributes such as electron charge per layer-unit-cell is quite justifiable.

Having illustrated groups on such a basis, further subdivision is possible on the nature of the octahedral sheet. Thus, each group has two subgroups, depending upon whether only two out of three of the octahedral positions are occupied by, e.g., Al^{3+} (dioctahedral), or all octahedral positions are occupied by, e.g., Mg^{2+} (trioctahedral). Eventually, therefore, one arrives at species, which may be related either structurally or chemically. A classification scheme for the phyllosilicates based on six-membered rings of SiO^4, tetrahedra is given in Table A.1 (Mackenzie, 1965). Individual minerals might have formulas departing from those shown in Table A.1, but closely related to them, because of isomorphous substitutions.

Diek *et al.* (1996) present a more detailed description of each mineral group described in the above table. In this Appendix, only the most relevant clay minerals for shale stability purpose, kaolinite, illite, smectite, and chlorite are described.

Table A.1: Classification scheme for phyllosilicates with six-membered rings of SiO_4 tetrahedra (Mackenzie, 1965).

Type	Group x — electron charge/layer-unit-cell	Subgroup	Species	Ideal formula
2:1	Pryophyllite-talc $x \sim 0$	Pyrophyllites	Pyrophyllite	$Al_4Si_8O_{20}(OH)_4$
		Talcs	Talc	$Mg_6Si_8O_{20}(OH)_4$
			Minnesotaite	$(Fe, Mg)_6Si_8O_{20}(OH)_4$
	Montmorillonite-saponite $x \sim 0.5$–1	Montmorillonites	Montmorillonite	$0.67M^+ \cdot (Al_{2.33}Mg_{0.67})Si_8O_{20}(OH)_4$
			Beidellite	$0.67M^+ \cdot Al_4(Si_{7.33}Al_{0.67})O_{20}(OH)_4$
			Nontronite	$0.67M^+ \cdot Fe_4(Si_{7.33}Al_{0.67})O_{20}(OH)_4$
			Volkonskoite	$0.67M^+ \cdot (Fe, Cr, Al)_4(Si, Al)_8O_{20}(OH)_4$
		Saponites	Saponite	$0.67M^+ \cdot Mg_6(Si_{7.33}Al_{0.67})O_{20}(OH)_4$
			Sauconite	$0.67M^+ \cdot (Mg, Zn)_6(Si_{7.33}Al_{0.67})O_{20}(OH)_4$
			Hectorite	$0.67M^+ \cdot (Mg, Li)_6(Si, Al)_8O_{20}(OH)_4$
	Vermiculite $x \sim 1$–1.5	Dioctahedral vermiculites	Dioctahedral vermiculite	$1.73M^+ \cdot (Al, Fe, etc.)_4(Si, Al)_8O_{20}(OH)_4$
		Trioctahedral vermiculites	Vermiculite	$1.73M^+ \cdot (Mg, Fe, etc.)_6(Si, Al)_8O_{20}(OH)_4$
	Illite $x \sim 2$	Dioctahedral illites	Illite	$(K, H_3O)_2(Al, Fe, Mg)_4(Si, Al)_8O_{20}(OH)_4$
		Trioctahedral illites	Glauconite (?)	$(K, H_3O)_2(Fe, Al, Mg)_4(Si, Al)_8O_{20}(OH)_4$
			Ledikite	$(K, H_3O)_2(Mg, Fe, Al)_6(Si, Al)_8O_{20}(OH)_4$
	Mica $x \sim 2$	Dioctahedral micas	Muscovite	$K_2Al_4(Si_6Al_2)O_{20}(OH)_4$
			Paragonite	$Na_2Al_4(Si_6Al_2)O_{20}(OH)_4$
		Trioctahedral micas	Phlogopite	$K_2Mg_6(Si_6Al_2)O_{20}(OH)_4$
			Biotite	$K_2(Mg, Fe, Mn)_6(Si_6Al_2)O_{20}(OH)_4$
			Lepidolite	$K_2(Li, Al)_6(Si, Al)_8O_{20}(OH)_4$
			Zinnwaldite	$K_2(Li, Fe, Al)_6(Si, Al)_8O_{20}(OH)_4$
	Brittle mica $x \sim 4$	Dioctahedral brittle micas	Margarite	$Ca_2Al_4(Si_4Al_4)O_{20}(OH)_4$
		Trioctahedral brittle micas	Seybertite	$Ca_2(Mg_4Al_2)\,(Si_{2.5}Al_{5.5})O_{20}(OH)_4$
			Xanthophyllite	$Ca_2(Mg_4Al_2)\,(Si_{2.5}Al_{5.5})O_{20}(OH)_4$
2:1:1	Chlorite x variable	Dioctahedral chlorites	Sudoite	$Al_6(Si, Al)_8O_{20}(OH)_{16}$
		Trioctahedral chlorites		$(Mg, Fe, etc.)_{12}(Si, Al)_8O_{20}(OH)_{16}$
1:1	Kaolinite-serpentine $x \sim 0$	Kaolinites	Dickite	$Al_4Si_4O_{10}(OH)_8$
			Nacrite	$Al_4Si_4O_{10}(OH)_8$
			Kaolinite-Tc	$Al_4Si_4O_{10}(OH)_8$
			Kaolinite-Md	$Al_4Si_4O_{10}(OH)_8$
			Metahalloysite	$Al_4Si_4O_{10}(OH)_8$
			Halloysite	$Al_4Si_4O_{10}(OH)_8 \cdot 4H_2O$
			Anauxite (?)	$Al_4Si_6O_{14}(OH)_8$ (?)
		Serpentines	Antigorite	$Mg_6Si_4O_{10}(OH)_8$
			Chrysotile	$Mg_6Si_4O_{10}(OH)_8$
			Amesite	$(Mg, Fe)_4Al_2(Si_2Al_2)O_{10}(OH)_8$
			Cronstedtite	$Fe_3(Si_2Fe_2)O_{10}(OH)_8$
			Berthierine	$(Fe, Mg, Al)_6(Si_2Al)O_{10}(OH)_8$
2:1 Ribbon	Hormite $x \sim 0.2$	Mixoditrioctahedral hormites	Palygorskite	$(Al, Mg)_{2.5}Si_8O_{20}(OH)_2(H_2O)_4$
		Trioctahedral hormites	Sepiolite	$Mg_8Si_{12}O_{30}(OH)_4(H_2O)_4$
			Xylotile	$(Mg, Fe)_8Si_{12}O_{30}(OH)_4(H_2O)_4$

Kaolinite minerals

The chief minerals that occur in this group are kaolinite, dickite, nacrite, and halloysite (Brindley, 1961). There is little, if any, isomorphic substitution in the crystal lattice of these dioctahedral 1:1 layer type clay minerals. The dominant structural feature of these minerals appears to be from the regularly distributed cation site vacancies in the octahedral sheet and the distortions these vacancies create with respect to joining the octahedral and the tetrahedral sheets (Figure A.8 (a)). They differ from one another in the manner the layers are stacked. Kaolinite and the two halloysites are single-layer structures, whereas dickite and nacrite are double-layer polytypes, they contain two kaolinite layers each of 7 Å thickness (14 Å).

Kaolinite

The structure of kaolinite is composed of a single tetrahedral sheet and a single alumina octahedral sheet combined in a unit (7 Å in thickness) so that the tips of the silica tetrahedrons and one of the layers of the octahedral sheet form a common layer (Figure A.9). All the tips of the silica tetrahedrons point in the same direction and toward the center of the unit made of the silica and octahedral sheets. In the layer common to the octahedral and tetrahedral groups, two-thirds of the anions are shared by the silicons and aluminums, and they are oxygens instead of hydroxyls.

Only two-thirds of the possible positions for aluminum in the octahedral sheet are filled, and there are three possible plans of regular population of the octahedral layer with aluminums. The aluminum atoms are considered to be placed so that two aluminums are separated by a hydroxyl above and below, thus making a hexagonal distribution in a single plane in the center of the octahedral sheet. The hydroxyl groups are placed so that each hydroxyl is directly below the perforation of the hexagonal net of oxygens in the tetrahedral sheet. Departures from the ideal structure are consequences of repulsive and attractive forces between the ions within a single layer and in adjacent layers, adjustments because one-third of the octahedral cation sites are empty, the lack of fit between unrestrained octahedral and tetrahedral sheets, and the presence of hydrogen bonds between adjacent layers. The ideal structural formula is $Si_4Al_4O_{10}(OH)_8$. The charges within the structure are balanced, i.e., there are no charges on the lattice due to substitutions within the lattice. The charge imbalance is principally caused by broken bonds on the edges of the mineral, giving a net negative charge, but the CEC of kaolinite minerals is generally less than 15 meq/100g.

Because of the superposition of oxygen and hydroxyl planes in adjacent units, the units are held together fairly tightly by hydrogen bonding between the layers. The plane between the unit layers is a cleavage plane which is not as weak as in other clay minerals where opposing oxygen planes cannot tie with hydrogen bonds. Thus, the mineral is not dispersible in water into extremely small units. However, treatment of kaolinite with some organic

chemicals, e.g., formamide or dimethyl sulfoxide, will open up its structure, or cause it to swell (see Diek *et al.*, 1996 for more detail). Electron micrographs of kaolinite reveal that the mineral exist as plates usually with many hexagonal angles (Swindale, 1975). The maximum lateral dimensions of plate surfaces range from about 0.3 to 4 μm, and the thicknesses from 0.05 to <2 μm.

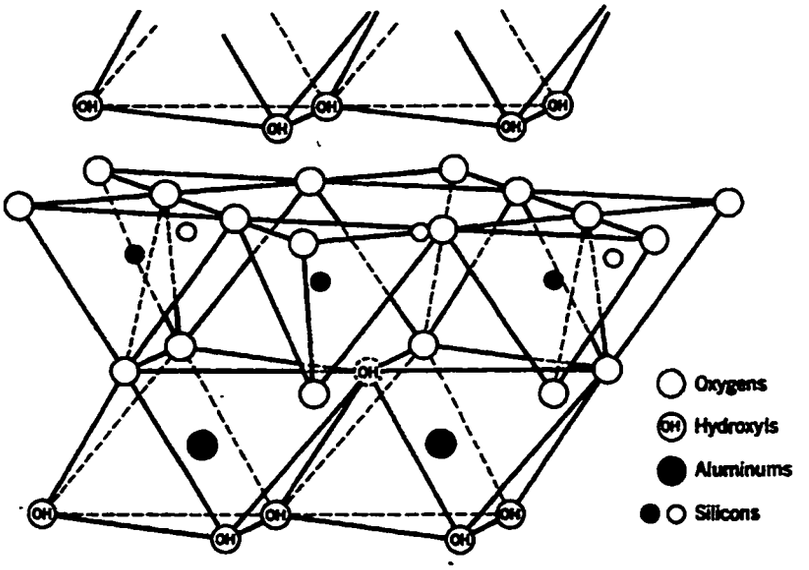


Figure A.9: Kaolinite layer structure (Gruner, 1932).

Halloysite

There are two forms of halloysite, one with a composition $Si_4Al_4O_{10}(OH)_8$ and the other with a composition $Si_4Al_4O_{10}(OH)_8.4H_2O$. The latter form has a layer of water about 2.9 Å thick between the 7 Å kaolinite layers, giving a 10 Å unit spacing. Figure A.10 shows arrangements of both kaolinite and halloysite

proposed by Hendricks (1938) and Bates *et al.* (1950). The CEC of the dehydrated form of halloysite is the same as for kaolinite, but the CEC of the hydrated form is about 10 to 40 meq/100g. According to Brindley (1961), the dehydration is irreversible, only partial dehydration takes place at low temperatures (60 to 75°C), and temperatures of the order of 400°C are necessary for complete removal of the interlayer water. Brindley (1980) suggested that halloysite is a highly disordered form of kaolinite, disordered enough to take water into the interlayer space. The interlayer water may be replaced by other polar molecules but not by more than a single layer of them. Halloysite minerals are made up of successive layers with the same structural composition as those composing kaolinite. The layers are stacked one above the other in the direction perpendicular to the sheets (*c*-axis direction) and are displaced randomly in both the *a*-and *b*-directions (lateral directions). Wada (1959) has shown that the mineral may interact with various salts causing variations in the c-direction and, therefore, indicating emplacement of salts in interlayer-water positions. The minerals have imperfect structures and occur as tubes, laths, and hollow prisms (Swindale, 1975).

According to Bates *et al.* (1950), the outside average diameter of the tubular particles of halloysite is 0.07 μm and the average wall thickness is about 0.02 μm. The tubes may range in length up to several microns. The ease of dispersion of the mineral mainly depends on the state of hydration. Partially dehydrated forms break down more easily into individual units than do the fully hydrated or the completely dehydrated form. In general, there are no

unsatisfied charges on the surface of halloysite particles; however, Bates (1959) found that few isomorphic substitutions may occur in hydrated halloysite, Al^{3+} and Fe^{3+} substitutions in the tetrahedra, and Mg^{2+} in the octahedra, giving rise to excess negative charges in the crystal that would contribute to the likelihood of disorder.

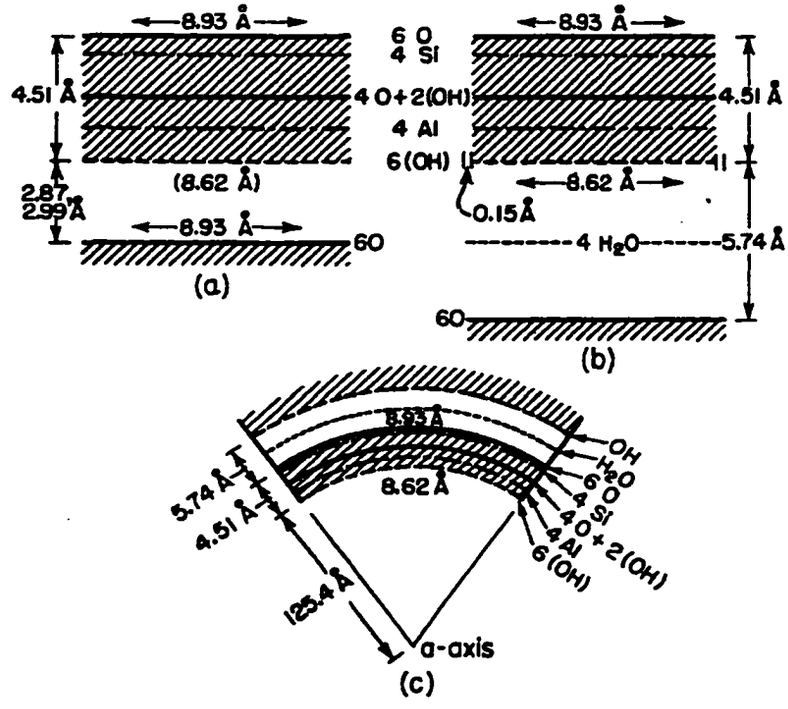


Figure A.10: Diagrammatic representation of the structure of kaolinite and halloysite $4H_2O$. (a) Arrangement of layers in kaolinite; (b) arrangement of layers in halloysite according to Hendricks (1938); (c) proposed arrangement of halloysite layers by Bates *et al.* (1950).

Smectite or Montmorillonite-Saponite Minerals

Smectite are composed of units made of two silica tetrahedral sheets with a central alumina octahedral sheet (Figure A.8 (b)). All the tips of the

tetrahedrons point in the same direction and toward the center of the unit. The tetrahedral and octahedral sheets are combined so that the tips of the tetrahedrons of each silica sheet and one of the hydroxyl layers of the octahedral sheet form a common layer. The atoms common to both the tetrahedral and octahedral layer are oxygens instead of hydroxyls. The layers are continuous in the *a*- and *b*-directions and are stacked one above the other in the *c*-direction. In the stacking of the silica-alumina-silica units, oxygen layers of each unit are adjacent to oxygens of the neighboring units with a consequence that there is a very weak bond and an excellent cleavage between them. An important feature of the smectite structure is that water and other polar molecules, such as certain organic molecules (i.e., ethylene glycol), can enter between the unit layers causing the lattice to expand in the *c*-direction. Unlike halloysite, interlayer sheets of polar molecules with many molecular layers thick may develop. The *c*-axis dimension of smectite varies from 9.6 Å, when no polar molecules are between the unit layers, to substantially complete separation in some cases. Exchangeable cations occur between the silicate layers, and the *c*-axis spacing of completely dehydrated smectite depends somewhat on the site of the interlayer cations, being greater the larger the cation. The thickness of the water layers between the silicate units also depends on the nature of the exchangeable cations at a given water-vapor pressure. Smectite with sodium as the exchangeable cation has discrete thicknesses of 9.6, 12.4, 15.2, 18 Å, where one molecular water layer is

approximately 2.8 Å in thickness. The CEC of smectite minerals varies between 80 and 150 meq/100g.

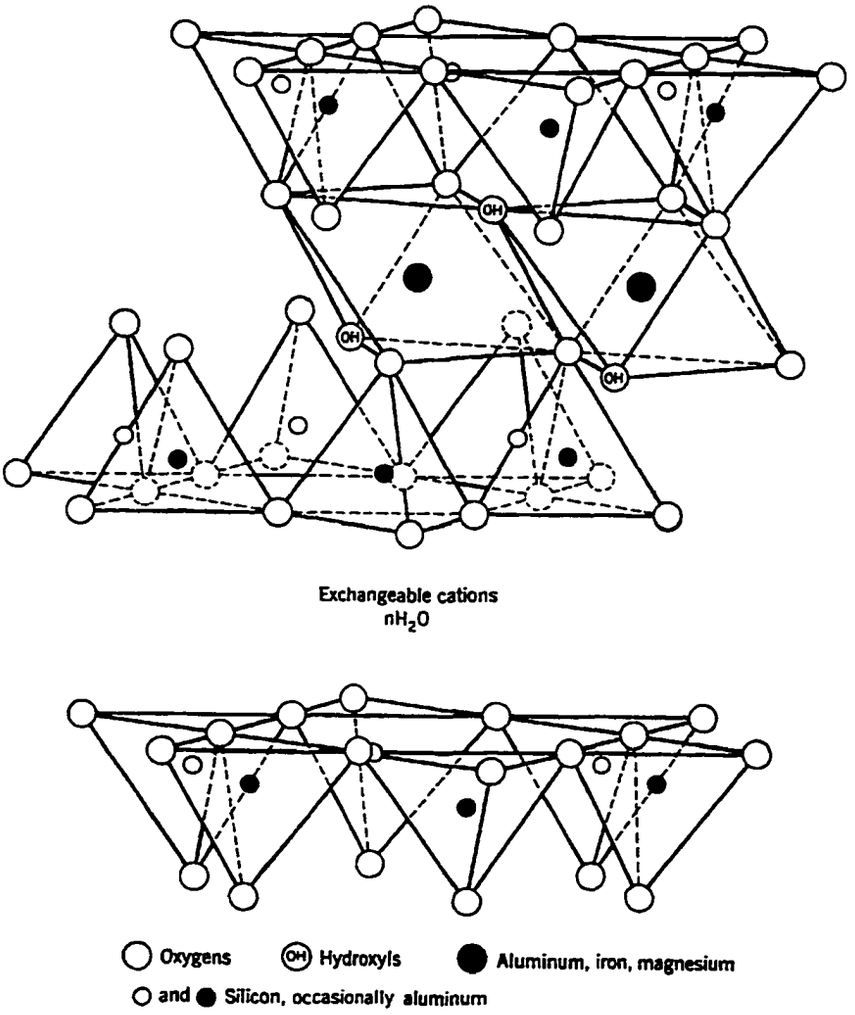


Figure A.11: Montmorillonite layer structure (Hendricks, 1942).

Smectite is found in dioctahedral and trioctahedral forms. Within the dioctahedral smectite group, montmorillonite (Figure A.11) has the origin of the layer charge primarily in the octahedral sheet due to the replacement of octahedral Al by Mg atoms. The ideal structural formula of a planar unit cell is

written as $[Si_8]^{IV}Al_{4-x}Mg_x]^{VI}O_{20}[OH]_4.R_x$ where IV and VI indicate tetrahedral and octahedral positions, respectively. The symbol R indicates the presence of compensator or exchange cations totaling x valences per cell. The charge x is generally between 0.5 and 0.9. Two other minor replacements are: Fe^{3+} replaces Al^{3+} and Fe^{+2} replaces Mg^{+2}. The other two dioctahedral smectite varieties are beidellite and nontronite in which the layer charge is the result of substitution primarily in the tetrahedral sheet: Al^{3+} replaces Si^{4+} in beidellite and Fe^{+3} replaces Al^{3+} in notronite. In trioctahedral smectites, hectorite resembles montmorillonite with dominantly octahedral substitution while saponite is a bit different than the other smectites in that it has a positive charge on the octahedral sheet that partially compensates for a large negative charge on the tetrahedral sheet.

Smectites tend to occur in equidimensional, extremely thin flake-shaped units. In some instances these units are elongate and are lath- or needle-shaped. Probably such elongate forms are due to substitutions within the lattice of ions of a size which does not easily fit into octahedral positions, thereby causing a directional strain on the lattice. Forms in which there is substantial substitution of iron and/or magnesium for aluminum possess this elongate form. Figure A.12 shows a transmission electron image of an ultra-thin section of typical smectite layers bifurcating, curling, and folding. A diagrammatic sketch of this texture in Figure A.13 illustrates interparticle pores (0.01-0.2 μm) and interaggregate pores (0.2 to several micrometers). The smectites are relatively readily dispersible in water down to extremely

small particle sizes. This seems to be particularly true when sodium is the exchangeable cation, in which case the particles may separate into units of about unit-cell thickness. The areal dimensions of the flakes are of the order of 100 to 1000 times the thickness of the flakes.

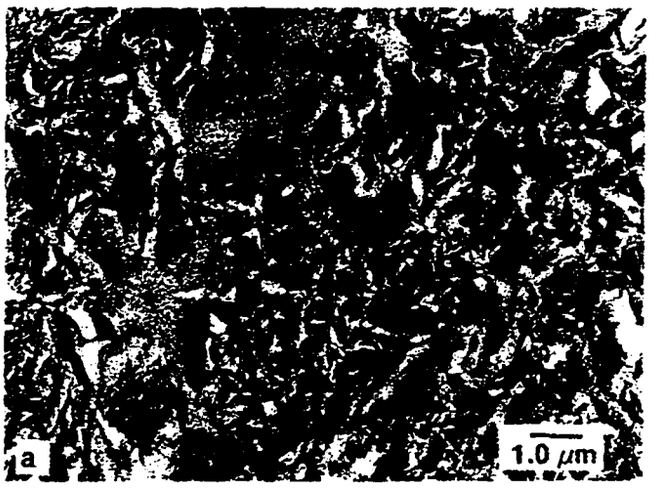


Figure A.12: Picture of an ultra-thin section of a smectite clay (Wyoming bentonite) showing stacks of smectite layers bifurcating, curling, and folding (Push & Guven, 1990).



Figure A.13: Sketch of Figure A.12 displaying interparticle and interaggregate pores in smectites (Push & Guven, 1990).

Illite Minerals

Illite minerals are clay-size mica minerals commonly found in argillaceous rocks (Grim *et al.*, 1951). The basic structural unit is a layer composed of two silica tetrahedral sheets with a central octahedral sheet. The tips of all the tetrahedrons in each silica sheet point toward the center of the unit and are combined with the octahedral sheet in a single layer with a suitable replacement of hydroxyls by oxygens. The unit is the same as that for montmorillonite except that some of the silicons are always replaced by aluminums, and the resultant charge deficiency is balanced by potassium ions (Figure A.8 (c)). In many of the well-crystallized micas one-fourth of the silicons are replaced by aluminums. The potassium ions occur between unit layers where they just fit into the hexagonal perforations in the surface of the oxygen layer. Adjacent layers are stacked in such a way that the potassium ion is equidistant from 12 oxygens, six of each layer (Figure A.14). The thickness of the silicate unit is approximately 10 Å.

The micas may be dioctahedral or trioctahedral, and there is considerable possible variation in the population of octahedral positions and also possible variations in the manner of stacking of the silicate layers above each other. Thus, muscovite is dioctahedral with a structural formula $(OH)_4K_2(Si_6Al_{12})Al_4O_{20}$, whereas biotite micas are trioctahedral with octahedral positions populated mostly by magnesium and iron. Illite minerals appear to differ from the well-crystallized micas in having relatively less

replacement of aluminum for silicon, less potassium, and some randomness in stacking of the silicate layers. Also, a small amount of water may be present between the silicate layers.

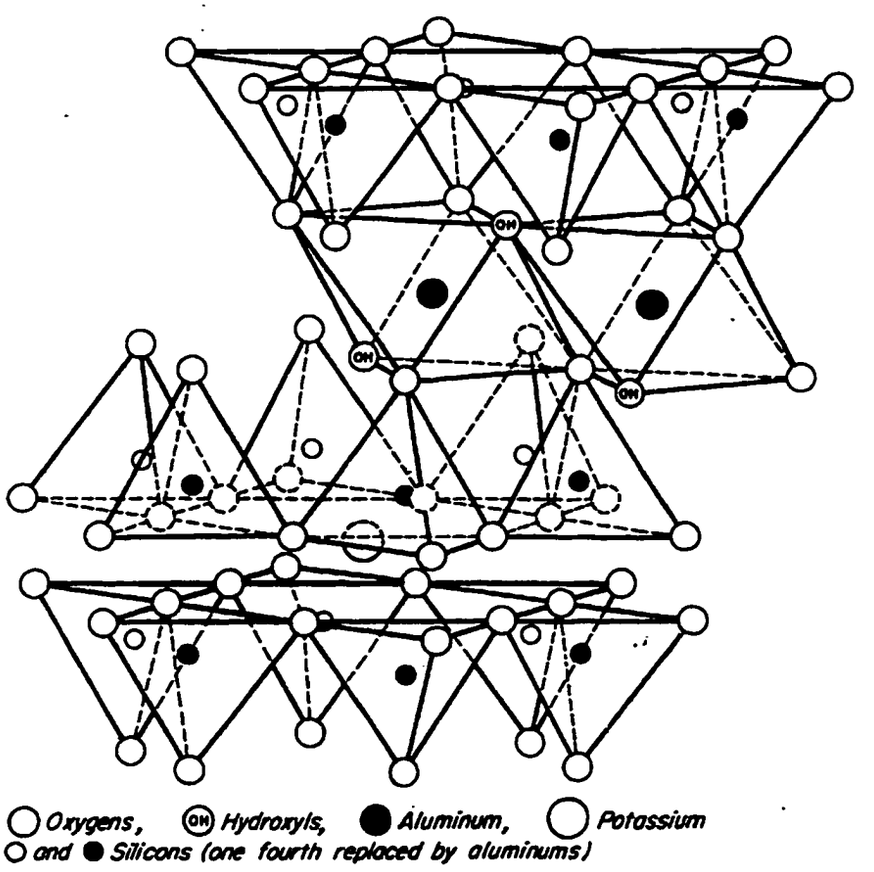


Figure A.14: Illite layer structure (Jackson & West, 1930).

The structure of illite differs from that of montmorillonite in several important ways. The charge deficiency due to substitutions per unit layer is about 1.30 to 1.50 for illite as compared with about 0.5 to 0.9 for montmorillonite. The seat of this charge deficiency in illite is largely in the silica sheet and therefore close to the surface of the unit layers, whereas in

montmorillonite it is frequently in the octahedral sheet at the center of the unit layer. Also, in the case of illite, the balancing cation between the unit layers is mainly potassium. Because of these differences the unit layers of the illite structure are relatively fixed in position, so that polar ions cannot enter between them and cause expansion. In addition, the interlayer balancing cations are not exchangeable except as they occur at the edges of the layers. The CEC of illite minerals varies between 20 and 40 meq/100g.

Electron micrographs of illite show generally small, poorly defined flakes commonly grouped in irregular aggregates without any distinct outline. Many of the flakes have a diameter of 0.1 to 0.3 μm, but larger particles up to several microns in diameter can occasionally be seen under the microscope in thin sections of illitic clays. When placed in water, the illite particles tend to disaggregate considerably in the poorly crystallized varieties and only slightly in the well-crystallized variety.

Chlorite Minerals

The structure of the true chlorites consists of alternate mica-like and brucite-like layers (Brindley & Robinson, 1951) as shown in Figure A.8 (d). The layers are continuous in the *a*-and *b*-dimensions and are stacked in the *c*-direction with basal cleavage between the layers Figure A.15. The mica-like layers are trioctahedral with the general composition $(Si.Al)_8(Mg.Fe)_6O_{20}(OH)_4$. The brucite-like layer has the general composition

$(Mg.Al)_6(OH)_{12}$. The mica layers are unbalanced by the substitution of Al^{3+} for Si^{4+}, and this deficiency of charge is balanced by an excess charge in the brucite sheet as a consequence of substitutions of Al^{3+} and Fe^{+3} for Mg^{2+}.

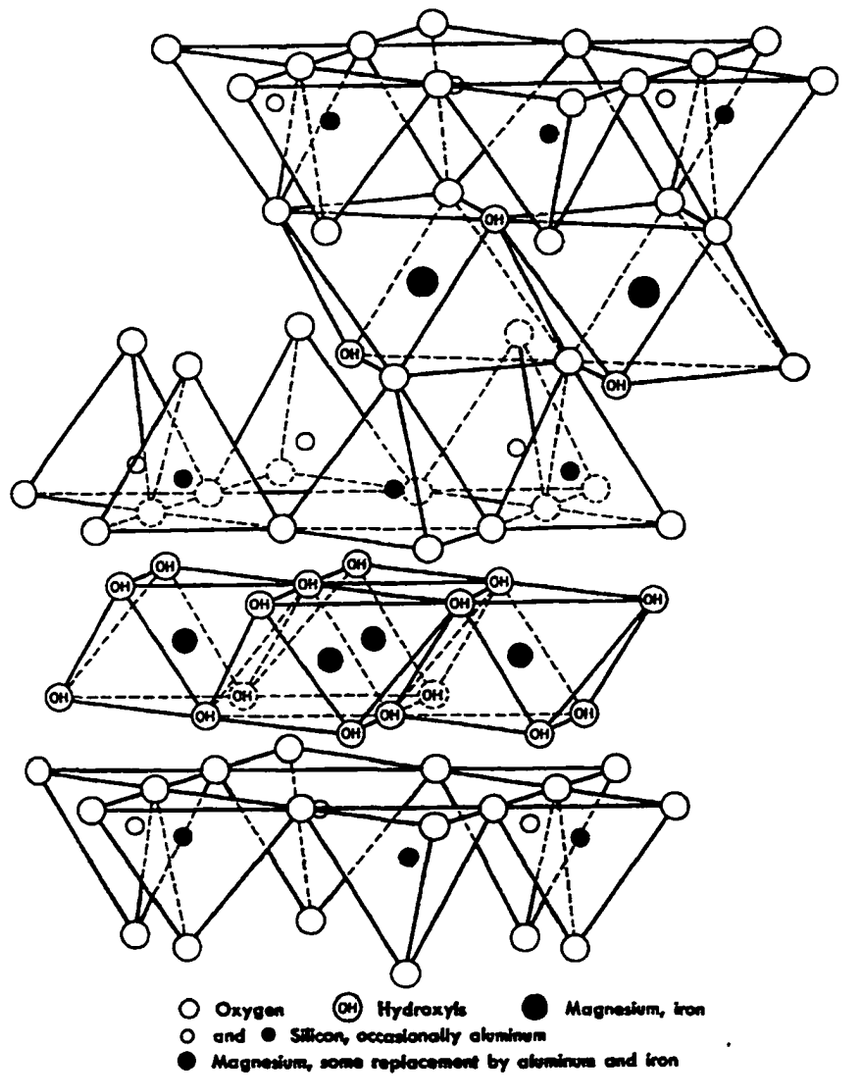


Figure A.15: Chlorite layer structure (McMurchy, 1934).

Because there is an overall electrostatic balance within the crystal the CEC only ranges between 10 to 40 meq/100g. The thickness of the layer consisting

of a mica and brucite sheet is 14 Å, which is just about twice that of kaolinite. Various members of the chlorite group differ from each other in the kind and amount of substitutions within the brucite layer and the tetrahedral and octahedral positions of the mica layer. They also differ in the detailed orientation of successive octahedral and tetrahedral layers, in the relation of the mica to the brucite layers, and in the stacking of successive chlorite units. Most clay mineral chlorites are trioctahedral in both octahedral sheets but some are dioctahedral.

Appendix B

Properties of Clay Minerals - Literature Review

Introduction

This Appendix presents three of the most important properties of clay minerals that are of interest for wellbore stability studies: (1) interaction with water, (2) cation exchange capacity (CEC), and (3) interaction with organic compounds. As in Appendix A, the focus is to present a literature review in order to help understanding the overall mechanisms of shale-fluid interaction. Because of their size clay minerals have a large ratio of surface area-to-volume. They have layer charges on (001) surfaces and charges from broken bonds on edges. An important consequence of these charges is that ions and molecules, water most commonly, are attracted to and held by clay mineral particles. In most cases, cations are attracted to the (001) surfaces, anions to the edges.

Interaction with Water

Although there is not a consensus, the water in shales can be generally divided into free water and bound water. Free water basically fills pores between clusters of accessory minerals (≥ 4 μm), between clay aggregates (interaggregate pores ≥ 1 μm; Touret *et al.*, 1990), and between clay particles within aggregates (interparticle pores 0.01-0.2 μm; Pusch & Guven, 1990). On the other hand, bound water fills the interlayer spacing within expandable clay particles. Clay particles composed of several unit layers can also contain internal lenticular pores up to 10 nm thickness as confirmed by scanning electron microscopy (Touret *et al.*, 1990). The most energetically bound water is associated with the exchangeable cations forming water-layer-complexes (Berend, 1991).

Many of the properties of clay minerals and other clay-size materials are related to water attached to edges and to basal planes (001) of clay minerals. This is because attached water is largely responsible for such characteristic properties of these materials as plasticity, nutrient-holding and nutrient-exchange capacities, as well as bonding, compaction, and suspension capabilities. In general, the amount of free water and bound water in clays depends on the clay type, texture (size and shape), and fabric (orientation and arrangement), the type and concentration of interlayer cations, temperature, and pressure. Temperature and salinity tend to decrease the amount of bound water. It should be noted that the bound water molecules are not completely

immobilized and they do exchange with free water, albeit more slowly (Israelachvili, 1991). Nevertheless, there is no general agreement concerning the mechanisms of water movement into or out of the interlayer.

On heating, free water in pores, and between particles or aggregates of the minerals composing clay materials is lost completely about 110°C. In the case of vermiculite, smectite, and the hydrated form of halloysite, the interlayer or bound water between the unit silicate layers of these minerals which causes their swelling and expansion characteristics is driven off by heating to about 250°C, but some remains up to 400°C (hydrated halloysite) at which slow loss of the crystalline or constitutional (OH) water begins. Smectites, however, present a two-stage dehydration; one stage occurs below 100°C, and the second depends on the cation present (Bish & Duffy, 1990); this water loss can only be separated and differentiated from the free water in the sample with TGA experiments. Rapid loss of (OH) water, herein called crystalline water, takes place at 550°C and is complete at about 750°C.

The amount of water adsorbed on clay surfaces for a given pressure and temperature depends on (Berend, 1991):

1) the adsorption energy of water molecules on the solid substrate, the first layer adsorbs with a higher energy than subsequent layers. Beyond the third layer, the adsorption energy is of the same order of magnitude as the condensation energy; and,

2) the density of water which increases with the number of adsorbed layers.

Structural Water

Structural Forces

Modern theories of surface forces (Derjaguin *et al.*, 1987; Israelachvili, 1991) have demonstrated that liquids confined within thin films can have properties that are both quantitatively and qualitatively different from their bulk properties. The molecules can structure into discrete layers whose properties vary with the number of layers, and such films may behave more like liquid crystals than normal liquid. The specific characteristics of thin films of water which delimit it from bulk water is restricted to relatively short surface separations up to 2 nm or even more depending on the nature of the clay surfaces and the interlayer ions.

In addition to van der Waals and electric double-layer forces, the surfaces sandwiching such a film of liquid experience oscillatory or monotonic structural (solvation or hydration) forces that originate from the difference in properties (e.g., density) between the film surface and the bulk liquid. The forces can be either repulsive (hydrophilic) or attractive (hydrophobic) or oscillating between attraction and repulsion. If the surface-liquid interaction is much more attractive than the liquid-liquid interaction, a dense packing of molecules at the surfaces develops. This leads to an overall repulsive force (Figure B.1, upper curve).

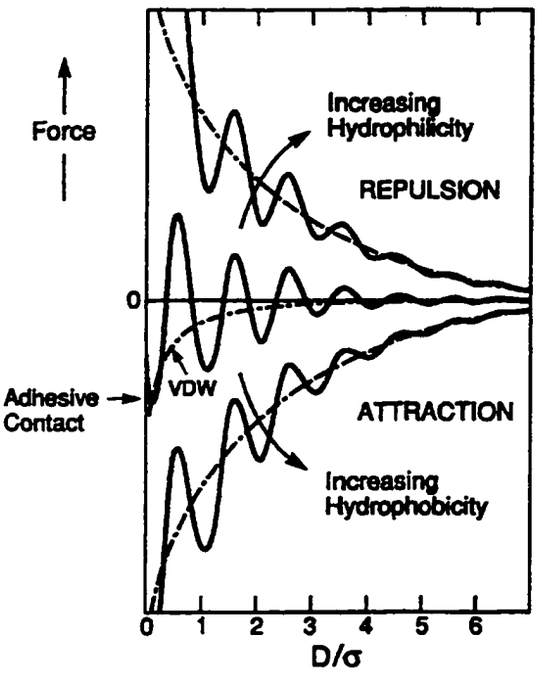


Figure B.1: van der Waals forces, and oscillatory and monotonic structural forces decaying with distance of separation D of clay surfaces per liquid molecular diameter σ (Israelachvili, 1991).

On the other hand, if the surface-liquid interaction is less attractive than the liquid-liquid interaction, an overall attractive force results (Figure B.1, lower curve). These forces comprise oscillatory short-range forces and monotonic long-range forces. However, if the liquid is water, the monotonic part arise from polarization and H-bond correlation interactions. Accordingly, water would come out of the interlayer space (surfaces coming together) if it were less dense than free water, or free water would move into the interlayer space (surfaces moving apart) if it would be more dense in the interlayer space.

Arrangement of Water Molecules between Silicate Layers

Hendricks & Jefferson (1938) have suggested a hypothetical arrangement of the interlayer water molecules adsorbed by hydrogen bondings to silicate sheets. A water layer is composed of water molecules joined into hexagons in an extended two-dimensional hexagonal lattice (Figure B.2).

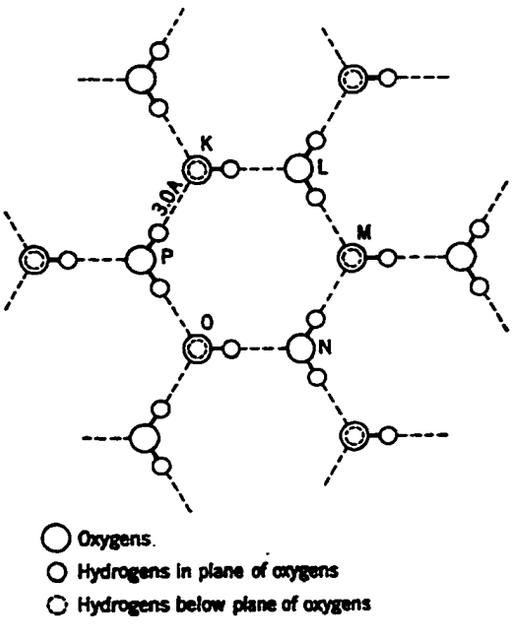


Figure B.2: Hypothetical arrangement of oxygens and hydrogens in layer of water molecules between clay mineral sheets. One hydrogen atom in each of the molecules K, M, and O is not involved in bonding within the net, but serves to join the net to oxygens of the neighboring silicate layer (Hendricks & Jefferson, 1938).

This arrangement was adopted in conjunction with the tetrahedral model of charge distribution within a water molecule in which two positive charges are centered on the two hydrogen atoms occupying two corners of the tetrahedron with the oxygen atom at its center and the two compensating negative charges

or pairs of unshared electrons on the other two corners. The oxygen atoms lie in the lattice plane, and each side of the hexagon represent a hydrogen bond, with the hydrogen of one water molecule being directed toward the negative charge of the neighboring molecule. One hydrogen atom in each of the water molecules K, M, and O (Figure B.2) is not involved in bonding within the lattice but serves to join the lattice to oxygens of the neighboring silicate sheet (Figure B.3).

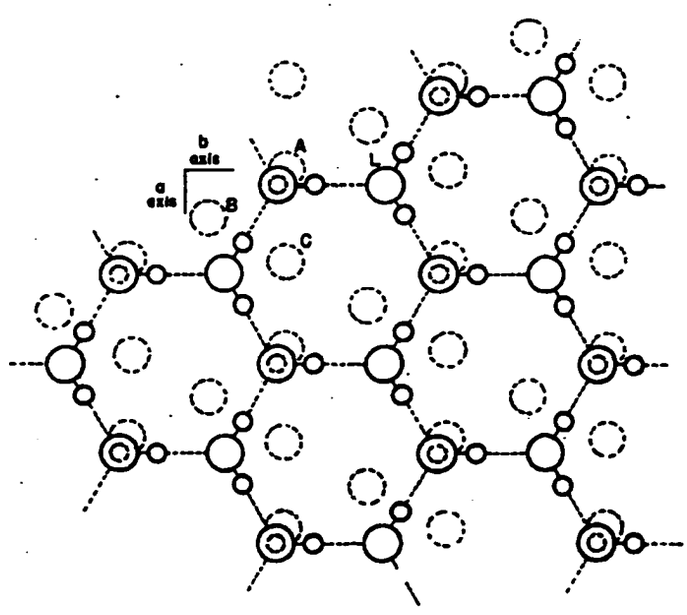


Figure B.3: Combination of water and vermiculite layers by binding through hydrogen. The oxygen atoms represented by large dotted circles are 2.73 Å below the plane of the water molecules (Hendricks & Jefferson, 1938).

Therefore, the water lattice is bound to the silicate sheet by hydrogen bonding of one-fourth of its hydrogen atoms with the clay oxygens. If the surface of the silicate sheet contains hydroxyl groups, part of the hydrogen of the hydroxyls are free to form hydrogen bonds with the oxygen atoms of the water layer.

Water molecules would be expected to form similar layers on the surfaces of clay minerals, and could be held in other layers (Figure B.4). It is for this structural reason that water is unique in many sorptive properties of the clays, such as swelling of montmorillonite. The hexagonal nets of water molecules are not complete and as a consequence hydrogen atoms are free for binding between the water layers. Even for complete layers there is probably some interlayer binding by hydrogen atoms of water molecules such as L of Figures B.2 and B.3. Water molecules of separate layers, therefore, might be expected to pack together, preserving tetrahedral coordination. A vermiculite containing only 8 water molecules in the unit of structure according to these concepts would have the schematic structure shown in Figure B.5. The energy of binding between the talc layers would be expected to be greater than that of completely hydrated vermiculite shown in Figure B.6, since there is the same number of bonds to each water molecule but more bonds between the water layers.

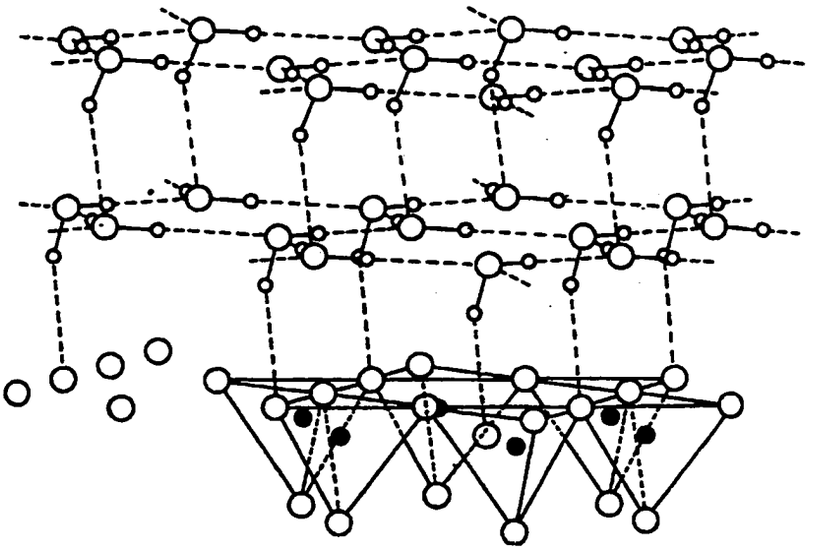


Figure B.4: Probable structure of multiple water layers on the surfaces of clays. Small black or shaded circles represent silicon atoms (Hendricks & Jefferson, 1938).

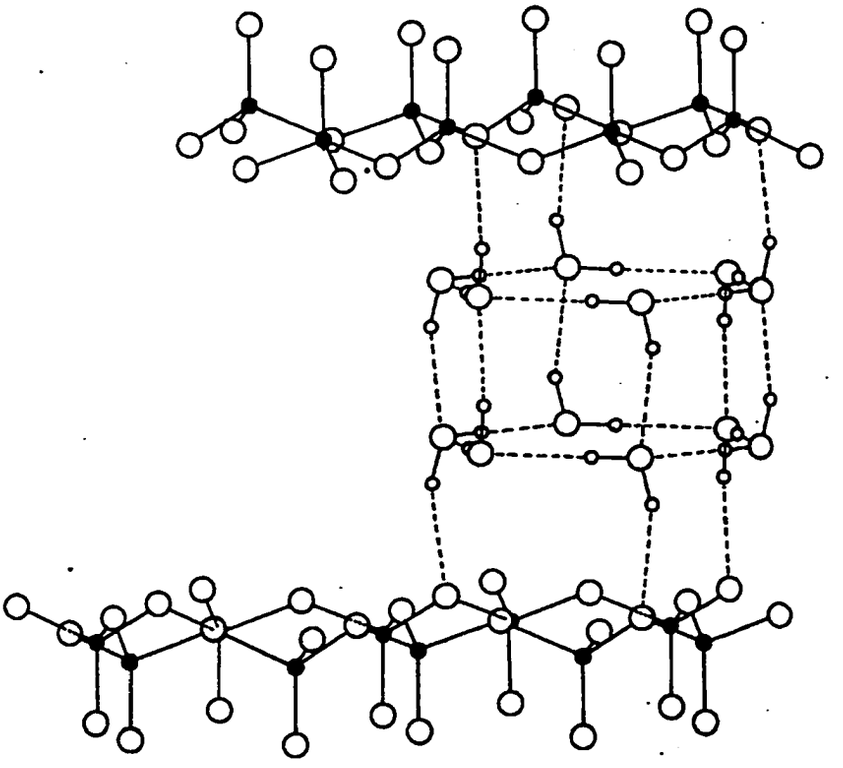


Figure B.5: Combined water layers in partially dehydrated vermiculite (Hendricks & Jefferson, 1938).

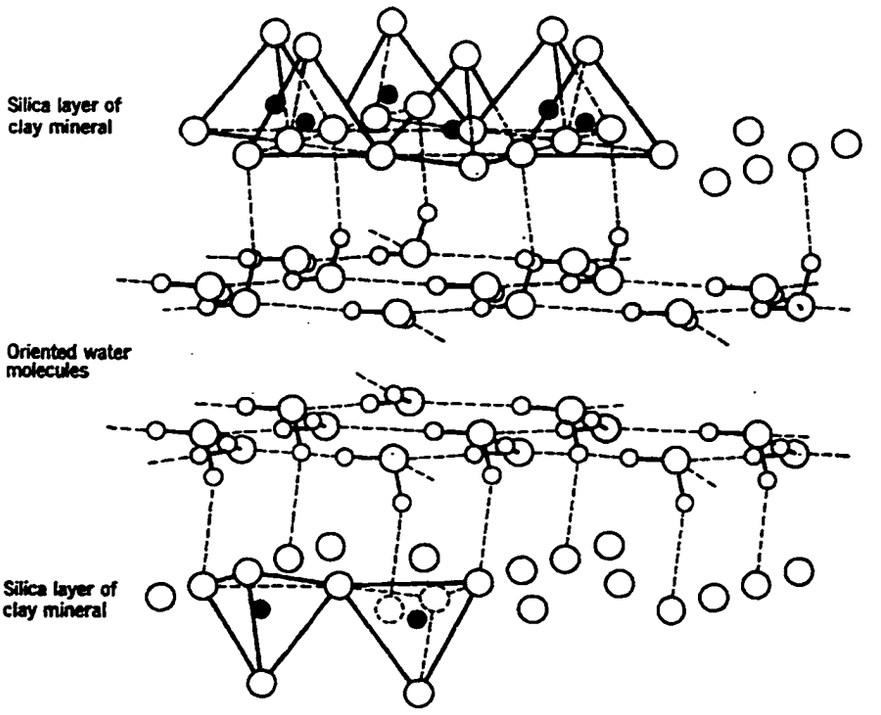


Figure B.6: Configuration of structured water bound to silicate sheets by hydrogen bondings (Hendricks & Jefferson, 1938).

Arrangement of Water Molecules in Hydrated Halloysite

Hydrated halloysite has been shown (Appendix A) to have the composition $Si_4Al_4O_{10}(OH)_8.4H_2O$ formed by superposition of two kaolinite layers $(OH)_4Si_2Al_2O_5$ and one layer of water molecules in between corresponding to four water molecules in the unit of structure. The arrangement of oxygen ions in one side of a kaolinite layer is the same as in the top of a talc layer; thus the structures shown in Figures B.2, B.3, and B.4 hold equally well for halloysite. The other side of a kaolin layer, however, contains only hydroxyl groups, and these in part are free for binding through hydrogen to oxygen atoms in the

water layer. The principle of the arrangement is that hydrogen atoms should be as far as possible from aluminum ions consistent with the requirements of binding to other hydroxyl groups (e.g., Figure B.7).

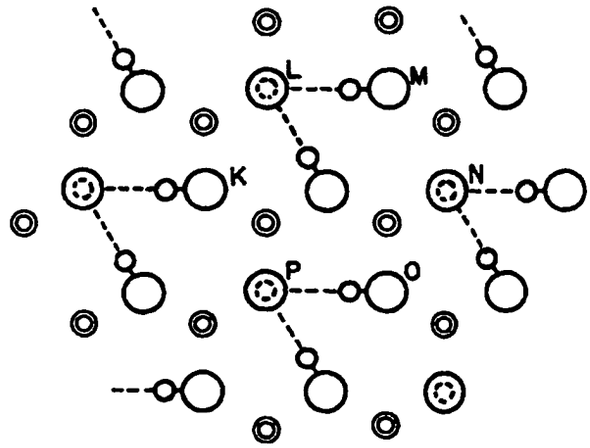


Figure B.7: Probable type of binding between hydroxyl groups in the kaolinite layers. Double circles represent aluminum atoms located about 1.1 Å above the plane of hydroxyl groups (Hendricks & Jefferson, 1938).

Hydrogen atoms of hydroxyl groups at L, N, and P of Figure B.7 are free for binding to oxygen atoms L, N, and P of water molecules in a layer of the type shown in Figure B.2. Each water molecule of the layer would be bound through hydrogen to four other oxygen atoms. The complete structure is schematically shown in Figure B.8.

Possibility of binding through the hydroxyl ions is apparently the factor that limits the water molecules to a single layer. If these are expelled by heating, the structure collapses to the ordinary type found for the kaolin minerals in which the hydroxyl groups give binding directly to oxygen ions of

the adjacent alumino-silicate layer. This structure would probably be more stable than that of the hydrate since the heat of formation of each hydroxyl bond would be expected to exceed that of a bond formed by hydrogen atoms of a water molecule, being more ionic in character. Ease of dehydration and failure of reversible hydration are thus quite reasonable.

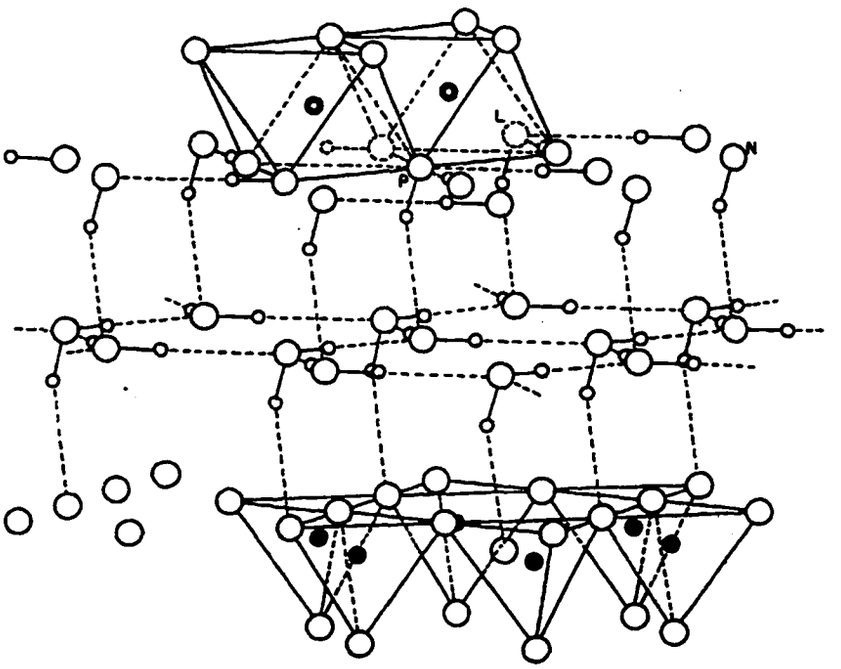


Figure B.8: Arrangement of a single layer of water molecules in hydrated halloysite (Hendricks & Jefferson, 1938).

Other Arrangements

Barshad (1949) suggested another arrangement of bound water on the basis of dehydration determinations. According to this author, at very low states of

hydration for montmorillonite, the water molecules tend to form tetrahedrons with the oxygens of the top layer of the linked silica tetrahedrons of the lattice. This type of packing would give rise to hexagonal rings of water molecules which are similar to the hexagonal rings of oxygens of the vertices of the linked silica tetrahedrons of the individual silicate sheets. In Figure B.9, *a* to *f* represent such water molecules forming tetrahedral units with oxygens of the underlying silica tetrahedral network. The packing in this configuration would be loose, as there would be only four molecules of water per unit cell per molecular layer. At higher states of hydration the water adsorbed by montmorillonite tends to form hexagonal rings of water molecules; these are similar to the hexagonal rings of the oxygens of the montmorillonite basal plane which forms the bases of the linked silica tetrahedrons.

In Figure B.9, 1 to 6 represent such water molecules. In this configuration the packing is more dense, and there are six molecules of water per unit cell per layer of water molecules. The height added for a single water layer would be about 2.55 Å, since the water molecules would be directly superimposed on the oxygens. At still higher states of hydration, it is believed that water molecules fill even the centers of these hexagonal water rings and the centers of the hexagonal oxygen rings of the linked silica tetrahedrons not occupied by exchangeable ions. Such water layers would consist of closely packed water molecules, and there would be eight water molecules per unit cell per molecular layer. Barshad (1949) stated that adsorption does not progress beyond the state of two molecular layers until dense packing is accomplished.

Furthermore, Mering (1946) suggested that, in Ca^{2+}-montmorillonite, the initially adsorbed water is packed octahedrally about Ca^{2+} and that, with increasing available water, a double water layer of superimposed water molecules first develops, followed by successive layers of superimposed water molecules; whereas in Na^{+}-montmorillonite, increasing amounts of water develop only successive layers of superimposed water molecules.

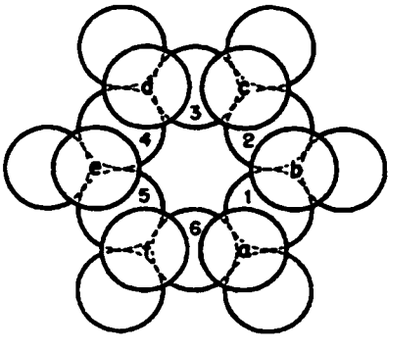


Figure B.9: Arrangement of the water molecules in the interlayer space of montmorillonite and vermiculite (Barshad, 1949).

In summary, there is a general agreement on the discreteness of water molecules between clay surfaces which imposes certain restrictions on surface separations due to packing constraints and to hydration of the cations and the surface groups. At short separations, these constraints reflect an oscillatory behavior of hydration or structural forces between the clay surfaces, as evident from the experimental curves obtained in direct measurements on mica plates in aqueous electrolyte solutions by Pashley & Israelachvili (1984). In general, in the interlayer space of expandable clay minerals, attached water tends to be

confined to two-dimensional structures, or sheets present in integral numbers 0, 1, 2, 3 ... as a function of relative humidity, i.e., the activity of water (Moore & Hower, 1986). However, the organization of water in the interlayer space is controlled by three factors: (1) the polar nature of the water molecule; (2) cation size, charge, and polarizability; and (3) the value and localization of the charge on the adjacent alumino-silicate layers.

Cation Exchange Capacity

Introduction

Especially in expandable clay minerals, cations may be exchanged when the clay minerals holding them come in contact with a solution rich in other cations. In the clay minerals in which cation exchange results from broken bonds, the exchangeable cations are held around the edges of the flakes and elongate units. In the clay minerals in which the exchange reaction is due to lattice substitutions, the cations are held mostly on the basal plane surfaces. In masses of clay with relatively small amounts of adsorbed water, i.e., with no more water than is required to develop plasticity, it is likely that the adsorbed cations are held directly in contact with, or at least very close to, the clay mineral surface. In clay-water systems in which the amount of water is at least greater than that required for the plastic state the exchangeable cations may be at greater distances from the clay mineral surfaces and separated from them by water molecules.

Exchangeable cations are important for at least three reasons: (1) they neutralize the layer charge; (2) they have a chemical influence on the organization of water molecules at the interface by restricting the amount of bound water or forming stable stoichiometric complexes with water depending on the type of cations; and (3) they have a physical influence on the intermolecular forces between clay surfaces (engineering properties and X-ray data for most clay minerals vary with the nature and number of the exchangeable cations).

Electric Charge

Two groups of mechanisms produce electric charges on clay mineral surfaces:

Isomorphous Substitution

When silicon atoms in a tetrahedral layer are substituted by aluminum atoms, or when aluminum atoms in an octahedral layer are replaced by magnesium or divalent iron atoms, the tetrahedral layer or the octahedral layer becomes negatively charged. This is called *isomorphous substitution*. Silicon and aluminum atoms have positive valences of 4 and 3, respectively, while magnesium and divalent iron have positive valences of 2. Each substitution leads to one negative elementary charge (1.6×10^{-19} C) in the layer. The distribution of cations in the interlayer space is probably controlled by the distribution of charges on the adjacent silicate layers that they neutralize. When there is Al^{3+} substituted for Si^{4+} in some of the tetrahedra, and the Al^{3+}

may be regularly or irregularly distributed, those pseudohexagonal holes with more Al^{3+} substituted tetrahedra around them are preferred spots for the location of cations (see Appendix A, Figure A.1).

Charge from Broken Bonds

Broken bonds around the edges of the silica-alumina units would give rise to unsatisfied charges which could be balanced by adsorbed cations. In kaolinite, halloysite, illite and chlorite minerals broken bonds are an important cause of exchange capacity. In montmorillonites and vermiculites broken bonds are responsible for a relatively small portion (20 per cent) of the cation-exchange capacity. The broken bonds at the edges could be between oxygen and silicon atoms, between oxygen and aluminum atoms, and between hydroxyl and aluminum atoms:

$$Si]-O^{-},\begin{matrix}Si]\\Al]\end{matrix}\rangle O^{\frac{1}{2}},Al]-O^{\frac{1}{2}},Al]-(OH)^{\frac{1}{2}}$$

The charges on these oxygens and hydroxyls depend on the pH of the outer solution. The reactions are represented by:

$$\begin{matrix} Si \\ Al \end{matrix}\Big\rangle O^{\frac{1}{2}-} + H^+ \rightarrow \begin{matrix} Si \\ Al \end{matrix}\Big\rangle O^{\frac{1}{2}+}$$

$$Si]-O^- + H^+ \rightarrow Si]-OH$$

$$Al]-O^{\frac{1}{2}-} + H^+ \rightarrow Al]-(OH)^{\frac{1}{2}+}$$

$$Al]-(OH)^{\frac{1}{2}-} + H^+ \rightarrow Al]-(OH_2)^{\frac{1}{2}+}$$

$$\begin{matrix} Si \\ Al \end{matrix}\Big\rangle (OH)^{\frac{1}{2}+} + OH^- \rightarrow \begin{matrix} Si \\ Al \end{matrix}\Big\rangle O^{\frac{1}{2}-} + H_2O$$

$$Si]-OH + OH^- \rightarrow Si]-O^- + H_2O$$

$$Al]-(OH)^{\frac{1}{2}+} + OH^- \rightarrow Al]-O^{\frac{1}{2}-} + H_2O$$

$$Al]-(OH_2)^{\frac{1}{2}+} + OH^- \rightarrow Al]-(OH)^{\frac{1}{2}-} + H_2O$$

As the pH of the outer solution decreases (i.e., as the hydrogen ion concentration of the outer solution increases), the reactions on the left are dominant. Consequently, the positive charges due to broken bonds increase as the pH decreases. As the pH of the outer solution increases, the reactions on the right are dominant and the negative charges due to broken bonds increase. At a certain pH, the amount of positive charge becomes equal to the negative charge. This value of pH is called the isoelectric point. Iimura (1966) shows the dependence of the charge of an alumina-silica gel on the pH of the outer solution. The isoelectric points of alumina gel and silica gel are pH 5.0 and 7.0, respectively.

Both kaolinite and montmorillonite possess charges due to isomorphous substitution and to broken bonds. As the ratio of isomorphous substitution to total charge is generally low in kaolinite, the charge of kaolinite depends

strongly on the pH of the outer solution. Measuring the amount of cations freed and replaced by others is a measure of both the negative charge on a layer and the cation exchange capacity (CEC). For expandable clay minerals, there is a linear increase in CEC with increasing layer charge. It is measured in mili-equivalents per gram (or per 100g) of dry sample. In general, the amount of net charge of a clay mineral is obtained by subtracting the anion exchange capacity (AEC) from the cation exchange capacity (CEC).

Chemical Influence

The cations adsorbed on the surface of the clay minerals may affect the adsorbed water as follows: (1) they may serve as a bond to hold the clay mineral particles together or to limit the distance to which they can be separated; (2) they may become hydrated and alter the configuration of adjacent adsorbed water molecules. Order is enhanced on the interface with the increase of cation charge. The more localized charge deficit in tetrahedral position induces stronger bonds and consequently better order than in the octahedral position. The cation size, polarizability, hydration state and charge dictate the organization at clay surfaces:

(a) K^+ cations which are large in size (bare ion radius 0.133 nm) and less hydrated (hydrated radius 0.33 nm) hold the clay unit layers tightly together dictating an ordered structure;

(b) Mg^{2+} having a small bare ion radius (0.065 nm) but strong polarizability (hydrated radius 0.43 nm), tends to form compact octahedral water-complexes held by hydrogen bonding to the surface oxygens of the silicate layers;

(c) Ca^{2+} and Na^{+} cations having larger bare ion radii (0.099 nm and 0.095 nm) than Mg^{2+} but lower polarizability (hydrated radii 0.41 and 0.36 nm) form less compact hydrated complexes.

In 1987, Tardy and Touret showed that less hydrated cations are favored when water activity decreases.

Cation Exchange Reaction

Many different equations have been proposed to model cation exchange reactions. Common features of these models are that they assume that the mineral surface has a constant total CEC at a given pH and that the exchange reaction is considered to be stoichiometric and reversible. The most general type of reaction model is the ***mass action equation***, which describes Ca^{2+}-Na^{+} exchange as follows (Bohn *et al.*, 1979):

$$CaX + 2Na^{+} \leftrightarrow 2NaX + Ca^{2+} \qquad \text{(B.1)}$$

where X represents the exchange phase of the cation. The equilibrium reaction coefficient for the reaction in (B.1) is therefore

$$K_k = \frac{(NaX)^2(Ca^{2+})}{(CaX)(Na^{+})^2} \qquad \text{(B.2)}$$

where the brackets ( ) denotes activity. All cation exchange models are limited by the fact that there are no models or measurements that characterize the activity of the adsorbed phases exactly. As an approximation, the activities in (B.2) are frequently replaced by concentrations. This approximate representation is called a Kerr model and may be reasonably valid over narrow concentration ranges. However, the reaction coefficient varies substantially over the entire range of cation concentration in the exchange phase (Marshall & Garcia, 1959). A modified mass action equation was developed by Gapon in 1933, who expressed the exchange reaction in terms of chemically equivalent quantities both for colloid exchange sites and exchanging cations and used concentrations in place of activities for soluble ions. The Gapon equation is written as

$$\frac{[NaX]}{[Ca_{1/2}X]} = K_G \frac{[Na^+]}{[Ca^{2+}]^{1/2}} \tag{B.3}$$

where exchangeable-cation concentration are in meq/g and soluble-cation concentrations are in mole/liter. The Gapon equation (B.3) corresponds to a mass action equation of the form:

$$Ca_{1/2}X + Na^+ \leftrightarrow NaX + \frac{1}{2}Ca^{2+} \tag{B.4}$$

It is inaccurate over large ranges of exchange concentrations, but it is reasonably accurate within important ranges of sodium exchange concentration (U.S. Salinity Laboratory Staff, 1954).

Ericksson (1952) developed an ion-exchange equation based on the electric double layer theory. He considered a system in which the colloidal phase is made up of negatively charged platelike clay particles in equilibrium with a solution of monovalent and divalent cations. The charge fraction of the monovalent ions to total ions in the double layer is written by Bolt (1955) as follows:

$$\frac{\Gamma_1}{\Gamma} = \frac{c_1 c_2^{-1/2}}{\Gamma\sqrt{\beta}} \sinh^{-1}\left(\frac{\Gamma\sqrt{\beta}}{c_1 c_2^{-1/2} + 4\sqrt{c_2}\cosh(e\phi_m / \kappa T)}\right) \tag{B.5}$$

where Γ is the surface charge density (meq/cm^2), Γ_1 is the portion of the surface charge neutralized by the monovalent cation, c_1 and c_2 are the concentrations of the monovalent and divalent cations in the bulk solution, ϕ_m is the electric potential at the midway plane between two surfaces, e is the electronic charge[1], k is Boltzmann constant, T is the absolute temperature, and

$$\beta = \frac{8000\pi F}{\varepsilon RT} \tag{B.6}$$

[1] e= 4.8 x 10^{-10} esu (CGS units) ≡ 1.6 x 10^{-19} C (SI units).

where F =2.892 x 10^{11} esu/meq, ε is the dielectric constant of the medium, and R is the universal gas constant. Equation (B.5) gives the fraction of the surface charge neutralized by the monovalent electrolyte and may therefore be considered an ion-exchange equation. An advantage of the double layer equation is that it permits calculations of ion distributions entirely from physically measurable parameters such as CEC, surface area, and bulk solution solute concentrations. In practice, $\phi_m \approx 0$ corresponds realistically, to particle separation of a few hundred Angstroms (theoretically, to infinite plate distance).

Physical Influence

In aqueous media, and at very small separations of clay surfaces (< 2 nm), the major intermolecular forces contributing to the adhesion or short-range stability of clay platelets are attractive van der Waals, attractive ion-ion correlation, and oscillatory hydration forces. Diek & Santos (1996) present a detailed description of the most relevant intermolecular forces.

On the other hand, oscillatory hydration forces favor the stability of H^+-montmorillonite with water interlayers thicknesses of 0.28, 0.58, 0.88, and 1.18 nm (Bradley *et al.*, 1937). As we mentioned earlier, interlayer cations form with water multi-layer hydrates. The relative ease with which one cation will replace or exchange another is not always predictable, but, in general, the ions' relative affinities for, or strength of retention by clays may be given as,

$$Li^+ < Na^+ < K^+ \approx NH_4^+ < Ca^{2+} < Mg^{2+} < H^+ \qquad (B.7)$$

K^+ seems to be more stable than Na^+ because of its larger bare size and less hydrated state, which translate into a stronger electrostatic attraction between the cation and the surface, a weaker monotonic repulsive hydration force (competing with the attractive van der Waals), and a more pronounced oscillatory force between the surfaces of the interlayer, such that a more stable state prevails between the silicate surfaces. On the other hand, Ca^{2+} is more stable in the interlayer space than is Na^+ because of its stronger polarizability and more compact hydrated complex formation. This series can vary with conditions or type of clay mineral, e.g., in acidic conditions H^+ is included in the series.

As discussed above, montmorillonite is capable of uptaking between basal planes a number of water layers, therefore, expanding the basal spacing stepwise from about 1 to 2.2 nm, corresponding to interlayer separations of about 0 to 1.2 nm. This type of expansion is referred to as crystalline or limited swelling (first stage), signifying that the overall crystal morphology is preserved. Swelling of clays in this region is primarily due to oscillatory repulsive hydration forces between the two opposite silicate surfaces, arising from the hydration of the interlayer cations and the arrangement of structural water. However, this crystalline swelling can be extended up to 10 nm under the influence of monotonic repulsive hydration forces.

In general, as the salt concentration increases, depending on the type of salt, the surface density of hydrated cations increases, and, hence, the monotonic hydration repulsion extends further the limited crystalline swelling.

This may explain the observed internal lenticular pores of 10 nm thickness in clay particles composed of eight unit layers (Touret *et al.*, 1990). These strongly attractive forces at small surface separations (< 4 nm), resulting from charge fluctuations[2] of polyvalent cations give rise to a stable state between the silicate surfaces that translates into a potential minimum at ~ 1 nm as seen in Figure B.10 in the absence of hydration forces[3] (Kjellander *et al.*, 1988).

The higher the surface charge density and the concentration of the polyvalent cations, the stronger are the ion-ion correlation effects and the deeper is the resultant minimum. Nevertheless, if hydration effects are taken into account, then, presumably, in pure water or dilute $CaCl_2$ solutions, repulsive hydration and EDL forces remain weaker than attractive ion-ion correlations around the separations 1-2 nm until the salt concentration reaches

---

[2] In the interlayer between the platelets, the local decrease in ion concentration around each ion (a "hole" in the ion cloud), due to ion-ion repulsions, constitutes a charge depletion and can be considered as a charge distribution of opposite sign. It can extend across the midplane between the surfaces if the ion is located nearby. The ion and the part of the ``hole'' on the other side of the midplane interact with an attractive force. The fluctuations or local change in ion density in one half of the interlayer due to an ion in the other half gives rise to an electrostatic attraction between the two halves. The sum of these forces for all ions constitutes the ion-ion correlation forces.

[3] In Figure B.10, the component of the solid line that represents the diffuse double-layer interactions was calculated using an advanced statistical mechanical method known as the *Anisotropic Hypernetted Chain approximation* (AHNC) which allows the determination of the total ion-ion interactions pressure (repulsive EDL and attractive ion-ion correlation effects), as well as the repulsive core-core contact pressure, and the repulsive ion-image charge interactions pressure. The last two have marginal influences on the net pressure, they are both very small compared to the other forces, except for the ion-image charge pressure at very small surface separations that are of no interest here. On the other hand, the component of the dotted line that represents the diffuse double-layer interactions was calculated using *nonlinear Poisson-Boltzmann* theory which only accounts for repulsive EDL effects.

1 mole/liter at which monotonic hydration forces dominate the interactions[4], thereby, extending the crystalline swelling of montmorillonite beyond 1 nm.

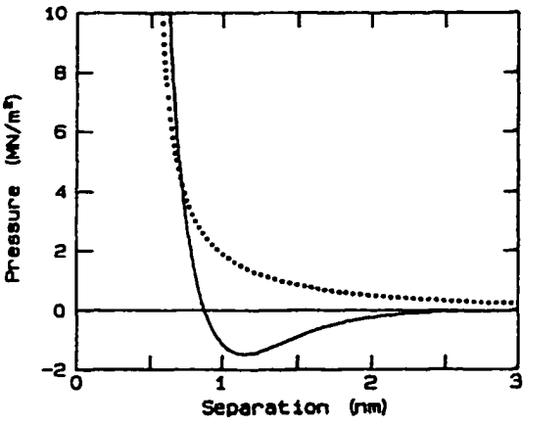


Figure B.10: Forces per unit area between platelets of Ca^{2+}-montmorillonite in pure water in the absence of hydration forces (Kjellander *et al.*, 1988). Net forces of van der Waals and electrostatic interactions including (solid line) or excluding (dotted line) ion-ion correlation effects.

Surely, van der Waals forces contribute to the net attraction, while structural effects of water modify the resultant force by introducing an oscillatory component. It should be noted that the question whether a state with zero disjointing pressure (a minimum in free energy) is a stable state or not at a specific separation (h_1) depends on the difference in free energy between the system at h_1 and at infinite separation (bulk free energy). The difference in free energy per unit area (ΔG_{total}) equals the integral of the pressure (Π) over all intermediate surface separations (h):

[4] Both repulsive hydration and attractive electrostatic correlation forces become stronger with increasing salt concentration, whereas repulsive EDL forces become weaker, while attractive London-van der Waals forces remain the same.

$$\Delta G_{total} = G_{total}(h_1) - G_{total}(\infty) = \int_{h_1}^{\infty} \pi dh \qquad (B.8)$$

such that for, $\Delta G_{total} < 0$, it is necessary to have a strong attractive pressure ($\Pi < 0$) in a reasonably large separation interval above h_1.

On the other hand, montmorillonite containing small, monovalent cations, such as Li^+ and Na^+, do not show a potential minimum at small separations due to the much weaker attractive ion-ion correlation between monovalent cations. The interlayer spacing then increases abruptly to 3-4 nm under the influence of hydration forces and continues to rise more or less linearly to some tens of nanometers with water content under the rising domination of electric double-layer (EDL) repulsion (Figure B.11). This is the second stage of swelling mostly controlled by the diffuse electrical double layers. On the scale of the interlayer (nanometers), the resultant osmotic EDL repulsion is mainly opposed by the weaker van der Waals and ion-ion correlation attractive forces. However, on a higher scale (microns), the gross effect of a clay particle expansion is restrained by frictional forces arising from edge-to-face particle association. At this stage, the consistency of the clay-water systems is that of a paste or thick gel. Note that edge-to-face association give rise to card-house structure (flocculation) if enough electrolyte is present in the suspension. This open structure can be disrupted by adding polyanions that are adsorbed at the positive edge surfaces of the clay particles neutralizing and then reversing its charge such that a negative double layer is formed between the edge and the

face of the particles promoting their dissociation and leading to the breakdown of the card-house structure (deflocculation).

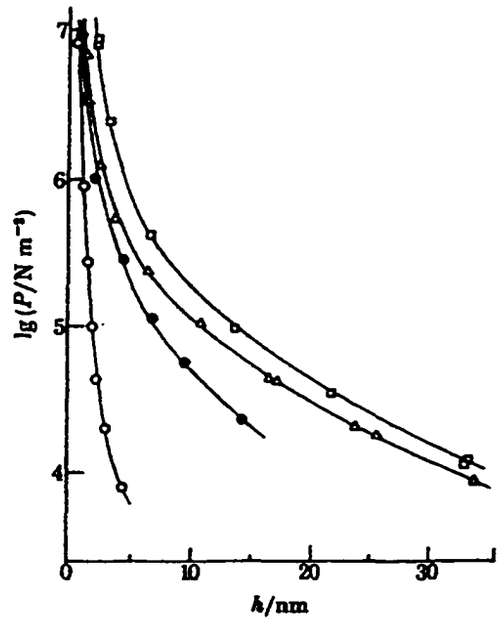


Figure B.11: Logarithm of the total pressure between clay platelets of Wyoming bentonite in 10^{-4} mole/liter salt solutions of various cations as a function of interlayer distance h: □-□ Li^+, Δ-Δ Na^+, •-• K^+, °-° Cs^+ (Lubetkin *et al.*, 1984).

In the near absence of edge-to-face contact, the system passes into the third stage which is characterized by unlimited dispersion. The individual silicate layers are separated by large distances, the extent of separation being limited only by the volume of water in the system. When this is large, the system is a dilute solution in which the particles are kept apart mainly through thermal motion. In relatively concentrated suspensions or gels, diffuse double

layer interaction is the stabilizing factor together with some residual edge-to-face bonding. Besides being dependent on the nature of the saturating cation, the ability of montmorillonite to show extensive or unlimited swelling is influenced by the amount and site of isomorphous substitution as well as by particle size. Thus, beidellites in which this substitution occurs mainly in the tetrahedral sheet do not swell beyond the crystalline or first stage. However, they may be made to swell extensively by mechanical treatment.

Finally, it should also be noted that non-expanding 2:1 type phyllosilicates, such as the illites and most vermiculites, do not form diffuse double layers on their interlayer surfaces but may do so on external surfaces (Quirk, 1968). Vermiculites containing Li^+, small alkylammonium ions, and some amino acids, however, can swell extensively (Diek *et al.*, 1996).

Interaction with Organic Materials

In nature, the net negative charges of clays are usually balanced by inorganic exchange ions, such as Na^+ and Ca^{2+}, which are strongly hydrated in the presence of water. The hydration of these exchangeable metal ions and the presence of Si-O groups in clays imparts a hydrophilic nature to the mineral surfaces. As a result, the adsorption of non-ionic organic compounds (NOCs) by clays is suppressed in the presence of water because relatively nonpolar organic chemicals cannot effectively compete with highly polar water for adsorption sites on the clay surface. In the absence of water, the clay acts as a

conventional solid adsorbent; the high adsorptive capacity for organic compounds is attributed to its large surface area (Chiou & Shoup, 1985). In general, organic ions are believed to be held by Coulombic forces, van der Waals forces (orientation, induction and dispersion) and C-H ··· O bonds between the organic molecule and the clay surface (Hendricks, 1941; Bradley & Grim, 1947). However, it is our opinion that the stability of one or more layers of organic molecules is also determined by solvation forces between the clay surfaces.

Clay minerals interact with organic materials by adsorption, intercalation and cation exchange. Intercalation reactions can be obtained with kaolinite which intercalates a limited number of neutral organic compounds. The adsorption of neutral organic compounds on 2:1 clay minerals dependent on the layer charge and the concentration of salts. The inability of clays to remove substantial amounts of NOCs from aqueous solution can be remedied by replacing natural metal cations with larger organic cations through ion-exchange reactions (McBride *et al.*, 1977; Boyd *et al.*, 1988a). Earlier studies indicated that exchanging quaternary ammonium cations for metal ions on clays greatly modified the sorptive characteristics of dry clays for organic vapors (e.g., White & Cowan, 1958; Barrer & Perry, 1961). Depending on the size of the organic cation, the exchanged organic ions have been shown to form either a microscopic organic phase, as in hexadecyltrimethylammonium-smectite (Boyd *et al.*, 1988b), or discrete organic-modified surface adsorption sites as in tetramethylammonium-smectite (Lee *et al.*, 1989).

Importantly, the substitution of organic cations reduces the hydration of the clay and concomitantly decreases the "free" alumino-silicate mineral surface area (i.e., that surface not covered by the organic exchange ions). As a result, the surface properties of the clay may change considerably from highly hydrophilic, if the clay contains mainly inorganic cations, to increasingly organophilic, as the inorganic cation is progressively replaced by the organic cation. In the petroleum industry, the interactions of cationic surfactants with clays are used to produce organophilic clays that substantially improve the properties and overall performance of oil-based drilling muds.

Interactions of Clays with Cationic Surfactants

Cation Exchange

Clays bind very different kinds of surfactants, and selectivity arises with increasing layer charge. Highly charged clays usually select distinct surfactants from surfactant mixtures. Cationic surfactants are exchanged for the inorganic interlayer cations from aqueous solutions. Depending on concentration, pH, kind of surfactant, alkyl chain length, and layer charge, the cation exchange is accompanied by intercalation of ionic pairs: surfactant cation plus its counterion. Most of the ionic pairs or the alkylamine molecules are removed by short washing; the fully quantitative removal (without showing any change in the X-ray diagram) requires intense washing of the samples.

The adsorption of organic ions on the basal plane surface of montmorillonite is shown by the shift of the basal plane (or *c*-axis) spacing in

Figure B.12. Hendricks (1941) demonstrated that more than one layer of organic molecules may be adsorbed on the basal surfaces of the montmorillonite planes. Figure B.13 displays the variation of the basal plane spacing of montmorillonite treated with aliphatic amines with increasing chain length. The stepwise separation of the planes in increments of 4 Å, which is about the thickness of a methyl group, indicates that the chains lie flat along the clay surfaces, with the planes of the zigzag carbon chains parallel to the mineral basal plane. When the organic chains occupy no more than half the surface area per cation-exchange position, the organic molecules on the top surface of one layer fit into the gaps between those on the bottom surface of the layer directly above it, so that the resulting separation of the two layers is 4 Å, or the thickness of one hydrocarbon chain. When the chains occupy more than 50% of the surface area per exchange position, adjacent laminae are unable to approach more closely than 8 Å, which is the thickness of two hydrocarbon chains. Long-chain quaternary amines form up to six-layer complexes (McAtee, 1958).

On intercalation of n-alkylammonium ions the resulting distance between the silicate layers depends upon the length of the alkyl chain and the layer charge. With increasing length of the alkyl chain, this distance increases alternately by a greater or lesser amount, depending on whether the resulting number of carbon atoms in the intercalated chain is even or odd (Figure B.14).

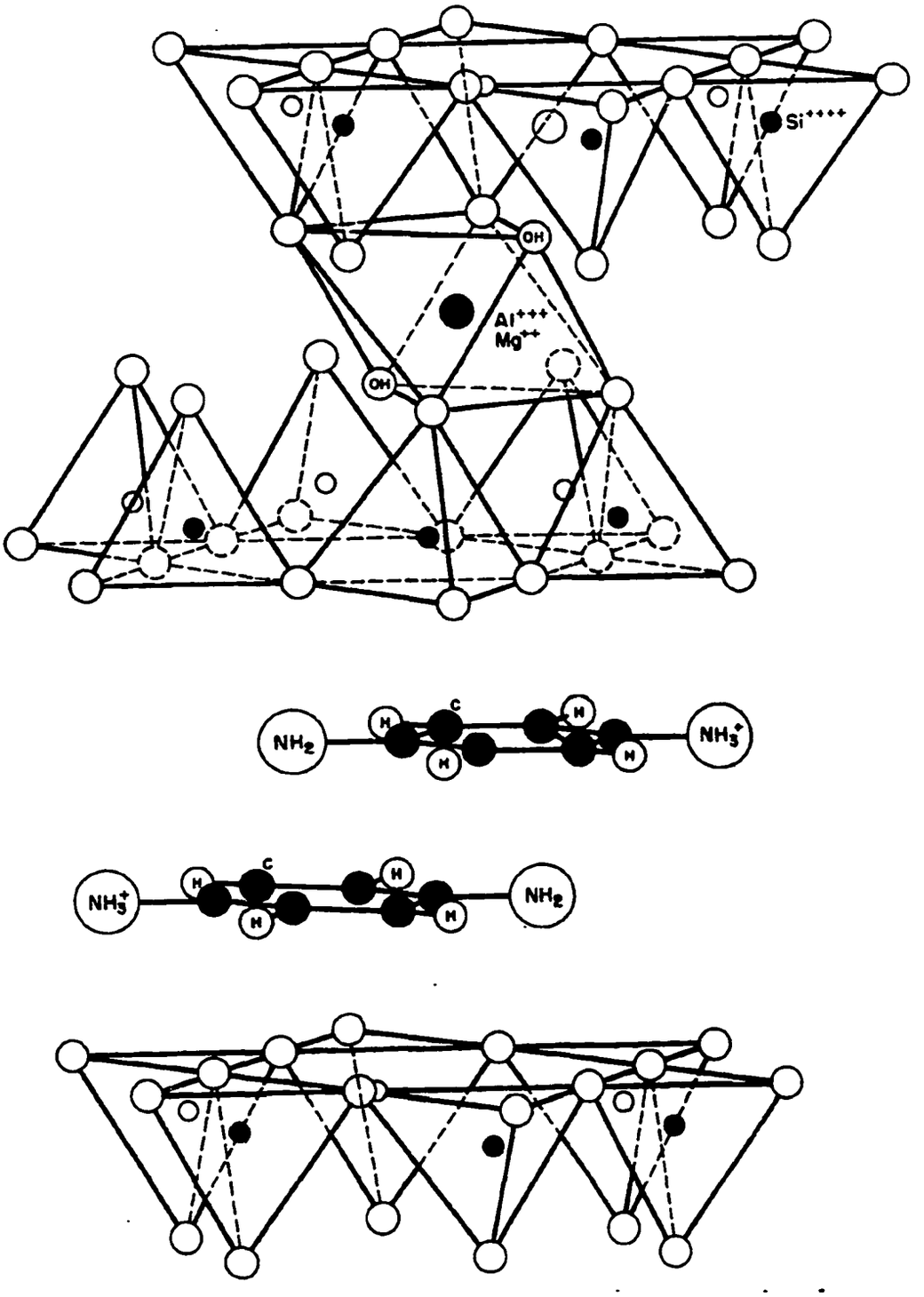


Figure B.12: Schematic drawing showing position of organic cation between montmorillonite layers (Hendricks, 1941).

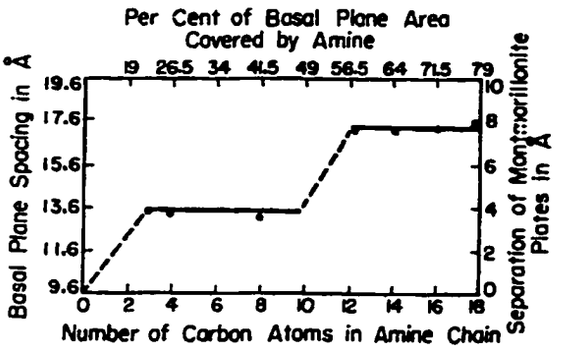


Figure B.13: Effect of amine chain length on montmorillonite basal spacing. The total internal surface area per cation-exchange position calculated as 165 $Å^2$ (Jordan, 1949).

When the layer charge is low, the alkyl chains remain flat until the layers are densely covered (Figure B.15 (a)). As the charge is increased, the chains begin increasingly to slip over one another (Figure B.15 (b)] and stand more erect, until finally the arrangement in Figure B.15 (e) is achieved. The energetically favored arrangement of the alkyl chains is illustrated in Figure B.15 (c) and (d) which shows the pronounced stepwise changes in the interplanar distance encountered when the alkyl chain is lengthened.

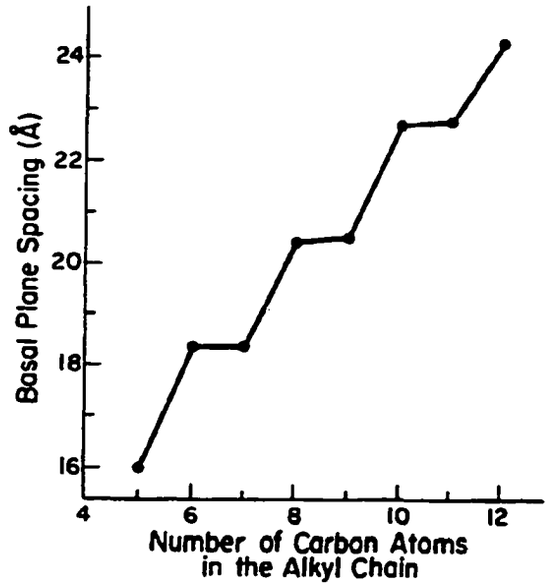


Figure B.14: Increasing basal plane spacing on intercalation of n-alkylammonium ions with increasingly long alkyl chains; charge per half unit cell, x=0.67, (Weiss, 1963).

According to Figure B.14, on passing from an odd to the next higher even number of carbon atoms, the interplanar distance increases by ~ 2 Å, but on passing from an even to the next higher odd number there is virtually no increase. The value of ~ 2 Å per carbon atom exceeds the length of the single C-C bond (1.54 Å). Weiss (1963) suggested that the additional distance originates from the coordination of the terminal CH_3 group with a six-membered ring of SiO_4 tetrahedra. The greatest variation in the interlayer distance to occur on transition from an odd to an even number of carbon atoms because the terminal CH_3 group can key into the six-membered SiO_4 ring only when there is an even number of carbon atoms. On transition to an odd number of carbon atoms, the distance between the silicate layers must increase by the entire thickness of a CH_3 group.

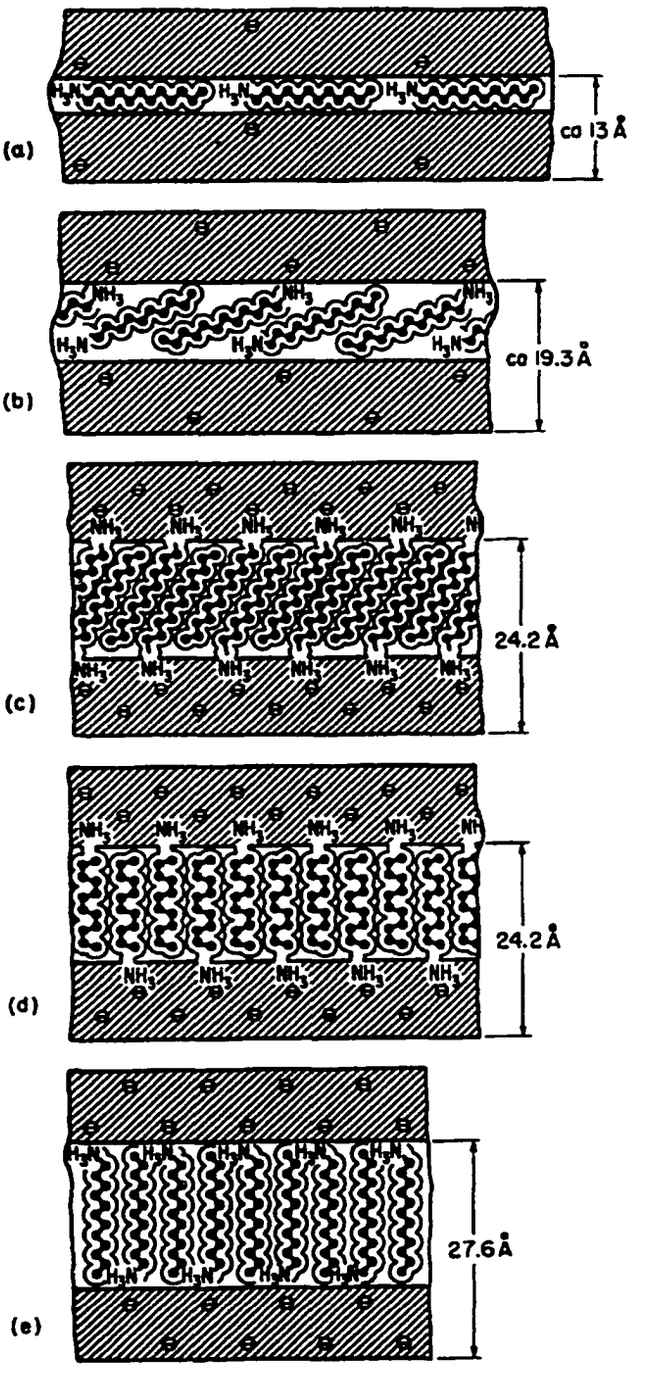


Figure B.15: Arrangements of alkylammonium mica-type layer silicates with different layer (Weiss, 1963). (a) Very low charge; (b) medium charge; (c) preferred arrangement with the formation of three hydrogen bonds per RNH_3^+ ion and with trans, trans-configuration; (d) as (c) but with cis, trans-configuration; (e) high charge. Hatched areas: silicate layers.

Hydrophobic, Hydrophilic and Electric Double-Layer Interactions

In general, the binding of surfactants by cation exchange on a clay surface makes the surface hydrophobic or inert to water, it cannot form ionic or hydrogen bonds with water. The resultant hydrophobic interaction causes an attraction between the surfaces called the *hydrophobic force* (or attractive structural forces) which exceeds van der Waals attraction and can manifest itself up to separations of 80 nm. The reorientation, or restructuring of water around non-polar solutes or surfaces is entropically very unfavourable, since it disrupts the existing water structure and imposes a new and more ordered structure on the surrounding water molecules. Consequently, hydrophobic molecules attract each other and water is ejected into the bulk decreasing the total free energy of the system[5]. In general, the hydrophobic interaction is based on a distinct association of polar molecules, especially water molecules, in the contact area to alkyl chains or low dielectric materials.

The limited or crystalline swelling of n-alkylammonium-montmorillonite system with water may be mainly attributed to the net result between hydrophilic (repulsion) and hydrophobic (attraction) forces between the hydrocarbon coated surfaces. The facts that the cation head group bind

[5] Note that the interaction between a hydrophobic molecule and water is actually attractive, due to van der Waals forces. However, the interaction of water with itself by hydrogen bonding is much more attractive. The strengths of most hydrogen bonds lie between 10 and 40 kJ/mol (Joesten & Schaad, 1974), which makes them stronger than a typical van der Waals' bond (~ 1 kJ/mole) but still much weaker than covalent or ionic bonds (~ 500 kJ/mole).

strongly to the silicate sheets via N-H ··· O bonds and the alkyl groups are hydrophobic restrict the uptake of water in the interlayer. Figure B.16 shows the relationship that exists between the charge density, length of the alkyl chains, and the swelling in water. A sample with layer charge x=0.42 swells in water only when the n-alkylammoniun ion contains more than eight carbon atoms. With a higher charge even the n-butyl and ethylammonium derivatives, respectively, swell in water. In contrast, the lower-charged montmorillonites swell only with n-decylammonium ions or still longer chains.

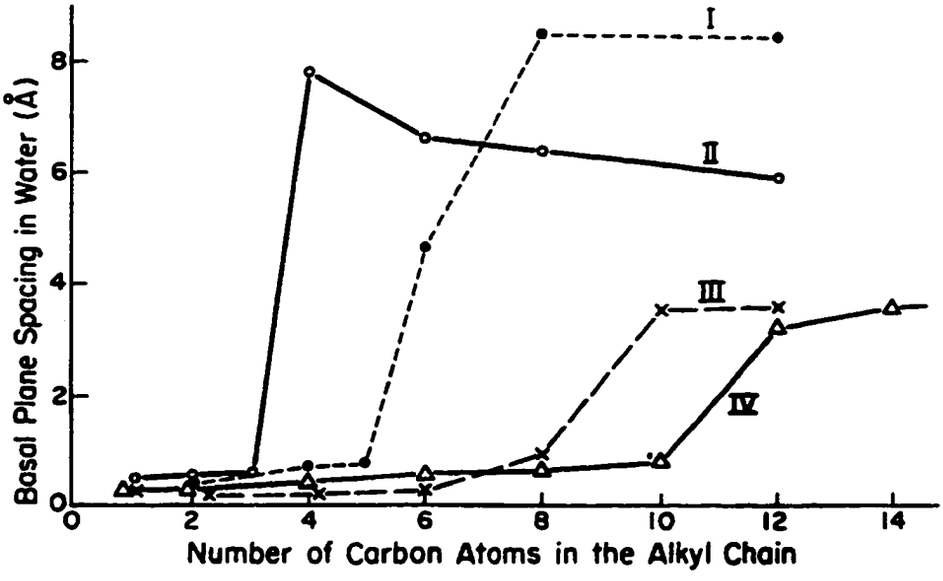


Figure B.16: Relationship between the length of the alkyl chain, the layer charge x, and the swelling power of n-alkylammonium montmorillonites in water (Weiss, 1963): curve I: x=0.55; curve II: x=0.66; curve III: x=0.42; curve IV: x=0.33.

The charge on the silicate layer is discrete rather than "smeared out" over the surface, an increase in layer charge leads to a decrease in the distance separating the negatively charged sites. This intercharge distance imposes an upper limit on the length of the cation's alkyl chain beyond which interlayer expansion, occurs: the higher the charge, the lower the upper limit. In our view, as the layer charge increases, the number of negative surface sites increases, the hydrophilicity of the clay surface increases, allowing water molecules to compete on hydrophilic centers on the clay surface between the chains. On the other hand, with low layer charge, an increase of the alkyl chain length would increase the distance between cation headgroups at negative surface sites, allowing a limited amount of water to invade hydrophilic centers on the surface between the chains. The orientation of hydrogen bonds at each surface may determine the resultant solvation forces whether attractive (hydrophobic), repulsive (hydrophilic) or oscillatory between attraction and repulsion. Of course, van der Waals attractive forces always exist between the surfaces, but their effect are about one order of magnitude smaller than solvation forces. Note that interlayers that do not contain alkylammonium ions or are partially saturated with them will uptake water molecules.

On the other hand, vermiculites saturated with certain short-chain n-alkylammo-nium ions (e.g., C_4) show extensive interlayer swelling (osmotic swelling) when the crystals are immersed in water. It is suggested that ordered water structures (icebergs) are arranged around the organic cations, acting as hosts of the cations which in turn act as supports for the water. The formation

of such structures, referred to as *clathrate compounds*, in the vermiculite interlayers evidently promotes the dissociation of the interlayer cations from the silicate surfaces, giving rise to the formation of diffuse double layers. Therefore, the repulsive electric double-layer forces determine the extension of the macroscopic swelling. Interestingly, montmorillonite containing about equal amounts of Ca^{2+} and short-chain alkylammonium ions swells in water almost as extensively as the sodium montmorillonite or alkyammonium-vermiculite, although the samples fully saturated with either Ca^{2+} or alkylammonium ions show only crystalline expansion as discussed above. This observation may be explained as follows: the inorganic divalent cations on the clay surface between organic cations hydrate causing crystalline swelling. The resulting structure is similar to *clathrate compounds* promoting the dissociation of the organic monovalent cations from the surface which form diffuse double layers that are weakly opposed by van der Waals forces. Note that in this case, attractive ion-ion correlation forces between opposing layers of organic cations are extremely weak not only because these cations are monovalent but also because they are screened by their alkyl chains.

Hydrophobicity does not require the chains to be close-packed, but their distance should not exceed a critical value. Under this condition, water or polar molecules between alkyl chains on an isolated clay surface may associate into ordered clusters creating discontinuities to the bulk water phase. For example, the cationic surfactant head groups may cover the negatively charged sites ($Si\text{-}O^-$) whereas the water clusters may be partially localized on

hydrophilic sites (e.g., Si-OH) between the charged sites. If the distance between the chains exceeds the critical value, the disordered water molecules of the bulk phase penetrate between the water clusters around the chains and the discontinuity disappears. The liquid clusters on the alkyl chain bearing surface are sensitively influenced by structure-breaking and structure-making ions. The structure-breaking power of ions can increase (for example, tetradecylammonium beidellite in water) or decrease the basal spacing (tetradecylammonium vermiculite in DMSO, tetradecylammonium beidellite in ethanol: Lagaly *et al.*, 1983). Consequently, the viscosity of organic dispersions of alkylammonium montmorillonites can be strongly influenced by inorganic salts.

Appendix C

Shale Coring Apparatus

Introduction

Shales are very sensitive rocks and require special handling when preparing the samples for laboratory testing (see Chapter 3) inorder to minimize damage and disturbance of the original properties. Any effort to prevent damage and loss of its water content will produce a better evaluation of the mechanical and/or chemical properties. In order to run triaxial tests, cylindrical plugs are required and the standard procedure is to cut them dry or with water as drilling fluid. For shales, however, the rock should be preserved at all times from air exposure; one of the ways is to keep the rock immersed in mineral oil. A simple apparatus was built at The University of Oklahoma allowing coring of plugs of different diameters and length while keeping the shale submersed in oil at all times. A detailed description of the apparatus and also the procedure to prepare the plugs is described in this Appendix.

Apparatus

The shale coring box is a cubic container made of aluminum 0.35 inches thick. The box dimensions are: 18 in. high, 24 in. long, and 18 in. wide. The box has eleven (11) holes along the two (2) bigger sides, near the top of the box. The holes are 0.35 inches in diameter and are spaced 2 inches apart and 1 inch away from the top of the box. The purpose of the holes is to hold up two (2) square aluminum bars (Figure C.1). The separation between the holes will allow to adjust the bars position at the top of the box, and their position will depend on factors in the coring operation such as core barrel size, clamp size, etc. The square aluminum bars in turn will hold two vertical threaded rods, which will tighten a piece of wood at the bottom of the box. A vise is bolted to the wood base and this vise is used to clamp the rock samples for coring (Figure C.2).

Flow System

In order to cut a plug, the shale coring box has to be filled with a non-contaminating fluid, which will be circulated while drilling with the core barrel. The fluid used for this purpose is light mineral oil. The box has a drainage valve (ball valve-valve 1), this valve is used to empty the coring box and to circulate the fluid contained in the box. The drainage valve is connected to a mineral oil container (five gallons in volume) through a plastic hose 1/2 in. in diameter, this type of hose is used in throughout the circulating system.

The oil container is attached to an electrical pump (115 volts, 50/60 Hz, 1.5 Amp.) which will supply the power necessary to circulate the oil. Finally the system has a needle valve (valve 2) to adjust the flow rate necessary to lubricate and preserve the rock sample when coring (Figure C.2).

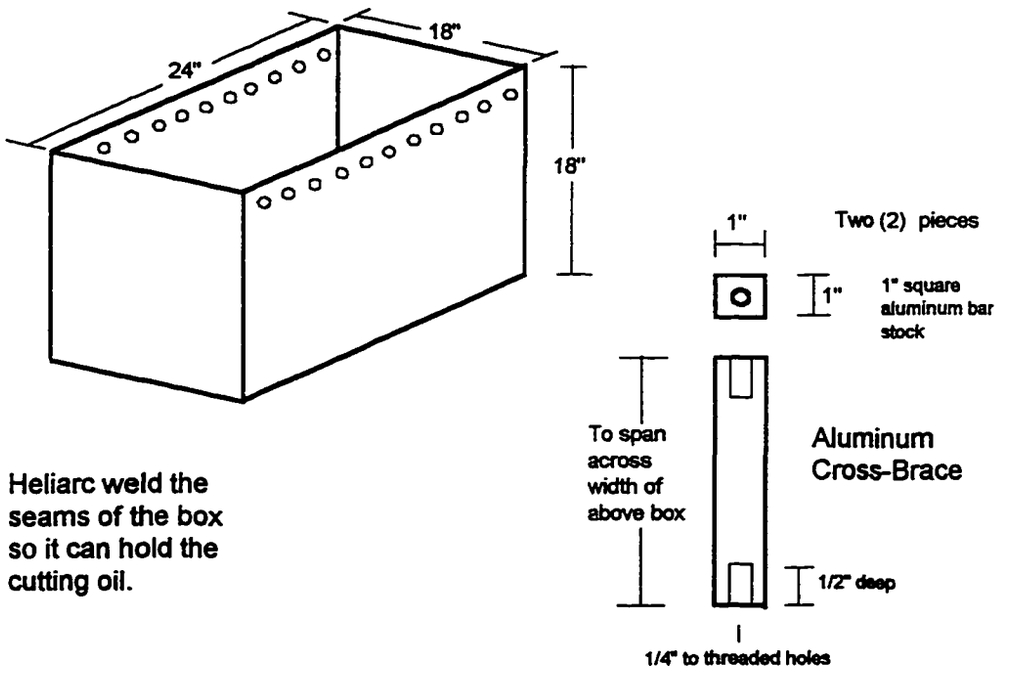


Figure C.1: Diagram of the shale coring box.

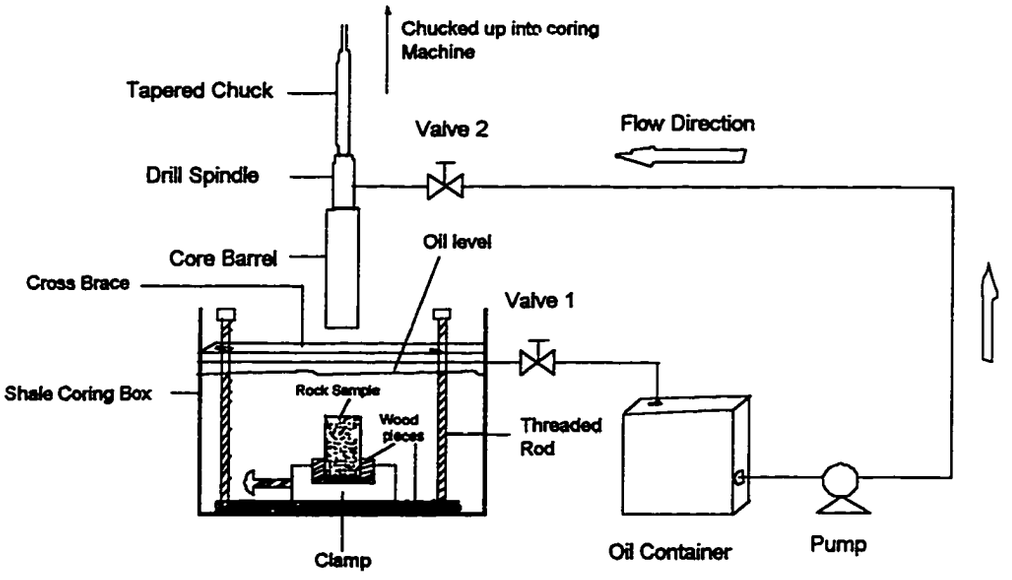


Figure C.2: Assembly diagram of shale coring set up.

Coring Procedure

The assembly used in coring is composed essentially of three parts: the coring machine, the pumping system and the shale coring box (Figure C.3). A schematic representation of the coring machine is given in Figure C.4. The coring procedure can be described as follows:

1) Place the shale coring box on the drill table.

2) Put the piece of wood which supports the clamp at the bottom of the shale coring box.

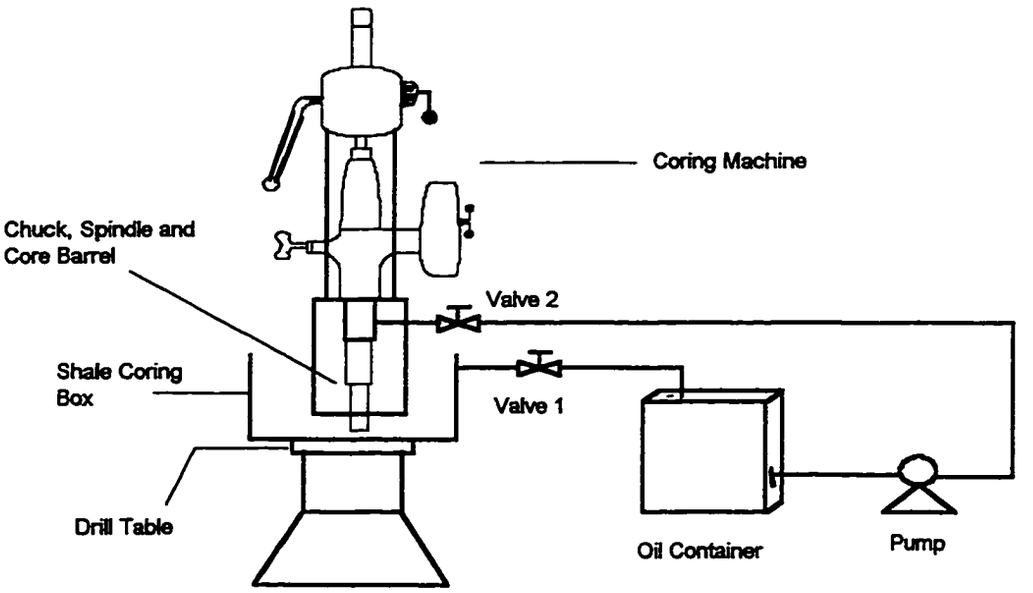


Figure C.3: Coring box, pumping system and coring machine.

3) Fill the shale coring box with mineral oil to a convenient level above the drainage valve (valve 1), and above the top of the sample to be cored.

4) Adjust the height of the drill head of the coring machine, to properly drill all the way through the sample. The previous adjustment can be done as follows (Two people are required for this step):

a) While holding up the drill head, loosen the two locking bolts on the drill head. Caution! The drill will fall when these bolts are loose! Do not have any core barrel in apparatus and keep hands and feet clear of drill head.

b) Move up or down the drill head adjusting its position according to need.

c) Tighten the smaller bolts, then take out the wrench from the largest bolt.

5) Insert the tapered chuck to the drill head.

6) Insert the barrel spindle to the tapered chuck.

7) Tighten the core barrel to the barrel spindle.

8) Put small pieces of wood in the jaws of the clamp to protect the shale sample. Put a piece of wood at the bottom of the clamp to avoid drilling into the steel vise.

9) Put the shale sample on the clamp, and carefully tighten it.

10) Adjust the position of the core and clamp assembly, by moving the piece of wood which supports the clamp and then clamp down the wood with the threaded rods.

11) Connect the flow system to the coring machine and to the core barrel spindle (drill spindle).

12) Open the valve 1 and turn on the electrical pump.

13) Adjust the flow rate of the coring fluid (mineral oil) using valve 2.

14) Turn the power of the coring machine on.

15) Set the drilling velocity at 4.

16) Move the drill head down using the up/down handle, until the core barrel reaches the top of the sample.

17) Start drilling by applying slight pressure to the core with the core barrel using the up/down lever. When the core barrel is stable, lock the lever into automatic feed by closing the two handles together.

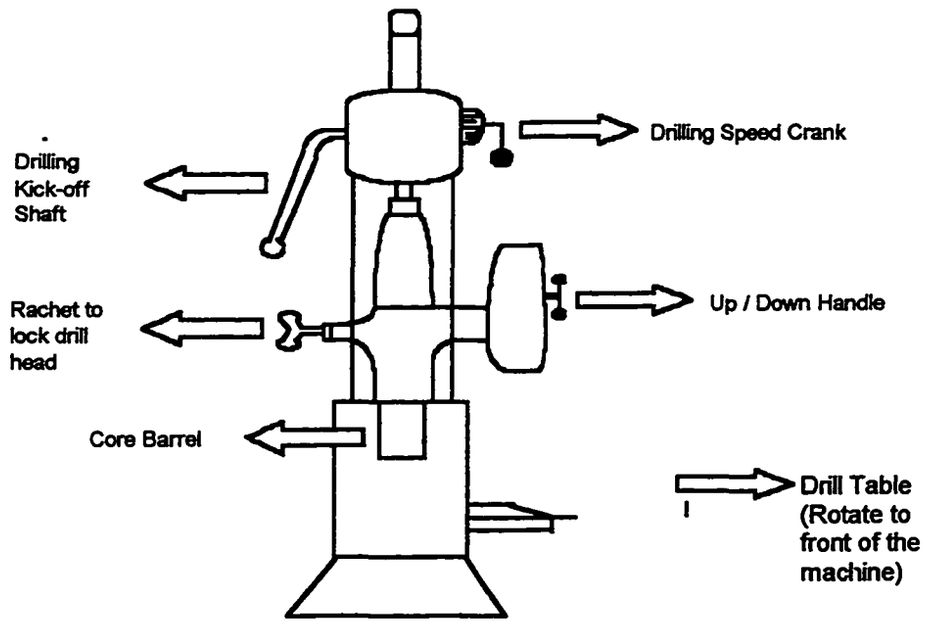


Figure C.4: Coring machine.

18) Once the coring has been completed, stop the drilling with the kick-off shaft, lock the coring string with the up/down handle and lift the drill head using the up/down handle.

Once the rock sample has been cored, the following procedure should be followed:

1) Turn off the coring machine

2) Unplug the power supply for the pumping unit.

3) Close the drainage valve in the shale coring box.

4) Take carefully the core out of the shale coring box.

5) Carefully take off the coring drill string, in the following order: first the core barrel, then drill spindle and then the tapered chuck.

6) Take out the hose from the oil container, open the drainage valve (valve 1) and drain the shale coring box.

7) Lift the shale coring box from the drill table and put the drill table in its initial position.

Conclusions

The apparatus here described have been used to cut shale plugs, from the Campos Basin, in Brazil, and from the Gulf of Mexico. Despite the relatively small experience with the equipment, some conclusions can be stated based on the plugs already cored:

. Drilling speed should be very small, without applying much weight on the bit. With a high drilling speed, the plug gets stuck with the bit, breaking it completely. Successful operation could only be achieved when the drilling speed was reduced. This problem is much more severe if the core has weakening planes or fractures. Norsk Hydro developed an apparatus that applies a pressure on the axial axis of the plug during the coring operation, avoiding the specimen to fall apart when weaking planes are present.

. A plug from a highly fractured core (from the Gulf of Mexico) was obtained, even with fractures filled with oil and almost opened, due to a low penetration rate.

. A complete operation to prepare a 4-in. long plug lasts about 1 hour. Tentatives to reduce this period by increasing drilling rate could lead to broken plugs.

. Encapsulating the core with a PVC tube and hose clamps helped the integrity of the plugs, once a confining stress is applied to the core.